2P
M 1X

FINAL REPORT

CR-103190

# RESEARCH STUDY ON INSTRUMENT UNIT THERMAL CONDITIONING PANEL

71-7133
May 1971





Prepared for

National Aeronautics and Space Administration
George C. Marshall Space Flight Center
Huntsville, Alabama
Contract No. NAS8-11291

GARRETT

AIRESEARCH MANUFACTURING COMPANY
Los Angeles, California

FINAL REPORT

# RESEARCH STUDY ON INSTRUMENT UNIT THERMAL CONDITIONING PANEL

71-7133
May 1971

Prepared by

D. W. Graumann
C. E. Richard
J. D. Duncan
J. C. Gibson
C. S. Coe
C. Albright

Prepared for

National Aeronautics and Space Administration
George C. Marshall Space Flight Center
Huntsville, Alabama
Contract No. NAS8-11291

AIRESEARCH MANUFACTURING COMPANY
Los Angeles, California

## FOREWORD

The work described in this report was accomplished under Contract Number NAS8-11291 initiated by NASA Marshall Space Flight Center for a Research Study on Instrument Unit Thermal Conditioning Heat Sink Concepts. The contract was under the direction of Mr. F. Huneidi at NASA and Messrs. I. G. Austin and E. W. Gellersen at the AiResearch Manufacturing Company. The following members of the AiResearch program staff contributed to this report: D. W. Graumann, thermal analysis; C. E. Richard, stress analysis; J. D. Duncan and J. C. Gibson, mechanical design and development; S. Coe, wick contamination investigations; and C. Albright, noncondensable gas investigation.

## ABSTRACT

A heat pipe panel 30 in. by 30 in. was designed, fabricated, and tested to the design requirements of the Saturn V vehicle. Investigations into wick materials, preservation of wick materials, and porous plate sublimation was performed in conjunction with a study of noncondensable hydrogen gas generator in 304 stainless steel heat pipes with water as the working fluid.

# SUMMARY

The Research Study on Instrument Unit Thermal Conditioning Heat Sink Concepts, performed by the AiResearch Manufacturing Company on NASA Contract NAS8-11291, was accomplished in two phases. The Phase I work was reported in the Annual Report entitled "Research Study on Instrument Unit Thermal Conditioning Heat Sink Concepts", NASA Report NASA-CR-97671 (AiResearch Report 67-2577). This final report describes the Phase II work entitled "Research Study on Instrument Unit Thermal Conditioning Panels - Design, Fabrication and Testing of a Heat Pipe Panel." This summary discusses both the Phase I and the Phase II work.

## PHASE I

The Phase I study consisted of (1) the investigation of wick-type evaporators, (2) the investigation and optimization of sublimator modules, and (3) an experimental and analytical investigation in the area of thermal conditioning panels.

### Wicking Materials

The initial part of the study was a basic investigation of wicking materials. Based upon past AiResearch development programs and information available in the literature, the best type of wicking material for this investigation was selected, and the various wick parameters were varied to determine their effect on water transport rate, evaporation performance, etc. Various methods of water flow distribution, water flow control, and heat transport fluid temperature control were analyzed. The evaporator module geometry was investigated with respect to wick-fin arrangement and flow configuration. A 1-kw boiler module and control system were designed, fabricated, and tested over a range of inlet temperatures and heat loads. Stacking studies were conducted to allow for heat loads larger than 1 kw. Based upon the wicking investigation, boiler operation analysis, and multiwick module testing, an optimized wick-type water boiler was designed.

The experimental and analytical investigations of wick-type water evaporators and the conclusions reached as a result of the study are summarized below.

Wicking rates may be successfully predicted analytically for a given wick as a function of pore size, contact angle, and tortuosity. The equations developed for pumping capacity and wicking rate in a zero-g environment were verified by horizontal wicking tests under 1-g conditions. Stringent cleanliness requirements are essential to assure optimum performance of a wick-type evaporator.

Good thermal control of a wick-type evaporator may be achieved by the use of a single valve which provides back pressure and water on-off regulation utilizing a vernatherm element which senses the heat transport fluid outlet temperature. The chief advantage of this valve is that the vernatherm generates its own driving force making the control system independent of external power requirements.

Proper evaporator design should include a pressure drop distribution system in order to assure equal quantities of supply water to all boiler wicks. The primary importance of this system was realized in a 1-g environment when the effects of gravity were normal to the evaporator wicks.

The optimum boiler module configuration incorporated water feed from both ends of the wick with a centrally located steam duct. This technique offered the advantages of low steam side pressure drop, the use of a minimum thickness wick due to the shorter wicking length, and more rapid distribution of water during a refill cycle.

A series of optimum 1-kw module water boilers may be combined to provide cooling for a wide variety of heat load applications.

Porous Plate Sublimators

Porous plate sublimator modules were studied to investigate possible sublimation mechanisms, the liquid breakthrough phenomenon, and the effect of water plenum configuration. An extensive experimental investigation of various porous plates and their operating characteristics was conducted. The effects of the heat flux and water plenum pressure were examined, and performance at startup, restart, steady state, and at no heat load were defined. Several water plenum configurations were tested and the potential advantageous use of hydrophobic coatings was established. A sublimator core incorporating several porous plates was designed, fabricated, and tested. Based on the investigation, an optimized 1-kw sublimator was designed with the potential of handling the large heat loads investigated in the stacking studies. The experimental and analytical investigations of porous plate sublimators and the conclusions reached as the result of the study are summarized below.

An optimum sublimator design should incorporate a steam plenum sized to ensure that all areas of the sublimator plates are exposed to pressure levels substantially less than the water triple point pressure. The use of a supply water plenum height on the order of 0.010 to 0.020 in. eliminates the possibility of a porous plate rupture during sublimator freeze up. The short water plenum does not, however, degrade the unit performance.

The optimum heat transport fluid side sublimator design in sublimator-type heat exchangers can be achieved by varying the heat transport fluid fin area density by increasing the number and thickness of the fins from the hot to the cold end of the unit. The resulting increase in overall conductance allows for operation of the sublimator over its entire length at the maximum allowable heat flux which can be withstood by a given porous plate without breakthrough.

Porous plates selected for use in a sublimator should contain pore sizes in the range of 2 to 10 microns. Porous plates with pore sizes smaller than 2 microns are subject to plugging by corrosion and system contaminants. Plates with pore sizes larger than 10 microns demonstrate poor startup characteristics due to the longer period of time required to form an ice block within each pore.

In general for porous plates with the same average pore size, the plate with the highest void fraction will demonstrate the best performance, measured in terms of the temperature difference between the heat transport fluid and the sink temperature.

A series of optimum 1-kw module sublimators may be combined or stacked to provide cooling for a wide variety of heat load applications.

## Thermal Conditioning Panels

The conclusions and recommendations in the area of thermal conditioning panels were formulated from the experimental and analytical investigations performed in the wicking and sublimators study portions of the program. The following summarizes the design concepts.

The heat pipe-sublimator and simple wick boiler were feasible panel concepts for thermal conditioning of electronic equipment in a zero-g environment. Development tests conducted on panel sections representing each of these concepts demonstrated that both panels successfully dissipated heat loads typical of those encountered on the Saturn instrument unit. The test sections achieved thermal control within a band of $\pm 10^{0}$F. The two panels studied can be equipped with mechanical controls and an integral water storage capacity making them independent of external loops or power requirements. The control system would be driven by a melting-wax vernatherm element and water would be supplied from a rechargeable storage tank within the panel.

The analytical techniques available for predicting the performance of the heat-pipe sublimator and the simple wick boiler have provided predicted values within 10 percent of the test results.

## PHASE II

The Phase II portion of the program included (1) the investigation of hydrophobic coatings and large pore porous plates on sublimator performance, (2) the investigation of wick preservation techniques, (3) additional testing of the two thermal panel sections built during Phase I, (4) the investigation of noncondensible hydrogen gas generation, and (5) the design, fabrication, and testing of a full-scale 30 in. by 30 in. heat pipe panel.

## Simple Wick Boiling

The 10 in. by 12 in. simple wick boiler test module was designed, fabricated, and tested to evaluate the performance characteristics of sintered fiber metal wicks. The testing was performed in a bell jar where the test module could be closely observed for wick wetting. Some difficulty due to wick contamination was experienced, but after cleaning the wick in a vacuum furnace at $1000^{0}$F testing was resumed and the maximum capacity of the sintered fiber metal wick was determined.

Heat Pipe Module Panel

A heat pipe thermal panel test module that was 1/6 scale of the 30 in. by 30 in. thermal conditioning panel was designed, fabricated, and tested to show the feasibility of a heat pipe of this size. Testing was performed that showed feasibility and also demonstrated the ability of the heat pipe to start up when the heat pipe fluid was frozen.

Hydrophobic Porous Plate Investigation

A conventional sublimator porous plate depends upon the existence of ice in the pores to restrain the water in the plenum from breaking through but there are two modes of operation in which ice may not exist and the sublimator fails. These modes are unit startup and high heat flux conditions. Startup breakthrough has been limited by regulating the water plenum pressure and water flow rate with additional controls. High heat flux breakthrough has been eliminated by limiting the maximum heat flux at which a unit operates.

Tests were performed based upon the hydrophobic coating analysis, and the MS122 Fluorcarbon mold release was found to be the most optimum coating. However, the coating should not penetrate more than a few thousands of an inch below the surface. The water retention pressure of the plate increased significantly over the uncoated plates, but the effect of the coating on permeability was inconclusive. The coating method used in this study produces significant penetration of the hydrophobic film into the plate as evidenced by the signficant degradation in thermal performance that occurs as a result of the coating.

Large Pore Sublimators

Tests were performed on large pore sublimator plates with pore sizes of 5, 20, 40, and 100 microns because of the possible pore plugging in conventional sublimator plates. Limited testing indicated that large pore sublimators will operate at steady-state conditions, but also showed that the large pore plates have higher temperature drops and lower heat flux breakthrough limits.

Wicking Preservation Study

A comprehensive program of research was directed toward understanding the principles involved in the wicking of water by sintered fibrous nickel wicks. A particular area of this program was the determination of the nature of the contamination responsible for loss of wicking action and development of methods for protecting the nickel wicks against the deleterious effects of the contaminants.

X-ray and microscopic examination were employed in an attempt to identify the contaminants responsible for loss of wicking action. X-ray examination indicates that nickel chloride dihydrate ($NiCl_2 \cdot 2H_2O$) was present on the surface of contaminated wicks and could be responsible for decrease in water transport rate. The chlorine in this compound may arise from a number of halogenated atmospheric contaminants such as ethylene dichloride, carbon tetrochloride, etc. X-ray examination of uncontaminated wicks which exhibited excellent wicking properties showed only nickel hydroxide on the wick surface.

Microscopic examination failed to correlate visible contamination with wick properties. An attempt was made to thermally desorb contaminants from wicks which had suffered loss of wicking ability and analyze the gas in a mass spectrometer. Data from these tests indicated that possibly sulfur dioxide may be an undesirable contaminant. It was concluded that a variety of contaminants can probably lead to a deterioration of wicking action and that only extremely small amounts of contaminants were required to affect wicking action, making specific identification difficult.

Attempts to protect the wicks from contamination by absorbing hydrophilic organic materials onto the nickel surface were unsuccessful. However, the use of chemically-bonded hydrophilic groups appeared promising. The best results were achieved by treatment with warm distilled water saturated with oxygen. This treatment, as demonstrated by X-ray analysis of surface material, formed nickel hydroxide on the surface. Other methods of oxidation were generally less successful than the oxygenated-water treatment. Treatment with ozone in water was equally effective but more complicated. Attempts to introduce other inorganic groups: fluoride, iodide, sulfide, and silicate were generally ineffective as far as protecting the wicks from contamination was concerned.

Oxidation of the wicks in air at elevated temperatures ($800^{0}$) failed to protect the wicks against contamination. Heating of the wicks in hydrogen was expected to make them hydrophilic, because of possible hydrogen bonding between the water molecules and the absorbed hydrogen on the wick surface. This treatment also failed to protect the wicks against contamination.

It was concluded that the formation of nickel hydroxide on the wick surface provided good protection against loss of water transport by wicks exposed to a contaminated atmosphere.

<u>Noncondensible Hydrogen Gas Investigation</u>

An investigation into the phenomena of hydrogen gas generation with stainless steel heat pipes using water as the working fluid was performed. Two configurations of tubular heat pipes were designed, fabricated and tested to investigate the rate of hydrogen generation and also the degradation effect of the entrapped hydrogen on heat pipe performance. The heat pipes with palladium (75%)-silver (25%) end caps and two heat pipes with stainless steel end caps were used for this evaluation.

No conclusions could be reached from the test results since hydrogen generation did not degrade the results of two of the conventional test specimens. The failure of the two heat pipes to show any degradation could be attributed to either the lack of sufficient hydrogen generation to show a detrimental effect on performance or the passivation by a mixture of nitric and hydrofluoric acids that may have removed a significant amount of sites in the stainless steel available for oxidation.

## Heat Pipe Panel

A heat pipe panel 30 in. by 30 in. using water sublimation for cooling was designed, fabricated, and tested. The panel was designed to carry 180 lb of electronic equipment at a vibrational load of 12-g. The heat pipe panel used a single 30 in. by 30 in. wick that was machined to accommodate the 168 equipment mounting bosses located in the panel. The heat pipe was designed to accommodate a thermal load of 420 watts with a maximum panel surface temperature of 90°F. However, due to unbrazed areas in the heat pipe, the maximum thermal capacity of the panel was 210 watts with a panel surface temperature of 90°F. A metallurgical evaluation of the brazed panel assembly was performed to evaluate the extent of the unbrazed areas and the results are presented in Appendix B.

CONTENTS


| Section | | Page |
|---|---|---|
| 1 | INTRODUCTION | 1-1 |
| 2 | TASK I--THERMAL PANEL MODULE AND RELATED SMALL SCALE TESTS | 2-1 |
| | Introduction | 2-1 |
| | Simple Wick Boiler Test Module | 2-1 |
| | Heat Pipe Thermal Panel Test Module | 2-9 |
| | Wicking Preservation Study | 2-21 |
| | Hydrophobic Porous Plate Investigation | 2-54 |
| | Large Pore Sublimator | 2-75 |
| 3 | TASK II--THERMAL PANEL CONCEPT SELECTION | 3-1 |
| 4 | TASK III--DESIGN AND FABRICATION OF FULL SIZE THERMAL PANEL | 4-1 |
| | Introduction | 4-1 |
| | Heat Pipe Sublimator Principle and Mode of Operation | 4-1 |
| | Thermal Design | 4-3 |
| | Sublimator Water Reservoir Design | 4-20 |
| | Sublimator Feed Water Valve Design | 4-22 |
| | Structural Design | 4-23 |
| | Noncondensable Gas Generation Investigation | 4-29 |
| | Fabrication | 4-39 |
| 5 | TASK IV--TEST OF FULL SIZE THERMAL PANEL | 5-1 |
| | Introduction | 5-1 |
| | Test Setup | 5-1 |
| | Performance Testing | 5-8 |
| | Test Results and Discussion | 5-15 |
| | Conclusions and Recommendations | 5-38 |
| 6 | REFERENCES | 6-1 |

CONTENTS (Continued)


| Appendix | | Page |
|---|---|---|
| A | TRANSIENT ANALYSIS TO APPROXIMATE PANEL COLD END TEMPERATURE DIFFERENCE | A-1 |
| B | AIRESEARCH REPORT 71-7343: METALLURGICAL EVALUATION OF BRAZED PANEL ASSEMBLY PN 189040-1 | |

## ILLUSTRATIONS


| Figure | | Page |
|---|---|---|
| 2-1 | Simple Wick Boiler Thermal Panel Test Section | 2-2 |
| 2-2 | Instrumented Simple Wick Boiler Thermal Test Module | 2-3 |
| 2-3 | Simple Wick Boiler Test Apparatus | 2-4 |
| 2-4 | Heat Pipe Thermal Panel Test Section | 2-10 |
| 2-5 | Instrumented Heat Pipe Thermal Panel Test Module | 2-11 |
| 2-6 | Heat Pipe Sublimator Test Schematic | 2-12 |
| 2-7 | Heat Pipe Sublimator Test Apparatus | 2-13 |
| 2-8 | Heat Pipe Test Module Performance | 2-15 |
| 2-9 | Frozen Startup of Heat Pipe Test Module | 2-17 |
| 2-10 | Liquid Resupply Limiting Heat Flux | 2-19 |
| 2-11 | Wicks Subjected to Various Treatments | 2-23 |
| 2-12 | Variation of Oxygen Solubility in Water With Temperature | 2-29 |
| 2-13 | Wick Rate Test-Observation of Wicking Height | 2-32 |
| 2-14 | Wick Rate Test-Weight of Water in Wick | 2-33 |
| 2-15 | Effect of Air Exposure Time on Wick Rate | 2-35 |
| 2-16 | Effect of Gas Exposure on Nickel Wick Behavior | 2-36 |
| 2-17 | Microscopic Examination of Wick Surface | 2-39 |
| 2-18 | Microscopic Examination of Wick Surface (450X) | 2-40 |
| 2-19 | Electrolytic Cell for Uniform Wick Oxidation | 2-53 |
| 2-20 | Depth of Penetration of Hydrophobic Coating as a Function of System Parameters | 2-58 |
| 2-21 | Porous Plate Bench Test Apparatus | 2-61 |
| 2-22 | Nitrogen Permeability With Vacuum Discharge | 2-63 |
| 2-23 | Nitrogen Permeability With Vacuum Discharge | 2-64 |

ILLUSTRATIONS (Continued)



| Figure | | Page |
|---|---|---|
| 2-24 | Bubble Point Data in Water | 2-67 |
| 2-25 | Permeability of Coated and Uncoated Plates | 2-68 |
| 2-26 | Porous Plate Sublimation Test Fixture | 2-69 |
| 2-27 | Sublimation Test Apparatus | 2-70 |
| 2-28 | Porous Plate Sublimation Performance | 2-71 |
| 2-29 | Coated Porous Plate Sublimation Performance | 2-73 |
| 2-30 | Nitrogen Permeability with Vacuum Discharge | 2-77 |
| 2-31 | Large Pore Porous Plate Sublimator Performance | 2-78 |
| 4-1 | Heat Pipe Sublimator Thermal Conditioning Panel | 4-2 |
| 4-2 | Vapor Pressures of Heat Pipe Fluids | 4-5 |
| 4-3 | Required Wick Thickness as Defined by Liquid Delivery Requirements | 4-7 |
| 4-4 | Conduction Temperature Drop Through Wick of Condensor End for Required Wick Thickness | 4-9 |
| 4-5 | Two-Path Liquid Flow | 4-9 |
| 4-6 | Worst Case Heat Input to Remote Coolant Loop | 4-13 |
| 4-7 | Effect of Sublimator Area on Temperature Drop Through Sublimator and Condensor End Wick | 4-17 |
| 4-8 | Instrument Unit Thermal Panel Structural Schematic | 4-23 |
| 4-9 | Sublimator Plate Support | 4-27 |
| 4-10 | Heat Pipes With Condenser End Ports Porous to Hydrogen for Noncondensable Gas Generation Studies | 4-30 |
| 4-11 | Heat Pipe Configuration A | 4-31 |
| 4-12 | Test Setup for Noncondensable Gas Generation Studies | 4-32 |
| 4-13 | Noncondensable Gas Study Hydrogen Flow Measuring System | 4-33 |

ILLUSTRATIONS (Continued)

| Figure | | Page |
|---|---|---|
| 4-14 | Heat Pipe-Stainless Steel Noncondensable Gas Generation Study With Palladium (75%)-Silver (25%) End Cap | 4-35 |
| 4-15 | Remote Cooling Loop Subassembly Prior to Brazing | 4-40 |
| 4-16 | Assembly of Structural Sandwich Prior to Brazing | 4-41 |
| 4-17 | Vacuum Furnace Braze Cycle Setup | 4-43 |
| 4-18 | Remote Cooling Loop Subassembly Ready for Brazing | 4-44 |
| 4-19 | Instrument Unit Thermal Conditioning Panel Structural Sandwich | 4-46 |
| 4-20 | Buildup of Details for Final Braze Cycle | 4-47 |
| 4-21 | IU Thermal Conditioning Panel | 4-49 |
| 5-1 | Schematic of High Altitude Test Setup | 5-2 |
| 5-2 | Heater and Thermocouple Installation | 5-3 |
| 5-3 | Thermocouple Installation | 5-4 |
| 5-4 | Configuration 1 Heater Installation - Heater Bonded to Panel Assembly | 5-5 |
| 5-5 | Configuration 2 Heater Installation - Heaters Bonded to Aluminum Plates | 5-6 |
| 5-6 | Thermocouple Installation with Configuration 2 Heater Installation | 5-7 |
| 5-7 | Heat Pipe Filling | 5-9 |
| 5-8 | Thermal Conditioning Panel Test Setup | 5-10 |
| 5-9 | Sea Level Thermal Performance Test System With Fill Apparatus and Simulated Sublimator | 5-12 |
| 5-10 | Sea Level Thermal Performance Test Setup | 5-13 |
| 5-11 | Ducting for Sea Level Performance Testing | 5-14 |

ILLUSTRATIONS (Continued)


| Figure | | Page |
|---|---|---|
| 5-12 | Remote Cooling Loop Pressure Drop | 5-16 |
| 5-13 | Remote Cooling Loop Thermal Performance | 5-18 |
| 5-14 | Panel Performance at a Heat Load of 105 Watts | 5-20 |
| 5-15 | Temperature Drop at Panel Hot End | 5-29 |
| 5-16 | Temperature Drop at Panel Cold End | 5-30 |
| 5-17 | Maximum Panel Surface Temperature for Heater Configuration 1 | 5-33 |
| 5-18 | Maximum Panel Surface Temperature for Heater Configuration 2 | 5-34 |
| 5-19 | Solid Aluminum Panel $\Delta P$ as a Function of Total Weight | 5-37 |
| 5-20 | Recommended Alternate Thermal Panel Design | 5-39 |

TABLES


| Table | | Page |
|---|---|---|
| 2-1 | Effect of Various Treatments on the Wicking Action of 15 Percent Dense Nickel Wicks (1 by 1.125 in. Wick Size) | 2-24 |
| 2-2 | Summary of Nickel Treating Results | 2-27 |
| 2-3 | Effect of Exposure to Air on Wick Rate | 2-34 |
| 2-4 | Results of Tests on Exposure of Wick Specimens to Various Gases | 2-34 |
| 2-5 | Comparison of Intermolecular Forces (Van der Waal's Type Forces) | 2-43 |
| 2-6 | Hydrophilic Groups | 2-43 |
| 2-7 | Compounds Tested for Ability to Render Nickel Surfaces Hydrophilic | 2-44 |
| 2-8 | Effect of Hydrophilic Agents on Wick Rate | 2-45 |
| 2-9 | Comparison of Quantity of Water Retained by Treated and by Untreated Wicks | 2-46 |
| 2-10 | Effect of Hydrophilic Agents on Wick Rate | 2-47 |
| 2-11 | Typical Hydrophilic Groups for Bonding to the Nickel Surface by Primary Chemical Bonds | 2-49 |
| 2-12 | Tests of Chemically Bonded Hydrophilic Groups | 2-50 |
| 2-13 | Chemically Bonded Hydrophilic Treatment Studies | 2-50 |
| 2-14 | Contact Angle of Water on Various Surfaces | 2-59 |
| 2-15 | Porous Plate Characteristics | 2-62 |
| 2-16 | Porous Plate Characteristics | 2-66 |
| 2-17 | Breakthrough Tests | 2-72 |
| 4-1 | Heat Pipe Potential Working Fluids | 4-4 |
| 4-2 | Heat Pipe Test Summary | 4-36 |

TABLES (Continued)


| Table | | Page |
|---|---|---|
| 5-1 | Remote Cooling Loop Test Conditions | 5-17 |
| 5-2 | Panel Thermal Performance Data for Heater Configuration 1 | 5-21 |
| 5-3 | Panel Thermal Performance Data for Heater Configuration 2 | 5-23 |
| 5-4 | Sea Level Thermal Performance Data Using Water and Methanol as Heat Pipe Working Fluids | 5-25 |
| 5-5 | Comparison of Analytical and Experimental $\Delta T$'s | 5-27 |

## NOMENCLATURE

| | |
|---|---|
| $a$ | fin spacing (reciprocal of number of fins per inch) |
| $A$ | area |
| $A_c$ | free flow area |
| $b$ | fin height |
| $B$ | wick friction factor |
| $C$ | experimental wicking content |
| $C_p$ | specific heat |
| $d$ | solvent density in gm/cc |
| $D$ | effective pore diameter |
| $D_h$ | hydraulic diameter |
| $E$ | heat pipe fluid evaluation parameter, Young's Modulus |
| $f$ | friction factor |
| $g$ | acceleration of gravity |
| $g_o$ | gravitational constant $\doteq 32.2\ lb_m\text{-}ft/lb_f\text{-}sec^2$ |
| $G$ | mass flux |
| $h$ | heat transfer coefficient |
| $h_{fg}$ | heat of vaporization |
| $\Delta h'$ | sublimating fluid enthalpy change |
| $H$ | difference in elevation |
| $k$ | thermal conductivity |
| $K$ | Henny's Law Constant |
| $l$ | coolant fluid passage width |
| $l'$ | width over which heat is input |
| $L$ | length |

## NOMENCLATURE (Continued)

| | |
|---|---|
| $N$ | number of fins per inch |
| $P$ | pressure, partial pressure, load |
| $\Delta P$ | pressure drop |
| $Q$ | heat transfer rate |
| $r'$ | effective pore radius |
| $\mathcal{R}$ | universal gas constant |
| $R$ | thermal resistance |
| $t$ | time |
| $T$ | temperature |
| $\Delta T$ | temperature difference |
| $w$ | wick width |
| $W$ | flow rate |
| $W_o$ | coolant flow rate |
| $x$ | distance |
| $X$ | MOL fraction |
| $\alpha$ | Bunsen absorption coefficient |
| $\beta$ | constant in Equation (2-1) |
| $\delta$ | thickness |
| $\eta$ | heat transfer fin effectiveness |
| $\theta$ | contact angle |
| $\mu$ | absolute viscosity |
| $\rho$ | density |
| $\sigma$ | surface tension, stress |
| $\phi$ | wick porosity |
| $\psi$ | angle of inclination |

NOMENCLATURE (Continued)

Subscripts

| | |
|---|---|
| A | alcohol |
| BA | alcohol bubble point |
| BL | liquid breakthrough |
| C | capillary |
| c | condenser |
| evap | evaporation |
| f | fin |
| fm | free molecular |
| HS | heated surface |
| HT | heat transfer |
| in | inlet |
| $\ell$ | liquid |
| m | maximum |
| n | nth section |
| o | overall |
| p | tube plate, facesheet |
| $p_{max}$ | panel maximum |
| s | sublimator |
| out | outlet |
| $O_2$ | oxygen |
| t | total |
| w | water |
| wi | wick |
| X | at location x |

## SECTION I

## INTRODUCTION

In a space vehicle, cooling of electronic packages located remotely to an active thermal conditioning system without resorting to lengthy and elaborate plumbing systems is possible only by providing the units with their own ultimate heat sinks. Since it is not practical to design a unique thermal conditioning unit for each heat producing electronic package, it becomes advantageous to develop an entirely self-contained thermal conditioning panel, capable of being located anywhere in the vehicle, upon which the various heat producing components may be mounted.

The previous heat sink study program performed an analysis of the relative advantages and disadvantages of various self-contained thermal panel concepts. This analysis and comparison was reviewed with the NASA and the two concepts which appeared to have the greatest potential were selected for further consideration. (The principle and mode of operation of each of the two concepts is described in Reference 1.) These two designs, the heat pipe-sublimator and the simple wick boiler were subjected to evaluation, and small scale test sections of each were built and tested.

The objective of the current study was to design, fabricate, and test a completely self-contained full-scale thermal conditioning panel. To achieve this objective, a 4-task program was performed consisting of

Task I — Additional testing of the two thermal panel test modules fabricated during the previous study and small scale testing pertinent to thermal panel development.

Task II — Selection of a thermal panel concept for continued development and eventual full-scale fabrication based upon information from Task I.

Task III — Detailed design and fabrication of the full-size thermal panel concept selected in Task II.

Task IV — Performance testing of the complete thermal panel to verify the operating characteristics.

The thermal panel problem statement developed in discussions with NASA is as follows:

(a) The thermal conditioning panel will be self-contained and not dependent on external power or pumping requirements to distribute evaporant within the panel.

(b) The thermal conditioning panel will include its own water supply and control system.

(c) The panel will be capable of dissipating heat from components mounted on its surface, or normal operation with an independent prime mover for conditioning of electronic packages with internal cooling shrouds.

(d) The panel will allow evaporant water to vent inboard to the spacecraft without the discharge of liquid water or ice.

(e) The overall panel size will be restricted to the 30 in. by 30 in. configuration used on the instrument unit cold plates. Although 10 watts cooling capacity per mounting boss must be maintained, the 420-watt maximum total heat load called out in the existing cold plate specification is not a rigid requirement. The heat transfer surface on the 30 in. by 30 in. thermal panel will therefore be reduced in order to provide area for the storage of water and the installation of control valves.

(f) The structural integrity of the thermal panel will be sufficient to withstand the environment of the Saturn instrument unit.

(g) The expendable water storage capacity shall be sized to handle 11.5 lb of water. This amount of water will provide 8 hr of cooling for a maximum heat load of 1450 Btu/hr, or 60 hr of cooling for a 50-watt heat load.

(h) Design and testing of the thermal panel to be fabricated should be oriented such that NASA and AiResearch are confident that a duplicate panel could pass those qualification tests required for its use on a Saturn mission.

(i) It may be necessary to operate the thermal conditioning panel in a preflight mode where low pressures would not be available for steam generation and cooling of mounted equipment. This type of panel operation would require that preflight cooling be obtained via ground support cooling equipment with quick disconnect fittings used to provide coolant flow directly to the panel and removed just prior to launch. This cooling flow would be supplied at approximately 60°F.

(j) Panel design should be such that the unit can be connected to the existing instrument unit cooling loop and operate using sublimator cooling for as long as its water supply lasts. Once the subliminator water supply has been expended, the panel mode of operation can be switched to its own water supply by means of a shutoff valve sensing a rise in the water-methanol loop temperature which normally runs below 60°F. Although design of this valve is not within the scope of the current contract, the panel design should make possible the type of operation described.

(k) In the selection of materials to be used for thermal panel fabrication, AiResearch will pay particular attention to the long term corrosion rates and material capability with those fluids that are exposed.

(l) The proposed panel concepts will be fabricated from stainless steel using nickel wicking material.

(m) The problem of thrust generated by steam flow during panel operation is of concern to NASA for particular panel applications. Resolution of this problem will ultimately be carried out by NASA; however, AiResearch will make a cursory examination of the problem to determine if thrust can be distributed by proper manifolding.

## SECTION 2

## TASK I--THERMAL PANEL MODULE AND RELATED SMALL SCALE TESTS

### INTRODUCTION

The first task of the panel development program involved testing of the two thermal conditioning panel test modules to evaluate their performance characteristics as well as additional small scale tests to obtain information pertinent to thermal panel development. These tests, their results, and the manner in which they apply to the thermal panel design are discussed below.

### SIMPLE WICK BOILER TEST MODULE

#### Description of Module and Test Apparatus

The 10 by 12 in. simple wick boiler test module is shown in Figure 2-1. This section represented approximately one quarter of a full-size thermal panel and empoyed a 0.060 in. thick, 20 percent dense, nickel fiber/metal wick on the evaporating surface. The supply wick, located on the opposite face, was 0.125-in. thick nickel felt metal and fed the evaporative wick through cellulose sponge packed on three sides of the test section. The fourth side of the test section was a lucite cover plate which allowed visual evaluation of fill procedures and examination of the wicks during operation of the unit. Electrical heaters were mounted on the surface adjacent to the thinner wick, and the unit was instrumented with 14 thermocouples and 2 pressure probes as shown in Figure 2-2. Temperature control of the panel test section was accomplished by manual adjustment of a back pressure valve, using panel temperature and steam plenum pressure to determine the correct valve setting.

The simple wick boiler test apparatus is shown in Figure 2-3. The test module was installed in a vacuum bell jar to permit adjustment of the saturation temperature to any level. The panel temperature was controlled during the testing by manual adjustment of the bell jar pressure. Separate switches were provided for each heater so that any combination of heaters could be tested, and the power could be set at any level with the variable power supply. Panel temperatures were recorded on a direct reading Honeywell-Brown potentiometer.

#### Predicted Performance

It was originally planned to perform tests to determine the limiting heat flux, the transient temperature response to step heat load changes, and the startup characteristics of the simple wick boiler. However, since it became evident during the initial testing that the wick contamination problem can be quite serious with this particular design, the decision was made to limit the amount of testing on this module. The contamination problem influenced this decision in two ways. First, the fact that this configuration contaminated easily was a point in favor of selecting the heat pipe as the concept to be

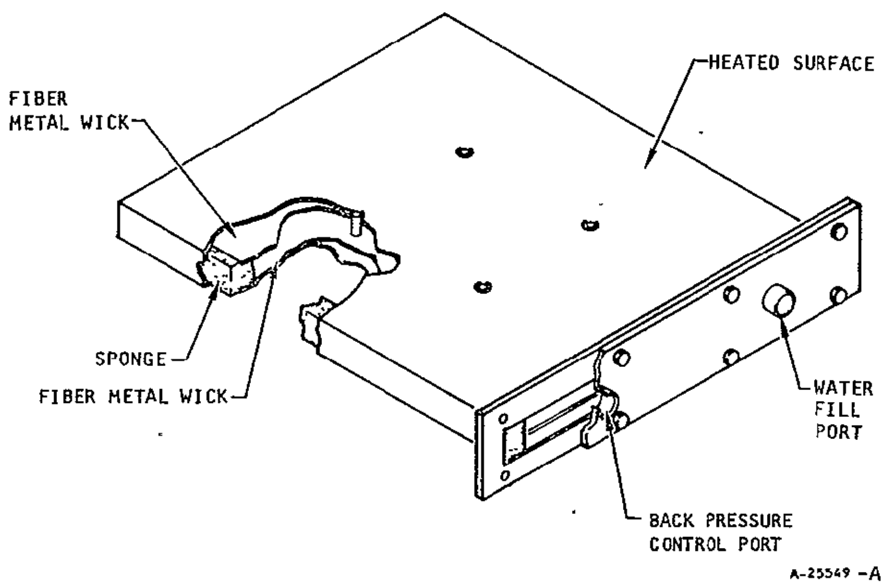


Figure 2-1. Simple Wick Boiler Thermal Panel Test Section

NOT REPRODUCIBLE

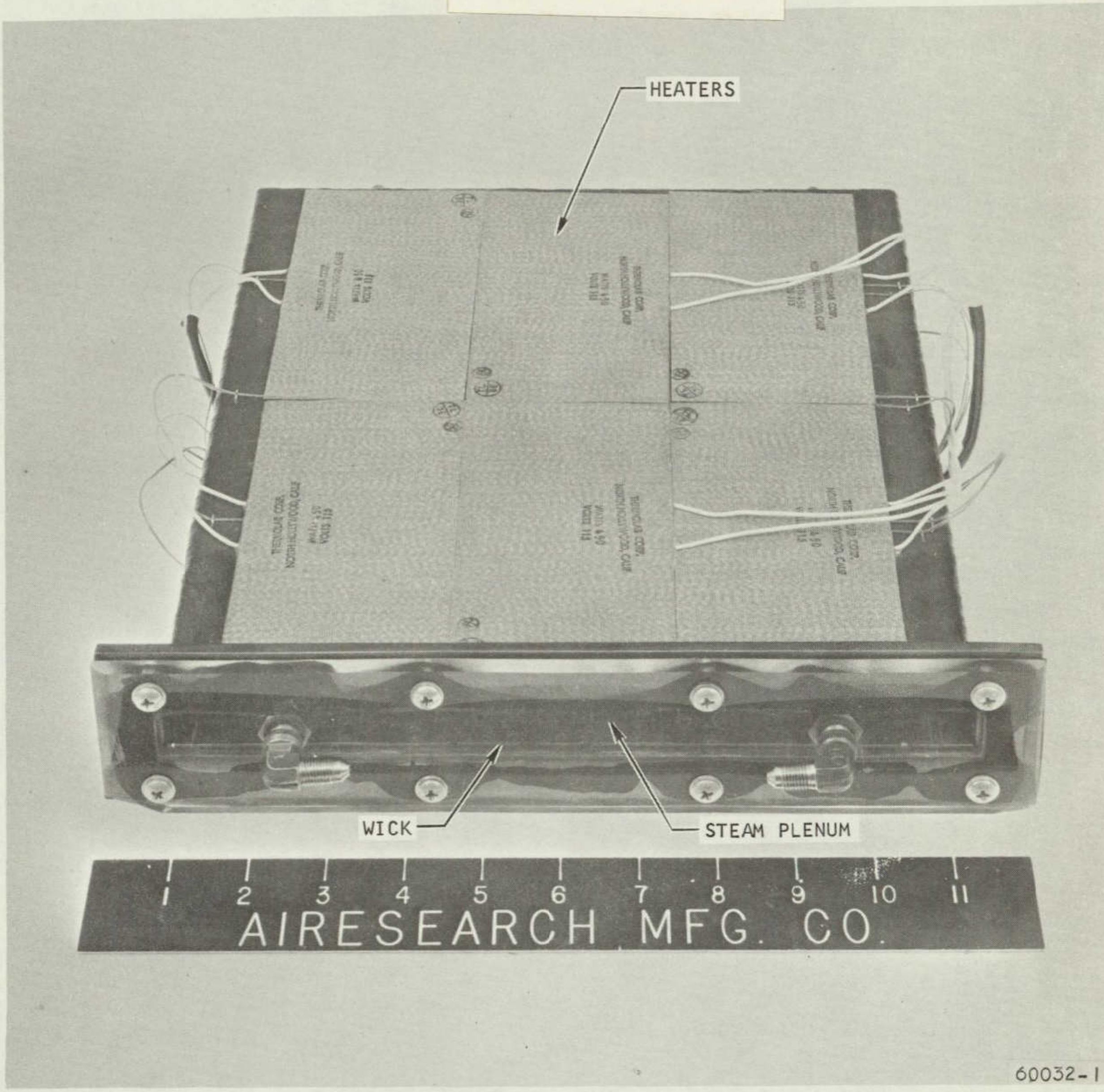


Figure 2-2. Instrumented Simple Wick Boiler Thermal Test Module

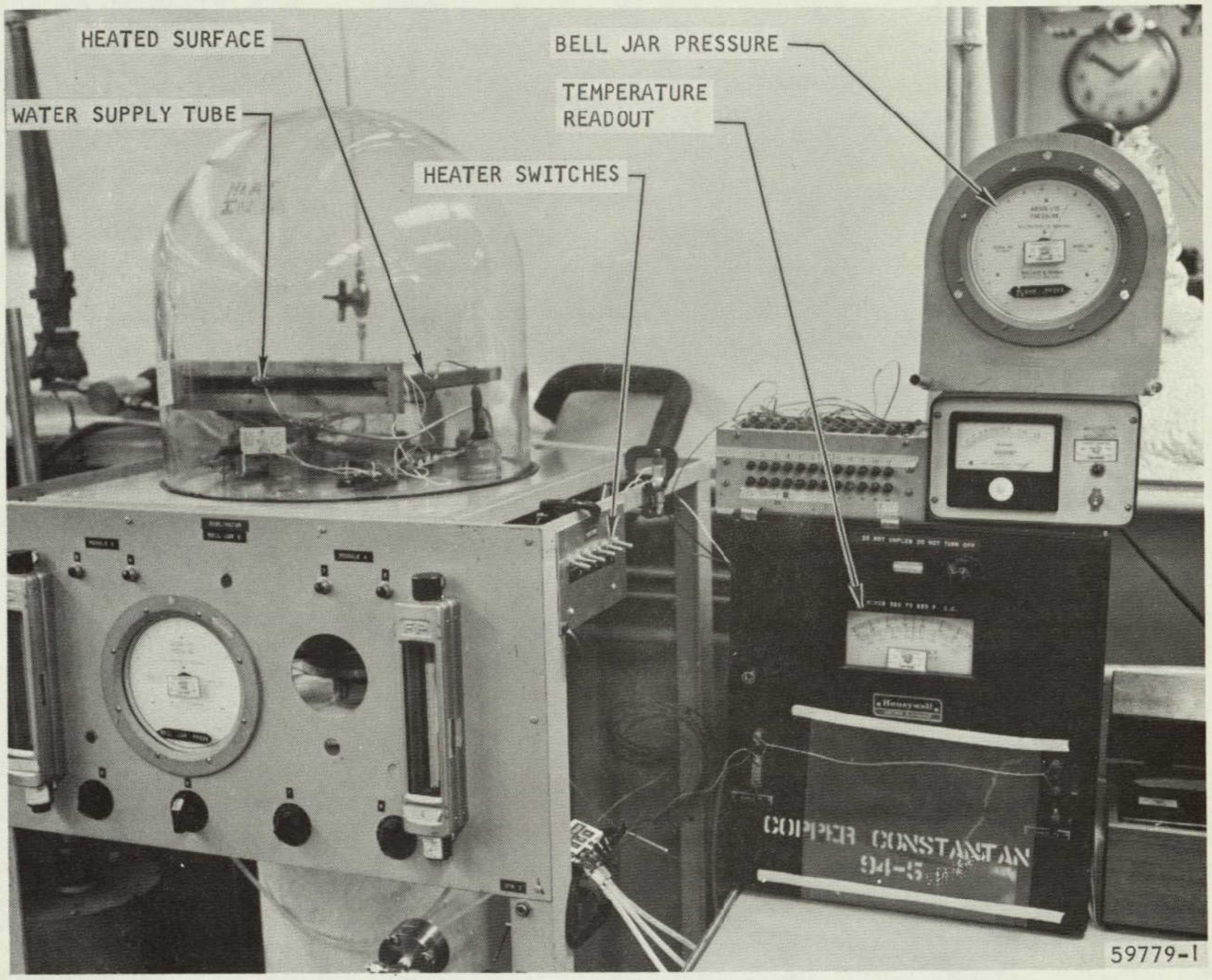


F-12545

Figure 2-3. Simple Wick Boiler Test Apparatus developed for the full size panel; if initial indications proved to be correct, the test time would be more wisely used for the heat pipe module. Second, the validity of the data obtained with a contaminated module would be open to serious question. For these reasons, the only test performed on the simple wick boiler was a portion of the limiting heat flux test.

As the heat load is gradually increased on a simple wick boiler, a condition will be reached at which the capillary forces in the wick are not adequate to deliver sufficient liquid to the areas of heat input. Sufficient water to meet the heat load is available in the unit for this condition; however, it cannot be transported to the area of high heat flux fast enough to keep this area from drying out. The basic analytical equation which defines this phenomenon is developed in Reference 2. In a slightly modified form, this equation is

$$Q_t = \frac{2\rho_\ell g_o h_{fg} A_c}{L \beta B \mu_\ell}\left[P_c - \frac{\rho_\ell g}{g_o} L \sin\psi\right] \tag{2-1}$$

where $Q_t$ = total heat transfer rate

$\rho_\ell$ = liquid density

$g_o$ = gravitational constant = 32.2 $lb_m$-ft/$lb_f$-$sec^2$

$h_{fg}$ = latent heat of vaporization

$A_c$ = wick free flow area

$P_c$ = experimentally determined capillary pressure

$g$ = acceleration of gravity

$L$ = total liquid delivery length

$\psi$ = angle of inclination from horizontal

$B$ = experimentally determined wick friction factor

$\mu_\ell$ = liquid dynamic viscosity

$$\beta = \frac{L_1}{L_n}\left(\frac{Q_1 + Q_2}{Q_T}\right) + \ldots + \frac{L_{n-1}}{L_n}\left(\frac{Q_{n-1} + Q_n}{Q_T}\right) + \frac{Q_n}{Q_t}$$

$L_1, L_2, \ldots L_{n-1}$ = lengths along wick at which heat flux changes

Ln = total wicking length

$Q_1, Q_2, \ldots Q_{n-1}, Q_n$ = local heat transfer rates along wick

$Q_T$ = total heat transfer rate

For the case of horizontal operation, the second term in brackets becomes zero because sin 0 deg = 0. $P_c$ and B have been determined experimentally for wicks of the type used in the simple wick boiler and are given as a function of the wick density in Reference 2. Equation (2-1) was solved for the maximum heat load due to liquid delivery limitations for the test condition in which only the two central heaters of the module were active. Dividing by the active heat transfer area, a theoretical maximum heat flux of 35,000 Btu/hr-ft$^2$ was predicted.

Early in the program it was postulated that the onset of nucleation in the wick would cause a severe degradation in performance and would be another limit on the applied heat flux. The normal mechanism by which heat is dissipated in the simple wick boiler is conduction across the wick water matrix and evaporation at the exposed wick surface. If nucleation occurs in the wick, it will likely occur at the wick-wall interface, the hottest location. It was thought that the vapor formed at the wall would remain there and form an insulating blanket decreasing the heat transfer capability significantly. Data published after the design of the IU Thermal Panel (Reference 2) has shown that upon nucleation, the performance does not degrade and that the vapor is not trapped at the wall. For this reason the onset of nucleation is not a design limitation.

Testing and Test Results

After a checkout of the test instrumentation and the test stand controls, an initial performance test run was made in order to obtain a comparison with previous test data. Using the electrical heaters bonded to the panel surface, a uniform heat flux of 1000 Btu hr-ft$^2$ was applied over the entire upper surface of the module. The bell jar pressure was adjusted to maintain a maximum panel temperature of 80$^\circ$F.

On startup it was discovered that the heated-surface-to-steam-plenum temperature difference was 4$^\circ$ to 5$^\circ$F greater than that previously recorded for the same test conditions. Steady state operation was maintained for 50 min, at which time local hot spots were observed. Results obtained during previous testing had yielded a heater-to-saturation $\Delta T$ of 2$^\circ$F compared to 7$^\circ$F obtained with these tests. Visual observation of the heated wick surface during the test run revealed localized areas of the wick that appeared lighter in color than the surrounding portions. These light sections indicate local dry spots in the wick that could be attributed to partial contamination of the wick in these areas. Also, on refilling the unit, water droplets formed on the wicks in those areas where dry spots had been detected. (The water contact angle on a clean wick is such that droplets of water cannot be formed on the wick surface.) This reluctance to absorb water, coupled with the high heater-to-saturation $\Delta T$ established that the unit was at least partially contaminated.

Work in the area of wick contaminants and wetting agents had shown that a partially contaminated wick could be recovered by a warm water soak with oxygen bubbling through the wicks. The unit with heaters and thermocouples attached was submerged in a tank of filtered and distilled water maintained at 190°F. Oxygen was then continuously bubbled through the unit for a 24-hr period. Following the soak, the unit was dried and tested with a hypodermic syringe for evidence of contamination. Although small areas of the wick appeared "slow wetting", the simple wick boiler module was placed back on test to establish its performance. The heater-to-saturation $\Delta T$ was slightly improved, but was still unsatisfactory. After removing the test instrumentation, the unit was cycled at 1000°F in a vacuum furnace in an attempt to clean the wicks.

After cleaning and reinstrumenting, the simple wick boiler was installed in the test stand for maximum heat flux determination testing. These tests were conducted to determine whether a degradation in performance due to heat flux limit was possible for the panel over the proposed range of operating conditions. The maximum heat flux determination testing was performed using only the two central heaters of the simple wick boiler test module. A heat flux of 1000 Btu/hr-ft$^2$ applied with these two heaters was used as a start point for these tests. The applied voltage was increased incrementally in order to determine the heat flux at which the unit could not deliver sufficient water. The heat flux was increased to about 4200 Btu/hr-ft$^2$-°F. Above this heat flux it was impossible to establish steady state conditions because of the limited volume of water that could be stored in the unit, and the test was concluded. While a liquid delivery heat flux was not reached in the test, a heat flux of almost four times that which was to be encountered in the thermal panel was established.

The heater-to-saturation $\Delta T$ remained at about 2.5 times that expected for all heat flux levels in spite of the fact that the wicks had been cleaned. It is unlikely that the unit was still contaminated after the 1000°F furnace cycle, since this method is standard procedure for cleaning wicks and making them wettable. A more likely explanation is one which was not known until similar results were obtained in a later study of heat transfer in wicks as reported in Reference 2. In that study, initial results of test modules of the same basic geometry as the simple wick boiler (heater-plate-water filled wick) yielded $\Delta T$'s as much as 1.7 times that predicted. It was found that when these modules, which had been filled with distilled filtered water at atmospheric pressure, were subjected to the low pressure required to give a 60°F saturation temperature upon evaporation, gas which was dissolved in the water at atmospheric pressure came out of solution.

The low pressure resulted in a low gas density so that only a very small amount of gas was required to displace a large percentage of the water from the wick. Since a large portion of the wick was full of gas instead of water, the effective thermal conductivity of the wick-water matrix was decreased and a larger $\Delta T$ resulted. Subsequent tests using degassed water yielded results which agreed closely with predictions.

It is possible that this phenomenon occurred in the simple wick boiler test module, causing the higher than expected $\Delta T$.

## Conclusions

The following conclusions were made based upon the analysis and testing of the simple wick boiler:

(a) Contamination of the wicks in the simple wick boiler and the subsequent degradation in performance was a serious problem. A method to prevent such contamination must be developed before this concept can be used.

(2) The simple wick boiler was capable of handling the maximum heat flux for which the thermal panel is to be designed.

## HEAT PIPE THERMAL PANEL TEST MODULE

### Description of Module and Test Apparatus

The heat pipe thermal panel test section is shown in Figures 2-4 and 2-5. The unit represented 1/6 of a full-size thermal panel and was 30 by 5 in. The 30-in. length was incorporated to examine the effect of the longest thermal panel dimension on the heat pipe operation. The heat pipe used a 0.060-in. thick nickel feltmetal wick in the condensing section and a 0.250-in. thick wick in the evaporating section to provide maximum pumping capability. The steam passage incorporated a 0.250-in.-high copper fin to obtain maximum conductance with minimum steam pressure drop losses. Electrical heaters were bonded to the surface of the panel for heat input, and thermocouples were attached to the panel surface for temperature measurement. The heat sink for the condensing water vapor was a single passage liquid heat exchanger located in the position that would be normally occupied by the sublimator on a full-size thermal panel.

The heat pipe panel was slightly modified from the original design by the addition of a plexiglass cover plate and was designed to eliminate void areas above the evaporator wick which had filled with water during previous module testing. In addition, the cover plate was modified to use a Veeco valve for better control of the system pressure level. The heat pipe was also provided with a vent port in the condenser area that can be used to bleed off non-condensable gases which were accumulated during startup.

A schematic of the test setup and instrumentation is shown in Figure 2-6 and the module installed in the test apparatus is shown in Figure 2-7. All testing was performed in a vacuum chamber. Power was supplied to the unit from a 115-v variac, and individual switches permitted use of any combination of heaters. Temperatures were read on a Honeywell-Brown Potentiometer. The temperature and flow rate of the coolant water were monitored and controlled from the coolant control panel.

### Testing and Test Results

Prior to the start of performance testing, the heat pipe was filled with 1.33 lb of 1/2-micron filtered, distilled and degassed water. The unit was then operated with all heaters switched on at a uniform heat flux of 1000 Btu/hr-ft$^2$ for a period of 1-1/2 hr. This initial run was made to cycle the water in the heat pipe from the liquid to vapor state in order to release any noncondensable gases that may remain entrapped in the working fluid. The presence of noncondensable gases was evidenced by panel temperatures in the condenser area that were 30 to 40 deg lower than the surface temperatures recorded for the remainder of the unit. After 1-1/2 hr, the noncondensable gas in the condenser area was bled off through the vent port provided for this purpose. Immediately following the gas removal, the panel temperature in the condenser area increased while the temperatures over the remainder of the panel decreased. However, continued operation at the 1000-Btu/hr-ft$^2$ heat flux produced a gradual decline in the temperatures recorded opposite the condenser. It was felt that

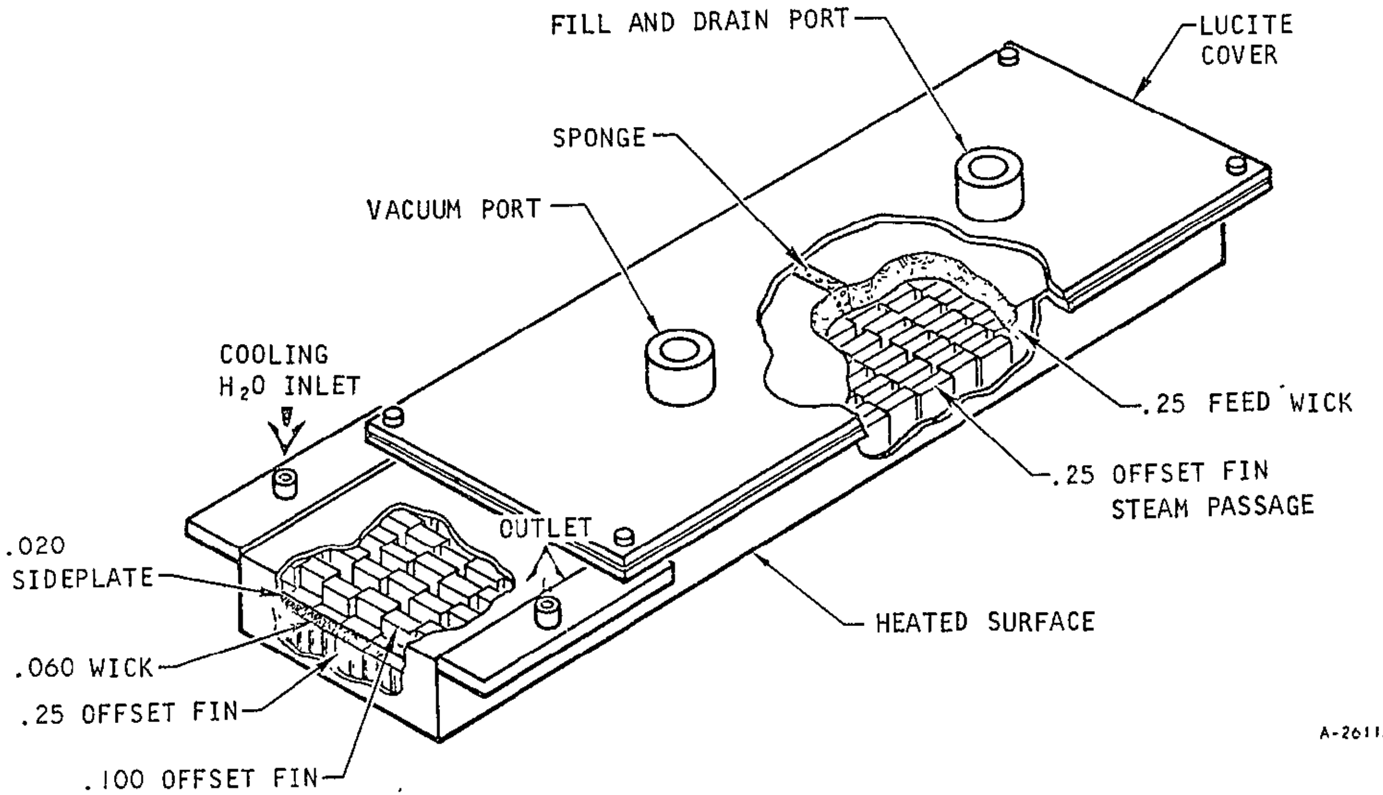


Figure 2-4. Heat Pipe Thermal Panel Test Section

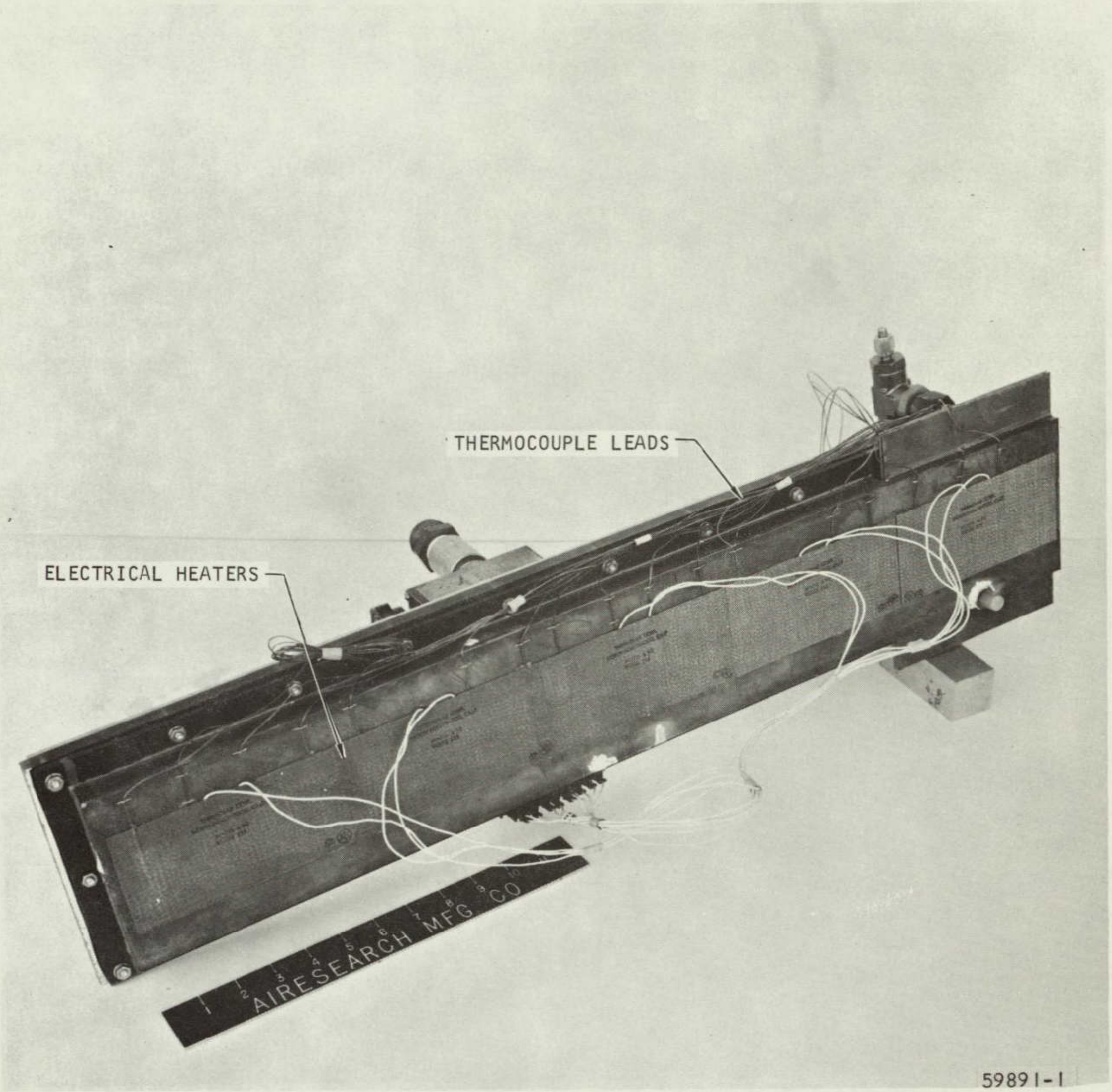


F-8103

Figure 2-5. Instrumented Heat Pipe Thermal Panel Test Module

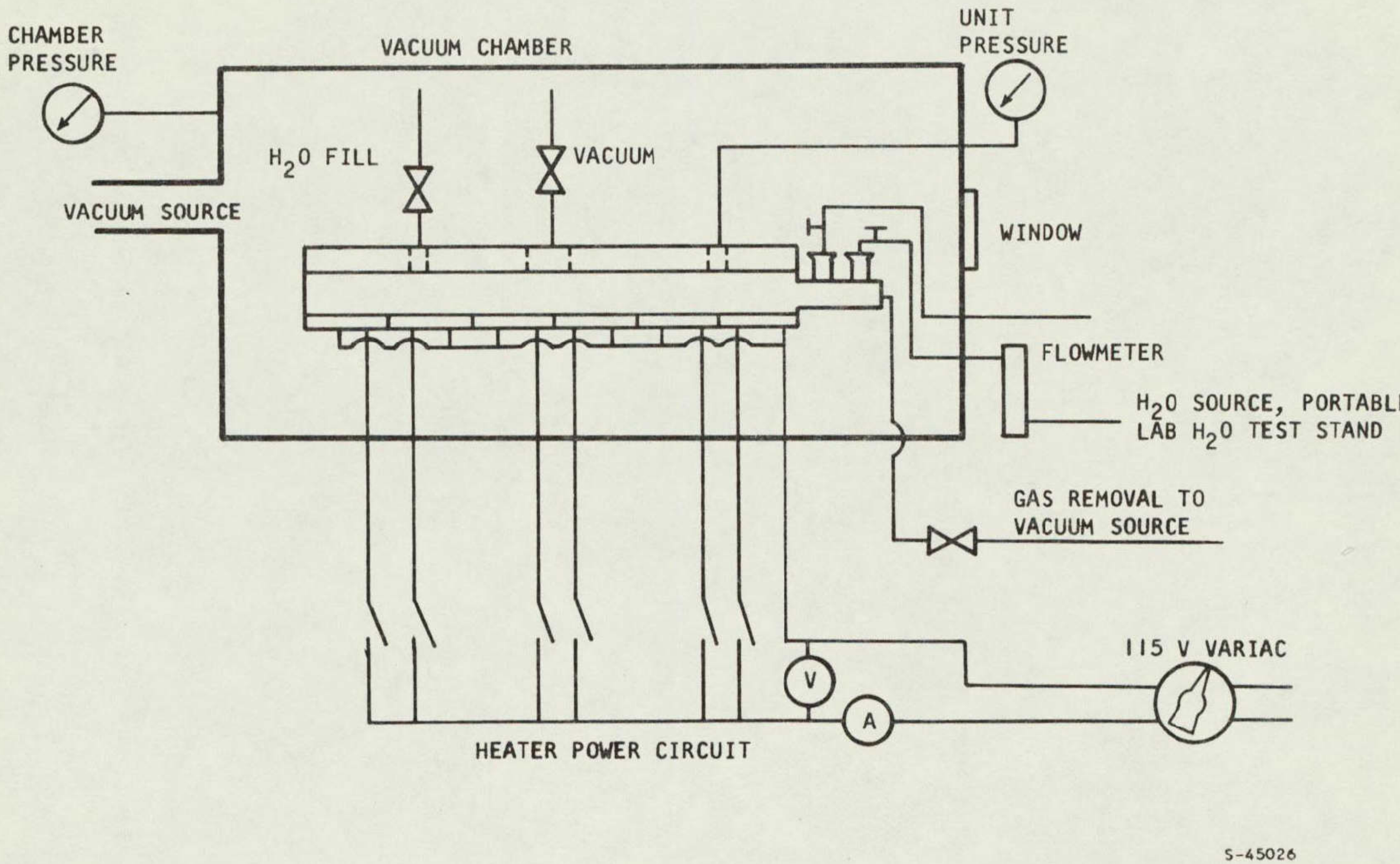


Figure 2-6. Heat Pipe Sublimator Test Schematic

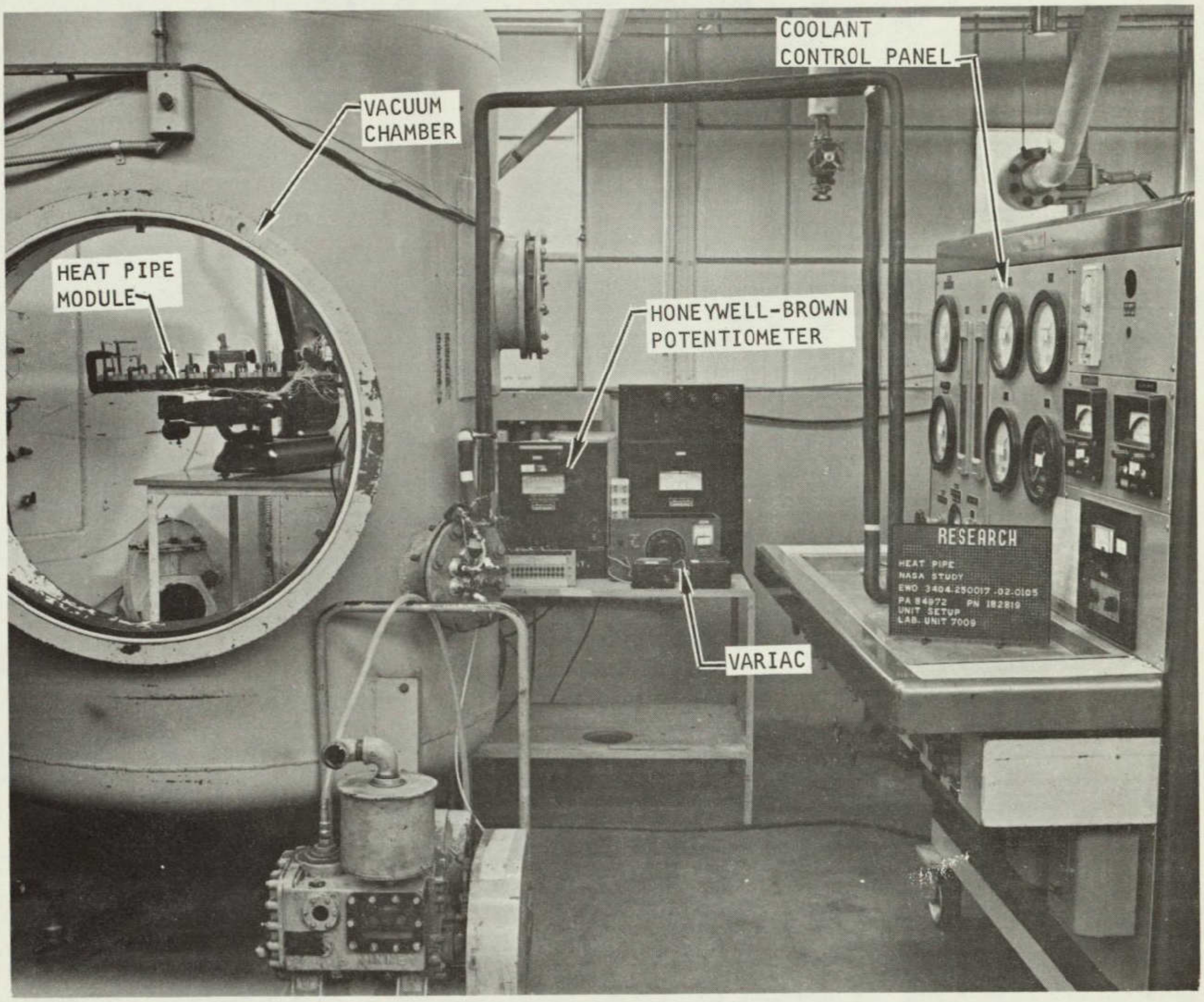


F-9745

Figure 2-7. Heat Pipe Sublimator Test Apparatus additional gas was being released to the heat pipe system for the wicks (which has been oxygenated to preserve their cleanliness). The heat pipe was cycled, bleeding off noncondensable gas at 8-hr intervals for a 48-hr period. At the end of 48 hr, the unit performance had been somewhat improved, but larger $\Delta T$'s than were observed during previous heat pipe tests were recorded over the 30-in. panel length. The unit was disassembled, the test instrumentation was checked out, and the evaporator wicks were tested for cleanliness. Water drops placed on the dry wick were immediately absorbed into the wick, indicating that the wick was clean. The unit water supply was replenished, and the cycling as described above continued. After approximately 100 hr of continuous operation, during which time noncondensable gas was vented intermittently, steady state performance of the heat pipe was achieved.

A comparison of the heat pipe temperature differential with previously obtained test data showed a fairly good correlation. Figure 2-8 shows both the results obtained when the heat pipe was first tested during the previous program and the results of current testing. Also shown was an entirely analytical prediction of the performance (the broken line) and a prediction of the current data based upon a semiemperical correlation of the data obtained previously (solid line). The predictions, as well as the data, change slope between the two sets of data because the heaters used in the latter testing covered the entire width of the panel while those used initially covered only 3 in. of the 5 in. width. This results in a 67 percent higher heat load in the latter testing for the same heat flux conditions.

## I. Frozen Startup Testing

A series of tests was conducted to explore the startup performance of a frozen heat pipe thermal panel. These tests simulate a condition wherein the heat pipe has been inoperative for an extended period in an environment which allows the entire heat pipe to soak below 32°F. Under these circumstances, water, the heat pipe working fluid, becomes frozen in the wicks. Startup from this frozen condition affords the possibility that the evaporating water will refreeze as it condenses on the ice filled portion of the wick, preventing resupply of the water to the areas where evaporation is taking place. The conditions for a frozen startup are most severe when high heat fluxes are applied locally to the unit. It has been reported by Deverall et al (Reference 3) and by L. G. Neal (Reference 4) that under this type of circumstances heat pipe restart was not possible, or at best produced operating temperature differentials which were unacceptable. The local starvation of the heat pipe due to solidified working fluid in nonheated areas is characterized by recorded temperature rises and hot spots not seen during steady-state operation. For the proposed heat pipe sublimator panel design, this type of failure would occur when a panel temperature greater than 90°F was reached while the panel temperature in the area of the condenser remained below the temperature at which water is supplied to the sublimator, about 65°F. That is, when the maximum heat pipe $\Delta T$ exceeded 25°F.

Due to the large size of the heat pipe test module and the amount of instrumentation needed to conduct a performance test, it was not possible to refrigerate the entire module in a conventional manner. Freeze up of the test

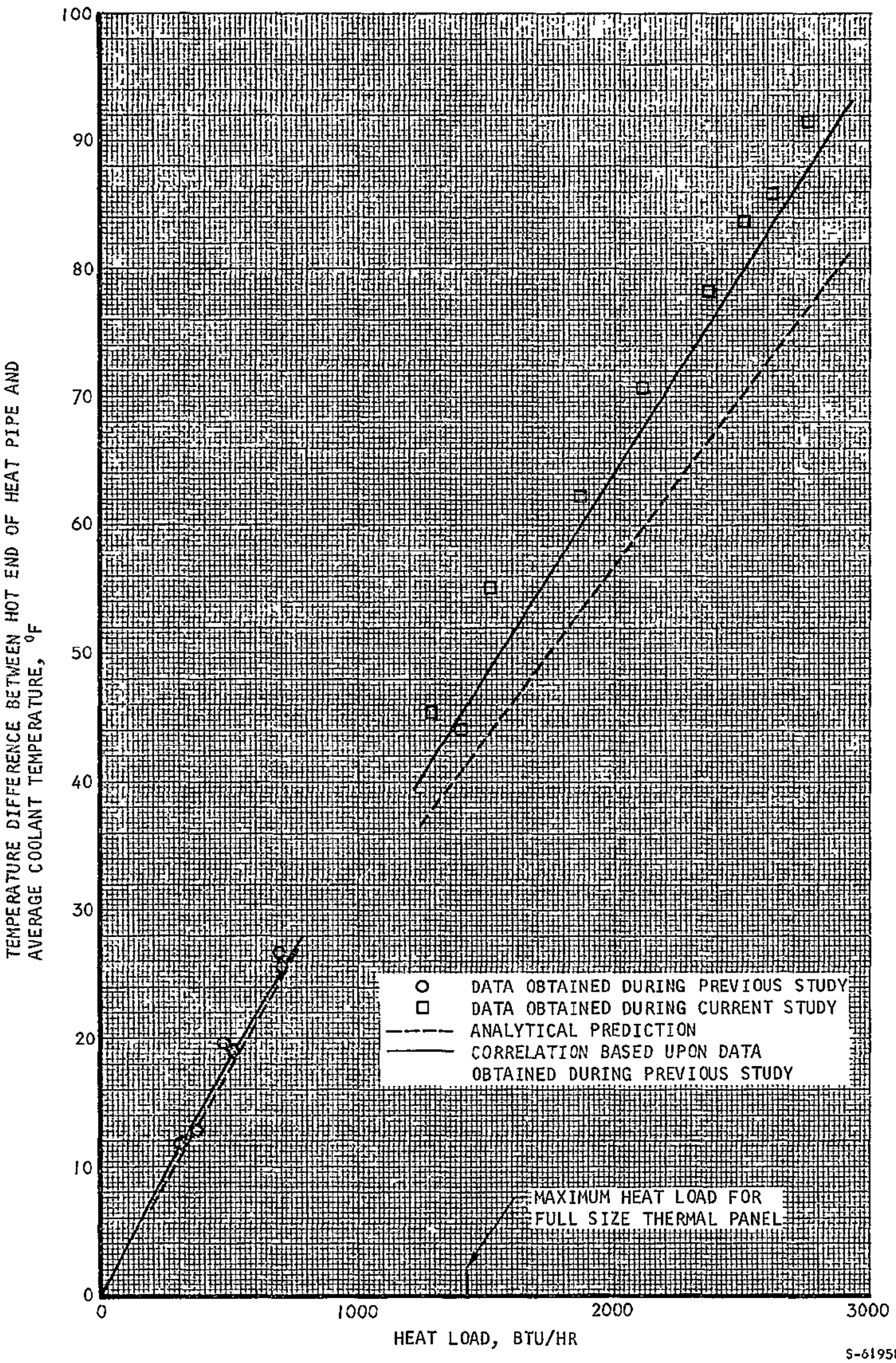


Figure 2-8. Heat Pipe Test Module Performance

module was accomplished by adding an additional two-tenths of a pound of water to the heat pipe and reducing the pressure inside the panel to a value below the triple point. (Two-tenths of a pound corresponds to the amount of water which when evaporated would absorb the latent heat of fusion of 1.33 lb of the working fluid.) A portable vacuum source located outside the test chamber was used for the freeze-up operation. One-half hour was allowed to freeze all the water in the unit at which time the panel temperatures were all below 32°F. The heat pipe was completely sealed and a single electrical heater covering an area 5 by 5 in. was switched on at the surface of the panel furthest from the condenser section. The applied heat flux for this single heater was 1000 Btu/hr-ft$^2$. The panel temperatures over the entire length of the unit were recorded at 2-min intervals. No coolant was supplied to the condenser heat exchanger during these tests. The absence of a heat sink simulates the mode of operation that will exist in a full-size panel where evaporant is not supplied to the sublimator below 65°F. During the tests the panel temperatures were allowed to rise to 130°F before the heaters were switched off. Figure 2-9 shows the surface temperature along the panel at various elapsed test times. Time zero corresponds to the instant at which the heater was turned on.

The tests conducted represented the worst case for startup of the heat pipe-sublimator thermal panel. That is, with a maximum heat flux applied in a small area of the 30-in. length, the possibility of wick starvation due to refreezing of the evaporated water is the greatest.

At the instant before heat is applied, all the panel temperatures were below 31°F. Two min after heat was applied, the area under the heater had thawed and the local temperature had risen to a maximum of 40°F while most of the panel remained below 32°F. Gradually, the ice in the wick melted at sucessive locations along the panel while the area under the heater continued to increase in temperature. The unheated area which was not frozen was fairly uniform in temperature and remained about 8°F cooler than the hottest location under the heater. When all the ice had melted and the coldest panel location had reached 65°F (the approximate temperature which would actuate the valve to supply water to the sublimator and initiate cooling in the full-size heat pipe-sublimator thermal panel), the hottest location was about 16°F hotter at 81°F. This is well below the maximum allowable surface temperature of 90°F. When the area under the heater reached 90°F, the coldest location was 79°F, sufficiently above the valve actuation temperature to assure that cooling would have been initiated in the full-size thermal panel.

This test demonstrated the ability of the heat pipe to start from a frozen condition.

2. Maximum Heat Flux Testing

The heat pipe literature cites four phenomena which limit the heat transfer capability of a heat pipe. These are (a) a liquid supply limit in which the capillary forces in the wick structures are not sufficient to resupply working fluid to the areas in which evaporation is occurring, (2) a burnout limit in which nucleation occurs inside the wick and vapor is generated at such a rate that it blankets the hot surface, preventing liquid from reaching the hot wall,

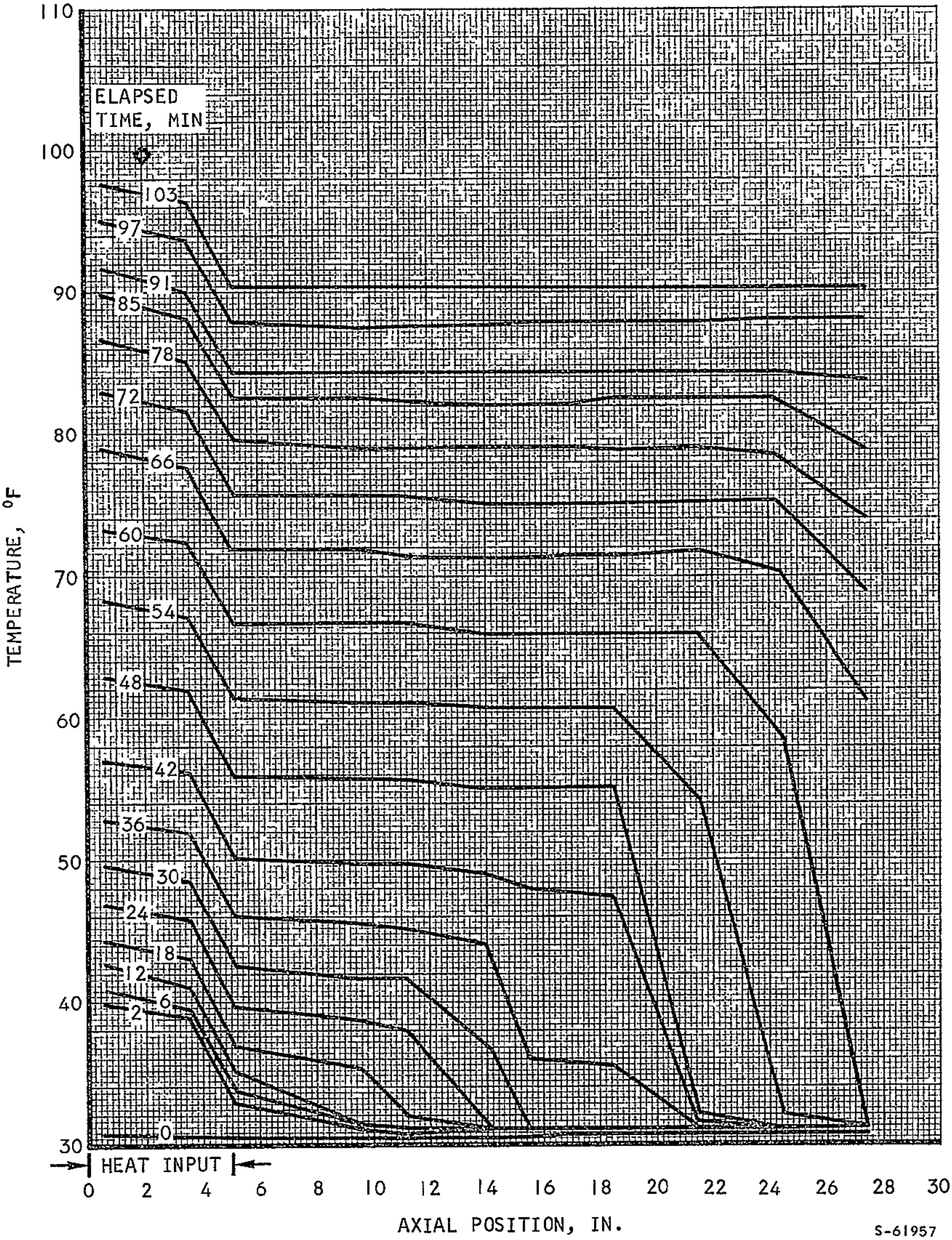


Figure 2-9. Frozen Startup of Heat Pipe Test Module

(3) a sonic limit which restricts the vapor flow as Mach 1 is approached, and (4) an entrainment limit in which liquid wicking toward the evaporator is entrained in the vapor flow and cannot reach the evaporator section. At the heat loads encountered in the heat pipe thermal panel test module, the vapor velocities are small enough so that no possibility of approaching either the sonic limit or the entrainment limit exists. The design of the module with a copper fin between the heated surface and the wick is such that the burnout limit does exist as it does in conventional heat pipes where the wick is against the heated surface. There does exist, however, a liquid supply limit for the heat pipe thermal panel, and this limit occurs at a heat flux of the order of magnitude that is encountered in the current application.

Dividing Equation (2-1) by the area over which heat is applied, the following equation is obtained for the case of a uniform heat flux along the panel:

$$\frac{Q}{A} = \frac{2\rho_\ell g_o h_{fg} A_c}{B\mu_\ell L^2 W} \left[ P_c - \rho_\ell \frac{g}{g_o} L \sin\psi \right] \qquad (2\text{-}2)$$

where $\frac{Q}{A}$ = limiting heat flux

$W$ = width of wick

Sin $\psi$ may be expressed as H/L where H is the difference in elevation between the two ends of the heat pipe. Analytical predictions of the limiting heat flux for the thermal panel module are tabulated below as a function of H.

| H, in. | Q/A, Btu/hr-ft$^2$ |
|---|---|
| 0 | 4090 |
| 0.31 | 3950 |
| 1 | 3650 |
| 3 | 2760 |
| 6 | 1430 |

The limiting heat flux was determined experimentally. The unit was tested in the vacuum chamber with the evaporator end 0.31 in. higher than the condenser section. Starting with a heat flux over the entire surface of 1360 Btu/hr-ft$^2$, the heat flux was increased in increments of approximately 280 Btu/hr-ft$^2$ and panel temperatures recorded at each increment. Several readings were taken at each heat flux to ensure that steady-state operation had been achieved. The data obtained in these tests is shown in Figure 2-10 where the panel temperature furthest from the condenser was plotted as a function of the applied heat flux. The data is given in this form since the area furthest from the condenser will show the water supply limit first. All temperatures up to a heat flux of

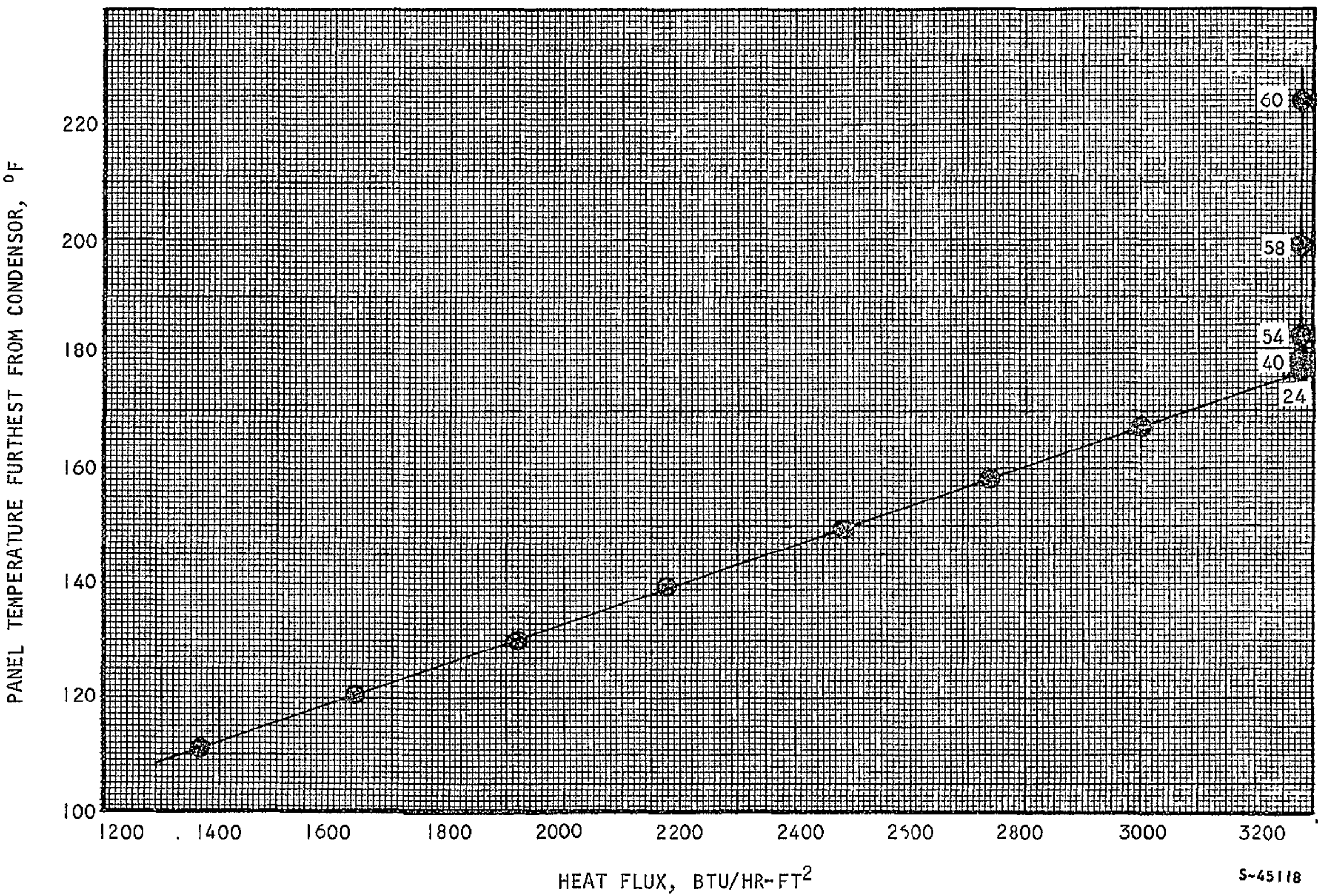


Figure 2-10. Liquid Resupply Limiting Heat Flux

3000 Btu/hr-ft$^2$ were steady-state temperatures taken anywhere from 31 to 108 min after the indicated heat flux was imposed. The temperatures shown at a heat flux of 3280 Btu/hr-ft$^2$ were not steady-state temperatures, but were recorded after imposing the heat flux at the time intervals that are indicated in minutes next to the data points. This data indicates a liquid supply heat flux limit between 3000 and 3280 Btu/hr-ft$^2$, about 80 percent of the analytically predicted value.

The 20 percent discrepancy may be due to uncertainties in the wick properties B and $P_c$ which exhibit a 20 to 25 percent data scatter. It is recommended therefore that the predictions of Equation (2-2) be reduced by 20 percent for use in establishing the maximum heat flux.

## Conclusions

Based upon the analysis and testing of the heat pipe-sublimator test module, the following conclusions were made:

(a) Startup from the condition in which the heat pipe working fluid is frozen is possible with the present configuration without exceeding the maximum allowable surface temperature.

(b) Analytical predictions of the maximum heat flux capability are higher than the experimental data and should be reduced by about 20 percent for design purposes.

WICKING PRESERVATION STUDY

## Introduction

The purpose of the wicking preservation study was to attempt to develop coatings for nickel wicks which enable these materials to transport water more rapidly and more reliably. To attain this objective, the approach taken was to first attempt to determine the factors which control wick water transport and to identify the contaminants and conditions which reduce the ability of a wick to transport water. In this latter area, recourse was made to test data previously obtained at AiResearch and to the literature, particularly that concerned with surface behavior. Numerous special tests and studies were made as reported herein.

While this study was being performed, a concurrent Apollo program at AiResearch was being conducted in the specific area of wicking preservation by the use of warm water and oxygen. That program was quite extensive, and included the effects of water temperature, oxygen bubbling rates, and exposure time. It was decided at the outset not to investigate the approach taken on the Apollo program to avoid duplicate effort. Moreover, since the success of that approach in preserving the wicking rate was not yet established, the pursuit of other methods (in this study) was justified.

## Past Experience

The ability of wicks to tranport water is a function of their surface properties. It is usually stated that wicks must possess hydrophilic surfaces in order to wick properly. The fluid transport rate in a wick is given by Equation (2-3):

$$\frac{dx}{dt} = \frac{Crg_o\sigma \cos \theta}{4\mu x} \qquad (2\text{-}3)$$

where
- $x$ = axial length in wicking direction
- $C$ = experimentally determined constant
- $r$ = wick capillary radius
- $\sigma$ = surface tension of wicking fluid
- $\theta$ = contact angle between fluid and wick surface
- $t$ = time

Examination of this equation indicates that surfaces which exhibit low contact angles with water are desirable for high wick rates. Such surfaces are generally termed "hydrophilic."

The possibility of introducing coatings onto the surfaces of wick fibers to render them more hydrophilic is attractive for increasing water transport rates. Another important consideration in the use of wicks is the permanence of wicking action. Many surfaces are readily contaminated by trace amounts of a variety of materials resulting in loss of wicking action. It is desirable that surface coatings be developed which resist the tendency of wicks to adsorb contaminants from the atmosphere.

Past studies of nickel wicks at AiResearch have indicated that contamination is a very serious problem in causing loss of wicking action. Tests of 15 percent dense nickel wicks which have been intially cleaned by heating in a vacuum ($5 \times 10^{-5}$ mm Hg) at 1000°F for 1 hr) show that exposure to relatively clean laboratory air causes serious loss of the ability of the wicks to transport water. It has also been found that the treatment of wicks with oxygen-saturated water to form nickel hydroxide on the surface is effective in combatting wick rate degradation. Additionally, treatment of the oxygen-saturated water-treated wicks with hydrogen gas for 1 hr (1000°F, 1 atmosphere pressure) was found to yield wicks of high wicking rate. This treatment was originally applied to remove white spots (identified as nickel hydroxide by X-ray diffraction) which form on the surface of the wick during the oxygenated water treatment. Photographs of these samples are shown in Figure 2-11 where sample A is the vacuum heated wick, sample B is the oxygen-saturated water treated wick and sample C is the hydrogen treated wick. Data from these tests are summarized in Table 2-1. The percentage shown after the wicking time in Table 2-1 is the percentage of the wick surface that appeared "wet" and the fraction shown is the fraction of the total wick height to which water advanced.

In order to select more effective hydrophilic coatings, it is desirable to have information on the nature of the nickel surface and the mechanism involved in the degradation of these surfaces when exposed to expected contaminants. To this end, a literature survey of nickel surface chemistry was implemented and a series of tests were carried out and various theories devised to explain this phenomenon.

## Results of Literature Survey

### 1. The Oxidation States of Nickel

Including the zero oxidation state, which can be represented by a compound such as nickel carbonyl, $Ni(CO)4$, there are at least four, and possibly as many as six, oxidation states for nickel. The +2 oxidation state is by far the most important so that NiO can be considered the most common oxide. Considerable discrepancy exists as to the oxidation states for higher oxides as to whether these are +3 state, +4 state, or mixtures of +2 and +4 state. The oxidizing agent in the Edison storage battery is an oxide mixture which approaches $NiO_2$ (Reference 5). The physical properties of nickel oxide, such as density, electrical resistance, solubility and catalytic activity vary with the temperature of preparation (Reference 6). A chemically active black oxide reportedly contaminated with +3 oxide and corresponding to a hydrate ($Ni_2O_3 \cdot 2H_2O$) is also known. This is not a true hydrate but loses a mole of water to revert to $Ni_2O_3 \cdot H_2O$ or $NiO(OH)$ (Reference 6). Nickel hydroxide $Ni(OH)_2$ is a green colloidal material when prepared from soluble alkalies, but under neutral or slight acid conditions recrystallizes to a micro-crystalline product. The solubility is low (Reference 6). Foust (Reference 7) reports that when nickel electrodes are in alkaline electrolytes in fuel cells at temperatures at or above about 100°C and the electrodes are in the presence of oxygen, they deteriorate rapidly due to corrosion. Foust reports that this corrosion can be prevented by the formation at high temperature of a coat of green nickel oxide on the surface. This green nickel oxide is also used to protect nickel when used as a material of construction in other parts of the fuel cell.

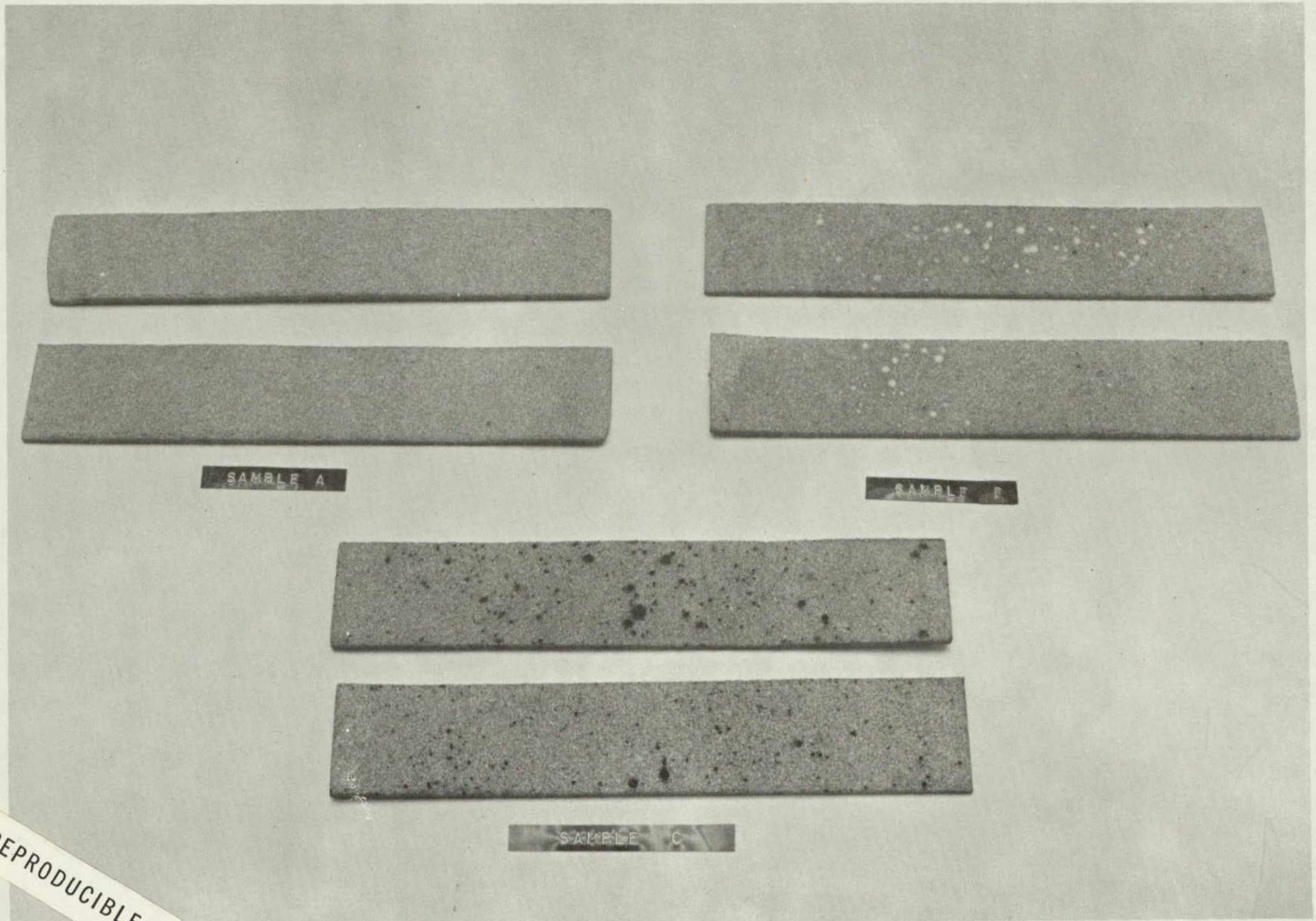




F-9457

Figure 2-11. Wicks Subjected to Various Treatments

TABLE 2-1

EFFECT OF VARIOUS TREATMENTS ON THE WICKING ACTION OF 15 PERCENT DENSE NICKEL WICKS
(1 by 1.125 in. Wick size)

| No. | Initial Treatment | Peak Wick Rate, Sec. Initial | Peak Wick Rate, Sec. 100-Hr Exposure |
|---|---|---|---|
| SC-1 | Distilled water (190°F, 24 hr) | 106 (100%) | 310 (80% wet) |
| SC-21,22 | Oxygen saturated $H_2O$ (100 hr, 190°F)<br>Air saturated water (190°F, 100 hr) | 89 (100%) | 123 (100%) |
| SC-74,75, 76 | Nitrogen saturated $H_2O$ (100 hr, 190°F) | 101 (100%) | 179 (100%) |
| SC-54 | Oxidation in air (1 Atm. 1 hr, 800°F) | 104 (100%) | 210 (3/4-65% wet) |
| SC-83,84 | Heating in hydrogen (1 Atm. 1 hr, 1000°F) | 117 ( 98%) | 110 (1/2-30% wet) |
| SC-55,56 | Oxidation in air (1 Atm. 1 hr, 800°F) followed by $H_2$ heating (1000°F) | 109 (100%) | 53 (1/2-30% wet) |
| SC-1,2 | Oxygen saturated $H_2O$ followed by $H_2$ treatment (1000°F) | 112 (100%) | 120 (100%) |
| SC-100 | Boiling in distilled water (24 hr) | 186 ( 75%) | |

In the presence of nonoxidizing acids, a supply of some oxidizing agent, such as dissolved oxygen, is necessary for the corrosion of nickel to proceed. Reducing conditions usually retard corrosion. However, nickel has the ability to protect itself against certain forms of attack by developing a corrosion resistant or passive oxide film so that oxidizing conditions do not always accelerate corrosion. Nickel is resistant to corrosion by the strongest alkalies, by chlorine, hydrogen chloride, fluorine, hydrogen fluoride, and steam. Sulfur gases cause intergranular attack (Reference 6).

The existence of such numerous oxidation states, forms of hydroxides and hydrates, and passive oxide films, makes an analysis of those surface conditions which facilitate wicking somewhat difficult. Erb (Reference 8) indicates that gross oxide surfaces facilitated the wettability of solid metals. The surfaces so produced were "low energy" surfaces. Laboratory investigations performed under this study, however, indicate that not all oxidation methods produce suitable surfaces and that when such surfaces are produced they may degrade into nonwicking surfaces, possibly by such methods as loss of water from hydrates or slow interaction of higher oxidation states of nickel with nickel metal. This would then produce a uniform oxidation state which may not be capable of the necessary capillary action. Thus, the passive oxide film could represent a stable oxidation state, incapable of being wetted.

## 2. Other "Wettable" Surfaces

Carbon, carbon monoxide, hydrogen and silicon will reduce nickel oxide to the metal when heated (Reference 6). The reduction by hydrogen as a method of eliminating "spots" has previously been noted. Cleaning at high temperatures under vacuum conditions can produce desorption of gases and evaporation of metal atoms from the surface. Such diverse phenomena as adsorption and chemisorption of gases on clean surfaces and thermal faceting (Reference 9) of the crystal may also contribute to surface wettability and account for the rapid wicking observed when oxides are not present. Such surface states are subject to degradation with time.

Nickel readily adsorbs hydrogen and carbon monoxide, but not nitrogen. Oxygen, particularly on the 110 face is strongly bonded by chemisorption and the 100 face undergoes structural rearrangement under the influence of oxygen. The composite surface is so stable that oxygen is difficult to remove even at temperatures at which nickel atoms evaporate (Reference 9). Thermal faceting is a phenomenon which takes place on a crystal face at high temperatures in which the crystal face becomes grooved or striated. The final crystal face is one of lower energy. These striations are not necessarily stable and have been observed to disappear under certain conditions. Conditions favorable to the formation of an adsorbed surface film appear to facilitate thermal faceting, but it is not known how an adsorbed film can promote rearrangement of surface atoms. (Reference 9).

In addition to oxides, hydroxides, adsorbed or chemisorbed gases, and thermal faceting of the crystal, the formation of other chemical compounds bonded to the nickel surface, either organic or inorganic, could be useful in forming a hydrophilic material.

Based on the success of the oxygen-saturated water treatment and the foregoing discussion, it was postulated that nickel hydroxide, $Ni(OH)_2$, or hydrous nickel oxide $NiO.XH_2O$ is formed on the nickel surface. This material is hydrophilic and thus induces good wicking action. To verify the presence of nickel hydroxide on the wick surface, wick samples which had been exposed to the oxygenated water treatment were subject to examination of the surface material by X-ray diffraction. Results of this examination demonstrate the presence of nickel hydroxide on the surface. Identical examination of the vacuum-heated nickel wick samples showed no nickel hydroxide or oxide to be present. In both samples small amounts of $\alpha$-alumina, apparently from the furnace liner, were observed. A summary of these analyses and corresponding wick performance is shown in Table 2-2.

The effect of oxygen compounds in making metal surfaces hydrophilic has been documented in the literature (Reference 8). Additional information in the literature (Reference 10) as well as information received privately from Dr. Malcom White of Bell Telephone Laboratories, indicates that nickel surfaces exposed to heated hydrogen are also hydrophilic (possibility of hydrogen-bond formation with water) and that they are less adsorptive than nickel hydroxide surfaces. This should render them less susceptible to contamination. Test data indicate that heating of the vacuum cleaned wicks in hydrogen was ineffective in preventing deterioration of the wicks on atmosphere exposure. On the other hand, heating of the oxygen-saturated water-treated wicks in hydrogen appears to be equally effective in protecting the wicks as the oxygen-saturated water treated wicks. The hydrogen treatment of these wicks makes them somewhat darker in color.

It has also been observed that wicks oxidized in an air atmosphere at 800°F give good initial wicking action. However, exposure of these wicks to the standard clean laboratory air causes serious deterioration in wicking ability. Also, air oxidized-wicks, post-treated by heating in hydrogen were found to show poor protection against airborne contamination.

It was postulated that the vacuum-heated wicks would possess an appreciable number of active surface sites and that if these wicks were boiled the sites would be converted to nickel hydroxide which would be effective in resisting contamination. Tests carried out along these lines indicated that such a reaction did not occur. Wicks treated in this manner suffered a serious loss in wick rate.

The action of oxygen saturated water in forming nickel hydroxide on the nickel surface is due, at least initially, to the solubility of oxygen in water. The solubility of oxygen in water follows Henry's law over a wide range of pressures and temperatures. Henry's law is expressed by

$$K = \frac{P_{O_2}}{X_{O_2}}$$

TABLE 2-2

SUMMARY OF NICKEL TREATING RESULTS

| Treatment | Effect on Initial Wick Rate | Resistance To Wick Rate Deterioration | Results of Surface X-Ray Diffraction Analysis |
|---|---|---|---|
| Vacuum heating | Good | Poor | Nickel |
| Oxygenated water | Good | Good | Nickel hydroxide |
| Air oxidation | Good | Poor | |
| Air oxidation followed by $H_2$ heating | Good | Poor | |
| Oxygenated water followed by $H_2$ heating | Good | Good | |

where $K$ = Henry's law constant (mm Hg/mol fraction)

$P_{O_2}$ = partial pressure of $O_2$ (mm Hg)

$X_{O_2}$ = mol fraction of $O_2$ in solution

The mols of dissolved oxygen is small with respect to mols of solvent so the total mols can be taken as the mols of solvent only. We can then define $\alpha$:

$$\alpha = \frac{9.454 \times 10^5 (d)}{K}$$

where $\alpha$ = Bunsen adsorption coefficient, or volume of gas (reduced to $0^\circ C$, 760 mm Hg) dissolved in one volume of solvent at the temperature of experiment when the partial pressure of the gas is 760 mm Hg

$d$ = density of solvent (g/cc)

For practical purposes $\alpha$ is a better measure of dissolved gas and can be taken as

$$\alpha = \frac{\text{std cc of gas}}{\text{cc of } H_2O}$$

Values for $\alpha$ $\left(\frac{\text{std cc } O_2}{\text{cc of } H_2O}\right)$ are plotted in Figure 2-12 as a function of temperature. The variation in the constant with pressure (recognizing the constant pertains to oxygen at 760 mm Hg only) has been shown at $26^\circ C$. At any pressure up to about 4000 mm Hg the dissolved gas can be read from the chart at the appropriate temperature as $\alpha$ and converted to the correct value of std cc $O_2$/cc of $H_2O$ by multiplying by the appropriate pressure ratio. Values will be within about 10 to 15 percent even with wide pressure changes.

## Wick Materials

AiResearch has a long history of experience with the wick material selected for tests. This nickel felt metal has a density of 15 percent of that for solid nickel. It was procured from Huyck Metals, Milford, Connecticut in sheets of a standard thickness of 0.088 in.

The wicks are prepared from selected 200 nickel containing a minimum of 99.6 percent nickel. A typical analysis of the nickel employed in making the wicks is given below:

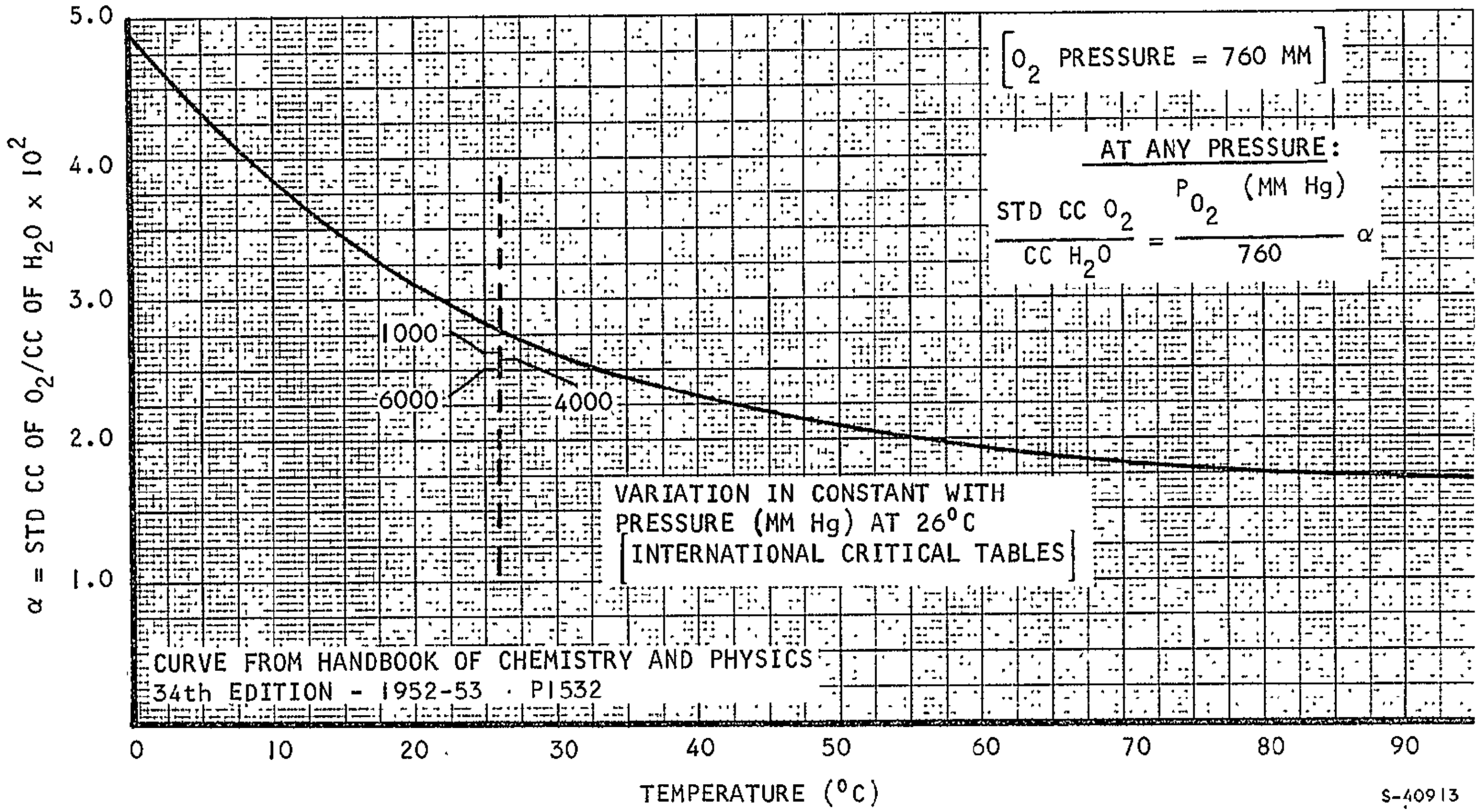


Figure 2-12. Variation of Oxygen Solubility in Water With Temperature

| | Weight Percent |
|---|---|
| Silicon | 0.00 to 0.01 |
| Manganese | 0.05 to 0.10 |
| Iron | 0.20 to 0.25 |
| Sodium | None |
| Zinc | None |
| Tin | None |
| Lead | None |
| Boron | None |
| Chromium | 0.00 to 0.05 |
| Titanium | 0.02 to 0.05 |
| Sulfur | 0.003 to 0.005 |
| Aluminum | 0.02 to 0.05 |

The remainder of the material is nickel.

After converting the nickel into fibers and cleaning, the fibers are made into a felt which is sintered in a pure hydrogen atmosphere. Details of the process are considered proprietary and have not been disclosed. The finished felt material is inspected by X-ray to establish uniformity. Quality control procedures are rigidly employed throughout the fabrication. The material is shipped in sealed nylon bags to protect it from contamination.

Upon receipt at AiResearch the wicks were cut to test size (1.125 by 6 in.) and heated to 1000°F for 1 hr at a vacuum of $5 \times 10^{-5}$ mm of Hg. After cooling under vacuum, the wicks were removed from the furnace with clean gloves and heat sealed in nylon bags until needed.

Test Methods

In order to attain rapid evaluation of the effects of various treatments on the water transport rates of the wicks it was necessary to develop a simple wick rate test.

The test developed at AiResearch involved the measurement of the rate of water rise in a vertical wick, the lower end of which was immersed in distilled water to a depth of 0.125 in. at the start of the test. The rate of water rise in the wick was observed visually and timed with a stop-watch. In most cases the boundary between the dry unwetted portion of the wick and the wetted portion was readily distinguishable. However, in some cases with wicks of poor performance, the surface of the wick was spotty and uneven. In such cases, touching the wick surface with a strip of clean filter paper causes the filter paper to become noticeably wet, thus allowing determination of the position of water in the wick.

Elapsed time in seconds was recorded when the water level reached 25 percent, 50 percent, 75 percent and 100 percent (peak) of the wick height. The time required for the water to completely fill the wick after the peak height was reached was also recorded. With good wicks the peak and the full values were almost identical. With wicks of poor performance, the water level in some cases did not reach the top; in such cases, the height at which the water level stopped was reported. In cases where the wick did not appear completely wet the percentage of the wick surface wetted was reported. This method is illustrated by the photograph of Figure 2-13. A second method of wick rate determination illustrated by Figure 2-14, involves the determination of rate of weight change of a wick dipping continuously in a container of water. This method has the advantage of yielding more accurate data when the wick is unevenly wetted and particularly in those cases where the wick may be wet internally without water appearing on the outer surface of the wick. Such situations were encountered in the oxidation of the wicks by chemical reagents. This method can also be used to measure evaporation rates and water holdup.

Wick Contamination

Determination of the nature of the contamination which induces loss of wicking action is of importance in devising methods to preserve wick activity. Extraction of wicks with organic solvents, followed by infrared spectral analysis of the solvent concentrate failed to demonstrate the presence of any organic material on the wick surface. In this connection it should be observed that contamination, even of as low a concentration as one-half of a monolayer or less, could cause serious deterioration of wicking action. It is doubtful if concentrations this low can be determined by most analytical methods. Because nickel strongly adsorbs atmospheric gases, particularly oxygen, it was postulated that the adsorption of such gases creates a hydrophobic surface. Exposure of the vacuum-cleaned wicks (1000°F) to clean, noncirculating air caused slow deterioration of wick rate (Table 2-3 and Figure 2-15). To determine the effects of specic gases on wick rate, samples of the vacuum-cleaned wicks were placed in glass tubes, and the tubes were evacuated, charged at 1 atmosphere pressure with the gest gas, and sealed off (fusion of the glass).

After two weeks, the tubes were opened and the wick rate determined. Gases studied were hydrogen, oxygen, nitrogen, carbon dioxide, and argon. Results of this test are given in Table 2-4 and plotted in Figure 2-16. The best wick performance was given by argon with nitrogen showing the poorest behavior. Hydrogen, surprisingly, exhibited poor wick performance.

Because argon is an inert gas one would expect it to be adsorbed the least strongly of those tested. Based on studies of adsorption of gases by a variety of materials (Reference 6) the strength of adsorption of gases is generally in the order:

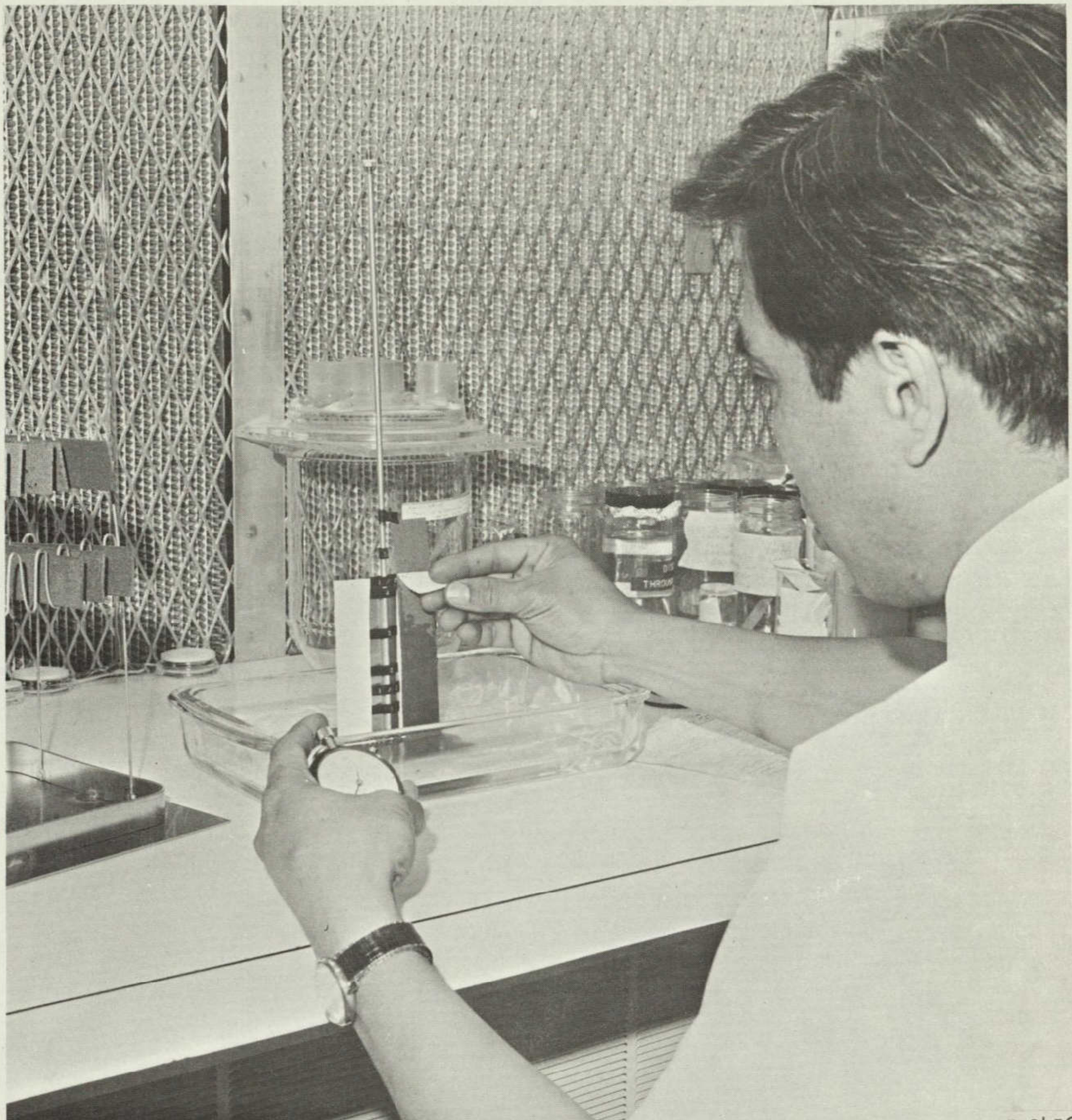


Figure 2-13. Wick Rate Test-Observation of Wicking Height

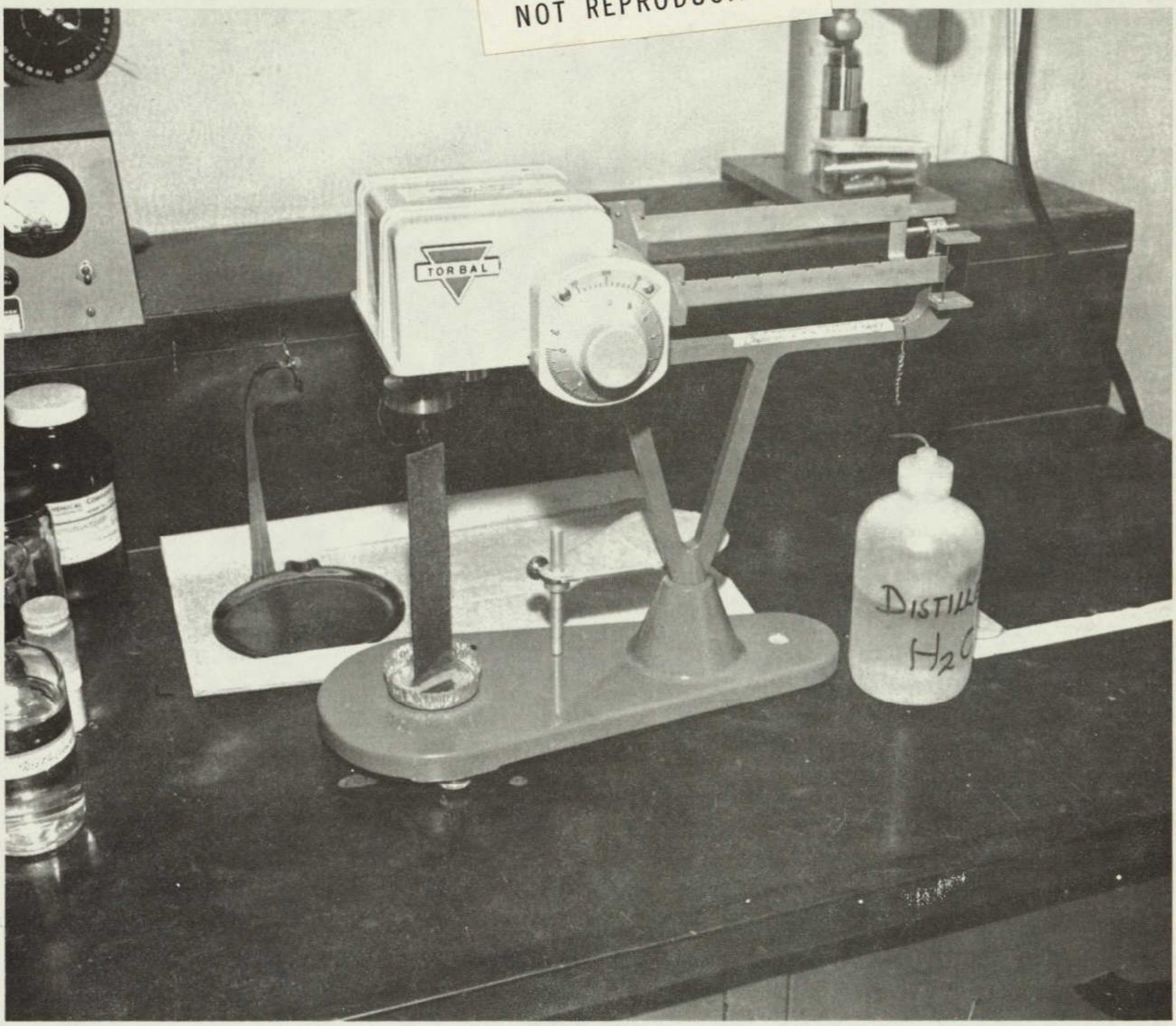


F-9301

Figure 2-14. Wick Rate Test-Weight of Water in Wick

TABLE 2-3

EFFECT OF EXPOSURE TO AIR ON WICK RATE

| Initial | Wick Rate After 150 Hr | Wick Rate After 550 Hr |
|---|---|---|
| 100 sec | 99 sec | 213 sec |

Wicks were exposed in closed glass bell jar originally filled with clean laboratory air. No sealants employed.

TABLE 2-4

RESULTS OF TESTS ON EXPOSURE OF WICK SPECIMENS TO VARIOUS GASES

| Test No. | Initial Wick Rate, Sec | Gas | Wick Rate After Exposure, Sec |
|---|---|---|---|
| SC 68, 69, 70 | 106 to 108 | $CO_2$ | 110 |
| SC 71, 72, 73 | 106 to 108 | $N_2$ | 131 |
| SC 77, 78, 79 | 106 to 108 | A | 105 |
| SC 80, 81, 82 | 106 to 108 | $O_2$ | 135 |
| SC 101, 102, 103 | 106 to 108 | $H_2$ | 125 |

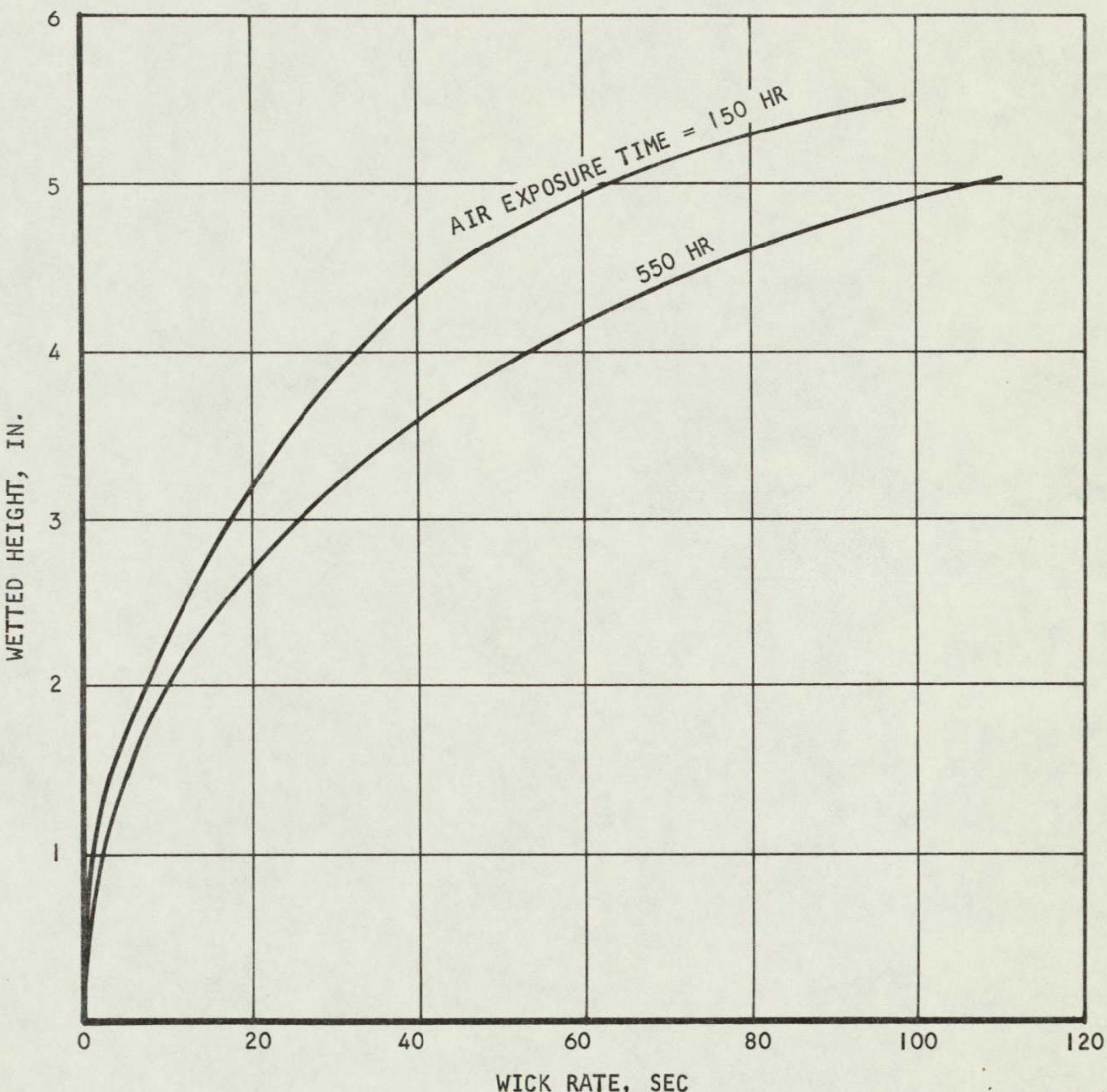


Figure 2-15. Effect of Air Exposure Time on Wick Rate

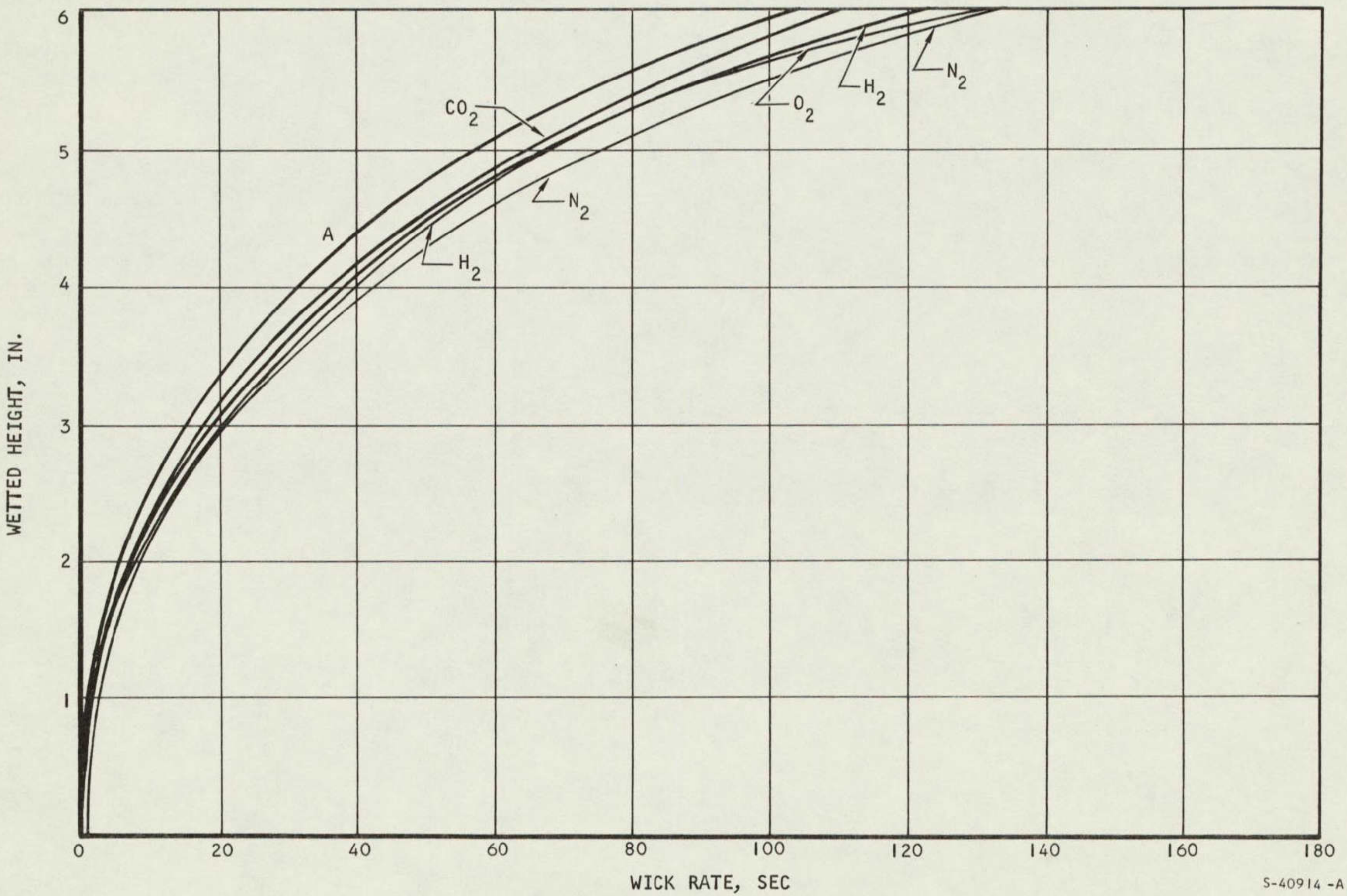


Figure 2-16. Effect of Gas Exposure on Nickel Wick Behavior

$O_2 > C_2H_2 > C_2H_4 > CO > H_2 > CO_2 > N_2$

The heats of adsorption of various gases on nickel (evaporated films) have been determined as follows in kcal/mole.

| | |
|---|---|
| Hydrogen | 29 ±1 |
| Acetylene | 67 |
| Ammonia | 37 ±1 |
| Ethylene | 58 |
| Oxygen | 107 to 150 |

The heats of adsorption of the noble gases are low because of the complete saturation of the electron levels. Results of the gas exposure test are somewhat difficult to interpret. Argon, adsorbed the least strongly, appears to give the best wick performance; however, nitrogen and hydrogen which are also weakly adsorbed show relatively poor wick rates. Oxygen, strongly adsorbed on nickel, also shows slow wick rates.

1. Examination By X-Ray Diffraction

Samples for X-ray diffraction referred to previously were obtained by scraping the surface of the wick under study with a razor blade. Material removed was thoroughly ground in a glass mortar under acetone and then the mixture subjected to ultrasonic radiation. The nickel metal was separated from the acetone mixture by a powerful magnet. After evaporation of the acetone the remaining material was mixed with cellulose nitrate-amyl acetate lacquer, and rolled in a 0.2-mm diameter fiber which was examined by rotation in a precision Debye/Scherrer powder X-ray diffraction camera.

Examination of wicks treated with oxygenated water and exposed to laboratory air indicated that a small amount of nickel chloride dihydrate may be formed (sample SC-23). A fresh nickel wick exposed to the laboratory atmosphere (SC-66) was found by X-ray diffraction analysis to contain both nickel carbonate ($NiCO_3$) and basic nickel carbonate ($NiCO_3.6H_2O$) on the surface.

2. Suspected Contaminants

Suspected contaminants include airborne materials which can coat the wick fiber surfaces and render them hydrophobic. Such contaminants can be present either in the form of vapors or as aerosols of liquid droplets or solid particles. Possible materials include those listed below.

Hydrocarbons (oils, solvents)

Chlorinated hydrocarbons (solvents, refrigerants)

Alcohols (solvents)

Aldehydes (smog)

Ketones (smog)

Silicones (oils, degradation products)

Carboxylic acids (smog)

Mineral acids, hydrochloric, sulfuric (smog)

Sulfur, hydrogen sulfide, sulfur dioxide (smog)

Sulfur trioxide, elemental sulfur (smog)

Inorganic oxides, chlorides, phosphates, etc. (aerosols)

Oxides of nitrogen (aerosols)

Ozone (smog)

Because less than a monolayer of these materials on the surface can cause serious loss of wicking efficiency, it is very difficult to detect and identify the actual contaminants by even highly sophisticated methods of analysis.

3. Microscopic Examination

Microscopic examination of the four wick samples listed below was made at a magnification of 450X in an attempt to discover contaminants on the surface.

| Sample No. | Treatment | Wick Rate Peak |
|---|---|---|
| SC-126 | Heated in vacuum at 1000°F for 1 hr | 108 (100%) |
| SC-23 | After vacuum heating, treated with oxygenated water (100 hr at 190°F) | 89 (100%) |
| SC-21 | Treatment identical to SC-23, after treatment exposed to laboratory air for 200 hr | 197 (100%) |
| SC-66 | Treatment identical to SC-126, after treatment exposed to laboratory air for 100 hr | 55 (only 1/2, ·30%) |

Photographs of these samples are shown in Figures 2-17 and 2-18. The photographs indicate some similarities between samples 126 and 66, and also between samples 23 and 21, as would be expected from the wick treatment. There is evidence of contamination on the surface of the nickel fiber of sample SC-21. However, no surface contamination appears to be visible on the surface of sample SC-66, which is the most heavily contaminated, as evidenced by its slow wick rate.

SC 126

SC 23

F-9454

Figure 2-17. Microscopic Examination of Wick Surface

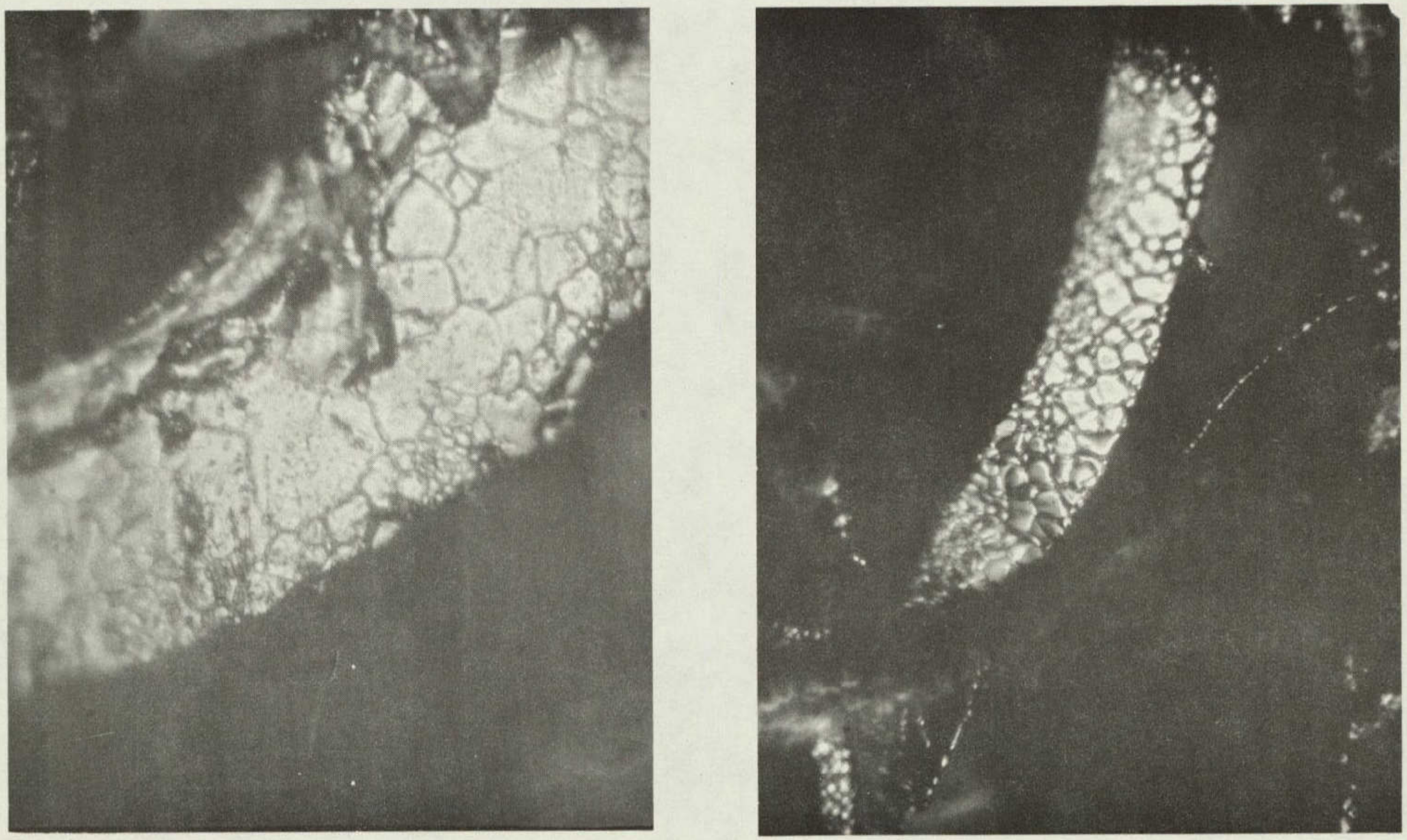

SC 21 SC 66 F-9455

Figure 2-18. Microscopic Examination of Wick Surface (450X)

4. Examination by Mass Spectrometer

Examination was made of four standard nickel wick samples which had been subjected to various treatments and exposures, as shown below. The samples were heated in quartz tubes so that the adsorbed gases were transferred immediately to a mass spectrometer. Results of this analysis indicate that the adsorption of sulfur dioxide may have something to do with the loss of wicking action of untreated wicks (vacuum-heated wicks) on atmospheric exposure.

GASES ADSORBED ON NICKEL WICKS

| Treatment | Exposure | Adsorbed Gases |
|---|---|---|
| Vacuum heated | None | $CO_2$, $H_2O$, hydrocarbons, dimethyl picoline |
| Vacuum heated | 100 hr, laboratory atmosphere | $CO_2$, $H_2O$, hydrocarbons, dimethyl picoline, $SO_2$ |
| Oxygenated water (100 hr, 190°F) | None | $CO_2$, $H_2O$, hydrocarbons |
| Oxygenated water (100 hr, 190°F) | 100 hr, laboratory atmosphere | $CO_2$, $H_2O$, hydrocarbons, dimethyl picoline |

Hydrophilic Coatings and Treatments

Coating or treatment of the wick surfaces to render them more hydrophilic, and especially, to give them greater resistance to loss of wicking action through contamination, appears to be a feasible and desirable effort.

This endeavor can be roughly divided into two types of surface treatment:

(a) Adsorption of hydrophilic materials on the wick surface.

(b) Chemically-bonding of hydrophilic chemical groups to the nickel surface to render them hydrophilic.

The first method of treatment may involve physical adsorption or chemisorption of surface active compounds onto the wick surface. Because physical adsorption involves only weak bonds with the surface, this type of surface coating can be expected to be only temporary. Chemisorption, involving bonds which approach primary valence bonds in strength (up to 50 kilocalories per mole) offers the possibility of attaching groups to the nickel surface which are retained more or less permanently to the surface and resist the leaching action of the water being transported.

Chemically bonding of hydrophilic groups to the wick surface offers the possibility of rendering the wick permanently hydrophilic. Such groups include the hydroxide ions discussed earlier. In many cases it was necessary to pretreat the nickel surface by an active reagent to form an intermediate surface compound which is then reacted with a second reagent to precipitate the hydrophilic group on the nickel surface. This process is exemplified by the formation of nickel chloride on the nickel wick surface. After washing to remove free nickel dichloride ($NiCl_2$) the surface contains bonded chlorine atoms which can be reacted with a second reagent such as dimethyl glyoxime. These reactions are illustrated by Equations (2-4) and (2-5).

$$Ni + Cl_2 \text{ -}NiCl_2 + \text{-}Ni\text{-}Cl \ (I) \tag{2-4}$$

$$\text{-}Ni\text{-}Cl + (CH_3(N\ OH)C\text{-})_2 \text{ - -}Ni \text{ -}ON\ C(CH_3)_2\ NOH\ (2) \tag{2-5}$$

Because of the presence of the hydroxylanimo groups the wick surface is expected to be hydrophilic.

## I. Adsorption of Hydrophilic Materials

In order to behave hydrophilically, compounds must be selected such that, when adsorbed onto the wick surface, the interfacial angle between that surface and water is lowered. Any leaching of the compound by the water being wicked will probably result in a decrease in wick rate since the surface tension of the water in contact with the wick will probably be lowered.

It is believed that compounds that present hydrophilic groups at the water interface when absorbed on the nickel surface will be most effective. Hydrophilic groups are those groups which are capable of entering into some type of bonding with water. Such bonding will probably include those roughly classified as due to Van der Waal's forces. The formation of hydrogen bonds between water molecules and groups on the wick surface may also be important. Van der Waal's forces may consist of dipole-dipole interaction, dipole-induced dipole interaction, as well as instantaneous dipole interactions as shown in Table 2-5. Groups which may be expected to form such bonds with water are listed in Table 2-6. These groups are often termed polar groups because their presence in a molecule usually infers polarity of the molecule.

It is recognized that the properties of such groups and their tendency to form these various types of bonds will depend strongly on the structure of the remainder of the molecule of which they form a part.

It is obvious that the molecules must be adsorbed onto the surface in a manner such that the hydrophilic end is extended toward the water side of the interface. This may pose a problem in the application of certain compounds, since it is possible that the polar (hydrophobic) groups may adsorb to the wick surface, thus presenting the opposite (hydrophobic) end of the molecule to the water.

Compounds selected for test included a number of organic esters and surface active agents. These compounds are listed in Table 2-7. In the initial tests the compounds were applied by dissolving them in reagent grade acetone. The wicks were immersed in the acetone solutions for a period of 15 min. After draining, the treated wicks were dried in the oven at 140°C for 1 hr.

TABLE 2-5

COMPARISON OF INTERMOLECULAR FORCES
(Van der Waal's Type Forces)

| Force | Energy Equation | Typical Values, kcal/mole |
|---|---|---|
| Dipole-Dipole | $E = \frac{-2/3\, M_1^2 M_2^2}{kTr^6}$ | 0.01 to 10 |
| Dipole-Induced Dipole | $E = \frac{3hv_1 v_2 a_1 a_2}{2r^6(v_1+v_2)}$ | 1 to 6 |

where a is the polarizability of the molecule

M is the permanent dipole moment of the molecule

r is the molecular radius

v is characteristics molecular frequency

h is Planck's constant

TABLE 2-6

HYDROPHILIC GROUPS

| | |
|---|---|
| Hydroxyl | -OH |
| Carboxyl | -COOH |
| Amino | $-NH_2$, -NRH |
| Aldehyde | -COH |
| Keto | -COR |
| Ether | -R-OR |
| Ester | -COOR |

TABLE 2-7

COMPOUNDS TESTED FOR ABILITY TO RENDER NICKEL SURFACES HYDROPHILIC

| | |
|---|---|
| Aerosol OT | $NaO_3S$ - CH COO $C_8$ $H_{17}$ ($CH_2COO$ $C_8H_{17}$) |
| Ethylene carbonate | $C_2H_4CO_3$ |
| Methyl crotonate | $CH_3$ OOC CH = CH $CH_3$ |
| Glycerol carbonate | $(CH_2\ CO_3)_2$ CH $CO_3$ |
| Polyglycol P 1200 | H(O CH $CH_2O$ $CH_2$ $CH_2)_n$ OH |
| Carbowax 400 | H(OCH $CH_2O$ $CH_2$ $CH_2)_n$OH |

On cooling, wick rates were determined for the samples. Results of these tests are given in Table 2-8. Perusal of this data indicates that none of these reagents is very effective in promoting water transport rates.

Two of the materials tested, glycerol carbonate and carbowax 400, appeared to give somewhat better performance than the others. The appearance of the gylcerol carbonate treated wicks indicated that they contained more water than fresh untreated wicks. For example, when removed from the water reservoir after the wick test, it was observed that water would drip from the wicks. This phenomenon was not previously observed.

In view of this, tests were made on the weight of water retained by the wicks after the wick test, both for gylcerol carbonate treated and untreated wicks. Results of this test presented in Table 2-9 indicate that the weight of water retained by the gylcerol carbonate treated wicks is actually less than that for the untreated wicks.

The discouraging results obtained with the acetone solutions, particularly the fact that reagent grade acetone itself caused poor wick performance, led to consideration of the use of distilled water as a solvent. Attempts were made to dissolve all of the materials, used previously in acetone, in water; where their solubility in water was limited, they were tested as saturated solutions rather than at the original concentration of 10 grams per 200 ml.

TABLE 2-8

EFFECT OF HYDROPHILIC AGENTS ON WICK RATE

| No. | Hydrophilic Agent* | Wick Rate (Peak) Initial | Wick Rate (Peak) Final, Exposed 100 Hr to Lab Air |
|---|---|---|---|
| SC-4, 5 | Reagent acetone only | 574 (80%, spotty) | |
| SC-6, 7 | Ethylene carbonate | 129 (3/4, 60% spotty) | |
| SC-8, 9 | Methyl crotonate | 120 (1/4, 20%) | |
| SC-10, 11 | Glycerol carbonate | 171 (100%) | 320 (80% - spotty) |
| SC-12, 13 | Polyglycol P 1200 | 280 (3/4 - 75%) | 100 (1/2 - 50%) |
| SC-14, 15 | Carbowax 400 | 193 (100%) | 198 (100%) |

*Acetone Solutions (10g/200 ml acetone

TABLE 2-9

COMPARISON OF QUANTITY OF WATER RETAINED BY
TREATED AND BY UNTREATED WICKS

| | Clean Untreated Wick* | Glycerol Carbonate Treated Wick |
|---|---|---|
| Weight after wick test, gm | 18.8633 | 18.8298 |
| Weight dry, gm | 11.5638 | 11.8152 |
| Weight water adsorbed, gm | 7.2995 | 7.0146 |

*New wick vacuum heated at 1000°F

Results of these tests are presented in Table 2-10. It was concluded from these tests, in similarity to those with the acetone solutions, that the hydrophilic agents selected have little merit in promoting rapid water transport rates or protecting the wicks from airborne contamination.

It appeared probable that the adsorbed reagents did not provide as low an interfacial contact angle with water as the vacuum heated or oxidized nickel surface (oxygen saturated water).

Agents which are soluble in water may be removed from the wick surface by the leaching action of the water as the wick test progresses. Because most of these reagents would be expected to lower the surface tension of water, this leaching action would cause a lowering of the wick rate. It was noticed from the data in Table 2-10 that in a number of cases cessation of wicking appeared to occur. This phenomenon is due to the establishment of an equilibrium between the gravitional force and the force of capillary attraction.

The failure of the hydrophilic reagents to protect the wicks against contamination was surprising since it was originally postulated that surface adsorbed reagents with the polar groups listed in Table 2-6 oriented toward the water would be less adsorptive to expected contaminants. Since the contaminants were unknown and efforts to identify them unsuccessful, it remained a possibility that they may enter into some type of chemical bonding with the surface coatings, causing loss of hydrophilic surface properties. Another possibility was that the reagents tested may be adsorbed in such an orientation that the nonhydrophilic portion of the molecule was presented to the fluid being transported.

## 2. Chemically-Bonded Hydrophilic Coatings

The first step in chemically bonding hydrophilic coatings to the nickel surface involved the introduction of reactive groups onto the nickel surface. Normally, complex hydrophilic molecules have low activity toward reaction with metals. Therefore, it was necessary to first treat the nickel surface with a reactive reagent such as nitric acid, sulfuric acid, or electronegative

TABLE 2-10

EFFECT OF HYDROPHILIC AGENTS ON WICK RATE

| No. | Hydrophilic Agent* | Wick Rate (Peak) Initial | Wick Rate (Peak) Final Exposed 100 Hr to Lab Air |
|---|---|---|---|
| SC-18 | Ethyl crotonate | Stopped (3/4) 50% | Stopped 1/2 (50%) |
| SC-19 | Ethylene Carbonate | 225 (95%) | Stopped 1/4 (25%) |
| SC-20 | Glycerol Carbonate | 135 (100%) | Stopped 3/4 (80%) |
| SC-52 | Gylcerol Carbonate | 163 (100%) | Stopped 1/2 (40%) |
| SC-53 | Carbowax 400 | 264 (100%) | 300 + (90%) |

*Aqueous Solution (10g/200 ml)

elements such as the free halogens. These reagents append ions to the nickel surface which can then be replaced by reaction with the desired surface active agents, provided reaction conditions are favorable.

Some of the groups which appeared interesting for this application are listed in Table 2-11.

As stated previously, hydroxyl, amino, and carboxyl groups, as well as the inorganic phosphate and silicate groups were expected to be hydrophilic. Groups which furnish a large concentration of hydroxyl groups on the surface were expected to increase hydrophilicity. It was probable that such groups may be less adsorptive to aliphatic organic contaminants than the bare nickel surface. The effect of the mobility of the hydroxyl groups on the surface which could be varied by altering the length of the hydrocarbon chain between the nickel surface and hydroxyl group (i.e., in going from the glycolyl group to the γ-hydroxyl propionyl group) was of interest.

Surface fluoride ions were not expected to be extremely hydrophilic because of the high strength of the nickel-fluorine bond, however, they were included in order to determine the effect of group electronegativity on wick performance.

Initial tests were performed on the dimethyl glyoximo and the fluoride coatings. The dimethyl glyoximyl groups were introduced by first treating the wicks with hydrochloric acid, washing to remove excess hydrochloric acid, and then treating the wick with an alcoholic solution of dimethyl glyoxime in a slightly alkaline solution. Results of these tests, shown in Table 2-12, indicated that the dimethyl glyoxime impairs the performance of the wicks. The wicks had a stained appearance after treatment and it appeared probable that the reagent was adsorbed in polymolecular layers, perhaps causing some wick plugging. The tests indicated that the material was not strongly hydrophilic.

The fluoride ions were applied to the surface by two different processes. In the first process, fresh, vacuum heated wicks were exposed to dilute 20 percent hydrofluoric acid at 50°C for 1 hr. After washing with distilled water and drying (1 hr at 140°C) wick rates were determined. Following this, and after redrying, the wicks were exposed to the laboratory atmosphere for 100 hr.

The second sample was subjected to the same treatment, except that the wicks were treated with oxygen saturated water (100 hr, 190°F) and dried prior to immersion in hydrofluoric acid.

Results of this test, also shown in Table 2-12, indicated that the wicks treated first with oxygen-saturated water give superior performance to those which had no pretreatment. The resistance of wicks treated by the second treatment to contamination was considerably greater. It was postulated that the hydroxide groups known to be present on the surface of the wicks treated with oxygen-saturated water were converted to fluoride ions so that these wicks probably had a higher concentration of fluoride ions on the surface. Thus it appeared that the fluoride ion offers some resistance to wick contamination by airborne contaminants. However, compared to the wicks treated with oxygen saturated water only, the fluoride gave poorer protection.

TABLE 2-II

TYPICAL HYDROPHILIC GROUPS FOR BONDING TO THE NICKEL SURFACE BY PRIMARY CHEMICAL BONDS

A. Organic

| | | |
|---|---|---|
| 1. | Dimethyl glyoximo | $(CH_3)_2\ C(NOH)\ NO_2^{=}$ |
| 2. | Oxalate | $HOOCCOO^-$, $(COO^-)_2$ |
| 3. | Dicyandiamido | $(NH_2)\ C\ (NH)\ NCO_2^{=}$ |
| 4. | Glycinyl | $NH_2\ C\ H_2\ COO^-$ |
| 5. | Acetyl | $CH_3\ COO^-$ |
| 6. | Glycolyl | $HO\ CH_2\ COO^-$ |
| 7. | Hydroxy propionyl | $HO\ (CH_2)_2\ COO^-$ |
| 8. | Hydroxy ethoxy | $HO\ CH_2CH_2O-$ |

B. Inorganic

| | | |
|---|---|---|
| 1. | Phosphate | $PO_4^{=}$, $HPO_4^{=}$, $H_2PO_4^-$ |
| 2. | Fluoride | $F^-$ |
| 3. | Sulfide | $S^{=}$, $HS^{=}$ |
| 4. | Silicate | $SiO^{=}_3$, $H\ SiO_3^{=}$ |

TABLE 2-12

TESTS OF CHEMICALLY BONDED HYDROPHILIC GROUPS

| Treatment | Wick Rate to Peak Heights (Average Values) | |
|---|---|---|
| | B<br>Initial | A<br>After Exposure to Atmosphere for 100 hr |
| Dimethyl glyoxime | 232(3/4-80%)* | |
| Fluoride | | |
| a. On fresh wicks | 120 (100%) | 218 (80%) |
| b. On wicks treated in oxygen-saturated water | 117 (100%) | 153 (85%) |

*Wicked to only 3/4 of its height; wick was 80 percent filled with water.

TABLE 2-13

CHEMICALLY BONDED HYDROPHILIC TREATMENT STUDIES

| | |
|---|---|
| Dimethyl glyoximo | Poor wick rate; no contamination protection |
| Fluoride | Poor wick rate; poor contamination protection |
| Phosphate | Good wick rate; poor contamination protection |
| Silicate (after iodide) | Good wick rate; some contamination protection |
| Iodide | Good wick rate; no contamination protection |
| Sulfide | Good wick rate; some contamination protection |
| Oxide, by ozone gas | Good wick rate; poor contamination protection |
| Hydroxide, by ozone saturated $H_2O$ | Good wick rate; good contamination protection |

Additional tests were performed on other chemically bonded hydrophilic groups and the results are summarized in Table 2-13.

Surface Oxidation

The success of the wick treatment with oxygenated water led to an investigation of other types and conditions of surface oxidation in an attempt to develop an improved treatment.

Oxidation in the presence of alkaline solutions was attempted using other processes with essentially the same results. Electrolysis in potassium hydroxide solutions (in which the wick is made anodic and produces oxygen) and immersion of wicks in an alkaline hydrogen peroxide solution produced surfaces which wicked temporarily but were subject to decay. A phenomenon which can only be described as "internal wicking" was observed with such surfaces. Apparently the outside of the wick deteriorated first with wicking degradation progressing inward. In many cases the wick was observed to have water in the interior, but this could be detected only by "feel" since on the exterior surface no water interface was seen nor did paper detect the presence of water.

One of the better methods of creating a surface comparable to that produced by the oxygenated water process but essentially free of discoloration or spots and which did not degrade appreciably was oxidation in an acidic potassium permanganate solution followed by removal of the permanganate stain with neutral hydrogen peroxide. In this case, continued wicking was probably attributable to a residue of manganese ion left on the surface, possibly bonded to the nickel through oxygen atoms, rather than to an oxidized nickel state.

Hydrogen peroxide was an attrative oxidizing agent because its products are gaseous. Thus, hydrogen peroxide decomposes to liberate oxygen and water vapor as shown by Equation (2-6).

$$H_2O_2 \quad H_2O + 0.5\ O_2 \tag{2-6}$$

Nickel wicks did not cause any significant decomposition of hydrogen peroxide to oxygen in a neutral solution. An alkaline solution, however, will spontaneously decompose when a nickel wick is immersed with liberation of oxygen from the wick surface. Similarly, wicks treated with potassium permanganate will react much more rapidly with basic $H_2O_2$ solutions, although permanganate will decompose neutral hydrogen peroxide. In all alkaline solutions noted above, however, the slow decay with "internal wicking" was observed.

Palladium chloride is a strong oxidizing agent. A palladium chloride solution can be made by dissolving Pd $Cl_2$ in hydrochloric acid (IN). If a nickel wick is immersed in such a solution, palladium will plate onto the nickel. It was expected that nickel chloride (soluble) is formed and goes into solution. There was some evidence to indicate such treatment might be beneficial, but wicks so treated wicked only partially. Exact methods, processes, solution concentrations, and immersion times that would optimize wick rate are not known. It can be theorized that the palladium sites would become cathodic in the presence of water. The electrochemical potential between palladium and nickel would be such as to maintain the nickel in an oxidized state (anodic) and possibly stabilize the initial hydrophilic surface.

An electrolytic cell was devised for subjecting wicks to anodic corrosion. To insure complete oxidation over the surface of the wick, the current density must be uniform over the entire face of the anode (wick). This was accomplished by using a platinum cathode (1 in. by 1/2 in.) which moved in grooves parallel to the anode face. The cathode was raised slowly by a synchronous motor (3 rpm) which drove a screw (28 threads/in.) such that the vertical velocity was about 6 in./hr. Both faces of the anode were subjected to oxidation. The anode connection was a platinum clip which contacted the wick at the top. A photograph of the cell is shown in Figure 2-19.

Initial electrolytic studies indicated that a green oxide was formed on the anode under suitable conditions. However, if a wick was made cathodic (that is, if hydrogen is liberated by electrolysis), the surface of the reduced metal wick became completely hydrophobic and the wick was completely "dead". This did not agree with high temperature reduction of nickel hydroxide by hydrogen so that the higher temperatures appeared to influence the nickel surface. Electrolytic studies in media other than the basic solutions used are necessary.

The most successful treatment found for preserving the wicking characteristics of nickel wicks was a warm water soak with oxygen bubbling through. Little work was done in this specific area in this program since a concurrent Apollo program at AiResearch was investigating this approach extensively. Wicks treated in this manner have maintained good wicking characteristics after long (800 hr) exposure to atmospheres which cause complete loss of wicking in untreated wicks after a few hours of exposure.

Conclusions

Based on the wicking preservation study, the following conclusions were reached:

(a) Treatment of nickel wicks with hydrophilic reagents in an effort to adsorb substances on the surface to lower the contact angle with water was not successful with any of the reagents tested.

(b) Attempts to chemically bond hydrophilic groups to the nickel surface were partially successful in the form of special oxidizing treatments.

(c) Nickel surfaces which were coated with nickel hydroxide as a result of a warm water soak with oxygen bubbling through were hydrophilic and showed resistance to airbone contaminants.

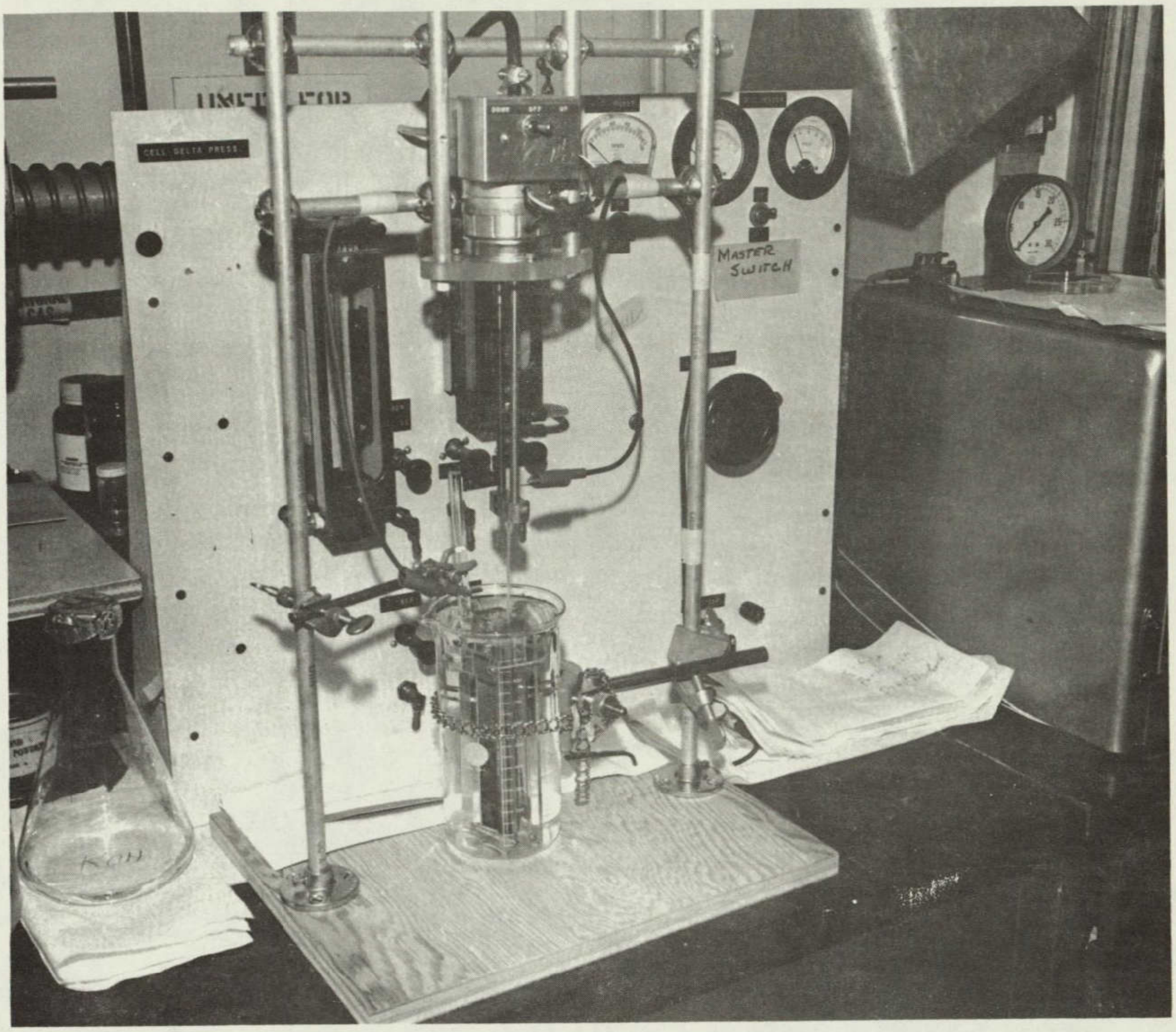


F-9300

Figure 2-19. Electrolytic Cell for Uniform Wick Oxidation

## HYDROPHOBIC POROUS PLATE INVESTIGATION

### Introduction

A conventional sublimator porous plate depends upon the existence of ice in the pores to restrain the water in the plenum from breaking through. There are two modes of operation in which ice may not exist and the sublimator fails. These modes are startup of the unit and high heat flux conditions. Startup breakthrough has been limited by regulating the water plenum pressure and water flow rate with additional controls. By limiting the maximum heat flux at which a unit operates, high heat flux breathrough has been eliminated.

An analysis of the effects of surface tension, contact angle, and pore geometry on the bubble point and liquid retention pressure of porous plates performed during the first phase of the heat sink study program indicated the possibility of another mechanism for restraining the liquid behind a functioning sublimator plate. (See Reference 1). This analysis indicated that as the contact angle increases, the liquid retention pressure of a porous plate increases. Therefore, by generating a large contact angle, surface tension effects could be used to restrain the liquid behind a porous plate without depending upon ice formation. Theoretically this would remove limitation on startup and maximum heat flux, as well as allowing operation with sink pressures above the triple point.

Based upon these potential operating advantages, an investigation of hydrophobic coatings for porous plates was performed. The investigation included development of selection criteria for porous plates and hydrophobic coatings used in the study, a survey of coating materials for rendering surfaces hydrophobic, investigation of application techniques for such coatings, and testing of the operating characteristics of coated plates.

### Selection Criteria - Alcohol Bubble Point and Contact Angle

To establish selection criteria related to pore size and contact angle for porous plate specimens to be used in the hydrophobic coating tests, an analysis of the characteristics of a hydrophobic pore was performed. A relationship between the water retention pressure (the pressure required to force liquid water through the plate) of a treated pore and the initial alcohol bubble point (the pressure required to force gas through a plate covered with alcohol) was developed so that plate specimens could be selected from bench test data. The normalized breakthrough pressure analysis presented in the Heat Sink Study Annual Report (Reference 1) was used. For a relatively dull pore exit, the water retention pressure, $P_{BL}$, is approximately equal to $-2 (\sigma_w/r') \cos \theta$ for $\theta$ angles between 95 deg and 180 deg. The pore exits of conventional sintered metal porous plates are well rounded and may be classified as dull, and the above expression $P_{BL}$ applies to such plates. Since the liquid breakthrough pressure is directly proportional to the cosine of the contact angle, it was obvious that large contact angles are desired.

The inverse proportionality to the pore radius indicated the desirability of a small pore. However, the small pore size must be compromised somewhat since the plate permeability is also a function of the pore size and high permeability is desirable.

The alcohol bubble point pressure, $P_{BA}$, is equal to $2\,\sigma_A/r'$. Since the contact angle of alcohol with most any surface is zero deg, the alcohol bubble point is dependent of the pore exit configuration. Expressing $P_{BA}$ in terms of $P_{BL}$:

$$P_{BA} = 2\,\frac{\sigma_A}{r'} = \frac{\sigma_A}{\sigma_W}\,\frac{P_{BL}}{(-\cos\,\theta)} \tag{2-7}$$

The surface tensions of alcohol and water are 23.1 and 75.0 dynes/cm respectively and Equation (2-7) becomes:

$$P_{BA} = \frac{.308\,P_{BL}}{\cos(180^\circ - \theta)} \tag{2-8}$$

Equation (2-8) gives the alcohol bubble point pressure which a plate with a water contact angle of $\theta$ must exhibit in order to function in a sublimator with a maximum feed pressure of $P_{BL}$. Tabulated below are the required alcohol bubble points as a function of the desired maximum operating feed pressure for a plate exhibiting a water contact angle of 130 deg. (It is shown below that such angle is obtainable).

| Maximum Feed Pressure, psia | Alcohol Bubble Point, psi |
|---|---|
| 5 | 2.4 |
| 10 | 4.8 |
| 15 | 7.2 |

This relationship establishes one of the selection criteria (alcohol bubble point) for porous plates used as hydrophobic plate test specimens.

Selection Criteria - Permeability and Hydrophobic Depth of Penetration

At the low pressures at which water vapor exits a porous plate in a sublimator, flow is in the free molecular regime. The equation for pressure drop in a uniform diameter tube in this flow regime is

$$\Delta P_{fm} = 1.88\sqrt{\frac{\Re T}{g_o}}\,\frac{L}{D\,A_c}\,W_{fm} \tag{2-9}$$

where $\Re$ = gas constant

$T$ = absolute temperature

$L$ = flow length

$D$ = diameter

$W_{fm}$ = flow rate

$\Delta P_{fm}$ = pressure drop

For flow through a porous plate however, Equation (2-9) cannot be applied directly because the effective flow length, the free-flow area, and the equivalent pore diameter are not known. A reasonable correlation of porous plate $\Delta P$ data can be obtained by multipling the right side of (2-9) by a constant $K_1$ and by taking L as the plate thickness, $A_c$ as the product of plate porosity $\theta$ and total plate surface area $A_t$, and D as the pore diameter defined by the initial alcohol bubble point. Permeability data for plates with varying characteristics (porosities ranging from 32 to 48 percent thicknesses of from 0.015 to 0.028 inch, and maximum pore diameter from 3.0 to 7.6 microns) were correlated to within ±18 percent using $K_1$ = 3.45. Therefore, for similar porous plates in this permeability range, Equation (2-9) may be rearranged to obtain

$$\frac{L}{\Phi} = \frac{D}{(1.88)(3.45)\sqrt{\frac{\Re T}{g_o}}} \quad \frac{\Delta P_{fm}}{W/A_t} \tag{2-10}$$

For a functioning sublimator plate, the flow rate per unit area may be expressed as a function of the heat flux applied to the surface, the enthalpy of the liquid entering the sublimator, and the enthalpy of the vapor exiting the sublimator.

$$\frac{W}{A_t} = \frac{Q}{A_t} \times \frac{1}{(h'_{out} - h'_{in})} \tag{2-11}$$

$$\text{or} \quad \frac{W}{A_t} = \frac{Q}{A_E} \frac{1}{\Delta h'}$$

Also, for an operating conventional sublimator porous plate, the pressure drop from the point of vapor formation to the sink, $\Delta P_{fm}$, must be no greater than 0.0885 psi, the triple point of water. Equation (2-10) becomes:

$$\frac{L}{\Phi} = \frac{0.154\ D\ \Delta h'}{\sqrt{\frac{\Re T}{g_o}}} \quad \frac{(0.0885\ \text{psi})}{Q/A_t}$$

or, for typical temperatures encountered:

$$\frac{L}{\Phi} = 8.3\ \frac{D}{Q/A_t} \quad \frac{\text{in.-Btu}}{\text{micron-hr-ft}^2} \tag{2-12}$$

The pore diameter may be expressed in terms of the water breathrough pressure with a hydrophobic coating.

$$D = 2r' = \frac{4\ \sigma_W}{P_{BL}}\ \cos\ (180^0 - \theta)$$

Equation (2-12) becomes:

$$L = \frac{350\ \Phi\ \cos\ (180^0 - \theta)}{P_{BL}\quad Q/A_t}\ \frac{\text{lb-Btu}}{\text{in.-hr-ft}^2} \qquad (2\text{-}13)$$

Equation (2-13) gives the maximum thickness of a porous plate with a hydrophobic coating on all surfaces which will still give a saturation pressure below the triple point as a function of the plate porosity, the contact angle, the desired water retention pressure (feed pressure), and the operating heat flux. It will be shown below that for reasonable values of the variable parameters such small values of L are obtained that plates of this thickness would be structurally unsound. However, Equation (2-13) may also be taken as defining the depth of penetration of a hydrophobic coating applied to one surface of a porous plate.

Equation (2-13) is plotted in Figure 2-20 for various maximum feed pressures for a contact angle of 130 deg and a plate porosity, θ, of 0.040. As an example, if it were desired to operate with a maximum feed water pressure of 10 psi at a heat flux of 3000 Btu/hr-ft$^2$, the depth of penetration of the hydrophobic coating must not exceed 0.003 in.

## Hydrophobic Coating Materials

A survey was made of possible materials for rendering surfaces hydrophobic. While all materials increased the water contact angle, only about half gave angles equal to or greater than 90 deg. The materials tested and the contact angles obtained are given in Table 2-14. Accurate measurements of contact angle were made on the first five specimens listed; however, the contact angles of the remaining samples were approximated by visual observation. As indicated by the data, MS-122, the fluorocarbon mold release, appeared most promising, yielding a contact angle of 132 deg.

Another material which appeared promising was pentadecalfluorotylacrylate, which has a relative surface energy of 10.5 compared to 20 for teflon. Since in general the contact angle increases with decreasing surface energy, it was thought that a contact angle greater than that obtainable with Teflon (~130°) could be achieved. A small quantity of this material was secured; however, the inability to develop a method of application to the porous plate curtailed any further investigation of this compound.

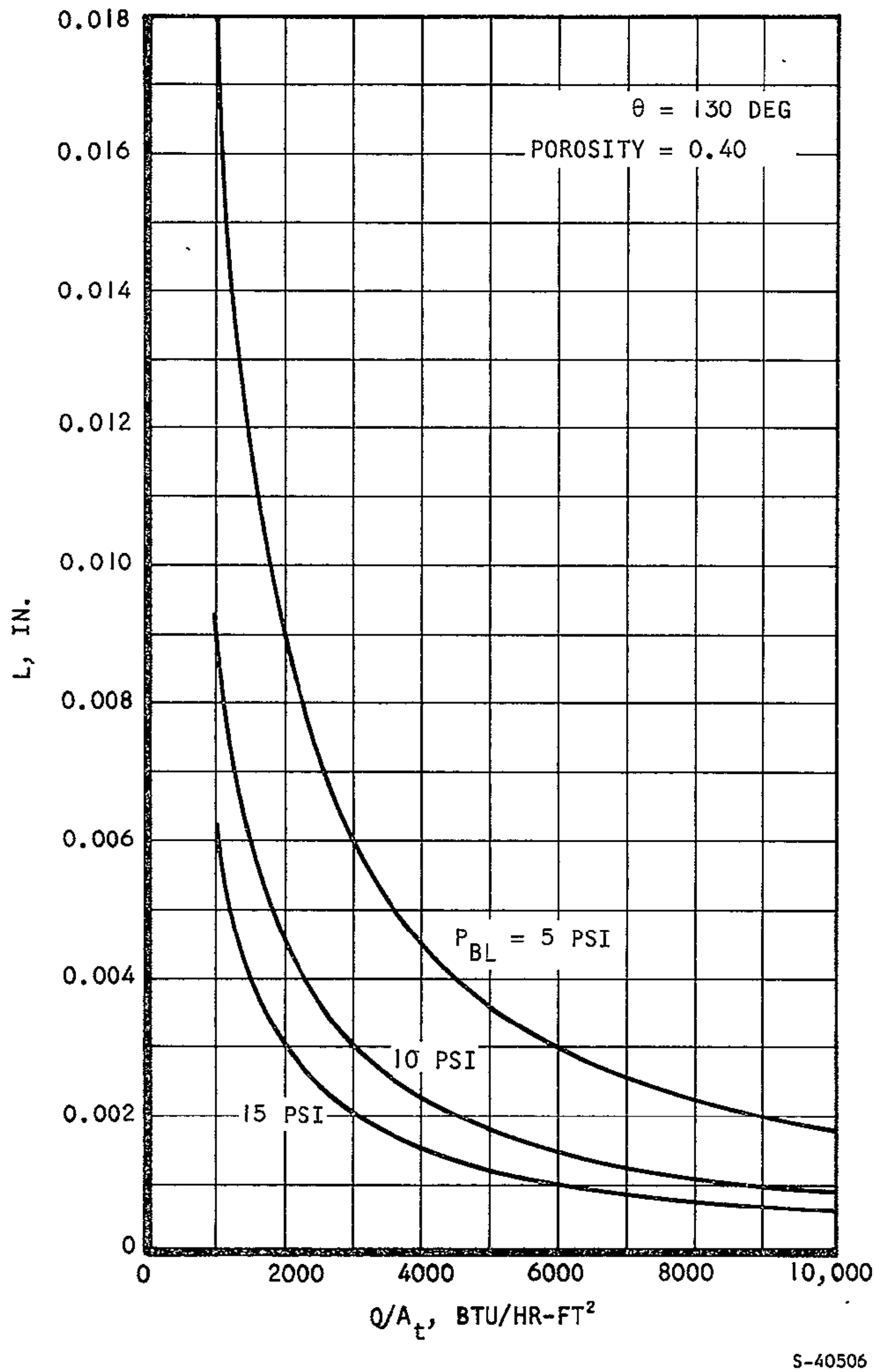


Figure 2-20. Depth of Penetration of Hydrophobic Coating as a Function of System Parameters

TABLE 2-14

CONTACT ANGLE OF WATER
ON VARIOUS SURFACES

| Material | Distilled Water Contact Angles, deg |
|---|---|
| Teflon (green) 958-207 Type S | 85 |
| Fluorocarbon (Sherman Williams) | 62 |
| MS-122 fluorocarbon mold release (Teflon) | 132 |
| Vydax (Dupont) | 90 |
| MX-136 | 95 |
| Nylon | 60 |
| Delrin | 90 |
| Phenolic | <90 |
| Lecton (acrylic) | <90 |
| Alkyd | <90 |
| Bakelite | 90 |
| Celcon | 90 |
| Diallyl phthalade | 90 |
| Epoxy glass | 90 |
| Fluorosint TFE | 60 |
| Fluoroloy "A" | 90 |
| TFE and Molysulfide | 90 |
| KEL F | 90 |
| Lexan (polycarbonate) | 60 |
| Mylar polyester | 60 |
| Teflon FEP | 90+ |
| Silicone (glass filled) | 60 |

Of the compounds investigated, the best material for coating, therefore, was the fluorocarbon mold release. The plates were coated in the following manner: Two passes with MS-122 teflon spray were made with the nozzle tip about 6 in. from the plates. The fusion process was performed on an iron plate heated in a furnace to 800$^{\circ}$F. The plate was removed from the oven and the porous plate placed on it for 2 min. The coating weight resulting from this application was between 0.006 and 0.010 gm/sq in. Contact angles of approximately 130 deg were measured on plates coated in this manner.

## Porous Plate Bench Tests

Twenty-two porous plates were selected from those purchased during the heat sink program for potential use in the hydrophobic coating investigation. All plates selected had alcohol bubble points (determined during the heat sink study) greater than 2.4 psia so that potentially they could have a water retention pressure greater than 5 psia. A series of bench tests were performed on these plates to define the permeabilities, relative pore sizes, and heat flux-temperature characteristics before coating with hydrophobics. To some extent, these tests duplicated those performed on the plates during the heat sink study. However, it was desired to establish the repeatability of the tests and to determine if the plate characteristics changed during extended storage.

The bench test apparatus is shown in Figure 2-21. In the water retention pressure test, distilled 1/2-micron filtered water was supplied at steadily increasing pressure to the back face of a porous plate clamped in a holder. The water retention pressure was the pressure at which water initially appeared on the top face of the plate. In the bubble point testing, distilled 1/2-micron filtered water or 95 ethyl alcohol was poured onto the top face of a porous plate clamped in a holder, sufficient to form a layer approximately 1/2-in. thick. Air was applied to the bottom face at a slowly increasing pressure. The pressure was recorded when the first dynamic bubble was seen and when 80 percent of the surface was seen to be bubbling. The permeability with vacuum discharge was determined by supplying filtered nitrogen gas to the back face of a porous plate in a holder which was situated in an evacuated bell jar. The pressure drop across the plate was recorded at various flow rates, the downstream pressure being maintained at less than 500 microns pressure. The same procedure was used for permeability with ambient discharge except that the plate and holder were situated in laboratory ambient conditions.

Table 2-15 gives the initial and 80 percent bubble points in alcohol and water and the water retention pressure for the porous plate specimens. In general, these results were in agreement with those obtained previously. Nitrogen permeability data with vacuum discharge was also obtained and again most plates performed as before. The results are shown in Figures 2-22 and 2-23. It was noted, however, that three plates had significantly higher pressure drops and it was decided not to use these plates in the hydrophobic tests.

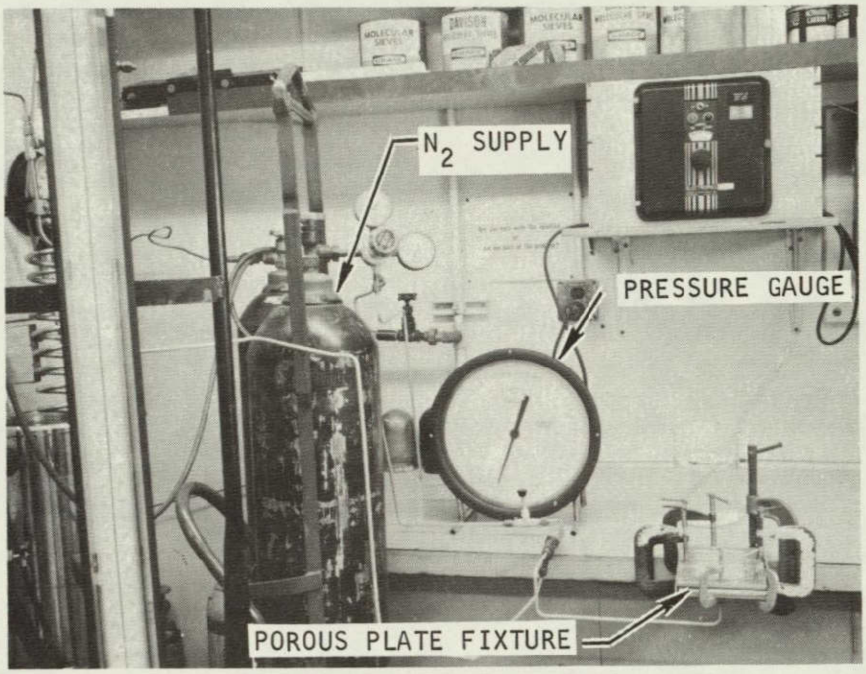


F-12546

Figure 2-21. Porous Plate Bench Test Apparatus

AIRESEARCH MANUFACTURING COMPANY
Los Angeles California

TABLE 2-15

POROUS PLATE CHARACTERISTICS

| Plate | Initial Alcohol Bubble Point, psi | 80% Alcohol Bubble Point, psi | Initial Water Bubble Point, psi | 80% Water Bubble Point, psi | Water Retention Pressure, psi |
|---|---|---|---|---|---|
| L-1A | 6.28 | 9.82 | 11.0 | - | - |
| L-2A | 5.25 | 10.45 | 16.4 | - | - |
| L-3A | 5.84 | 9.77 | 15.37 | - | - |
| L-4A | 5.84 | 10.35 | 12.1 | - | 0.10 |
| L-5A | 5.45 | 9.82 | 16.75 | - | 1.08 |
| UC-1C | 5.60 | 7.07 | 13.35 | - | - |
| UC-2B | 5.53 | 5.90 | 18.2 | - | 0.93 |
| UC-2B-1 | 4.47 | 11.3 | 8.83 | - | 1.18 |
| UC-2B-2 | 4.81 | 11.77 | 18.65 | - | 1.96 |
| UC-2B-3 | 4.07 | 5.45 | 11.9 | 16.95 | 0.74 |
| UC-2B-4 | 4.71 | 6.13 | 9.38 | 18.15 | 0.05 |
| UC-2B-5 | 4.12 | 6.04 | 8.34 | 16.75 | 0.15 |
| UC-2B-6 | 3.73 | 6.28 | 11.85 | 17.15 | 0.15 |
| UC-2C-1* | 3.83 | 9.32 | 14.25 | - | 6.04 |
| UC-2C-2 | 8.40 | 21.1 | 18.4 | - | 1.38 |
| UC-2C-8 | 5.35 | 21.1 | 14.45 | - | 1.18 |
| UC-3A | 2.75 | 8.25 | 10.9 | 16.9 | 0.49 |
| UC-3A-1 | 4.47 | 6.28 | 13.6 | 16.6 | 0.74 |
| UC-3A-2 | 4.47 | 7.41 | 13.3 | - | 0.88 |
| UC-3A-3 | 4.96 | 7.66 | 14.7 | 19.45 | 0.88 |
| UC-3A-4 | 4.47 | 5.94 | 11.4 | 17.0 | 0.54 |
| UC-3A-5 | 4.76 | 6.63 | 9.28 | 18.65 | 0.39 |

*Teflon coated plate

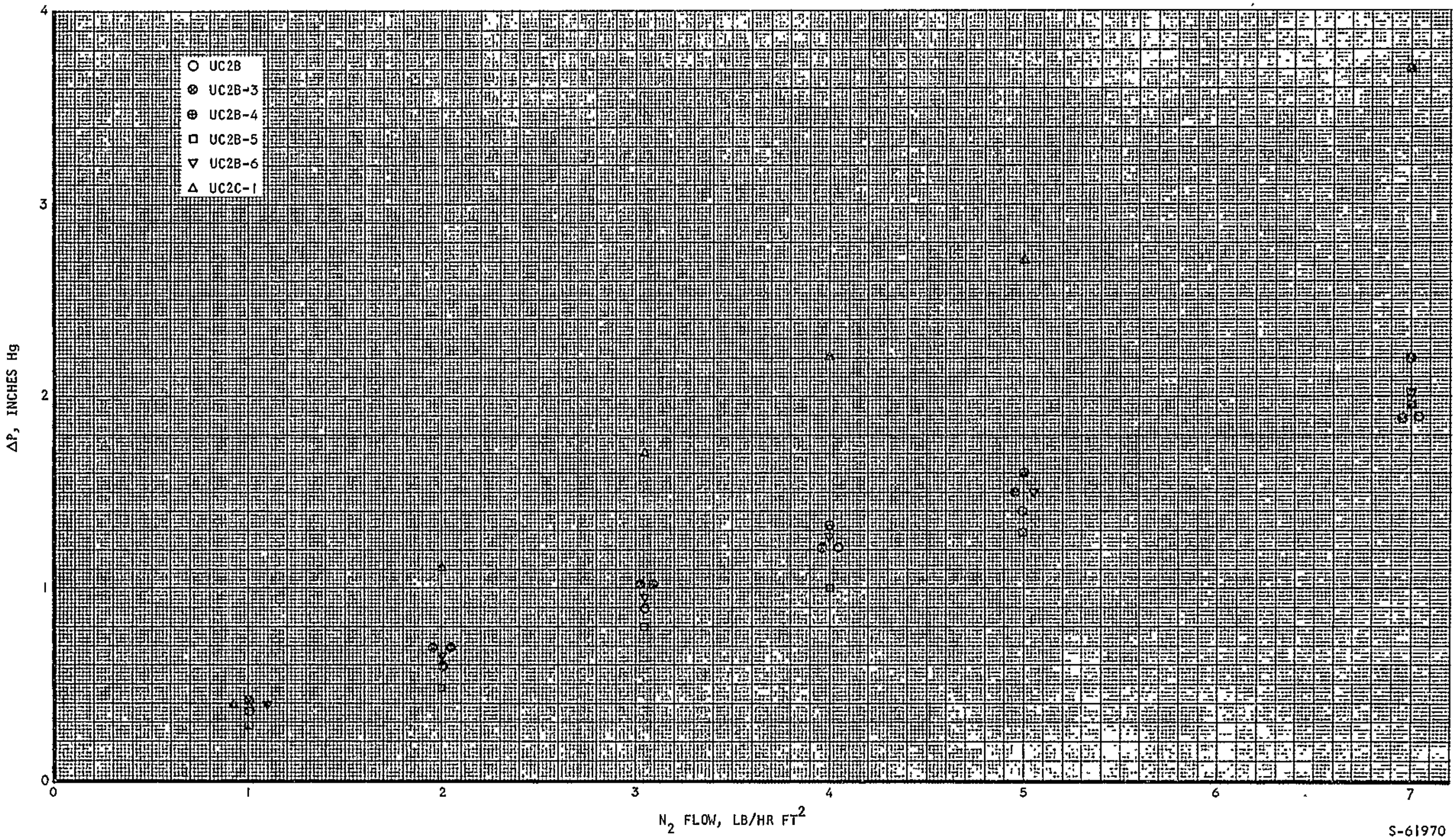


Figure 2-22. Nitrogen Permeability with Vacuum Discharge

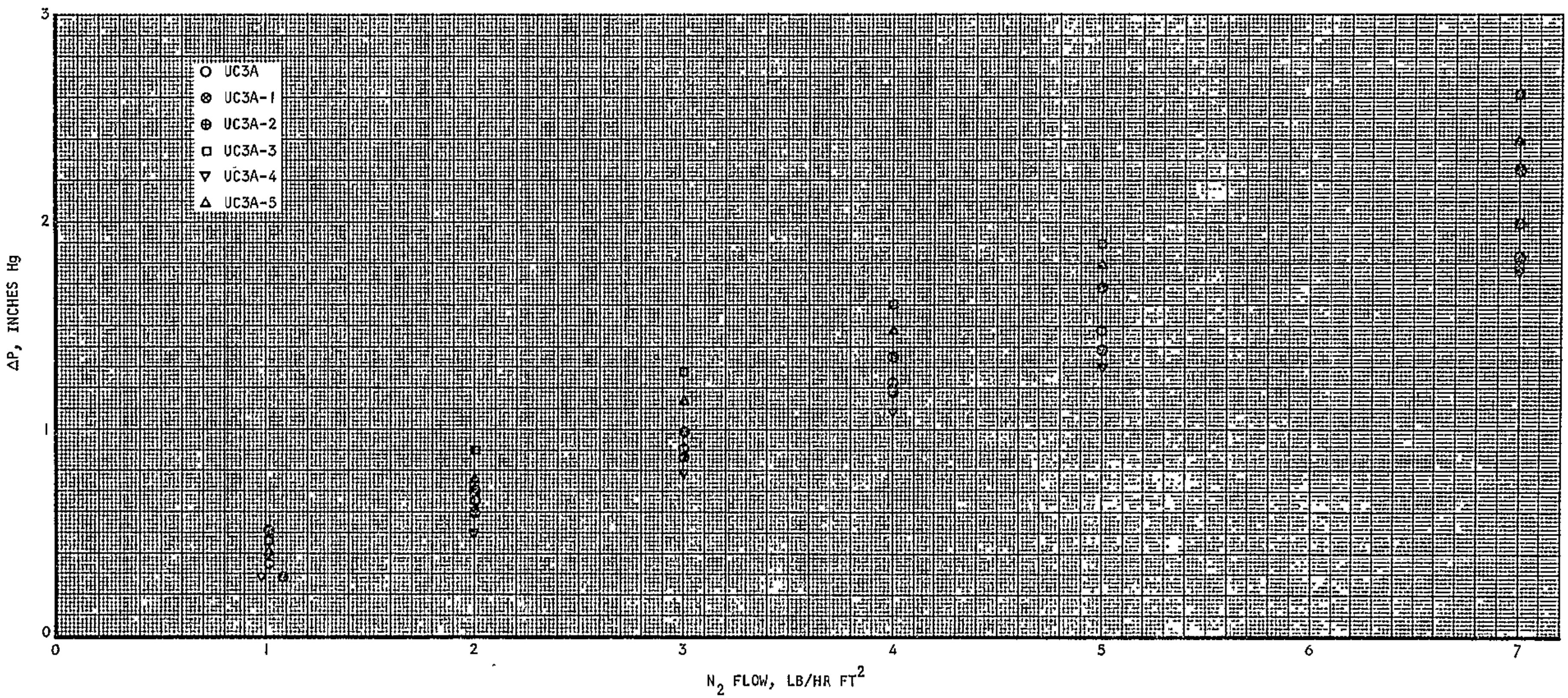


S-61969

Figure 2-23. Nitrogen Permeability with Vacuum Discharge

Six porous plates were coated with MS-122 in the manner described above. Those plates were then bench tested to determine what effects the coating had on the bubble point and permeability. Table 2-16 shows a comparison of the initial and 80 percent bubble points in alcohol, initial bubble point in water, and the water retention pressure before and after coating. As was expected, the alcohol data did not change significantly since the alcohol contact angle was not greatly increased on Teflon. However, the water data changed markedly due to the large contact angle of water on Teflon. As predicted by the theory, the bubble point (gas breakthrough) pressure decreased and the water retention (liquid breakthrough) increased sharply. This increased water retention pressure is highly desirable for a sublimator as this would prevent breakthrough with no ice present in the pores to restrain the water. Figure 2-24 shows bubble point in water data being taken on Teflon coated plates (UC2B-1 and UC2B-4).

Plates UC2B-4 and UC2B-6 were also permeability tested after coating and a comparison of the data before and after coating is shown in Figure 2-25. The permeability of plate UC2B-6 was unchanged by the coating process. However, the permeability of plate UC2B-4 was reduced by a factor of 0.5. The decreased permeability of plate UC2B-4 was due to plugging of some of the pores by the hydrophobic coating.

Sublimation tests also were performed on coated and uncoated plates using the fixture and apparatus shown in Figures 2-26 and 2-27. The first of these figures shows a porous plate mounted in the support fixture. The fixture has a phenolic frame with aluminum support bars. Below the porous plate was a finned water plenum with a water inlet tube located at one end and a pressure tap at the other. Below the water plenum was a copper block to which the electrical heater was bonded. The block was instrumented with six copper-constantan thermocouples. Figure 2-23 shows the test apparatus. The porous plate fixture was placed inside a bell jar vacuum chamber which was connected to a vacuum line through a cold trap. Liquid nitrogen was used as the heat sink for condensing the water vapor in the cold trap. Power input to the heater was regulated with a variac and measured with a voltmeter and ammeter. Water was fed to the sublimator from a degassed water supply tank through a flowmeter. Feed water pressure, plenum pressure, and bell jar pressure were measured and recorded, as were the temperatures.

Sublimation data was obtained in the form of heater temperature vs heat load. The data for uncoated plates agreed quite well with data reported previously (Reference 1). Typical performance is shown in Figure 2-28 for two plates with a plenum pressure of about 6 in. Hg abs. All the data takes this general shape giving a somewhat linear increase in heater temperature with heat flux.

Two plates which had been coated with Teflon were tested in the sublimation apparatus. One of these plates, UC2B-6, had not been plugged by spraying while the other, UC2B-4, had its permeability cut in half by the hydrophobic application. The heat transfer test was to ascertain if there were any differences in the performance as well as to determine if the Teflon had penetrated the pores. As discussed in Reference 1, if the hydrophobic material

TABLE 2-16

POROUS PLATE CHARACTERISTICS

| Plate | Initial Bubble Point in Alcohol, psi | | 80 Percent Bubble Point in Alcohol, psi | |
|---|---|---|---|---|
| | Before Coating | After Coating | Before Coating | After Coating |
| UC2B | 3.53 | 3.00 | 5.90 | 5.16 |
| UC2B-1 | 4.47 | 3.83 | 11.30 | 8.50 |
| UC2B-2 | 4.81 | 4.32 | 11.77 | 8.01 |
| UC2B-3 | 4.07 | 3.34 | 5.45 | 5.21 |
| UC2B-4 | 4.71 | 3.64 | 6.13 | 5.56 |
| UC2B-6 | 3.73 | 3.34 | 6.04 | 5.61 |

| Plate | Initial Bubble Point in Water, psi | | Water Retention Pressure, psi | |
|---|---|---|---|---|
| | Before Coating | After Coating | Before Coating | After Coating |
| UC2B | 18.20 | 7.52 | 0.93 | 6.99 |
| UC2B-1 | 8.83 | 5.61 | 1.18 | 6.29 |
| UC2B-2 | 18.65 | 3.49 | 1.96 | 3.34 |
| UC2B-3 | 11.90 | 2.26 | 0.74 | 6.59 |
| UC2B-4 | 9.38 | 4.67 | 0.05 | 6.83 |
| UC2B-6 | 11.85 | 2.11 | 0.15 | 6.64 |

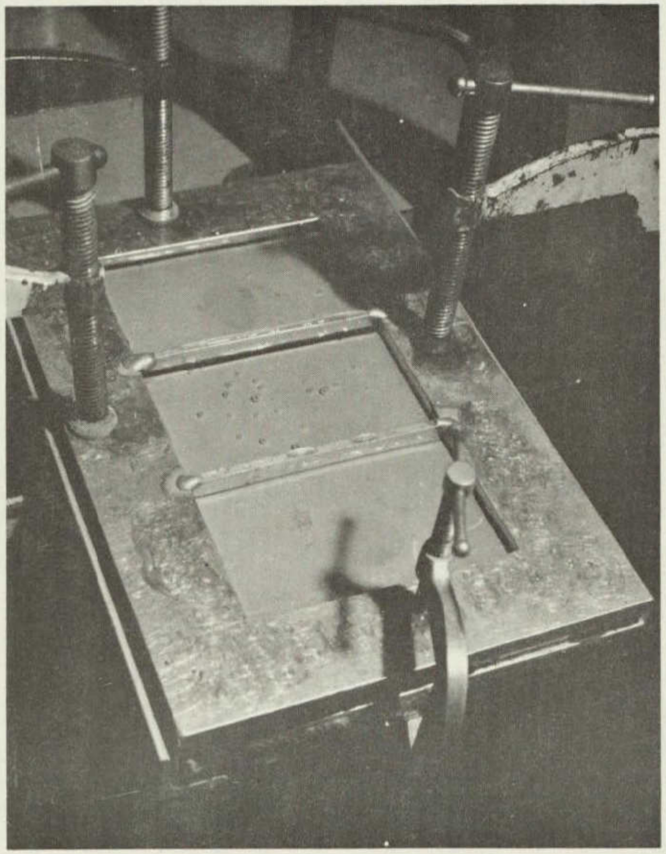

UC2B-1

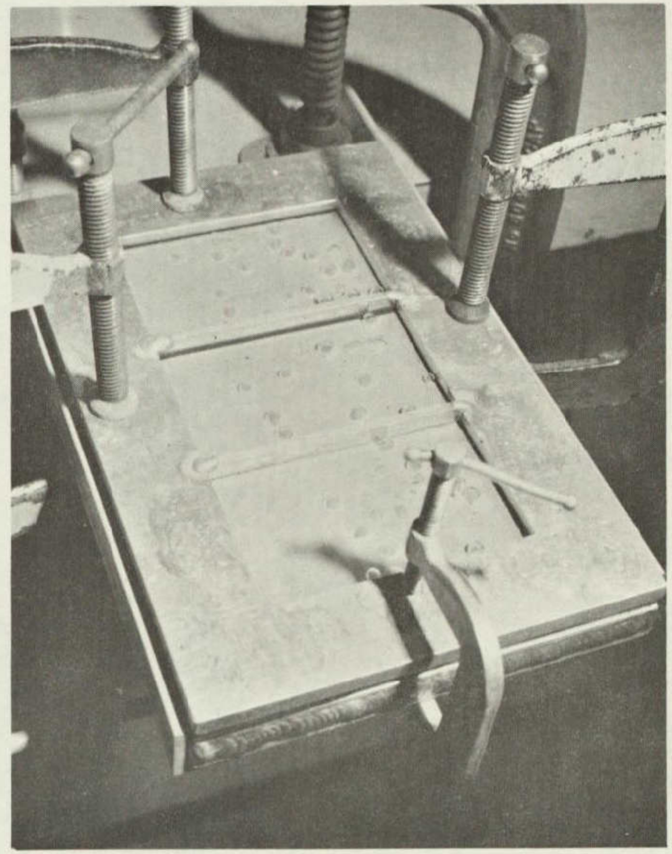

F-9740

UC2B-4

Figure 2-24. Bubble Point Data in Water

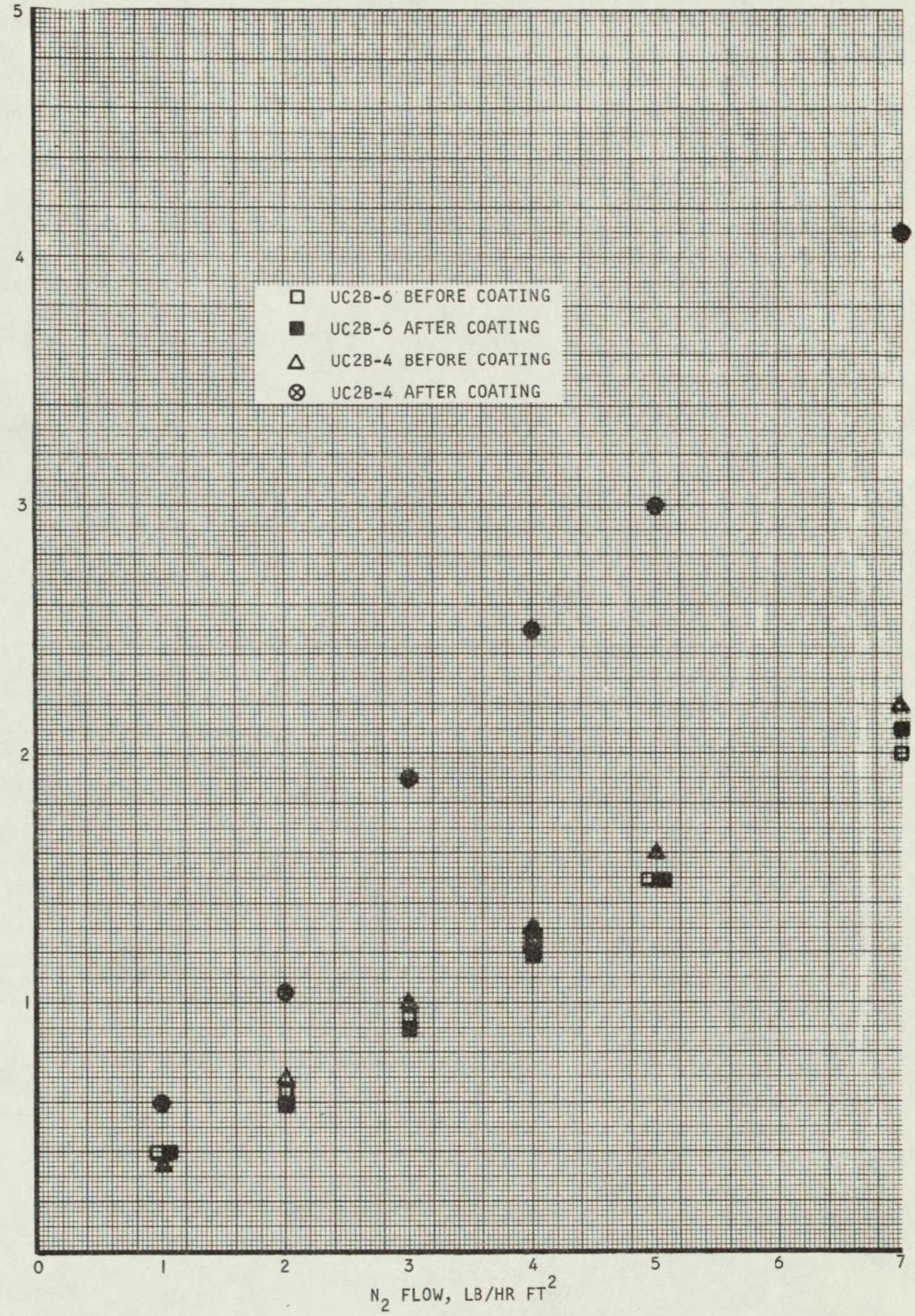


Figure 2-25. Permeability of Coated and Uncoated Plates

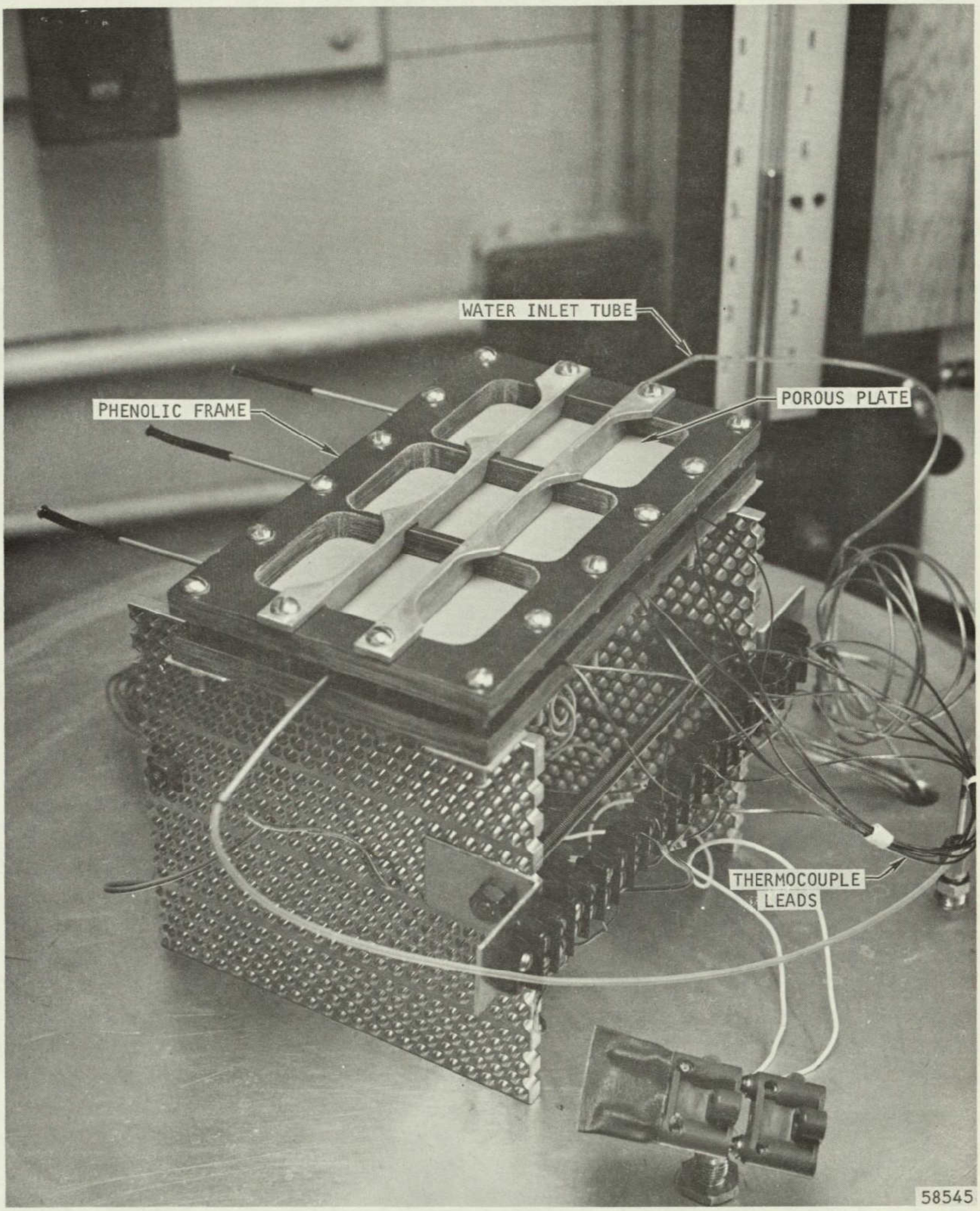


Figure 2-26. Porous Plate Sublimation Test Fixture

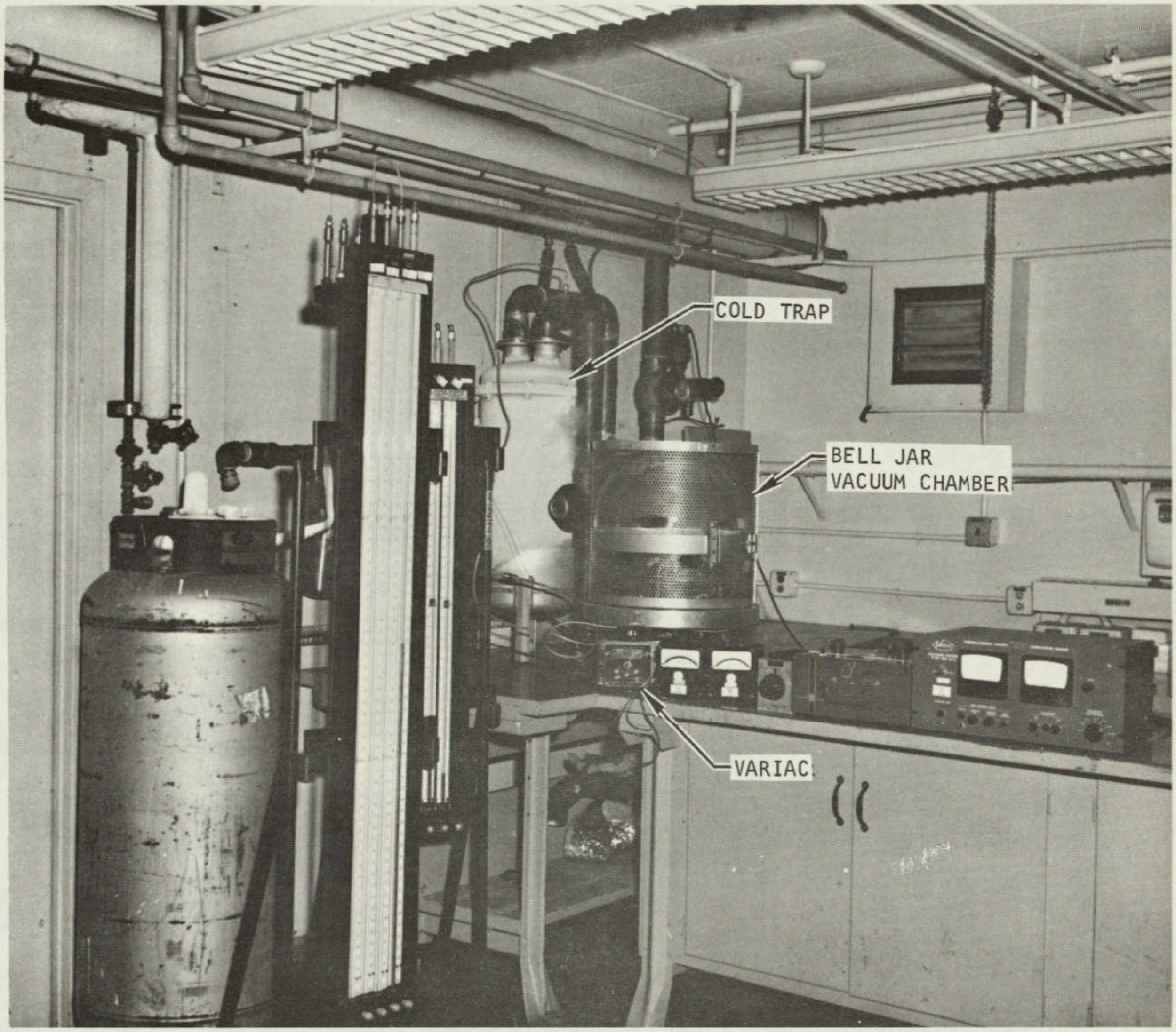


F-9741

Figure 2-27. Sublimation Test Apparatus

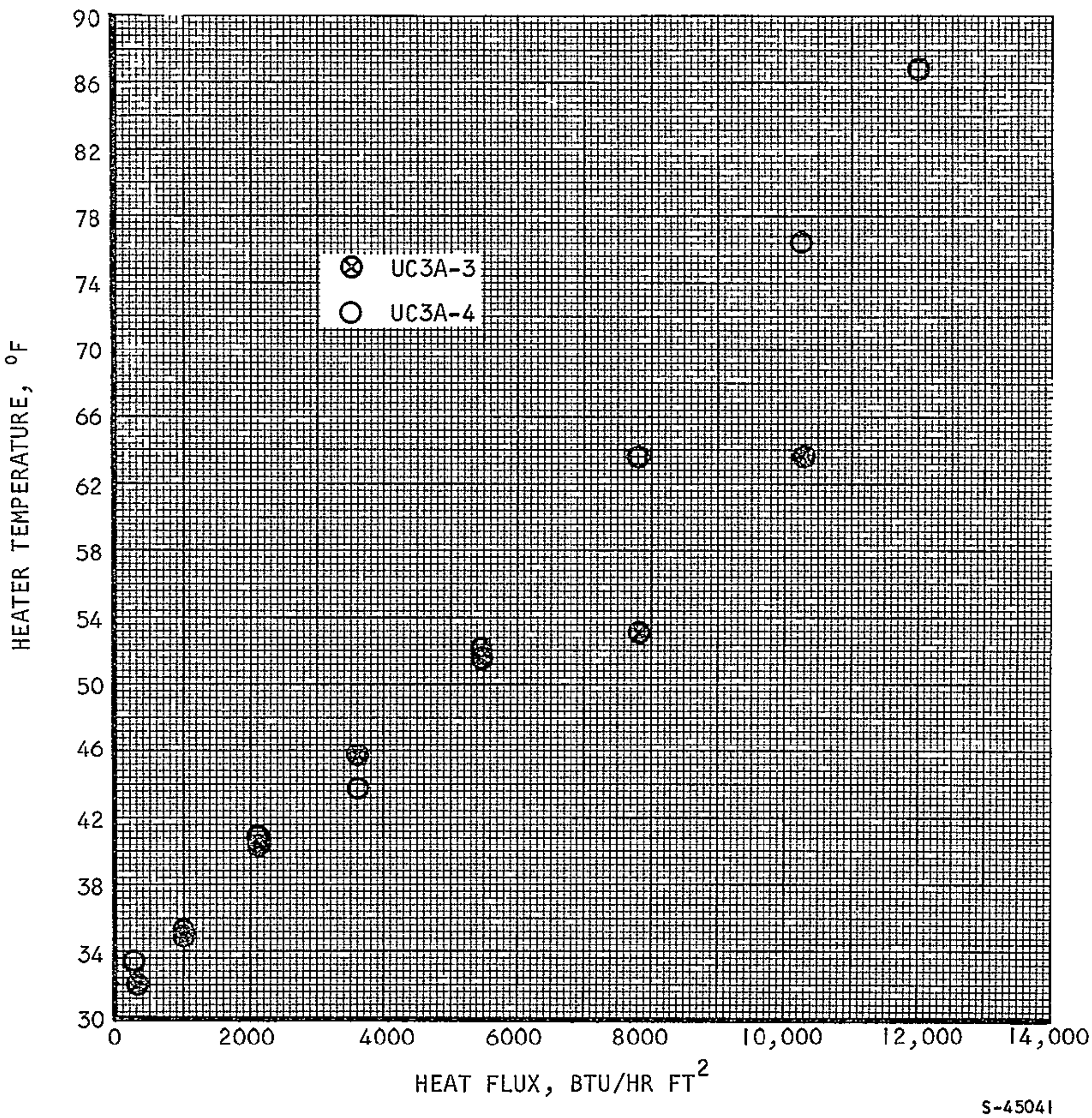


Figure 2-28. Porous Plate Sublimation Performance

penetrated deeply into the pores, poor sublimator performance would be expected since the evaporating interface would be near the upstream face of the plate and the pressure drop associated with vapor flow out of the plate would raise the local saturation temperature significantly. The data for these two plates is shown in Figure 2-29 along with the data for UC2B-4 before coating. While little difference existed between the two plates, the heat transfer performance of the coated plates was reduced significantly from their uncoated performance. This was undoubtedly due to penetration of the hydrophobic coating into the pores.

Tests were performed to determine whether or not the hydrophobic coating could restrain liquid in the porous plate and prevent breakthrough with no ice in the pores to block the liquid. Two plates were operated with downstream pressure above the triple point. This assured that no ice was present in the plates and was verified by the presence of liquid concensation on the inside of the bell jar. A heat flux of 3600 Btu/hr-ft$^2$ was applied to the plate and the plenum pressure increased incrementally. Observations of breakthrough were made and the results are shown in Table 2-17. It was seen that the hydrophobic coating does restrain the liquid in the plate when no ice is present.

TABLE 2-17

BREAKTHROUGH TESTS

| Plate | Plenum Pressure, psi | Bell Jar Pressure, in. Hg vac | Breakthrough |
|---|---|---|---|
| UC2B-4 | 3.00 | 29.2 | none |
| | 4.77 | 29.2 | none |
| | 4.91 | 29.2 | none |
| | 6.35 | 29.3 | minor |
| UC2B-6 | 2.61 | 29.2 | none |
| | 4.77 | 29.2 | none |
| | 6.64 | 29.3 | minor |

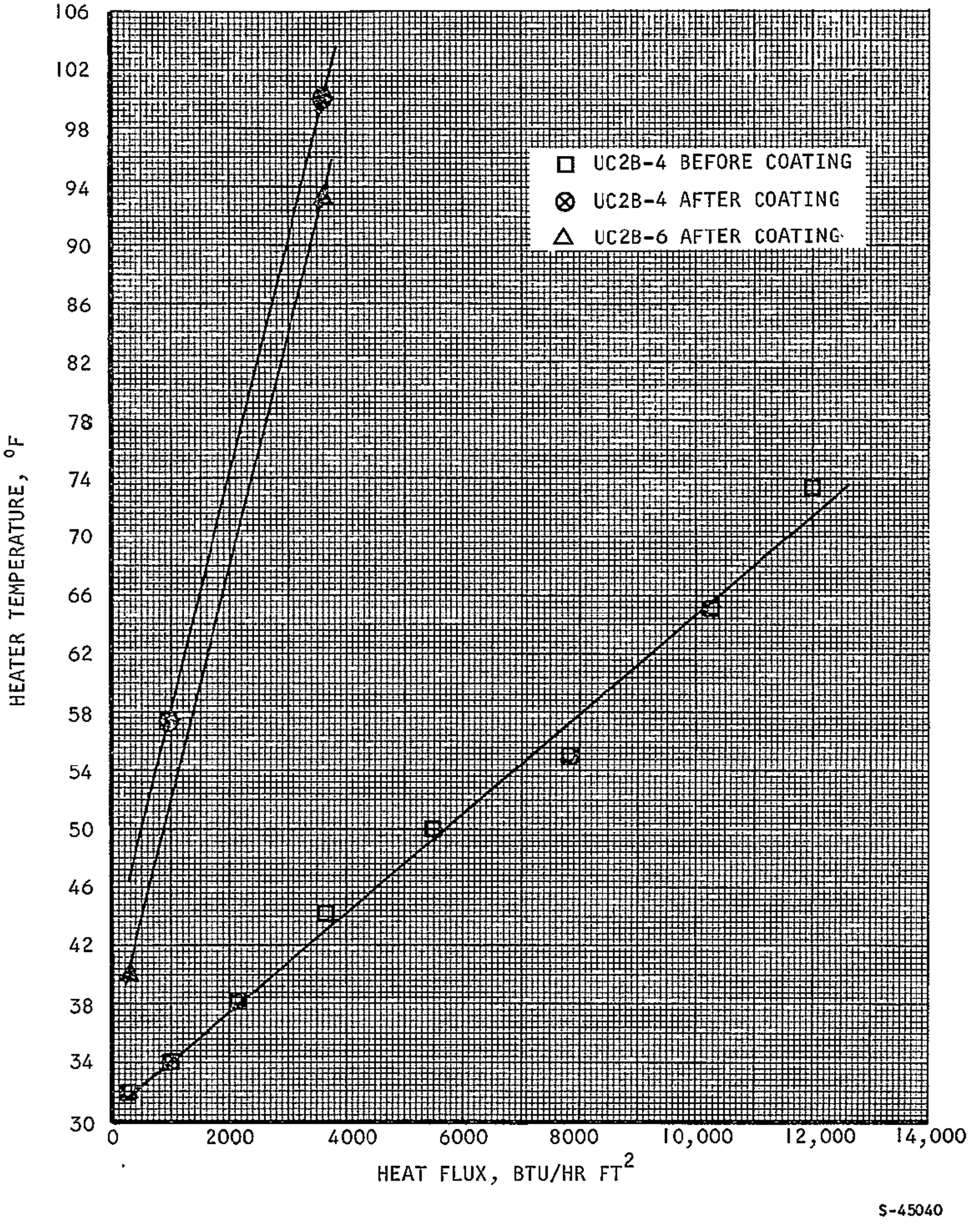


Figure 2-29. Coated Porous Plate Sublimation Performance

## Conclusions

Based upon the hydrophobic coating analysis and testing, the following conclusions were made:

(a) In order for a hydrophobic porous plate to give thermal performance close to that of an uncoated plate, the hydrophobic coating must not penetrate more than a few thousandths of an inch beneath the surface.

(b) Of the 22 compounds tested, MS-122 Fluorocarbon mold release appeared to be the most optimum as it gave the largest water contact angle (and thus the largest water retention pressure).

(c) The water retention pressure of coated hydrophobic plates increased significantly. The effect of coating on the plate permeability was inconclusive as tests indicated both no reduction and a 50 percent reduction in permeability on two coated plates.

(d) The coating method used in this study results in significant penetration of the hydrophobic film into the plate as evidenced by the significant degradation in thermal performance over that of the same plate in an uncoated condition.

(e) The presence of ice in the pores to restrain liquid was not necessary with a hydrophobic plate as evidenced by tests performed above the triple point.

## LARGE PORE SUBLIMATOR

### Background

An important problem associated with sublimator design and porous plate selection is the suspected gradual plugging of the plates due to the depositing of dissolved solids from the water. Obviously this phenomenon is a function of the length of operation of the sublimator, and, for extended operation, it may result in serious performance degradation. While it is possible to build the sublimator with enough plate area so that adequate performance will be obtained with a large percentage of the plate area plugged, it would be advantageous if sublimators could be designed with porous plates having pores large enough so that plugging problems would be greatly reduced. A large pore subbimator incorporating a bed of glass beads instead of a conventional porous plate was operated successfully during the previous study program. A further investigation of a large pore sublimator was performed during the current study.

### Testing and Test Results

It was decided to use sintered metal porous plates with large pores instead of the glass bead bed because a more meaningful comparison between large and small pore performance can be made if the porous structures were basically the same and various pore sizes were readily available in porous plates. Plates with manufacturer's quoted pore sizes fo 5, 20, 40, and 100 microns were ordered. Two 4 in. by 7 in. by 1/16 in. plates of each pore size were obtained. These samples represent nominal pore sizes ranging from those found in conventional plates to an order of magnitude larger than those normally encountered. In order to more completely define these plates, bench tests were performed on them. Initial and 80 percent bubble point in alcohol tests and water retention pressure tests were conducted on all the plates, and the results are tabulated below. Comparison of the tabulated values with those given in Table 2-15 showed the bubble points to be one to two orders of magnitude smaller than those recorded for the "conventional" plates. The smaller pressures were expected since bubble point is inversely proportional to the pore size.

| Plate | Initial Bubble Point in Alcohol, psi | 80 Percent Bubble Point in Alcohol, psi | Water Retention Pressure, psi |
|---|---|---|---|
| MM5-1 | 0.34 | 0.69 | 0.89 |
| MM5-2 | 0.34 | 0.69 | 0.89 |
| MM20-1 | 0.15 | 0.29 | 0.44 |
| MM20-2 | 0.15 | 0.29 | 0.44 |
| MM40-1 | 0.07 | 0.15 | 0.29 |
| MM40-2 | 0.07 | 0.15 | 0.29 |
| MM100-1 | 0.02 | 0.10 | 0.05 |
| MM100-2 | 0.02 | 0.10 | 0.05 |

The maximum equivalent pore size may be calculated from the alcohol initial bubble point data using:

$$\Delta P = 4\sigma/D$$

where $\sigma$ = surface tension of alcohol

$D$ = maximum equivalent pore diameter

The bubble point pressure is also a function of the contact angle and pore exit geometry (Reference 1). However, for a contact angle very nearly 0 deg, the effects of these other two parameters become negligible. It has been shown that the contact angle of alcohol is very nearly 0 deg on most reasonably clean surfaces (Reference 11), so use of the simplified equation is justified. The maximum equivalent pore diameters of the large pore plates are tabulated below:

| Plate | I.B.P., psi | Maximum Equivalent Pore Diameter, microns |
|---|---|---|
| MM5 | 0.34 | 39 |
| MM20 | 0.15 | 91 |
| MM40 | 0.07 | 182 |
| MM100 | 0.02 | 682 |

Specimen number MM5-2 was tested for permeability. Nitrogen gas was flowed through the plate with a vacuum (~400 microns Hg) discharge. The pressure drop across the plate as a function of mass flux is shown in Figure 2-30. Also shown for comparison was the most permeable conventional plate in the group of UC-2C series plates. The permeability of plate MM5-2 was approximately ten times that of plate UC3A-1. It was noted that the maximum equivalent pore diameter of plate UC3A-1 based upon previously reported bubble point data was 3.0 microns as compared with 39 microns for MM5-2. Therefore the permeability of these two plates correlated somewhat with the maximum pore size.

Plate MM5-2 was also heat transfer tested in the apparatus described previously with a plenum pressure of about 2 in. Hg abs. Heater plate temperature as a function of applied heat flux is shown in Figure 2-31. At the lower heat fluxes, the performance was comparable to that of the smaller pore plates; however, at the higher heat fluxes the performance dropped off. At the highest heat flux achievable, 7850 Btu/hr-ft$^2$, the heater-to-sink temperature difference (32$^\circ$F) was about 50 percent greater than that obtained with the small pore plates. With some of the small pore plates tested previously no minor or uncontrolled breakthrough was experienced up to a heat flux of 12,000 Btu/hr-ft$^2$. However, the large pore plate tested experienced minor breakthrough at 5500 Btu/hr-ft$^2$ and uncontrolled breakthrough at 8000 Btu/hr-ft$^2$.

The startup characteristics of the large-pore sublimator plates were not investigated since this was beyond the scope of the present work.

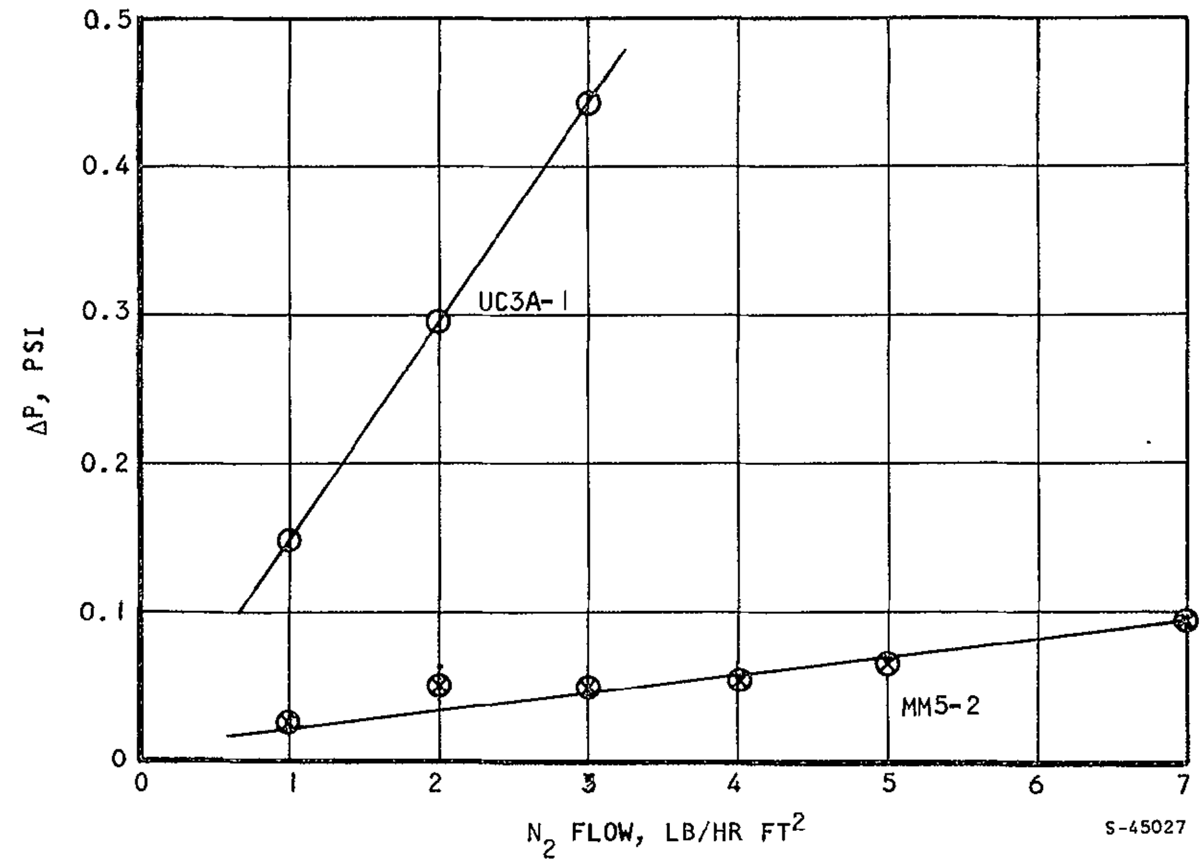


Figure 2-30. Nitrogen Permeability with Vacuum Discharge

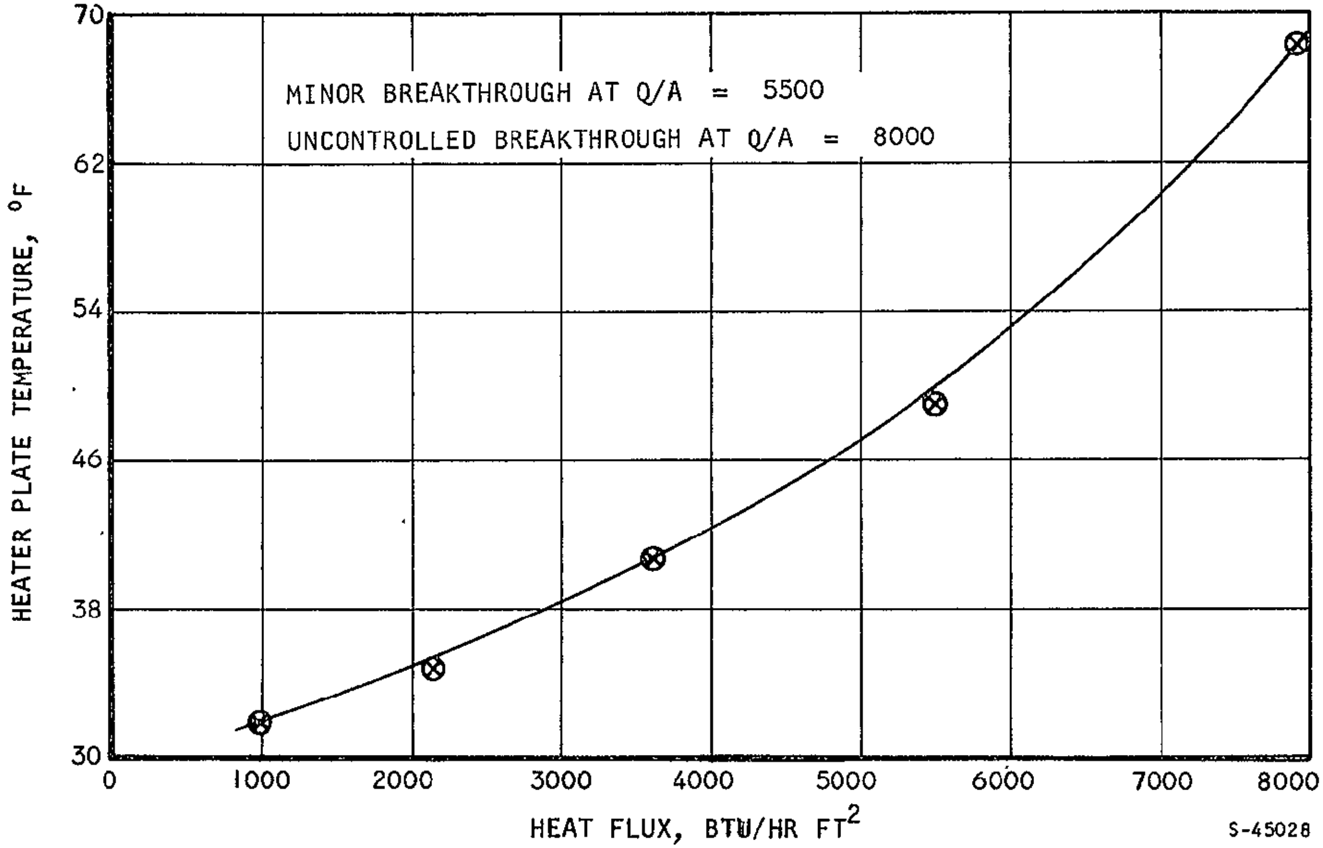


Figure 2-31. Large Pore Porous Plate Sublimator Performance

## Conclusions

The conclusion made based upon the large pore sublimation tests was that the large pore sublimations will operate at steady state. However, limited tests indicate that they have higher temperature drops and lower heat flux breakthrough limits than conventional porous plates.

## SECTION 3

## TASK II--THERMAL PANEL CONCEPT SELECTION

The basic panel designs, the simple wick boiler concept and the heat pipe concept that were retained throughout Task I, were tested in the form of panel modules. After a review of the performance of the test modules, the heat pipe sublimator concept was selected for further study because it offered the following advantages over the simple wick boiler concept.

Module testing had demonstrated the vulnerability of the simple wick boiler to airborne contamination of the wicking materials. Testing of this module had been repeatedly interrupted for recleaning of the wicking material. The data indicated that the simple wick boiler with the wick passages open to the atmosphere during nonuse or storage periods would present insoluble cleanliness problems. The heat pipe, on the other hand, is a permanently sealed device where, following the initial charge with the working fluid, the wicks are exposed only to a saturated water atmosphere.

The use of a sublimator to provide the ultimate heat dissipation for the panel simplifies the thermal controls requirements. The sublimator, with the formation of an ice block or the use of a hydrophobic substance, is self-regulating in its use of coolant water. The use of an 0.025-in. water passage ensures a minimum waste of stored coolant and allows less sensitive control of the expendable water feed rate. Further, the surface area available for heat dissipation in the sublimator will fix the operating temperature control band in the panel. A simple wick boiler would require accurate steam back-pressure control in order to provide temperature control within the desired range. The use of a steam pressure control valve would present possible real problems with the poppet during nonuse periods, and water that had been stored for the cooling of mounted components would be wasted.

The two important reasons for selecting the heat pipe sublimator over the simple wick boiler were the following:

(a) The heat pipe sublimator has freedom from contamination that the simple wick boiler does not.

(b) The heat pipe sublimator requires simpler controls than the simple wick boiler.

## SECTION 4

## TASK III--DESIGN AND FABRICATION OF FULL SIZE THERMAL PANEL

### INTRODUCTION

The heat pipe sublimator thermal conditioning panel designed and fabricated during Task III is shown in Figure 4-1. The primary component parts of the panel are the heat pipe, the remote coolant loop, the sublimator, the water reservoir, the water feed valve, and the structural sandwich. The panel surface to which heat generating equipment may be mounted has 168 mounting bosses which extend into the panel. As indicated in the magnified cut-away view, a heat exchanger passage is located immediately beneath the panel surface. This passage is the remote coolant loop that (1) provides thermal conditioning to the panel in conjunction with ground cooling during a preflight mode of operation, (2) provides cooling to the panel in conjunction with a remote heat sink during flight, or (3) provides cooling for remotely located equipment using the panel sublimator as a heat sink. These various functions are described in detail below.

### HEAT PIPE SUBLIMATOR PRINCIPLE AND MODE OF OPERATION

The heat pipe consists of a 15 percent dense nickel wick and a high thermal conductivity (copper) fin structure. The heat pipe is located beneath the remote coolant loop. The coolant loop extends over the entire panel surface. Heat generated by equipment mounted on the panel is conducted first through the fins of the remote coolant loop and then through the fins of the heat pipe layer to the surface of the wick. At the surface of the wick, heat is dissipated by the evaporation of water stored within the wick. The vapor generated travels outward from the point of evaporation through the steam passage fins, and is condensed either on the cooler portions of the thermal panel, or on the wick adjacent to the sublimator heat sink. The heat given up in condensing steam on the wick adjacent to the sublimator is conducted through the wick and dissipated by the sublimation of expendable water.

Expendable water is supplied from the bladder-type reservoir located on the panel surface immediately opposite the sublimator. The sublimator and water reservoir are located at the extreme edge of the 30 by 30-in. panel surface to provide a maximum-size uninterrupted area for mounting the cooled equipment. Water is delivered to the sublimator on demand through an on-off water flow control valve located in the area of the condensor and operating as a function of the vapor temperature.

The sublimator which serves as the ultimate heat sink is located at the condensor end of the panel with fins behind the sublimator plate to provide water dispersion to the entire porous plate. A plate-fin structural sandwich is brazed behind the heat pipe passage.

The design of the various panel components and a more detailed description of the operating characteristics of each are discussed below.

THERMAL DESIGN

Heat Pipe

The heat pipe portion of the thermal panel incorporates the liquid transporting wick material, the vapor passage, and the working fluid. A primary consideration in design of this portion of the panel is the selection of the working fluid because the design of the wick and vapor passage depends upon the working fluid properties. The desirable physical and thermodynamic properties may be identified based upon the heat pipe structure and operating mechanisms. Since the heat transfer principle involved in heat pipe operation utilizes the latent heat of vaporization of the circulating fluid, desirable fluid characteristic is a high heat of vaporization. The greater the heat of vaporization, the lower the flowrate of fluid required to transport a given amount of heat.

Resupply of fluid from the condensing surface to the evaporating surface is accomplished through capillary action, and thus, fluid properaties which aid wicking should be maximized. The wicking rate increases with higher surface tension, indicating the desirability of wicks with high values of surface tension. Wicking is also improved when the fluid wets the wick material well. Good wetting, which is indicated by a small contact angle between fluid and wick, is a function of both the fluid and the wick material; optimization of this property is therefore dependent upon both.

Low viscosity of the fluid in both its liquid and vapor states reduces the pressure drop associated with fluid flow, aiding in fluid recirculation and minimizing temperature losses inherent in the selected design.

Heat pipe working fluids should also (1) be thermally stable, (2) be chemically inert with the wicks, (3) have good structural properties, and (4) possess a low freezing point.

High thermal conductivity of the liquid is desirable in order to minimize temperature differences across the wick in the condensor area.

Certain of these properties may be grouped into a dimensional parameter which is proportional to the maximum heat transfer rate obtainable in a heat pipe for a given geometry. This fluid evaluation parameter is

$$E = \frac{\rho h_{fg} \sigma}{\mu}, \frac{\text{Btu-lb}_f\text{-hr}}{\text{ft}^3\text{-lb}_m} \tag{4-1}$$

where $\rho$ = fluid density

$h_{fg}$ = latent heat of vaporization

$\sigma$ = surface tension

$\mu$ = liquid viscosity

Table 4-1 lists values of E for various heat pipe working fluids at two temperatures which bracket the desired operating temperatures. The freezing points are also shown.

The choice of fluid also depends upon the desired operating temperature. At the operating temperature of the heat pipe, the fluid vapor pressure should be in the portion of the pressure-temperature curve that produces essentially isothermal conditions. Pressures should not be so high that pressure containment is a problem, since thin walls are desirable for heat transfer and weight economy. Figure 4-2 shows the pressure-temperature relationship of the working fluids given in Table 4-1, indicating the pressure levels associated with the range of operating temperatures.

From Table 4-1 and Figure 4-2, it is seen that water appears to be the best overall choice of working fluid in the temperature range of the current application. While dP/dT is larger for ethanol, methanol, and Freon 113, the parameter E is 4 to 28 times as large for water as for these other fluids. E for ammonia is fairly close to that for water; however, in the required temperature range, the vapor pressure of ammonia is 100 to 200 psia. Therefore, water was chosen as the working fluid for the full-sized thermal panel.

TABLE 4-1

HEAT PIPE POTENTIAL WORKING FLUIDS

| Fluid | Freezing Point, °F | E, $\frac{Btu\text{-}lb_f\text{-}hr}{ft^3\text{-}lb_m}$ 50°F | 100°F |
|---|---|---|---|
| Water | +32 | 108 | 186 |
| Ammonia | -112 | 60.5 | 40.7 |
| Methanol | -140 | 24.5 | 31.4 |
| Ethanol | -170 | 8.8 | 12.8 |
| Ethylbenzene | -130 | 7.4 | 11.7 |
| Freon 113 | -31 | 5.8 | 6.7 |
| Propyl alcohol | -196 | 4.1 | 6.5 |

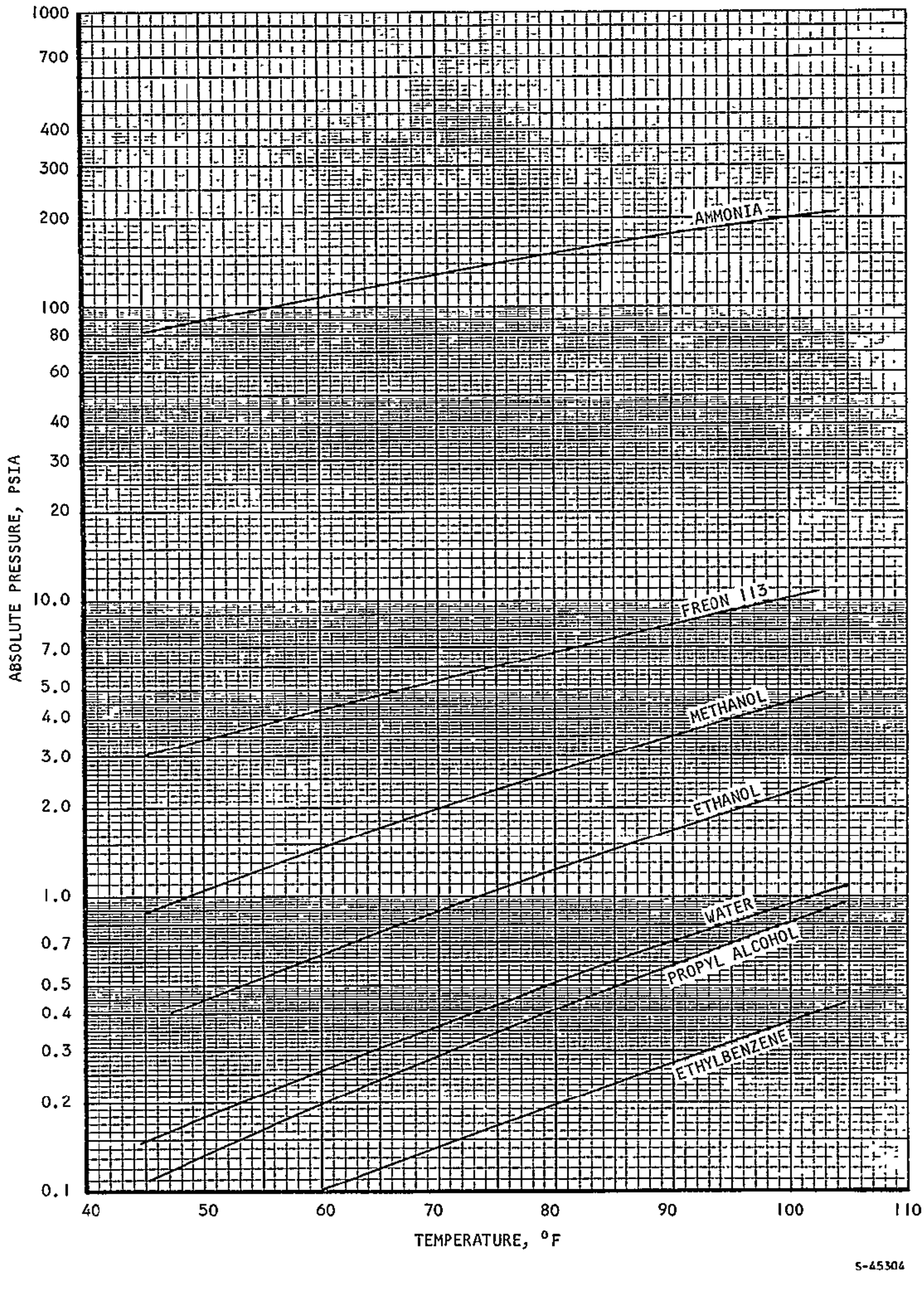


Figure 4-2. Vapor Pressures of Heat Pipe Fluids

Once the working fluid has been chosen, it is possible to size the wick. The two factors which are important in wick sizing are liquid transport and conduction temperature drop. The wick must be able to return liquid from the condensing area to the evaporating area at a sufficient rate to match the heat load requirements so that liquid is always available for evaporation. At the condenser section of the heat pipe, all the heat transferred out of the pipe to the sublimator must be conducted across the wick-water matrix. It is of course desirable to keep this conduction $\Delta T$ (as well as all $\Delta T$'s in the system) small.

The equation which is used to determine the required wick thickness based upon liquid transport requirements is developed from Equation (2-2) and the relationship $A_c = w\delta\phi$.

$$\delta = \left[\frac{Q_t \mu B \beta L}{h_{fg} w \phi 2 \rho g_o}\right] \left[\frac{1}{P_c - \rho L \frac{g}{g_o} \sin \psi}\right] \tag{4-2}$$

Equation (4-2) was solved as a function of nickel wick density for water at $70^oF$. Since the thermal panel is designed to operate in zero gravity, the second term in the bracketed denominator becomes 0. With the 3-in. wide sublimator heat sink located 1 in. from the edge of the panel and with the test load applied along the three furtherest rows of bosses, L is 27 in. and $Q_t$ is equal to the total heat load, 420 watts. Parameter $\beta$ is a function of the distribution of the heat load, and for the worst case (i.e., all the heat concentrated at one end of the panel) $\beta$ is equal to 1.74. The wick width w was taken as 28.49 in., accounting for the portion of the wick that is removed to allow room for structural webs. The wick properties B and $P_c$ were obtained as a function of wick porosity $\phi$ from Reference 2.

The required wick thickness as a function of wick porosity is shown in Figure 4-3. The solid line is for Equation (4-2), and the broken line incorporates a 0.8 factor that is recommended for use in liquid delivery equations. (The 0.8 factor was determined as a result of heat pipe module testing; refer to Figure 2-10 and the related discussion.) It is seen that a thinner wick is possible with a more porous structure.

The other consideration in the heat pipe wick design is the conduction $\Delta T$ across the wick at the condensor section. This temperature drop is characterized by the fundamental one-dimensional heat conduction equation.

$$\Delta T = \frac{Q}{A}\frac{\delta}{k} \tag{4-3}$$

In this case, k is the effective thermal conductivity of the wick-water matrix and $\delta$ is the wick thickness. The heat is dissipated through an area equal to that of the sublimator plates, and therefore the plate area determining the heat flux to be used in Equation (4-3). The required sublimator area is obtained from the total heat load and the available $\Delta T$ from the wick surface

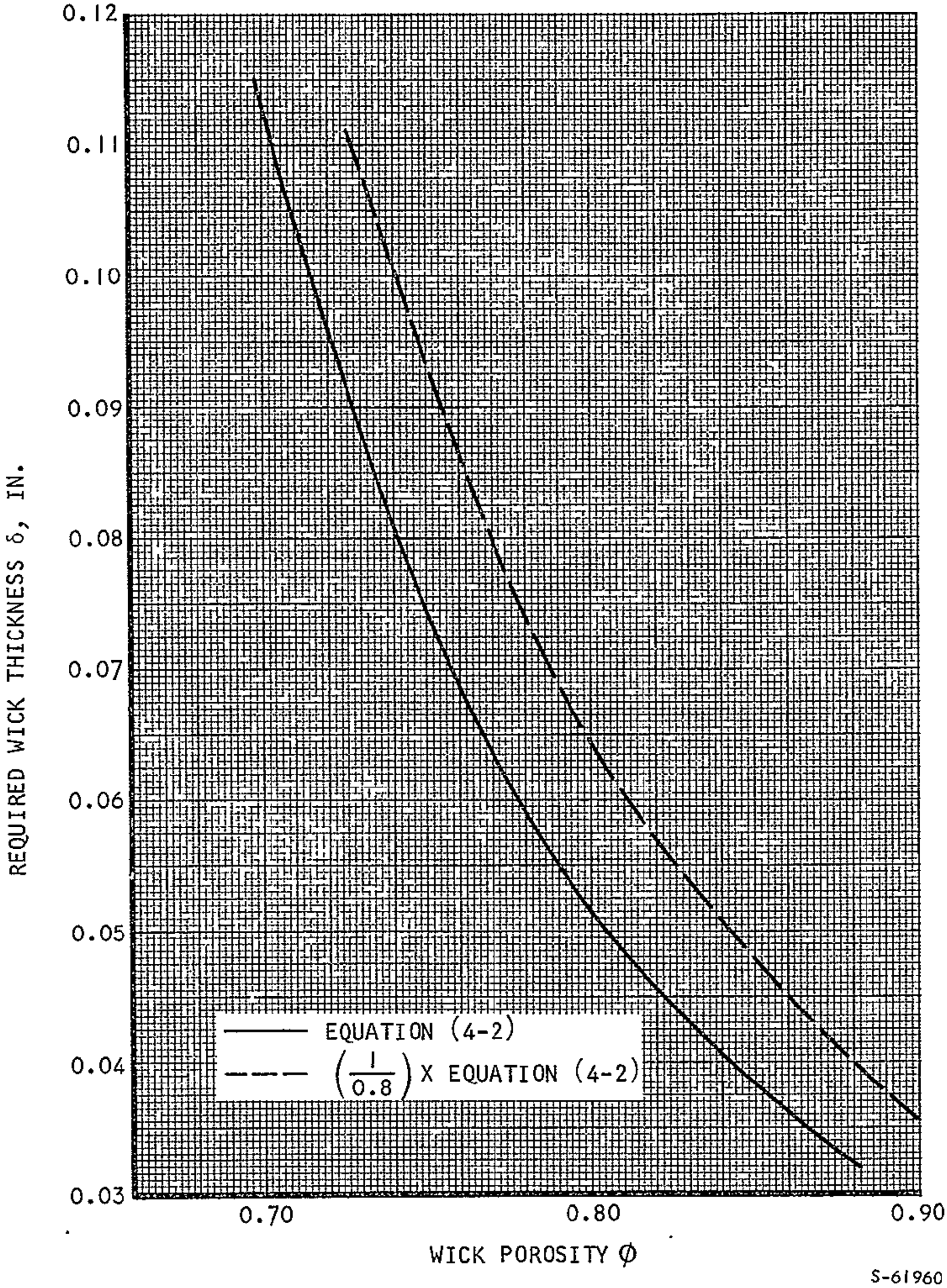


Figure 4-3. Required Wick Thickness as Defined by Liquid Delivery Requirements

to the sink temperature. This area is derived below in the discussion of sublimator design. In order to illustrate the relationship between the wick liquid delivery requirements and the heat transfer requirements, Equation (4-3) was solved for the temperature drop across the wick using the wick thickness required to meet the liquid delivery demands from the upper curve of Figure 4-3. The wick-water effective conductivity as a function of porosity was taken from correlations of experimental data in Reference 12. A heat flux defined by the sublimator final design area and the maximum heat load was used. The results are shown in Figure 4-4. At smaller porosities with the wick porosity increasing, the conduction $\Delta T$ decreases because the wick thickness $\delta$ defined by the liquid delivery requirements decreases faster than the effective conductivity. Above about 82 percent porosity, however, the $\Delta T$ increases because k now decreases faster than $\delta$. The lowest conduction $\Delta T$ is obtained with a wick in the 80 to 85 percent porosity range as indicated in Figure 4-4.

The plot of required wick thickness shown in Figure 4-3 was based upon the case of the heat load concentrated along the edge of the panel furthest from the sublimator and accounted for the wick area lost to the structural webs in the heat pipe. While this plot is valid for this particular case and illustrates the effect of porosity on thickness, a more severe condition exists for design purposes, i.e., the case in which the heat input is concentrated in one of the far corners. The liquid flow in the wick is two dimensional in this case and the equations describing this phenomenon are not developed. The analysis is further complicated by the intermittent webs which block liquid flow in the direction normal to their alignment. The wick was designed by assuming liquid flow over the two paths shown in Figure 4-5. A modified form of Equation (4-2) was used in the design. A wick porosity of 85 percent was selected for the heat pipe wick as this was in the range of porosities which gave the lowest temperature drop. The heat pipe wick was designed to be 0.080-in. tnick. Although this is somewhat thicker than the analytical requirement, it was considered advisable to provide a design margin for several factors that may affect liquid delivery rate. The first of these is a lack of uniformity in the wick porosity. Experience has shown that the local porosity of fiber metal wicks may vary across the surface and additional wick thickness is required to offset the reduced wick pumping capacity in those areas where the porosity is less than the overall average. The 168 mounting bosses extend through the heat pipe and local areas of the wick must be removed to allow for the bosses. The additional wick thickness offsets the local reduced wick flow area in these regions.

The heat pipe vapor passage in this design is somewhat different than that in a conventional heat pipe. The conventional design has no fins in the vapor passage; however, fins are required in this design to conduct heat to the wick since it is not located against the hot surface. The vapor passage design therefore is performed to minimize both the vapor pressure drop through the fin and the conduction temperature drop across the fin.

The overall heat transfer coefficient associated with evaporation, $h_o$, is defined for the current configuration by an emperical correlation given in Reference 2.

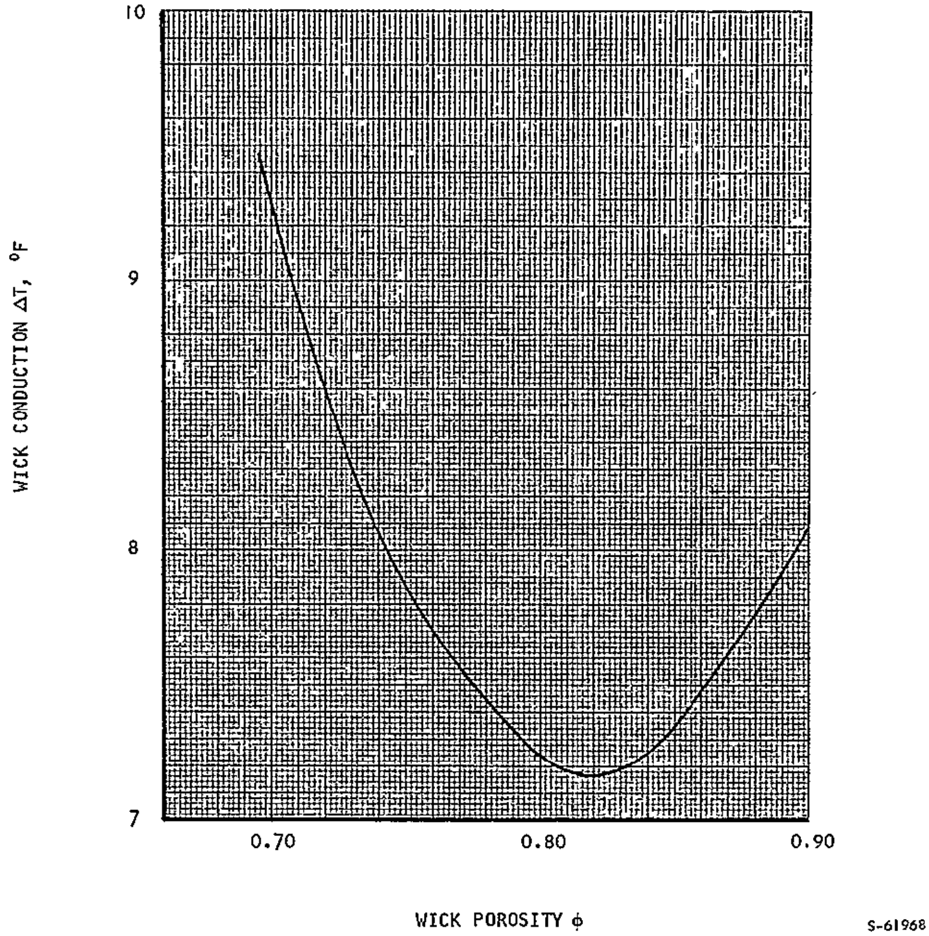


Figure 4-4. Conduction Temperature Drop Through Wick of Condensor End for Required Wick Thicknesses

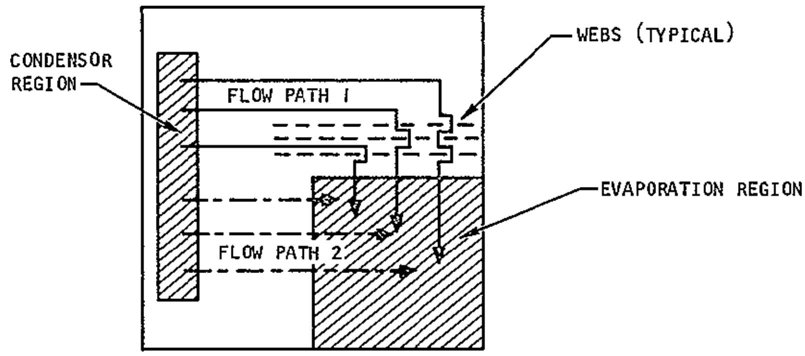


Figure 4-5. Two-Path Liquid Flow

$$\frac{1}{h_o} = \frac{1}{h_f} + \frac{1}{h_{evap}} \quad (4-4)$$

where $h_f$ is an effective fin conduction heat transfer coefficient defined as

$$h_f = \frac{k_f \, \delta_f \, N}{b} \quad (4-5)$$

where $k_f$ = fin thermal conductivity

$\delta_f$ = fin thickness

$N$ = number of fins per inch

$b$ = fin height

The evaporation heat transfer coefficient at the fin-wick interface, $h_{evap}$, was determined experimentally in Reference 2 and is given as 904 Btu/hr-ft$^2$-$^0$F at a saturation temperature of 35$^0$F and 1022 Btu/hr-ft$^2$-$^0$F at 60$^0$F.

To minimize the fin $\Delta T$, copper with its high thermal conductivity is specified as the fin material, and a large conduction area is achieved by using a high density fin. Several fins were analyzed and the same fin used in the steam passage of the heat pipe test module was selected for use in the full size panel, i.e., 28 fins/in., 0.25-in. high, 0.002-in. thick, and 1/8 in. offset. An offset fin is specified to allow for vapor flow in all directions which may be necessary as the locations of the mounted heat generating components is not fixed. Evaluation of $h_f$ is complicated because of the uncertainty in the fin thermal conductivity. During brazing of a copper fin, the braze alloy penetrates the copper and a lower conductivity alloy is formed. The copper fin used in the experiments from which Equation (4-4) was developed was 0.101-in. high and 0.008-in. thick with 16 fins/in., and the thermal conductivity measured after brazing was 115 Btu/hr-ft-$^0$F. The effective fin conductivities after brazing of the 0.008-in. and 0.002-in. thick fins were assumed the same (115 Btu/hr-ft-$^0$F). The time required at braze temperature and the aggressiveness of the EMS9-4778 braze alloy make this a valid assumption. It will be shown below that its validity is somewhat substantiated by the small scale heat pipe module test data.

For the specified fin, $h_f$ becomes:

$$h_f = \frac{k_f \, \delta_f \, N}{b} = \frac{(115)\ (0.002)\ (28)}{(0.25/12)}$$

$$= 309 \text{ Btu/hr-ft}^2\text{-}^0\text{F}$$

The overall evaporation coefficient $h_o$ is:

$$h_o = \frac{1}{\frac{1}{h_f} + \frac{1}{h_{evap}}} = \frac{1}{\frac{1}{309} + \frac{1}{1022}}$$

$$= 237 \text{ Btu/hr-ft}^2\text{-}^\circ\text{F}$$

The local heat flux to the wick is increased because the fin area must be reduced to allow for the bosses and webs. The fin area is 83 percent of the plan area so that for the maximum design heat flux of 1230 Btu/hr-ft$^2$ (10 watts/boss) the overall evaporation $\Delta T$ based upon a fin thermal conductivity of 115 is

$$\Delta T = \frac{Q/A}{h_o} = \frac{(1230/.83)}{237} = 6.3^\circ F$$

In the heat pipe test module (which incorporated this fin), a total $\Delta T$ (i.e., the difference in temperature between the top of the fin and the saturation temperature) of 4.7°F was obtained at a heat flux of 1000 Btu/hr-ft$^2$. Since the controlling heat transfer mechanism at these relatively low heat fluxes is conduction, the experimental $\Delta T$ may be ratioed by the heat fluxes. The total $\Delta T$ associated with conduction through the fins and evaporation for the full-size panel will be

$$\Delta T = \frac{(1230/.83)}{1000} (4.7^\circ F) = 7.0^\circ F$$

The experimental data indicates that the evaporation $\Delta T$ may be slightly higher than predicted analytically.

The pressure drop of the vapor flowing from the evaporator area to the condenser must be kept small in order to minimize the $\Delta T$ associated with the difference in saturation temperatures at the evaporator and condenser. For the case of all the heat input concentrated along the side furthest from the sublimator, the pressure drop is determined from the conventional one-dimensional flow pressure drop equation.

$$\Delta P = \frac{4fL}{D_h} \cdot \frac{G^2}{2g\rho} \qquad (4\text{-}6)$$

where $f$ = friction factor for the fin configuration used

$D_h$ = hydraulic diameter of steam passage

$G$ = mass flux

The friction factor is determined from experimental correlations of f as a function of the Reynolds number.

With the heat input concentrated along the end of the panel furthest from the sublimator, the flow length from the middle of the heat input area to the middle of the sublimator area is 23.5 in. At the maximum water vapor flow rate, a Reyonlds number of about 6 (based upon the hydraulic diameter of the fin in the steam passage) is obtained, indicating operation in the laminar flow regime. Because the bosses extend through the heat pipe, the free-flow area is smaller over that portion of the flowpath between the bosses, and the pressure drop was calculated separately for each section of the flowpath with a different free flow area. The pressure drops were summed and an overall pressure drop of 0.046 psi was obtained for maximum heat load conditions. For a 60°F temperature at the condenser end of the heat pipe, a 0.046 psi pressure drop results in a 4.6°F change in saturation temperature from one end of the heat pipe to the other.

Remote Coolant Loop

The remote coolant passage must be capable of serving several functions. In the preflight mode, it must serve to cool electronic components mounted on the panel using ground support cooling equipment. The passage should be such that it could be hooked into the existing instrument unit cooling loop and operate using sublimator cooling as long as the expendable evaporant supply lasts. It must also function as the transport loop for cooling of remote equipment, i.e., the fluid in the passage would circulate to equipment located remotely to the thermal panel, cool that equipment, and return to the panel where the fluid would be cooled using the thermal panel sublimator as the heat sink.

The instrument unit thermal panel problem statement was used to design the remote coolant passage. The coolant was taken as 60 percent methanol and 40 percent water by weight, flowing at 3.60 lb/min at an inlet temperature of 60°F. For the maximum heat load of 420 w, the coolant bulk outlet temperature is

$$T_{out} = T_{in} + \frac{Q}{W_o C_p} \tag{4-7}$$

$$= 60 + \frac{(420\ \text{w})\ (3.414\ \text{Btu/hr-w})}{(3.60\ \text{lb/min})\ (0.8\ \text{Btu/lb-}^{\circ}\text{F})\ (60\ \text{min/hr})}$$

$$T_{out} = 60 + 8.3 = 68.3^{\circ}\text{F}$$

It is possible to encounter a local outlet temperature higher than 68.3°F if the heat input is concentrated along the edge of the panel as shown in Figure 4-6. Since the Reynolds number is below 100 and the flow is laminar, very little mixing occurs across the passage and the fluid under the unheated section heats up very little while that under the heated section absorbs all the heat. For this worst case condition:

$$T_{max\ out} = T_{in} + \frac{Q}{W_o C_p}\ \frac{\ell}{\ell'} \tag{4-8}$$

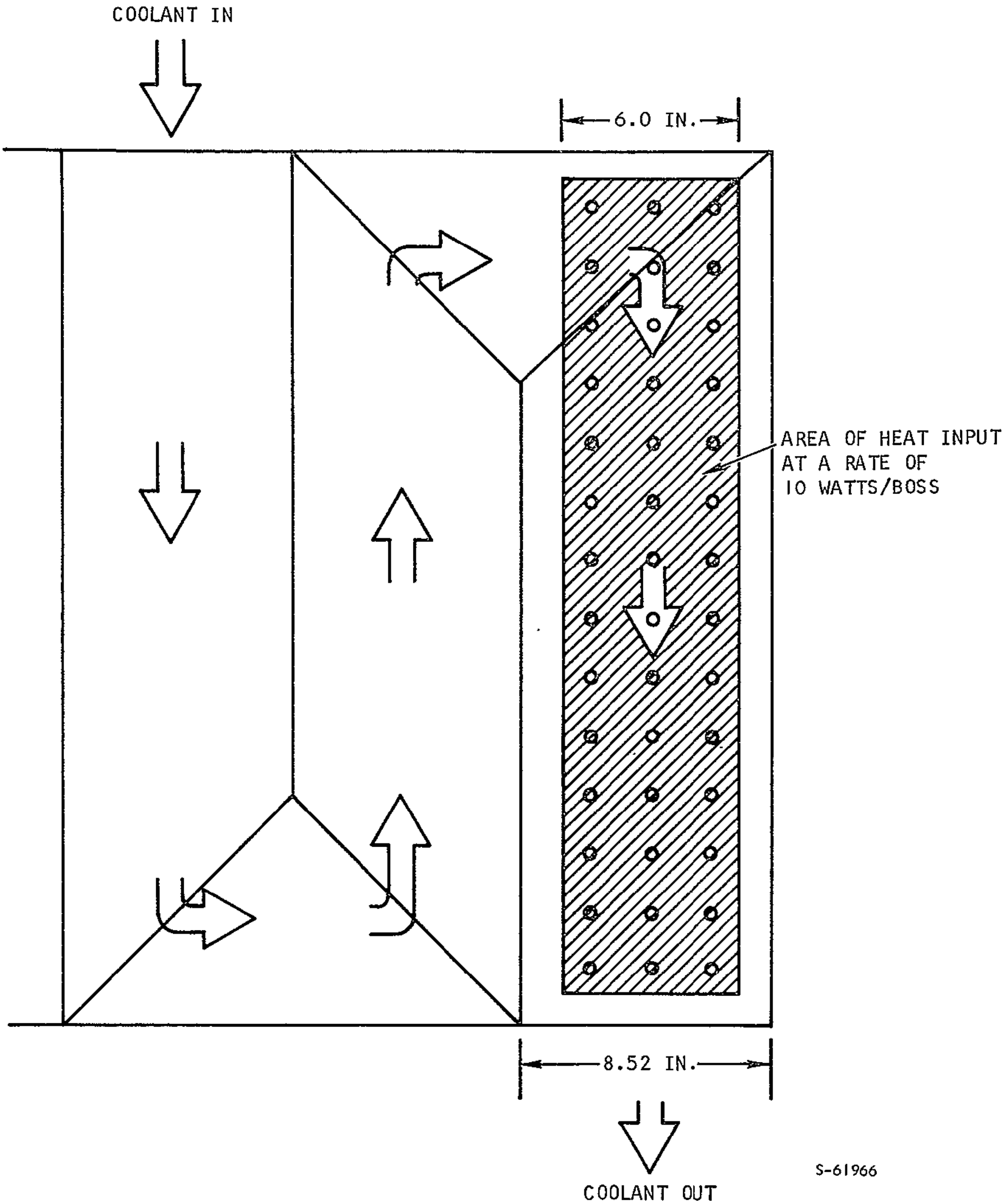


Figure 4-6. Worst Case Heat Input to Remote Coolant Loop

where $\ell$ = fluid passage width

$\ell'$ = width over which heat is input

With 420 watts input over the last three rows of bosses ($\ell' \approx 6$ in.), Equation (4-8) gives for the maximum local fluid outlet temperature:

$$T_{max\ out} = 60 + 8.3\,\frac{8.52}{6.0} = 71.8^{\circ}F \tag{4-9}$$

The coolant loop must be designed so that maximum panel surface temperature $T_{P\ max}$ does not exceed 90°F. The required conductance per unit area of the panel surface, $\frac{\eta h A_{HT}}{A}$, may be determined from the maximum design heat flux and the basic convection equation.

$$\frac{Q}{A} = \frac{\eta h\ A_{HT}}{A}\left(T_{P\ max} - T_{max\ out}\right)$$

$$\frac{\eta h\ A_{HT}}{A} = \frac{Q/A}{T_{P\ max} - T_{max\ out}} \tag{4-10}$$

For the maximum heat flux of 1260 Btu/hr-ft$^2$, the required conductance is

$$\frac{\eta h\ A_{HT}}{A} = \frac{1260}{90.0 - 71.8} = 69.1\ \frac{\text{Btu/hr-}^{\circ}\text{F}}{\text{sq ft of panel surface}}$$

The design of the remote loop must be such that the pressure drop is not excessive. A pressure drop of 6 psi was taken as the maximum allowable, and the conventional pressure drop equation with experimental friction factors was used for the calculation.

A major consideration in the design of the remote loop is the requirement for a small thermal conduction resistance across the passage. When the loop is not functioning, the heat generated on the panel is conducted across this passage to the heat passage to the heat pipe, and it is desirable to have a small conduction temperature drop across the panel. The conventional conduction equation was used to calculate the conducton temperature drop across the panel at the maximum heat flux.

For this design, obtaining a small conduction ΔT was a more severe design condition than obtaining the required conductance of 69.1 Btu/hr-ft$^2$-°F. The small conduction ΔT was obtained by designing with a relatively short and thick fin configuration. Several fin configurations were analyzed, and a 20 fins/in., 0.050-in. high, 1/10-in. offset, 0.004-in. thick nickel fin was selected. With this fin and a 3- pass remote coolant loop design, the conductance per unit area, $\frac{\eta h A_{HT}}{A}$, at the design flow rate is 835 Btu/hr-ft$^2$-$^0$F, an order of magnitude larger than that required, resulting in a predicted maximum panel temperature of about 74$^0$F at the design flow rate. The predicted drop with this configuration is 3.5 psi. When the loop is not functioning, the conduction temperature differential across it at the maximum heat flux is 3.5$^0$F if there is fluid in the passage or 4.3$^0$F if it is empty.

There is also a temperature drop associated with conduction through the stainless steel plates on each side of the remote loop fin. The conventional one dimensional conduction equation applies, and at maximum heat flux, $\Delta$Ts of 0.8$^0$F and 0.4$^0$F were calculated for the upper .063 inch thick plate (actual part thickness) and the lower 0.032-in. thick plate respectively.

Sublimator

The sublimator is the ultimate heat sink of the thermal panel. All the heat input to the panel is dissipated in sublimation of the expendable water stored in a reservoir attached to the termal panel. The heat from the heat pipe condenser region is conducted through the heat pipe wick, through the tube plate, through the sublimator plenum, and into the porous plate where it is dissipated in sublimation. The temperature drop through the sublimator is a function of the plenum geometry and the sublimator plate area.

Tests conducted during the previous program and reported in Reference 1 showed that plate damage during water plenum freeze-up is also important. These tests indicated that plate damage can be eliminated by reducing the plenum height to a small value. Reduction of the plenum height also decreases the thermal resistance across the plenum. A plenem height of 0.025 in. was chosen for the thermal panel sublimator since this height is small enough to reduce plate rupture problems while not introducing serious fabrication problems.

A 40 fins/in., 0.001-in. thick nickel finned structure is inserted in the plenum to support the porous plate at the 0.025-in. spacing and to increase the conductance of the water plenum.

The following equation defines the temperature drop through the heat pipe wick, the tube plate, and the sublimator:

$$\Delta T = Q\,(R_{wi} + R_p + R_s) \qquad (4\text{-}11)$$

where $Q$ = rate of heat transfer

$R_{wi}$ = wick thermal resistance = $\frac{\delta_{wi}}{k_{wi} A}$

$R_p$ = tube plate thermal resistance = $\frac{\delta_p}{k_p A}$

$R_s$ = sublimator thermal resistance = $\frac{1}{h_s A} + \frac{1}{\frac{k_f A_f}{b} + \frac{k_w A_w}{b}}$

$h_s$ = sublimation heat transfer coefficient

$A$ = sublimator plate area

$k_f$ = water plenum fin thermal conductivity

$A_f$ = water plenum fin conduction heat transfer area

$b$ = water plenum fin height

$k_w$ = water thermal conductivity

$A_w$ = water conduction area in plenum

$\delta_p$ = tube plate thickness

$k_p$ = tube plate thermal conductivity

$\delta_{wi}$ = wick thickness

$k_{wi}$ = wick-water matrix effective thermal conductivity

The sublimination coefficient for the porous plate selected (plates of the UC-2C series) was determined from test data given in Reference 1 and found to be 1150 Btu/hr-ft$^2$-$^\circ$F. Equation (4-11) shows that the overall temperature drop in the sublimator region is inversely proportional to the area. Therefore, the temperature level at which the heat pipe operates at maximum heat flux will be fixed by the area of the sublimator. Equation (4-11) was solved for $\Delta T = f(A)$ using the selected wick and fin and the results are shown in Figure 4-7. A sublimator area 3.0 in. by 19.5 in. (0.407 sq ft) was selected, and this area gives a steady state $\Delta T$ of 28$^\circ$F. Adding this to the 32$^\circ$F sink temperature yields a heat pipe cold end temperature of about 60$^\circ$F. The temperature drop of 28$^\circ$F is made up of a 14.9$^\circ$F drop through the sublimator, a 1.2$^\circ$F drop through the tube plate, and a 11.9$^\circ$F drop through the heat pipe wick. The control system will have an effect on the cold end $\Delta T$ since the water feed is intermittent. With a heat pipe cold end steady-state temperature below the temperature at which the water valve is activated, the actual $\Delta T$ will be transient. This aspect is discussed in Appendix A.

The analtyical temperature drops associated with the various elements of the heat pipe-sublimator thermal panel are tabulated below.

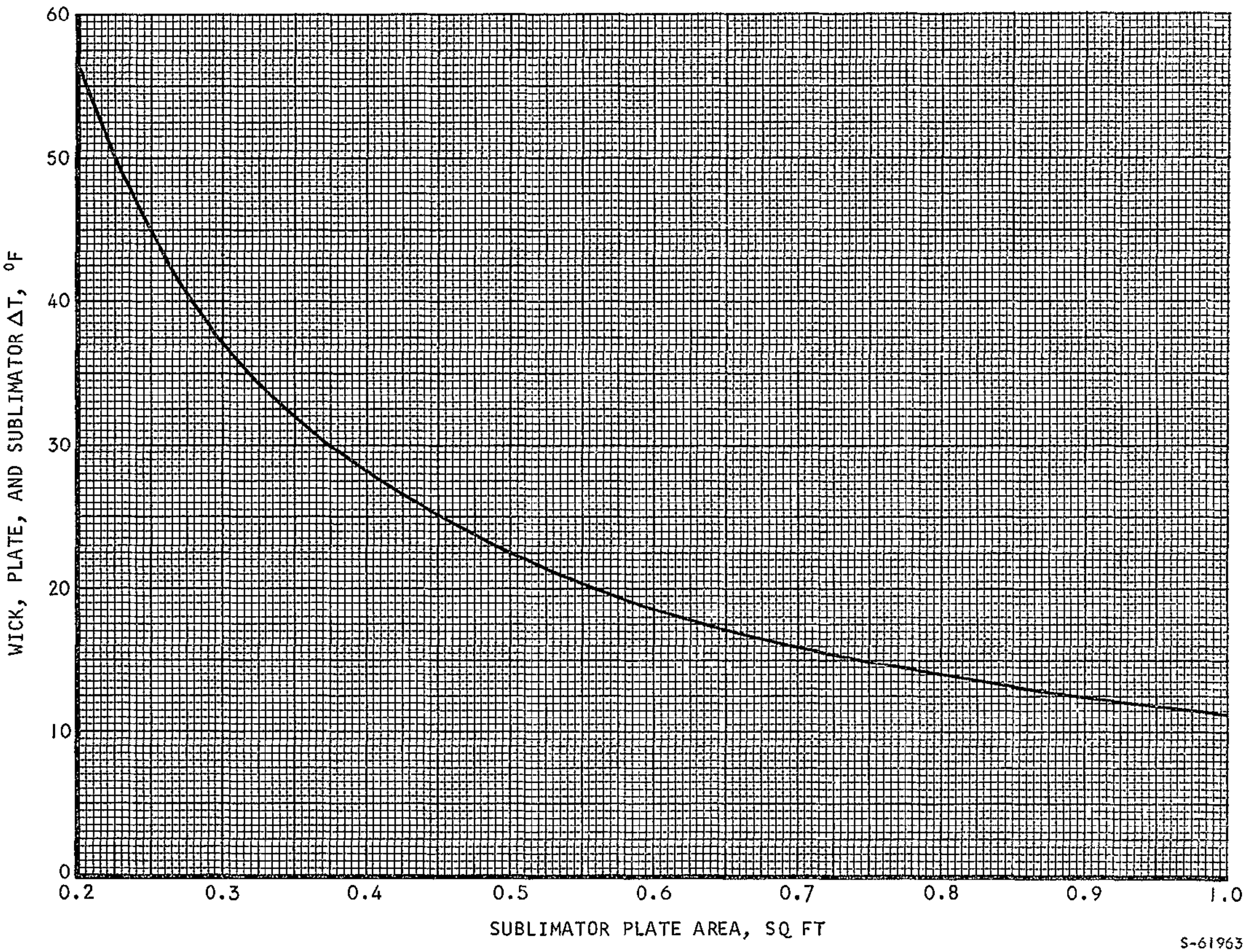


Figure 4-7. Effect of Sublimator Area on Temperature Drop Through Sublimator and Condenser End Wick

| Panel Element | Temperature Drop, $^{\circ}F$ |
|---|---|
| Sublimator (conduction and sublimation) | 14.9 |
| Tube plate (conduction) | 1.2 |
| Heat pipe wick (conduction) | 11.9 |
| Vapor passage (change in saturation temp.) | 4.6 |
| Evaporator end (conduction in fin and evaporation) | 7.0 |
| Tube plate (conduction) | 0.4 |
| Remote loop fin (conduction) | 4.3 |
| Upper tube plate (conduction) | 0.8 |
| | 45.1 |

With a sublimator sink temperature of 32°F, the 45°F temperature differential results in a predicted surface temperature of 77°F.

The use of individual heat pipes instead of one large heat pipe plenum was considered during the panel design phase. The individual heat pipes could have been of the conventional circular cross section, or they could have been planar heat pipes of rectangular cross section. It should be noted that the heat pipe thermal panel test module was designed in January 1967 and the selection of the design was based on the current heat pipe state of the art.

Circular-cross-section heat pipes at that time used multilayer screens as the wick structure. AiResearch had no experience with screen wicks at that time. It was thought advisable to use sintered fiber metal wicks, because AiResearch had gained experience with these wicks during the initial phase of the study. Fabrication of fiber metal wicks into the inside of small diameter heat pipe tubes appeared to be a very difficult problem, and this was considered an important factor against the use of circular cross section heat pipes.

Design requirements stipulate that the heat load can be arranged in any configuration on the panel surface. With individual heat pipes, a situation in which all the heat load must be carried by a few of the heat pipes could occur. This is shown schematically on the following page. This means that the wicks and vapor passages must be larger than in the single heat pipe concept where "cross-flow" of both liquid in the wick and vapor in the vapor passage can occur. Also, with the heat load concentrated along a few individual heat pipes, only that portion of the sublimator adjacent to the active heat pipes would recieve the heat load. The temperature drop through the sublimator would be significantly greater than that which would occur if heat were dumped to the entire sublimator. With one large sublimator, there can be ice in the areas adjacent to the inactive heat pipes (no local heat load), while the area under the active heat pipes may have dried out. If only one temperature-actuated control were used and if that control were located in a "cold" inactive

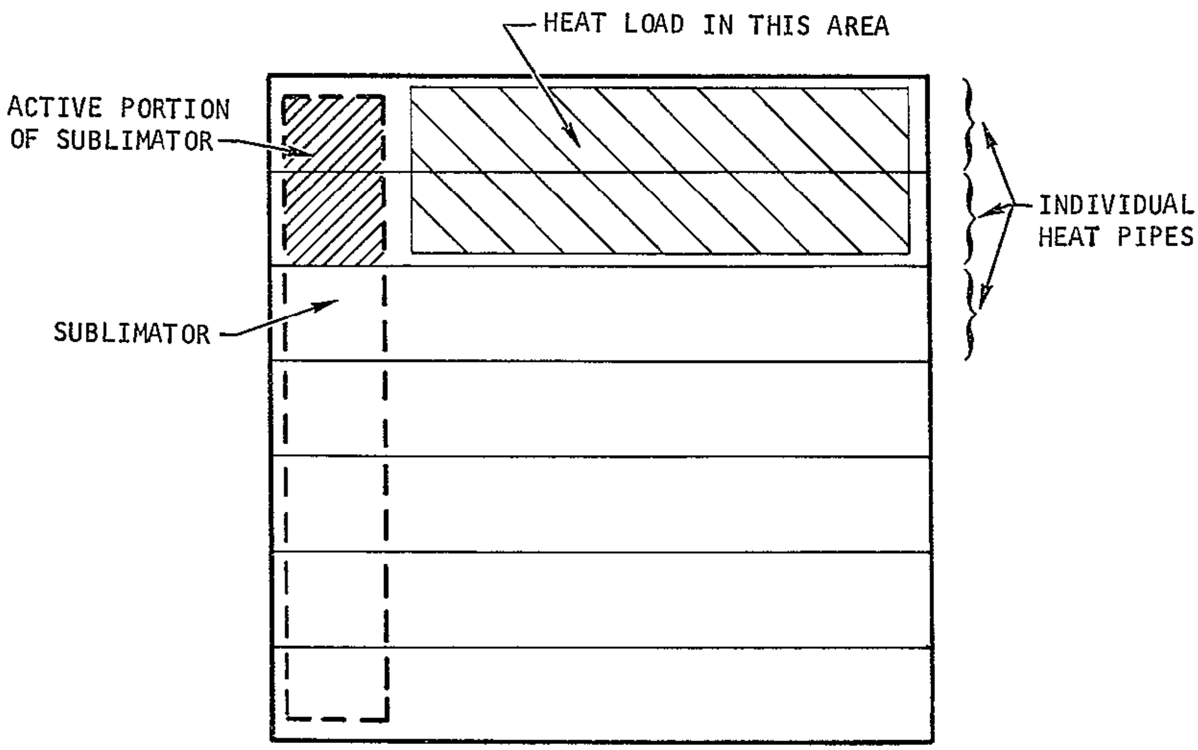


area, no more water would be fed to the sublimator and, with the sublimator dry under the active heat pipes, the panel surface temperature would increase above the allowable level. Thus, individual heat pipes would require individual sublimators, each with their own control system. The only configuration that permits the use of individual heat pipes is one with another layer of heat pipes at right angles to the primary heat pipes. In this way, the heat would be distributed more uniformly to the sublimator; however, the additional temperature drops associated with heat transfer from one heat pipe to another heat pipe and the additional weight made this approach undesirable.

In order to use one sublimator with one temperature sensing control valve and to assure that the entire sublimator would be used, the most practical solution was one large heat pipe plenum.

SUBLIMATOR WATER RESERVOIR DESIGN

The sublimator water reservoir was sized to hold 11.5 lb of water to provide 8 hr of cooling at the maximum heat load of 420 watts. The reservoir is located on the front face of the panel opposite the sublimation and uses a pressurized reversible bladder for water expulsion. The reservoir is charged by filling one side of the bladder with water and pressurizing the other side with nitrogen gas. As water is used, the volume on the gas side of the bladder increases and the pressure decays.

The reservoir was sized and the initial pressurization level established such that (1) the maximum feed pressure (water reservoir fill) did not exceed the breakthrough pressure of the porous plate and (2) the minimum pressure (water reservoir almost empty) was sufficient to deliver enough water to meet the maximum required heat dissipation rate. If the temperature of the reservoir remains constant, the initial and final pressures and volumes on the gas side of the bladder are related by the following equation.

$$P_i V_i = P_f V_f$$

Where $P_i$ = initial gas pressure

$P_f$ = final gas pressure

$V_i$ = initial gas volume

$V_f$ = final gas volume

The final gas volume is equal to the total available volume in the reservoir and the initial gas volume is the total volume less the initial stored water volume. The ratio of the initial and final gas pressures becomes

$$\frac{P_i}{P_f} = \frac{V_T}{V_T - V_W}$$

where $V_T$ = total available reservoir volume

$V_W$ = initial stored water volume

Extrapolated data from Reference 1 indicated a breakthrough pressure of between 10 and 13 psia at the maximum sublimator heat flux of 3500 Btu/hr-ft$^2$. This range limits the maximum allowable pressure to which the reservoir may be pressurized, i.e., the maximum $P_i$. The pressure loss through the tubing valve, and distribution orifices for a water flow rate (1.4 lb/hr) sufficient to meet the maximum heat lead requirements, was calculated to be less than 0.01 psi. For a sublimator plenum saturation pressure of 0.18 psia at 50$^\circ$F, the minimum allowable pressure in the reservoir, $P_f$, is 0.19 psia.

The reservoir was designed with a total volume was designed with a total volume of 340 cu in., which yields $P_i/P_f$ = 15.5. For an initial gas pressure of 5 psia (half the breakthrough pressure) a final gas pressure of 0.32 psia results. These pressures are well within the allowable limits of 10 and 0.19 psia.

## SUBLIMATOR FEED-WATER VALVE DESIGN

The sublimator must be supplied with water at heat pipe vapor temperatures over $63^0$F to maintain panel temperature within the specified $80^0 \pm 10^0$F range. Since the sublimator uses only the water required to meet the heat load, the valve can be an on-off type. The valve selected was a poppet type valve with a melting wax thermal sensing device that monitors the heat pipe vapor temperature and supplies the driving force to open the valve without any external power required to operate the valve. The thermal sensing device was bonded to a copper cup that was brazed to the panel surface and extended into the vapor passage.

STRUCTURAL DESIGN

The panel structural design was established for the required inertia loads and for containment of internal fluid pressures. Panel requirements included provisions for attachment of electronic equipment to one surface by any combination of two-inch mounting intervals and, on the other surface, provisions for mounting to the vehicle at five points. In addition to its own weight, the panel must support up to 180 lb of electronic gear under a design load of 12g. These inertia load considerations were of primary importance in the selection of the panel structural configuration, although constraints arising from heat pipe operating characteristics and pressure containment requirements were also satisfied. Additional pressure containment design was performed for the water tank and the sublimator.

The selected panel design, shown in Figure 4-8, is a 3-layer sandwich panel consisting of the remote loop, heat pipe and plate-fin structural sandwich layer. The remote loop which is adjacent to the electronic equipment consists of the outer stainless steel sheet with a design thickness of 0.025 in., 0.050-in. high nickel fins, 20 fins/in., 0.004-in. thickness, and a sheet of 0.032-in. thickness which is common to the heat pipe layer. The heat pipe layer includes bosses, copper fins, and a nickel felt metal wick. The bosses were connected by ribs which are the full height of the passage. The 0.09-in. thickness ribs are required to provide strength for the heat pipe layer. The plate-fin structural layer consists of an 0.032-in. sheet common with the heat pipe, 0.25-in. high fins, and outer sheet of 0.040-in. thickness. This design incorporates the heat pipe and remote loop into an efficient, integrated sandwich structure to support the design inertia loads. The added structural layer is an integral part of the sandwich and, therefore, provides the required strength with a minimum of additional weight.

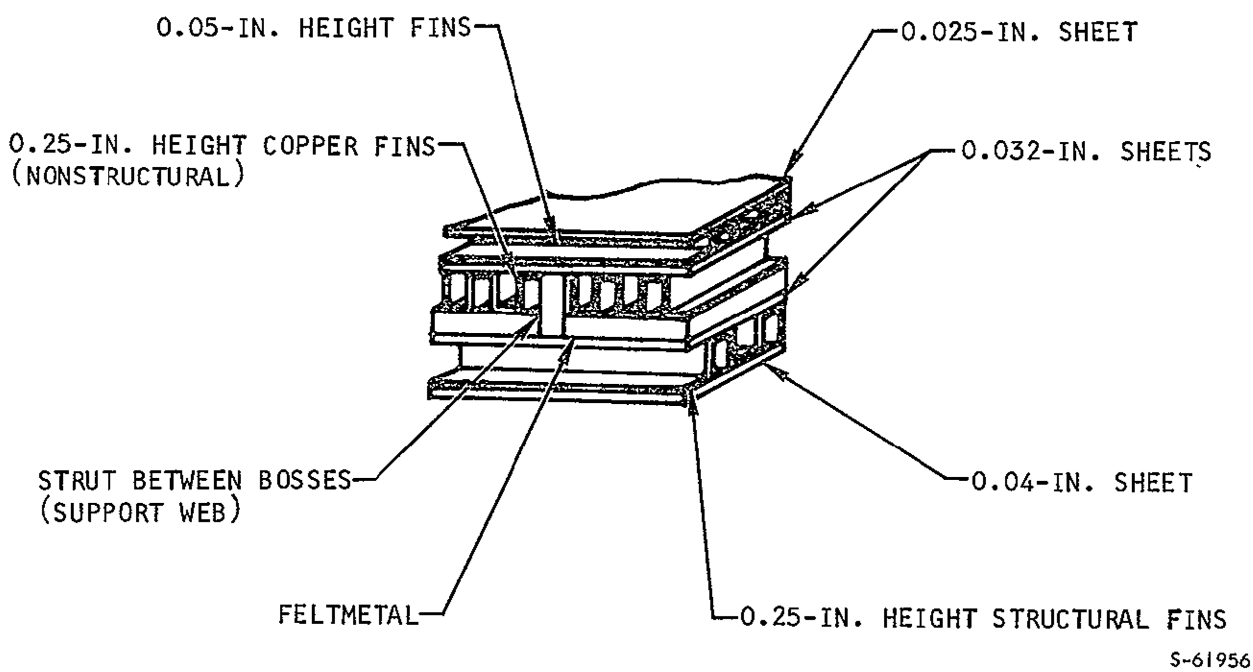


Figure 4-8. Instrument Unit Thermal Panel Structural Schematic

The estimated weight of the panel assembly was 82.9 lb including the filled water sublimator reservoir. The design was based upon current fabrication technology using Type 347 stainless steel as the basic structural material. A possible weight reduction of the order of 15 lb appeared available through the use of a stronger structural material such as PH14-8Mo which is a heat-treatable semiaustentic stainless steel. The weight reduction would have been achieved primarily through the use of thinner sheet material but would require a heat treatment operation. The panel design approach would not be altered by the introduction of a stronger structural material. Due to potential development problems associated with PH14-8Mo and the other high strength materials, 347 stainless steel was selected for the sheet material.

Inertia Loads

Inertia loads will cause bending moments in all directions in the plane of the panel with the specified 5-point mount system. It was therefore desirable to have an isotropic plate rather than the orthotropic properties of a typical plate-fin heat exchanger. It was further assumed that the loading due to the combined weight of the electronic equipment and the panel was uniform over the panel surface. The design pressure was 8 psi for a combined weight of 270 lb, which included 90 lb for the panel. The design was based on a safety factor of 1.5 and a 12-g loading. The design bending moment for this loading was determined to be 355 in.-lb based on the analysis of a plate simply supported at five points. Isotropic properties were achieved by selecting unidirectional sandwich layer properties which, when combined, gave equal stiffness in two directions.

The heat pipe layer with the rib and boss array and the two inner 0.032-in. sheets provided the required stiffness in one direction. The design strength was 32 ksi, the yield strength of 347 stainless steel at room temperature. The required section modulus for the heat pipe layer for a safety factor of 1.5 on yield was therefore

$$Z = M/\sigma = 355/32{,}000 = 0.011 \text{ in.}^3/\text{in.}$$

The section modulus of a two-layer sandwich, assuming that only the sheets were effective in bending, is given by

$$Z = t_f \, (h + t_f)$$

Therefore, the required face sheet thickness for a web height of 0.33 in. was 0.031 in.$^3$/in. The nearest standard sheet size of 0.32 in. was therefore selected for the design.

The combined stiffness of the remote coolant loop layer and the 0.25-in. structural layer was approximately equal to the heat pipe stiffness and oriented 90 deg to that layer. Similar calculations to those above were performed on the assumption that the required section modulus is the sum of the moduli of the two layers. This analysis therefore assumed that each layer contributes bending strength only in the direction of fin orientation. It was further assumed that the full strength of each sandwich can be obtained even though separate layers share common facesheets.

The sublimator replaces the 0.25-in. high structural sandwich over a 5.3 by 22 in. section on one edge of the panel (under the water tank). The structural layer was therefore extended to the mount points at either end of the sublimator using fins oriented 90 deg to the basic array in that layer. These fins therefore provided added strength for transmitting loads to these two mount points (the fins were oriented so that their bending stiffness added to the bending stiffness of the heat pipe layer). The effect of this deviation from the isotropic plate design approach was not evaluated.

The support ribs in the heat pipe layer join with equipment bosses (2-in. boss spacing) to form continuous rows in the direction of coolant flow. These ribs had 0.6-in. long notches so that the porous plate would not be completely interrupted by a row of ribs and bosses. However, bending strength continuity was maintained over the unsupported length by the 0.032-in. sheet which had a large buckling capability. The estimated critical buckling stress (Euler) for the segment, assuming fixed ends, was about 290 ksi compared to a maximum operating stress of 21 ksi (32 ksi/1.5). The main mount in the center of the panel was integral with two adjacent equipment bosses to provide load distribution to the panel, whereas the main mounts at the corners connect to the adjacent bosses with diagonal strut segments in the heat pipe layer.

Pressure Containment

Heat exchanger plate-fin structures rely on fin tensile loads and facesheet bending for pressure containment. The fin stress level is related to pressure P, fin spacing $a_f$, and fin thickness $\delta_f$, by

$$\sigma = 2P\ (a_f - \delta_f)/\delta_f \qquad (4\text{-}12)$$

The factor of 2 relates tested peformance to the theoretical stress based on pressure force divided by area. Facesheet bending stresses are computed for a fixed end beam under uniform pressure and with a thickness of $\delta_p$ by the following equation:

$$\sigma = 0.5P\ [(a_f - \delta_f)/\delta_p]^2 \qquad (4\text{-}13)$$

Standard pressure vessel design techniques were incorporated for the design of the water tank and sublimator. The major considerations are discussed below.

1. Remote Coolant Loop

The maximum operating pressure in this plate-fin heat exchanger was expected to be 50 psi. At this pressure, the fin stress for a spacing of 0.050 in. (20 fins/in.) and a thickness of 0.004 in. by Equation (4-12) is

1.1 ksi. This is a small fraction of the minimum specified nickel yield strength of 10 ksi, so the fins are satisfactory. The face sheet bending stress of Equation (4-13) for a 0.025-in. thickness was 0.3 ksi so facesheet strength is also more than adequate.

2. Heat Pipe

The maximum heat pipe loading was expected to be the 15 psi external pressure which occurs when the evacuated heat exchanger is located in an ambient environment. Pressure containment is provided by the 0.09-in. thick struts and 0.032-in. thick sheets. Strut compressive stress for a 2-in. spacing was 0.3 ksi and sheet bending stress was estimated to be 26 ksi so that the minimum safety factor was 1.2 for 347 steel. This is less than the desired 1.5 factor. However, this is a local bending stress and the design was considered to be satisfactory.

3. Structural Sandwich

The structural sandwich was subjected to the same pressures as the heat pipe due to a leak between the two layers. The fin buckling pressure was determined to be 70 psi by crushing a set of the 16 fin/in., 0.004-in. thick, 0.25-in. high nickel fins. The buckling safety factor on the 15-psi maximum pressure was therefore 4.7.

The test value was about one-sixth of the theoretical Euler buckling load of the fin. The simply-supported column buckling load of a 1-in. width of fin is

$$P_{critical} = 0.9\ E\delta^3/L^2$$

For an elastic modulus of $30 \times 10^6$ psi, a length of 0.25 in., and a thickness of 0.004 in., the calculated buckling load would be 28 lb, whereas at 70 psi, the tested buckling pressure, the calculated fin load was 4.4 lb.

4. Water Tank

The water tank was basically a square tank with a 0.05-in. wall thickness shell reinforced with 0.032-in. corrugated doublers on the three 28-in. sides and 0.05-in. sheet doublers on the ends. Tank material was 347 steel and the water pressure capability was 20 psi. The tank was joined to the sublimator by Nioro TIG brazing the mating sheet of the tank to the exposed heat pipe sheet. The braze alloy was applied around the edge of the 0.75-in. diameter holes drilled in the 0.05-in.-thick tank shell to provide for the water pressure seal and for transmission of the design inertia loads.

A typical pressure containment calculation for the rectanuglar water tank is illustrated for the reinforced tank ends. The combined thickness of the tank wall and doubler is 0.1 in. and the unsupported span is about 4.5 in. At a pressure of 20 psi, the beam stress, from Equation (4-13), is

$$\sigma = 0.5(20)(4.5/0.1)^2 = 20.2\ \text{ksi}$$

Since the allowable stress is 32 ksi, this is a satisfactory design.

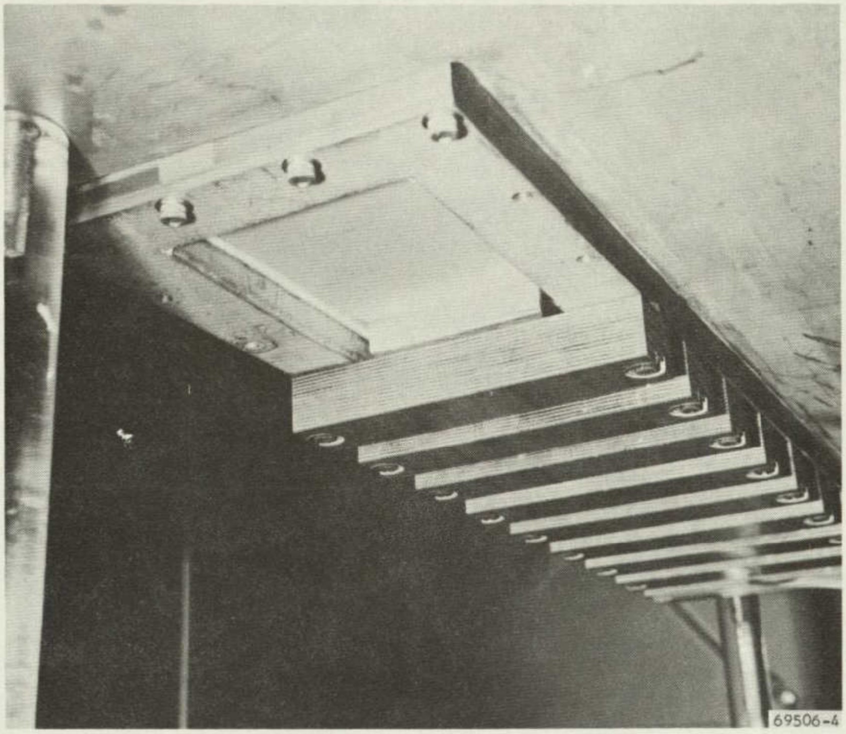


a. VIEW OF SUBLIMATOR WITH U-CHANNEL SUPPORTS

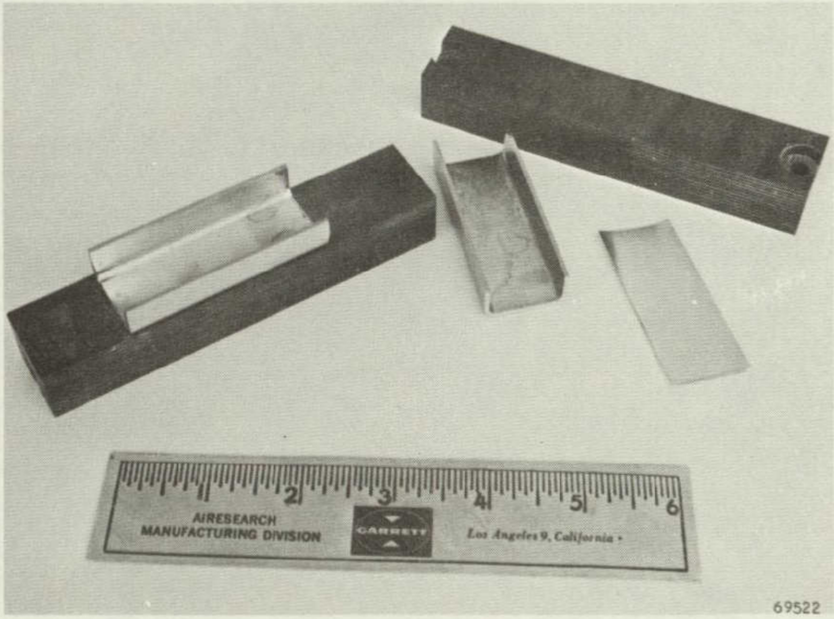


F-12536

b. U-CHANNEL AND SUPPORT BEAM DETAILS

Figure 4-9. Sublimator Plate Support

5. Sublimator Plate

The 0.028-in. porous sublimator plate required reinforcement due to bulging during performance tests (pressures were up to about 10 psi). The plate was reinforced by externally attaching the beams and channels shown in Figure 4-9.

Weight Analysis

The total weight of the heat pipe assembly including water (10.3 lb) was measured to be 101 lb. The fabricated panel weight would have been 93 lb if the 0.062-in. face sheet on the remote coolant loop had been machined to the design thickness of 0.025 in. The calculated weight of the panel was 91 lb based on the following component weights.

| | | |
|---|---|---|
| Remote coolant loop | | 8.0 lb |
| 0.025-in. sheet | 5.2 lb | |
| Nickel fins plus braze alloy | 2.3 lb | |
| Bosses | 0.5 lb | |
| Heat pipe | | 32.0 lb |
| Two 0.032-in. sheets | 16.7 lb | |
| Copper fins plus braze alloy | 4.7 lb | |
| Feltmetal | 2.7 lb | |
| Bosses and struts | 7.9 lb | |
| Structural sandwich | | 13.9 lb |
| 0.04-in. sheet | 9.1 lb | |
| Nickel fins plus braze alloy | 4.6 lb | |
| Bosses | 0.2 lb | |
| Water tank (including water) | | 28.5 lb |
| Sublimator | | 4.3 lb |
| Five percent allowance for fasteners, headers, and fluid connectors | | 4.0 lb |

## NONCONDENSABLE GAS GENERATION INVESTIGATION

Literature surveys indicated that a noncondensable hydrogen gas generation phenomenon occurs in stainless steel heat pipes which use water as the heat pipe fluid (References 20 and 21). A similar problem encountered with hydrogen gas entrapped in potable fuel cell water for Apollo was solved by installing a section of Palladium-silver tubing in the system to pass hydrogen overboard. An investigation was initiated to (1) verify the generation of noncondensable hydrogen gas in a water-stainless steel heat pipe, (2) determine the effectiveness of palladium-silver as a means of removing the hydrogen gas, (3) verify the degrading effect of the noncondensable gas generation upon heat pipe effectiveness, and (4) determine the hydrogen generation rate in a water-stainless steel heat pipe.

### Test Specimen

The heat pipes fabricated for the noncondensable hydrogen gas generation study were tubular heat pipes as shown in Figure 4-10. The Configuration A heat pipe illustrated schematically in Figure 4-11 was a 0.450-in. O.D. (0.028 in. wall) tubular stainless steel pipe 15.5 in. long with a double layer of 100 mesh screen wick in contact with the inside circumference along the entire length. A stainless steel end cap and a fill tube completed the A1 assembly and a palladium-silver end cap and a fill tube completed the A2 assembly. Heat pipe configuration B was identical to Configuration A with the exception that the Configuration B heat pipe used a 0.015-in. thick nickel feltmetal wick (20 percent density). The Configuration B heat pipes were fabricated but not tested.

### Test Setup And Procedure

Heat input was provided to the evaporator end of the heat pipe (10 in.) by a 20-watt electrical resistance strip heater wrapped around the circumference at the evaporator section and by the immersion of the condenser section (5.5 in.) in a water bath as shown in Figure 4-12. The strip heaters were installed on the heat pipe in a manner that did not cover the surface thermocouples. Instrumentation was provided to record heat sink temperature, electrical heat input, heat pipe surface temperature, ambient pressure and ambient temperature. A special hydrogen gas quantity measuring section shown in Figure 4-13 was attached over one of the heat pipes with the special palladium-silver end cap to measure the amount of hydrogen generation as a function of time. The hydrogen gas was vented into an oxygen atmosphere and the amount of oxygen lost due to the hydrogen-oxygen reaction was recorded.

Two Configuration A1 and two Configuration A2 heat pipes were tested simultaneously. Each heat pipe and its associated fill apparatus were helium leak checked with a maximum observed leakage rate of $1.4 \times 10^{-8}$ scc/sec. Prior to being filled with distilled, degassed water (filtered to 1 micron), each heat pipe was evacuated to $1 \times 10^{-6}$ mm Hg abs. One each of configurations A1 and A2 were filled with 4.0 cc and 5.0 cc of water. The heat pipes were then tested in the horizontal position to simulate a zero-g environment.

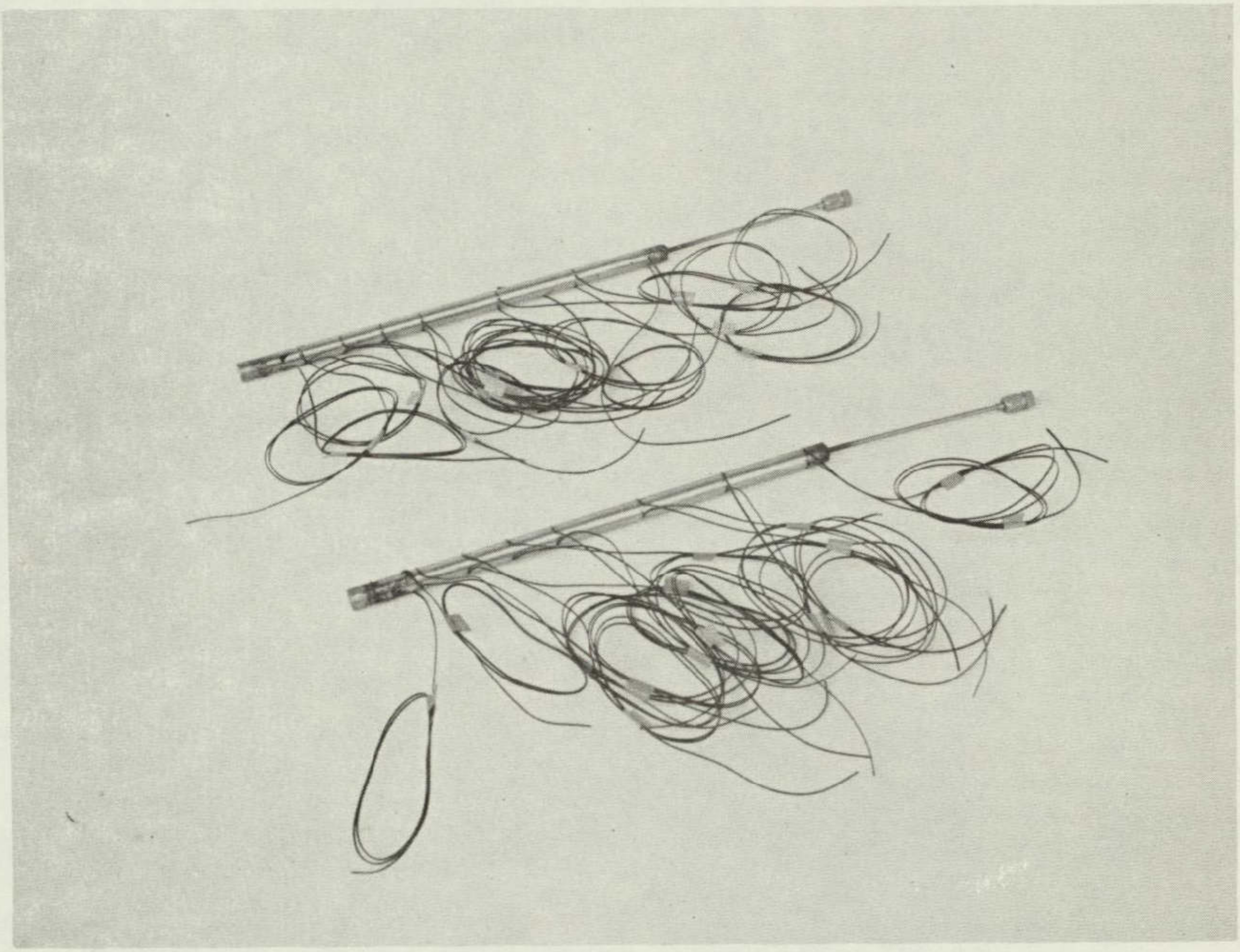

F-11742

Figure 4-10. Heat Pipes With Condenser End Ports Porous to Hydrogen for Noncondensable Gas Generation Studies

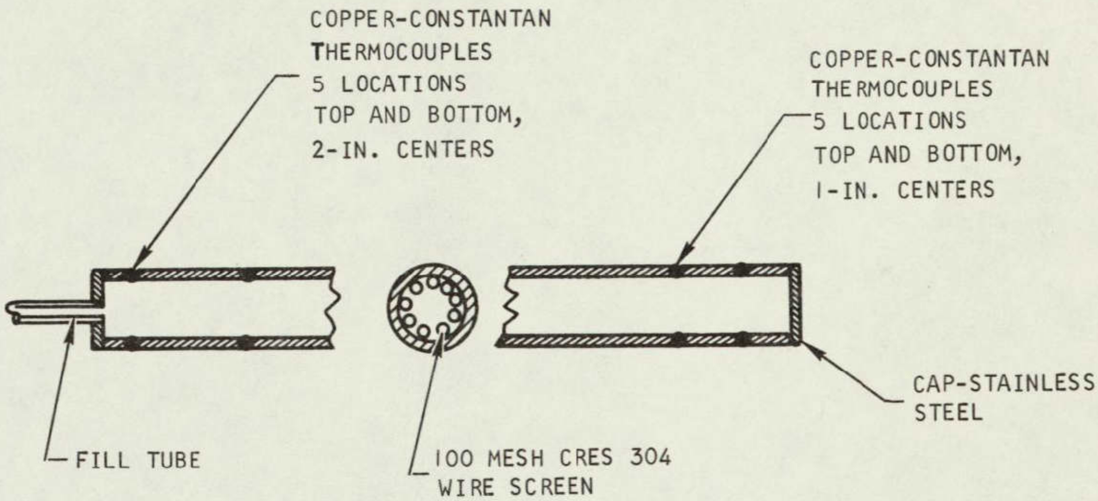


A. CONFIGURATION A1

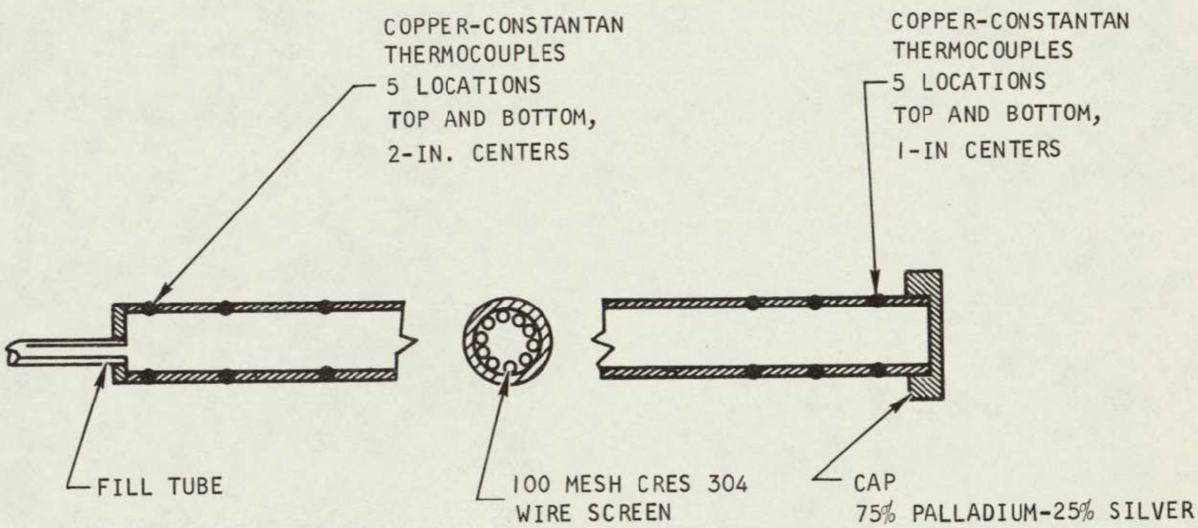


B. CONFIGURATION A2

S-61964

Figure 4-11. Heat Pipe Configuration A

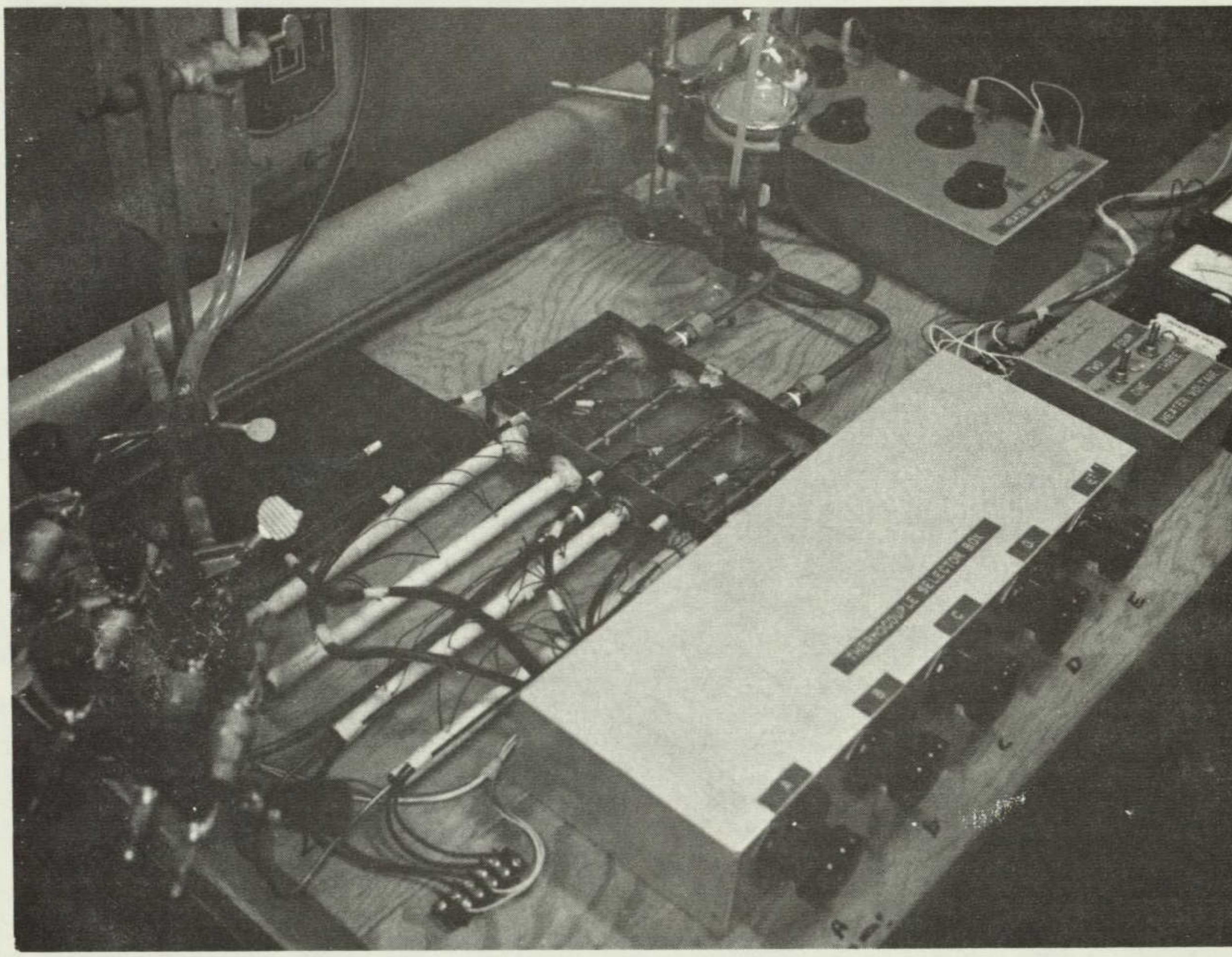


F-11743

Figure 4-12. Test Setup for Noncondensable Gas Generation Studies

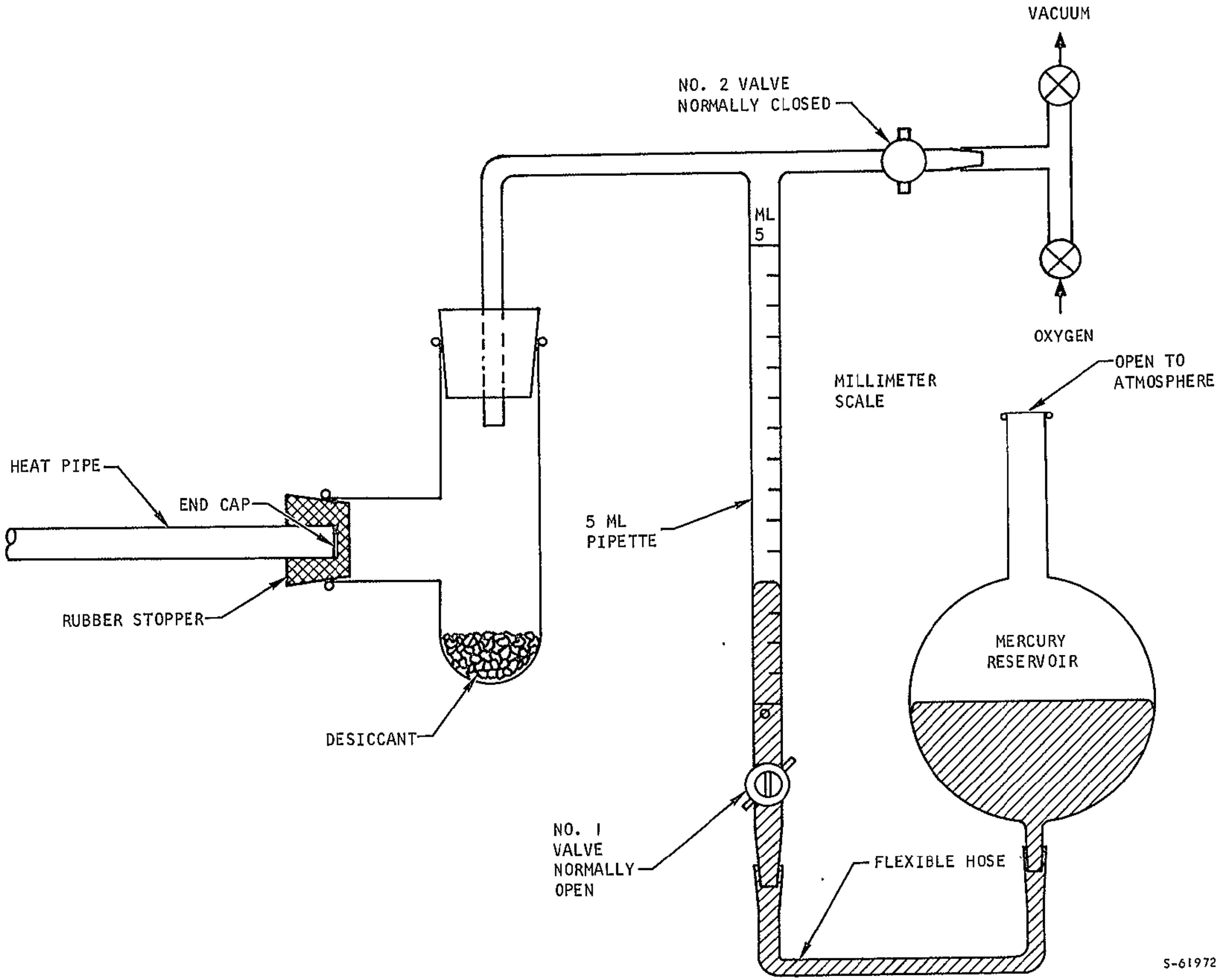


Figure 4-13. Non-Condensable Gas Study Hydrogen Flow Measuring System

Test Results and Discussion

The noncondensable hydrogen gas generation data is presented in Figure 4-14 and tabulated in Table 4-2 as volume of gas generated in standard cubic centimeters as a function of time. The rate of gas generation decreased with time, but not to the extent anticipated prior to initiation of testing. After reviewing the data, it became evident that an electrolytic cell was present between the 304 stainless steel in the tube and the palladium in the palladium-silver end cap through the silver braze joint and the water in the heat pipe.

The permeation of hydrogen through palladium-silver alloys at essentially ambient temperature and atmospheric pressure was studied at AiResearch during a prior program for NASA as part of the Apollo Applications Program (Reference 13). This program resulted in a hydrogen-water separator in which the partial pressure of hydrogen dissolved in fuel cell water was reduced to approximately one percent of its original value by passage of the hydrogen to space through a palladium (75 percent)-silver (25 percent) alloy. Special techniques were devised for application of a palladium black coating to the palladium silver alloy which is necessary to catalyze adsorption and desorption of hydrogen on the surface. This coating is resistant to water and removal by erosion. Coated palladium silver alloys were evaluated as a potential method for removal of hydrogen which collects as a noncondensable gas in heat pipes that are evacuated and sealed from the external environment. The heat pipe tested was a configuration A2 with the palladium alloy sealed to the stainless steel pipe with silver braze.

In theory hydrogen, liberated by water decomposition, migrates to the cold end of the heat pipe. The palladium black surface causes the molecular hydrogen to break up into protons, or single hydrogen atoms, which migrate into the palladium silver alloy, forming in effect a ternary alloy. In effect the hydrogen is absorbed within the tube, passes through the metal lattice, and is burned to water vapor by the catalytic coating on the exterior of the tube. The amount of hydrogen permeating through the alloy was monitored by measuring the rate of decrease in pressure of a known volume of oxygen surrounding the exterior of the tube. The water vapor formed during the reaction was continually removed by suitable drying agents.

It has been known that hydrogen is formed within sealed tubes by the reducing action of metals on water. Thus, where M is a metal,

$$M + H_2O = MO + H_2$$

In a previous program at AiResearch, it was found that sealed aluminum tubes containing distilled water would create substantial hydrogen pressure due to the metal surface water reaction (Reference 14). The formation of hydrogen from hydrogen ions in distilled water requires 0.414 volts (Reference 15):

$$2H^+ \ (10^{-7}M) + 2e^- = H_2 \qquad E = 0.414v$$

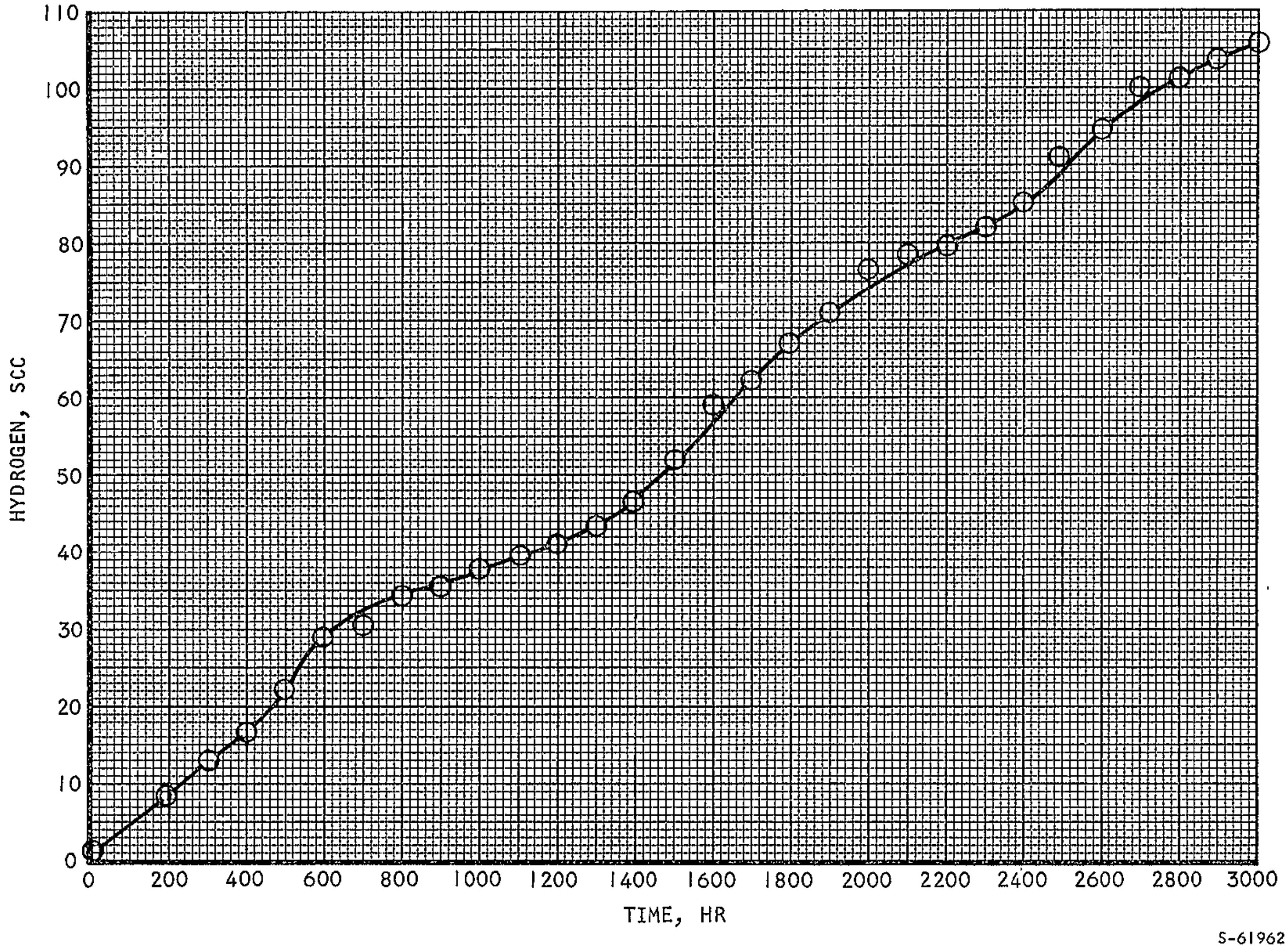


Figure 4-14. Heat Pipe-Stainless Steel Noncondensable Gas Generation Study with Palladium (75%)-Silver (25%) End Cap

TABLE 4-2

HEAT PIPE TEST SUMMARY

| Test Time, hr | Evaporator to Condensor Temperature Differential, °F | | | | Total Hydrogen Generation for A2 S/NI Unit, std cu cm |
|---|---|---|---|---|---|
| | AI SN I*** | AI SN 2** | A2 SN I** | A2 SN 2*** | |
| 0 | 15.1 | 19.8 | 122(12) | 13.4 | 1.10 |
| 50 | 17.1 | 22.7 | 76.0 | 12.1 | 1.47 |
| 100 | 16.5 | 20.0 | 11.6 | 11.2 | - |
| 200 | 16.8 | 21.2 | 11.3 | 9.8 | 8.0 |
| 300 | 17.9 | 21.1 | 11.0 | 12.6 | 13.0 |
| 400 | 19.2 | 21.6 | 11.3 | 13.6 | 16.6 |
| 500 | 19.6 | 24.1 | 11.8 | 14.2 | 22.0 |
| 600 | 18.6 | 21.1 | 12.5 | 13.0 | 28.8 |
| 700 | | | | | 30.8 |
| 800 | 18.7 | 21.5 | 13.8 | 13.2 | 34.6 |
| 900 | | | | | 35.6 |
| 1000 | 20.9 | 20.5 | 12.1 | 14.8 | 37.8 |
| 1100 | | | | | 39.2 |
| 1200 | 20.7 | 19.1 | 12.1 | 14.2(18) | 41.0 |
| 1300 | | | | | - |
| 1400 | 23.2(24) | 18.5 | 12.0 | 14.6(24) | 46.4 |
| 1500 | | | | | 52.0 |
| 1600 | 25.5(36) | 21.7 | 10.9 | 14.0(36) | 59.0 |
| 1700 | | | | | 62.0 |
| 1800 | 22.0(48) | 18.3 | 10.3 | 14.5(48) | 67.2 |
| 1900 | | | | | 70.8 |
| 2000 | 19.7(54) | 20.0 | 12.1 | 14.5(54) | 75.6 |
| 2100 | | | | | 78.4 |
| 2200 | 22.4(60) | 19.5 | 11.5 | 17.7(54) | 79.6 |
| 2300 | | | | | 81.0 |
| 2400 | 30.7(96) | 21.0 | 11.5 | 25.4(84) | 85.2 |
| 2500 | | | | | 90.0 |
| 2600 | 30.4(126) | 19.5 | 10.0 | 36.5(126) | 94.6 |
| 2700 | | | | | 99.4 |
| 2800 | 31.8(126) | 21.7 | 9.5 | 38.4(126) | 101.2 |
| 2900 | | | | | 103.8 |
| 3000 | 30.5(126) | 19.5 | 10.5 | 39.5(126) | 105.4 |

NOTE· *Heat input was 6.0 watts unless otherwise noted by numbers enclosed in parentheses.
**Heat pipe filled with 4.0cc of water.
***Heat pipe filled with 5.0 cc of water.

Any reducing agent with a couple more positive than 0.414v would liberate hydrogen from water. In particular, if we examime chromium, a constituent of stainless steel, we find for acid solutions

$$Cr = Cr^{3+} + 3e^- \qquad E = 0.74v \quad \text{(p. 247, Reference 15)}$$

$$Cr = Cr^{2+} + 2e \qquad E = 0.91v \quad \text{(p. 248, Reference 15)}$$

$$Cr^{2+} = Cr^{3+} + e \qquad E = 0.41v \quad \text{(p. 248, Reference 15)}$$

Both chromium, as metal, and the divalent chromium ion, $Cr^{2+}$, thus constitute potential reducing agents for water and can be expected to be unstable with respect to the evolution of hydrogen from water even at low acid concentrations, i.e., distilled water. Similarly, for nickel in a basic solution we find

$$Ni + 2OH^- = Ni\ (OH)_2 + 2e^- \qquad E = 0.72v \quad \text{(p. 200, Reference 15)}$$

so that oxidation of a nickel surface would be expected to occur.

With considerable surface area of nickel and chromium present and with these metals unstable with respect to hydrogen evolution, it would be expected that the metal-water reaction would slowly occur and that hydrogen would accumulate within the heat pipe. It is probable that the surfaces already contained a monomolecular oxygen layer since such oxygen layers are extremely difficult to eliminate and constitute the basis for passivation of such surfaces. In the absence of palladium alloy the metal-water reaction might be expected to cease after all active metal sites capable of reacting with water have been oxidized. With the palladium alloy present, however, there exists an additional driving force represented by the absorption of hydrogen into palladium. This constitutes approximately 0.2v (Reference 16). The metallic contact of the palladium alloy with the stainless steel tube in the test specimen formed a battery in which water was slowly decomposed on the interior of the palladium surface, which was kept depleted by oxidation of the hydrogen on the exterior surface; the metal conducts the electrical current to the interior metal surface which oxidizes, and ionic transfer through the water was carried by a hydroxyl or hydrogen ions. The elimination of concentration gradients would be facilitated by the water flow through the screen. Under such circumstances, it can be expected that oxygen layers considerably deeper than a monomolecular layer can be built upon the interior metallic surfaces and the decomposition of water could slowly take place almost indefinitely. It can be shown that liberation of a 1 std cu cm of hydrogen gas per day is almost exactly equivalent to a current of 100 $\mu$a ($1 \times 15^4$ amp). It also constitutes the transfer of $7.15 \times 10^{-4}$ gm of oxygen per day from water molecules to the surface of the metal, equivalent to the decomposition of 8.05 x 154 gm of water per day. It would take approximately 3.4 years to decompose 1 cu cm of water at this rate.

In the absence of extensive testing for extended periods of time the effect of the palladium alloy on the continuous reduction of water by metallic surfaces cannot be known. It was apparent that the removal of the hydrogen by the palladium silver end cap was accomplished. The battery effects could be eliminated by the use of a nonconducting bonding medium between the palladium alloy and the stainless steel tube. However, it would also be necessary to insure such a bonding medium was not permeable to the passage of gases such as nitrogen, oxygen, or carbon dioxide which would then collect in the heat pipe and be even more detrimental than the hydrogen since they are also noncondensable and cannot be readily removed.

The performance degradation effects of the noncondensable gas generation was to be evaluated by the comparison of the temperature profiles of two heat pipes with the palladium silver end caps, configuration A2, and two heat pipes with stainless steel end caps, configuration A1. The temperature profile of the heat pipes was recorded and the averages of the six thermocouples at the extreme evaporator end and the six thermocouples at the extreme condensor were tabulated in Table 4-2 as heat pipe temperature differential. The heat load into the heat pipe is also presented in the table.

The two pipes with stainless steel end caps showed no evidence of hydrogen generation and buildup. However, the data of Swartz (Reference 17) showed a significant increase in the heat pipe $\Delta T$ within 800 hr due to the generation of hydrogen gas. If gas had formed in these pipes at the rate experienced by Swartz, there would have been a significant $\Delta T$ increase since the gas had no way of escaping. The lack of active oxidization sites in the stainless steel available for oxidation, and therefore hydrogen generation, may have been minimized due to cleaning and passivating the detail parts in a nitric-hydrofluoric acid bath prior to final assembly of the heat pipes. Hydrogen generation data for the first palladium-silver capped heat pipe indicated that hydrogen was being generated in these units, probably by electrolysis as discussed above. Neither pipe exhibited an increasing $\Delta T$ as long as the heat load remained constant. Since the pipes were generating hydrogen gas, the relatively constant $\Delta T$ establishes that the gas was being passed through the palladium-silver end cap.

It was noted that one of the palladium-silver heat pipes exhibited a large initial $\Delta T$ which, after about 100 hr, dropped to a steady-state level. This behavior was attributed to nonuniform distribution of the working fluid which eventually redistributed itself through repeated evaporation and condensation.

## FABRICATION

### Introduction

A 30 in. by 30 in. thermal conditioning panel consisting of three sandwiches, a remote cooling loop, a heat pipe sandwich, and a structural sandwich was fabricated. The panel also contained equipment mounting bosses, structural webs and five bosses for mounting the panel. Auxiliary equipment included with the panel were a consumable water reservoir with two shut-off valves, a bladder, and a thermostatic flow control valve. A sublimator plate and water distribution fins were an integral part of the panel required to furnish the heat sink for vacuum operation. The flow of water from the reservoir to the sublimator was controlled by the thermostatic valve mounted to the panel.

### Detail Fabrication

1. Remote Cooling Loop

The remote cooling loop consisted of fins, sheets, flow divider bars, and header bars. The fins in the remote loop were 20 fins/in., 0.050-in. high made from 0.004-in. thick nickel material on the AiResearch universal fin machine. The header bars and divider strips were cut to length from standard head bar stock made from upset wire stock. The two sheets that cover the fins and bars completing the plate fin sandwich were standard stock 347 stainless steel (0.063- and 0.032-in. thickness). The sheets were drilled and the fins electric discharge machined at the detail level to accept the equipment and structural mounting bosses. Figure 4-15 shows the remote cooling loop fins placed on the top sheet prior to brazing.

2. Bosses and Webs

The bosses, equipment mounting, and four of the mounting bosses were machined from bar stock. The webs were milled and drilled from standard sheet stock. The center mounting boss was machined from plate stock. The machining tolerance on the fabrication processes was set by the need to maintain acceptable braze tolerances.

3. Structural Sandwich

The structural sandwich consisted of fins, sheets, header bars, and also the water plenum. The fins were 16 fins/in., 0.250-in. high and made from 0.004-in. nickel on the AiResearch universal fin machine. The header bars were cut to length from standard stock made from upset wire. The water plenum was made from a thin walled square tube. The sheets that enclosed the structural sandwich were standard stock 347 stainless steel (0.032- and 0.040-in. thickness). The sheets were drilled and the fins electric discharge machined at the detail level to allow placing the mounting bosses in position. The structural fins are shown in Figure 4-16.

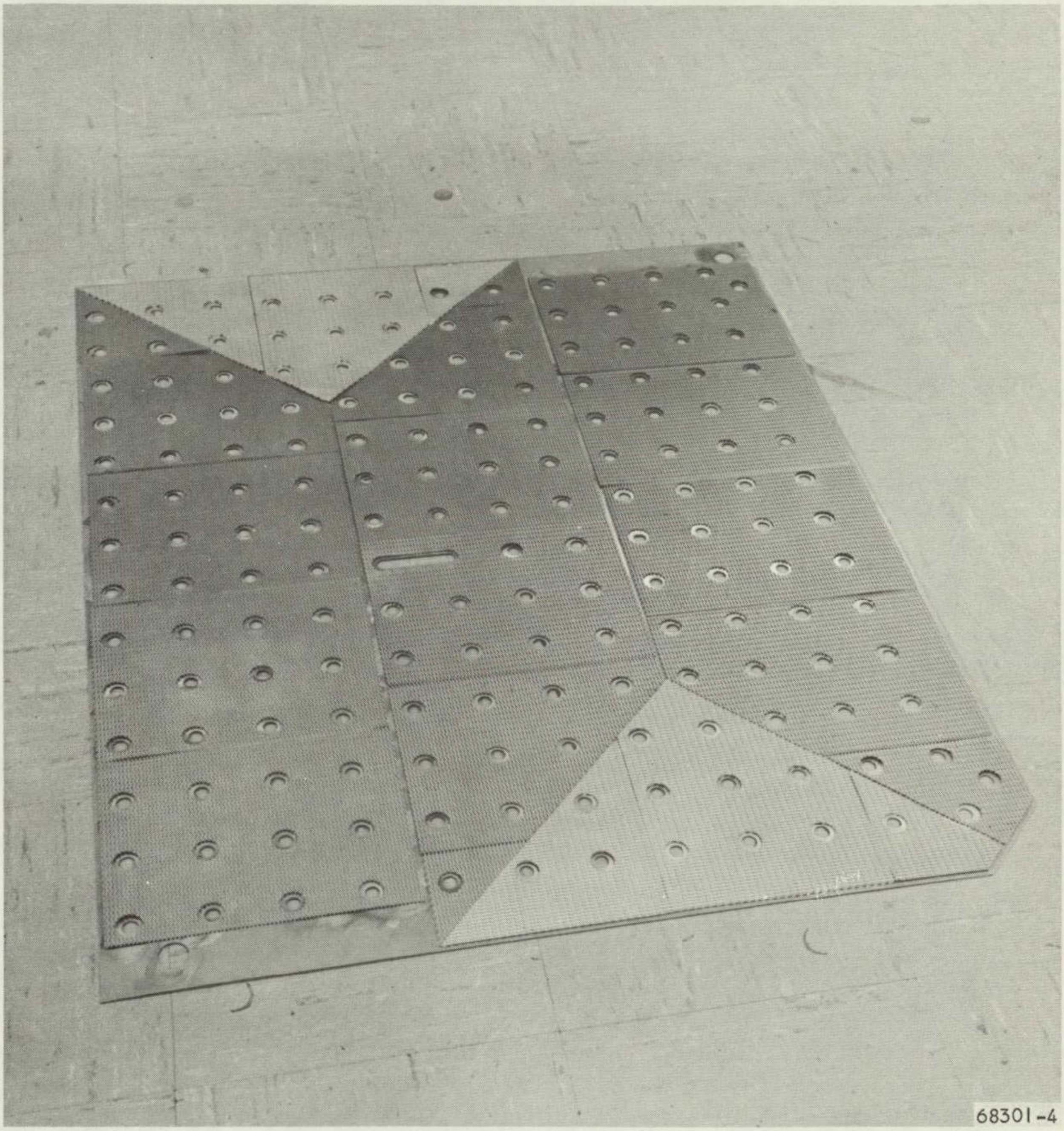




Figure 4-15. Remote Cooling Loop Subassembly Prior to Brazing

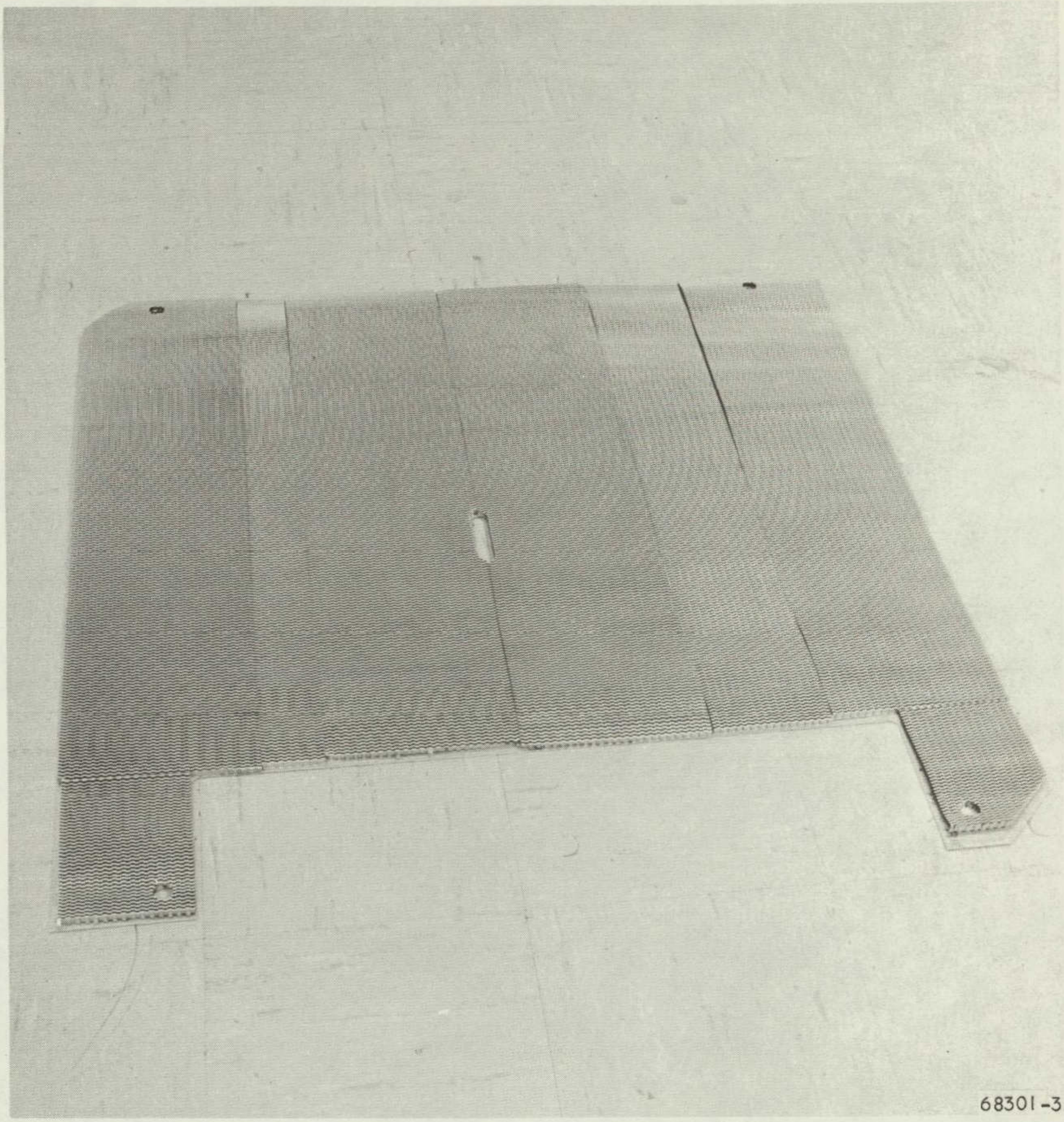

Figure 4-16. Assembly of Structural Sandwich Prior to Brazing

4. Heat Pipe

The details of the heat pipe sandwich consisted of the 15 percent density nickel wick and copper fins. The wick was purchased from a vendor and then machined to accept the bosses and webs. The fins in the heat pipe were made from 0.002-in. thick copper formed into 28 fins/in., 0.250-in. high on the AiResearch Universal fin machine. The fins were cut to the desired length to fit between the webs prior to being electric discharge machined to fit around the bosses.

5. Palladium-Silver Plates

The palladium-silver plates were treated with palladium black to promote the catalytic reaction. After the surfaces were treated the plates were cut to size and stored for later assembly.

6. Water Reservoir

The water reservoir details consisted of two halves each containing a threaded connection for a valve, flanges, and a bladder. The halves of the reservoir were fabricated from one piece of standard 0.050-in. 347 stainless steel sheet. The flanges were cut from 347 stainless steel plates, machined and brazed to the reservoir halves. The bladder was formed from Dow Corning 93-072 RTV Silicon Rubber. A half reservoir was used as the female mold to form the bladder. The reinforcing ribs on the reservoir were formed on standard tooling from 0.032-in. 347 stainless steel and brazed to the reservoir halves.

7. Thermostatic Flow Control Valve

The thermostic flow control valve consisted of the valve body, thermostat, lines and fittings, bellows seal, and reaction load spring. The thermostat was a vendor item purchased to an AiResearch source control drawing. The bellows was purchased from a vendor. The remaining parts of the flow control valve were fabricated from standard material stock.

8. Sublimator

The sublimator consisted of a porous metal plate, a mounting frame, and water distribution fins. The porous metal plate (vendor supplied) was welded to the frame assembly that was fabricated from standard material stock. The water distribution fins (38 fins/in., 0.025-in. high and made from 0.001-in. 347 stainless steel) were made on a punch press fin machine.

Panel Assembly

The details of the remote loop were brazed in a vacuum furnace using EMS9-4779 braze alloy. A typical furnace setup is shown in Figure 4-17. The second step of the assembly sequence was to braze the bosses and webs into the remote loop using Palniro RE in a vacuum braze cycle. The remote loop with the bosses and webs in position for brazing is shown in Figure 4-18.

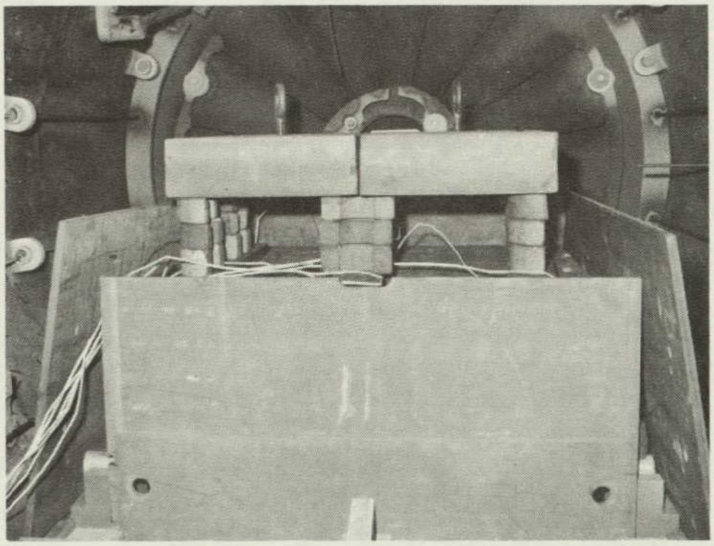

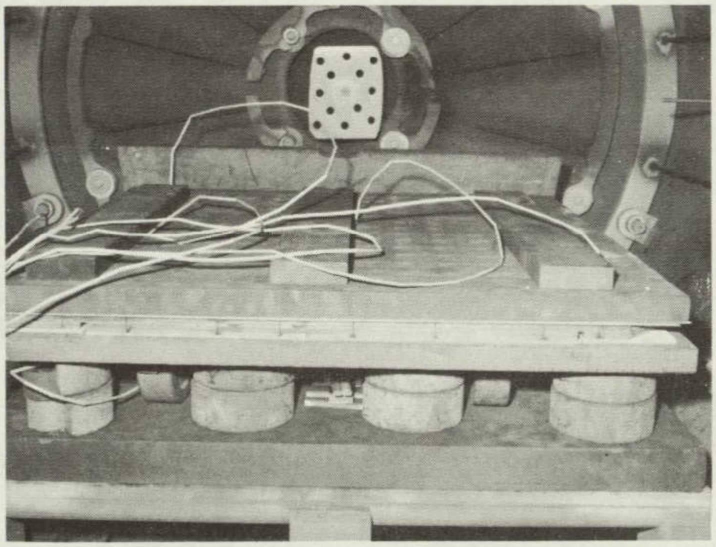

F-12530

Figure 4-17. Vacuum Furnace Braze Cycle Setup.

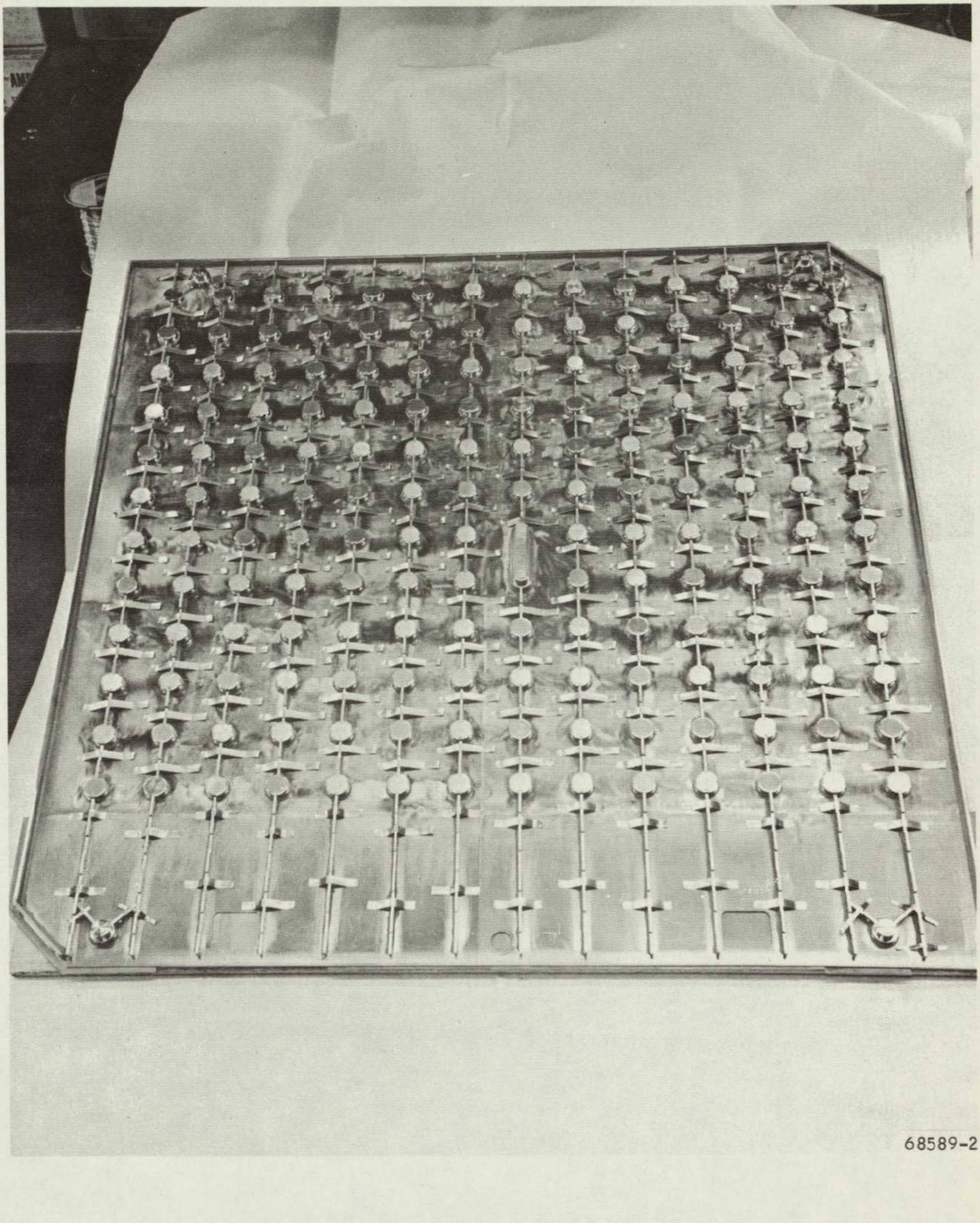

68589-2

Figure 4-18. Remote Cooling Loop Subassembly Ready for Brazing

Following this braze cycle the remote loop was subjected to a helium leak check which indicated several areas requiring repair. Several of the bosses were repaired by TIG brazing with Palniro RE braze alloy. However, one of the mounting bosses could not be sealed by TIG brazing or TIG welding repair procedures. This mounting boss was removed from the brazed assembly by machining and a combination boss, webs, and doubler plate was fabricated and brazed into the remote loop with EMS 9-4778 in a vacuum braze cycle. Following the repair braze cycle, the remote loop was subjected to a helium leak check and one boss showed excessive leakage. The helium leak was repaired by a TIG braze repair operation with Palniro RE alloy. The structural sandwich was assembled from the details and brazed with EMS 9-4779 in a vacuum braze cycle. Upon completion of the braze cycle, the water plenum holes were drilled in the square tube water plenum. Figure 4-19 shows the completed structural sandwich.

The last vacuum furnace braze cycle was to complete the heat pipe braze assembly. In this braze cycle the remote loop, structural sandwich, heat pipe details, sublimator mounting frame, and the sublimator fins were brazed with EMS 9-4778. Figure 4-20 presents the build up of details for the final braze cycle. The braze cycle was closely controlled to minimize the panel bowing due to temperature differentials through the panel assembly. Following the braze cycle, the completed assembly was X-rayed. While the quality of the braze joints could not be determined, the X-ray verified that all detail parts remained in the proper position during the braze cycle. The first helium leak check performed was between the remote cooling loop and the heat pipe which showed that the joints remained helium leak tight. The second helium leak check performed was an air leakage check of the heat pipe to the atmosphere which indicated two areas of leakage, one at the header bar to tube sheet and the other at the mount bosses. The header bar to tube sheet leaks were repaired by TIG brazing with Nioro alloy, as were the leaks at the mount bosses. By sealing the mounting bosses with the external TIG brazing repair, the structural sandwich became subjected to the heat pipe vacuum. When the heat pipe section was subjected to a helium leakage check, an additional leak was located in the header bar between the water plenum and the heat pipe. Initial TIG brazing repairs were unsuccessful as this leak was not readily accessible from the exterior. However, the repair was accomplished using Silver Solder in lieu of TIG brazing, with the heat pipe helium leak check indicating a maximum leakage of $1 \times 10^{-6}$ scc/sec.

The assembly procedure continued with Nioro TIG brazing of the water line bosses, the thermostat cup, and the palladium-silver plates to the heat pipe. A helium leak check following these TIG brazing attachments indicated that the palladium-silver plates were cracked and these were repaired by additional Nioro TIG brazing. The repair of the palladium-silver plates was confirmed by an additional helium leak check. The next step in the assembly sequence was to Nioro TIG braze one half of the water reservoir to the heat pipe and then helium leak check the heat pipe which ensured that no leak paths had been opened. Following the attachment of the reservoir, the equipment mounting bosses were drilled and tapped on a tape-controlled drilling machine.

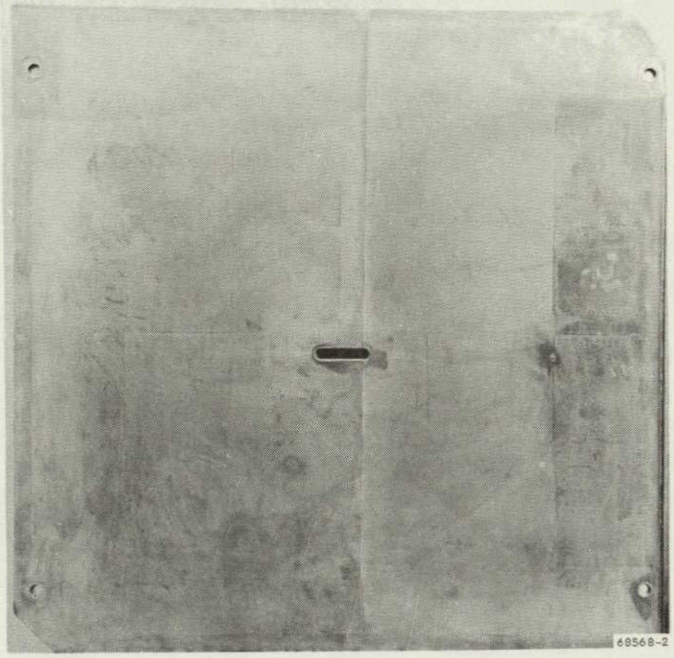


a. VIEW OF STRUCTURAL SANDWICH FROM HEAT PIPE SIDE

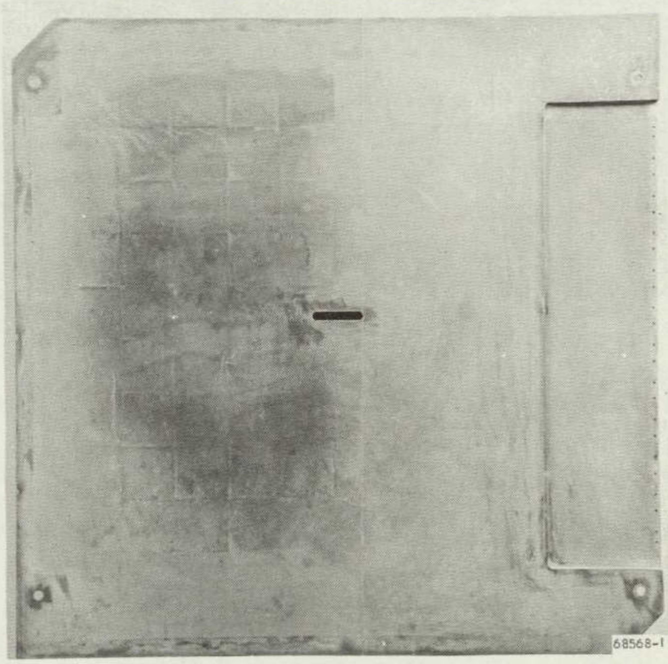


b. VIEW OF STRUCTURAL SANDWICH FROM SUBLIMATOR SIDE



F-12538

Figure 4-19. Instrument Unit Thermal Conditioning Panel Structural Sandwich.

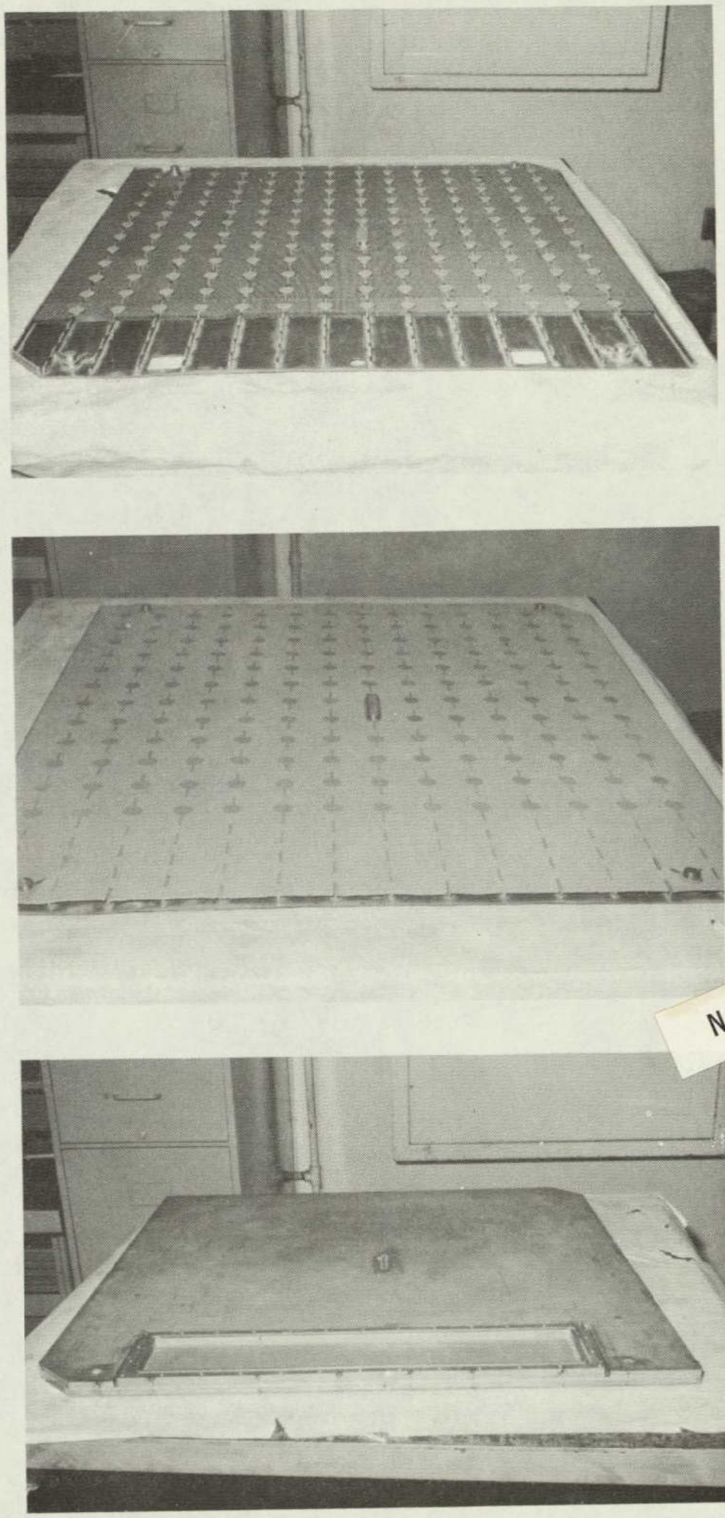



F-12539

Figure 4-20. Buildup of Details for Final Braze Cycle

The wick was conditioned by holding the assembly at $600^{o}F$ for 1 hr in a vacuum atmosphere. Following the wick conditioning cycle, the heat pipe was subjected to the final helium leak check which indicated a leakage rate of $2.7 \times 10^{-7}$ scc/sec of helium with the entire external surface of the assembly exposed to a helium atmosphere. Following the helium leak check, the heat pipe was filled with water and the copper fill tube sealed.

The final assembly of the heat pipe panel was accomplished by bolting on (1) the thermostatic flow control valve and its associated lines, (2) the upper half of the reservoir and bladder, (3) two bellows type shut off valves on the reservoir, and (4) the sublimator plate assembly. The completed assembly is shown on Figure 4-21.

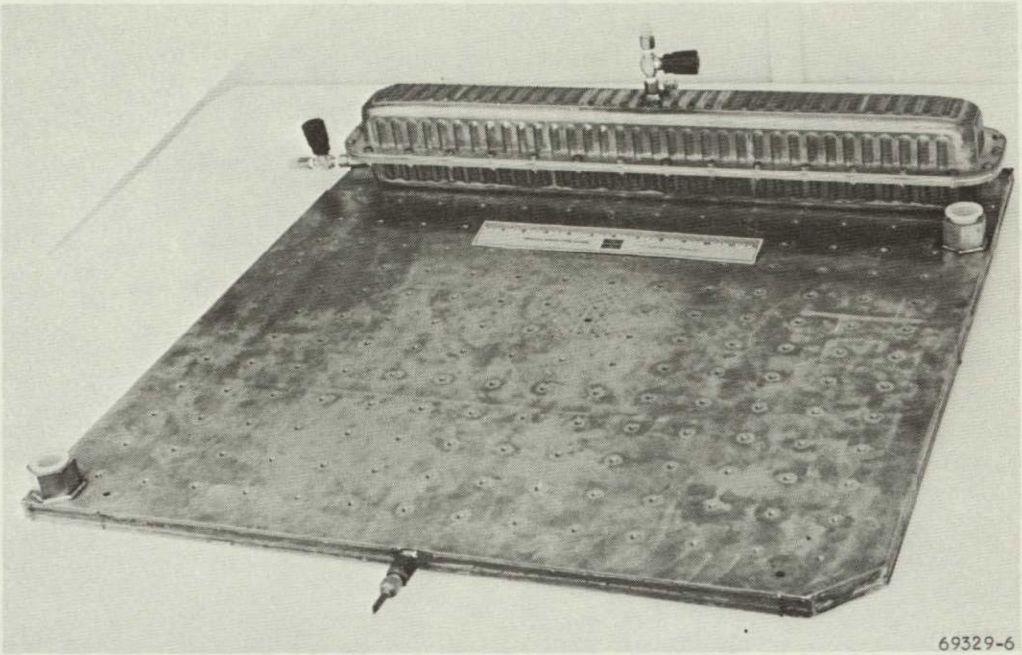


a. OVERALL VIEW OF PANEL ASSEMBLY

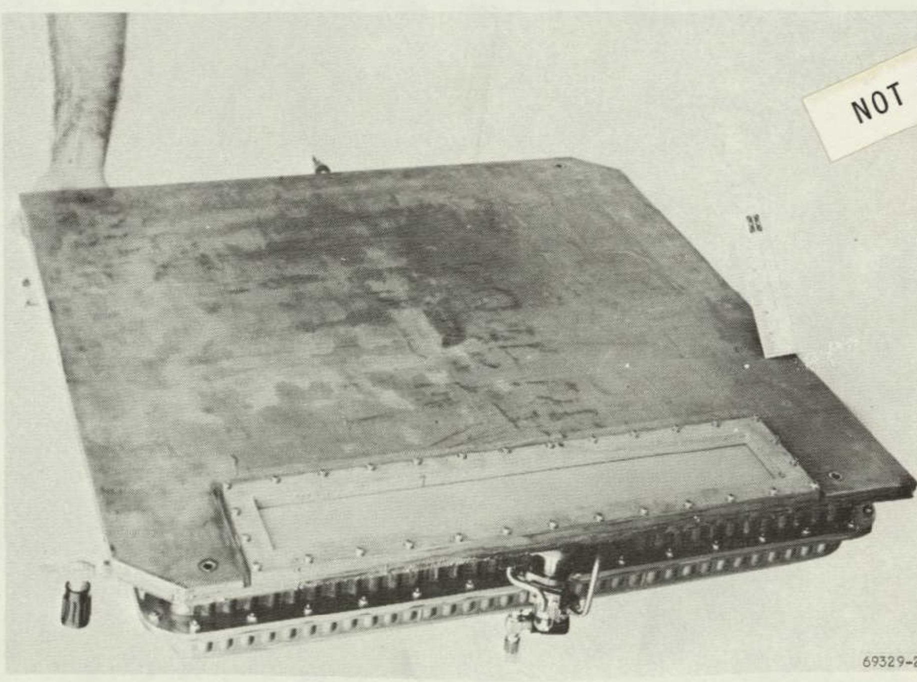


NOT REPRODUCIBLE

b. VIEW OF SUBLIMITOR AND THERMAL SENSING VALVE

F-12540

Figure 4-21. IU Thermal Conditioning Panel

## SECTION 5

## TASK IV--TEST OF FULL SIZE THERMAL PANEL

### INTRODUCTION

The heat pipe thermal panel module was tested with heat loads up to 420 watts to evaluate sublimator and heat pipe performance. This heat load is the maximum load which the panel will experience. Instrumentation was provided to record representative panel temperatures at selected locations.

### TEST SETUP

The panel test setup included installation of heaters, thermocouples, the remote cooling loop water cooling system, and the water reservoir filling apparatus. A setup schematic is presented on Figure 5-1.

Thermocouple instrumentation was installed on the panel surface using Copper-Constantan type thermocouple wire at locations indicated in Figure 5-2. The bead of the thermocouple was attached to the plate and the lead was attached to an insert placed in the mounting boss as shown in Figure 5-3.

The electric heater blankets (7-1/2 by 13-1/2 in. strip heaters) were installed by two different techniques. The configurations 1 and 2 installations are shown in Figures 5-4 and 5-5, respectively. Heater locations 1, 2, and 3 are designated in Figure 5-2. The configuration 1 heater was attached to the surface of the panel using RTV 732 as a bonding agent. Weights were placed on the heater blankets during the bonding process to ensure that the thickness of the bond did not exceed 0.015 in.

The configuration 2 heaters were attached to 7-1/2 by 13-1/2 by 1/4 in. thick aluminum plates with RTV 732 using the same installation technique as the configuration 1 installation. The aluminum plates were thermally bonded to the panel surface with a silastic and oxide mixture manufactured by G. C. Electronics (No. 8109-S). Bolts were used to hold the aluminum plates against the panel. The thermocouples were fed through 3/8-in. holes drilled in the aluminum plate in order to record panel surface temperatures (Figure 5-6).

The temperature sensing valve was stored below 32°F with a 20-lb load prior to assembly on the panel. For calibration the temperature sensing valve was placed in a fixture using backup hardware from the panel assembly to simulate the actual panel installation. The valve was placed in a closely controlled fluid calibration both with a 19-psia air supply connected to the valve inlet. The valve was cycled from 58° to 65°F three times in 1°F temperature increments every 5 min. The valve opened and closed as shown in the table below.

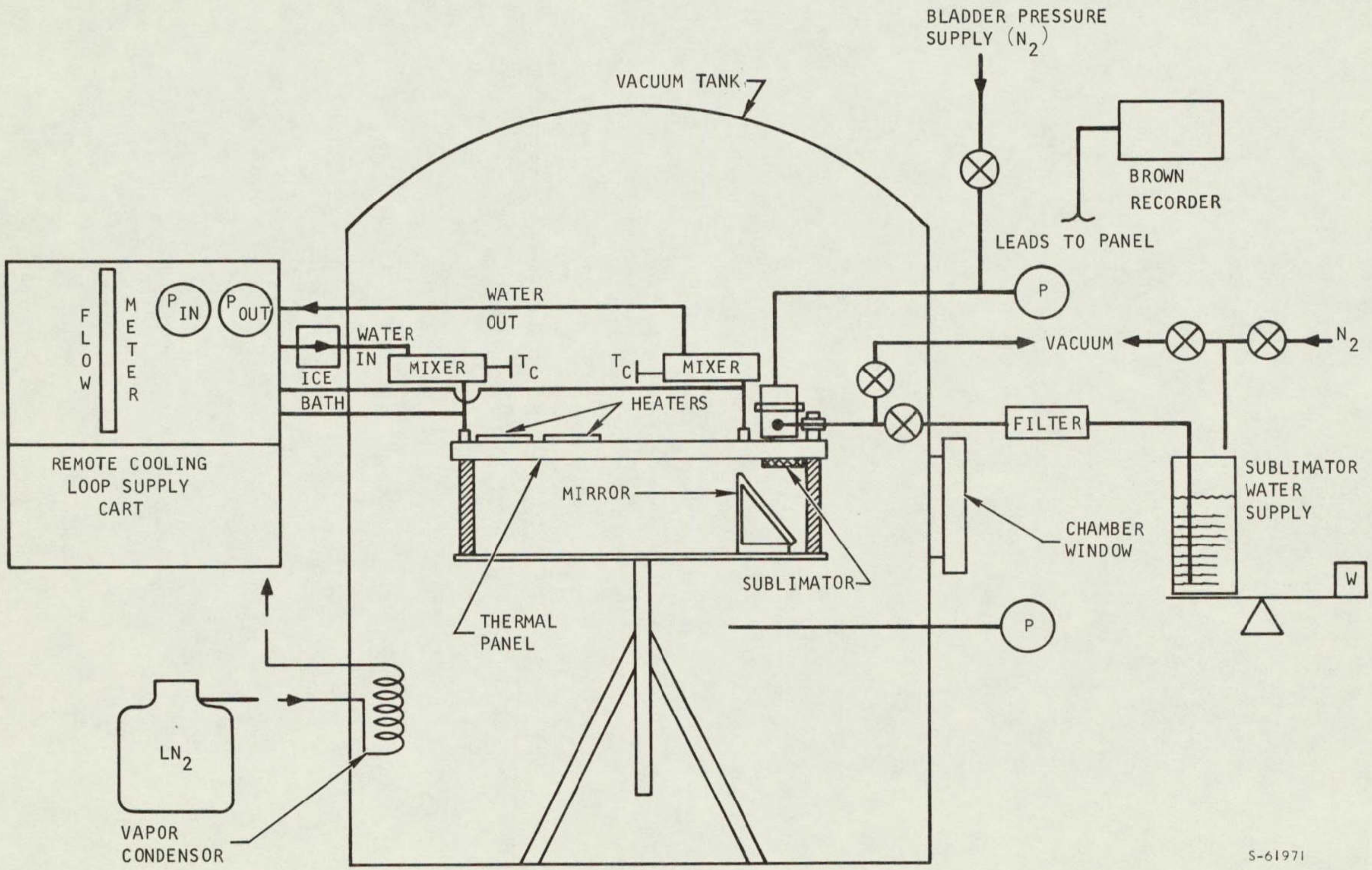


Figure 5-1. Schematic of High Altitude Test Setup

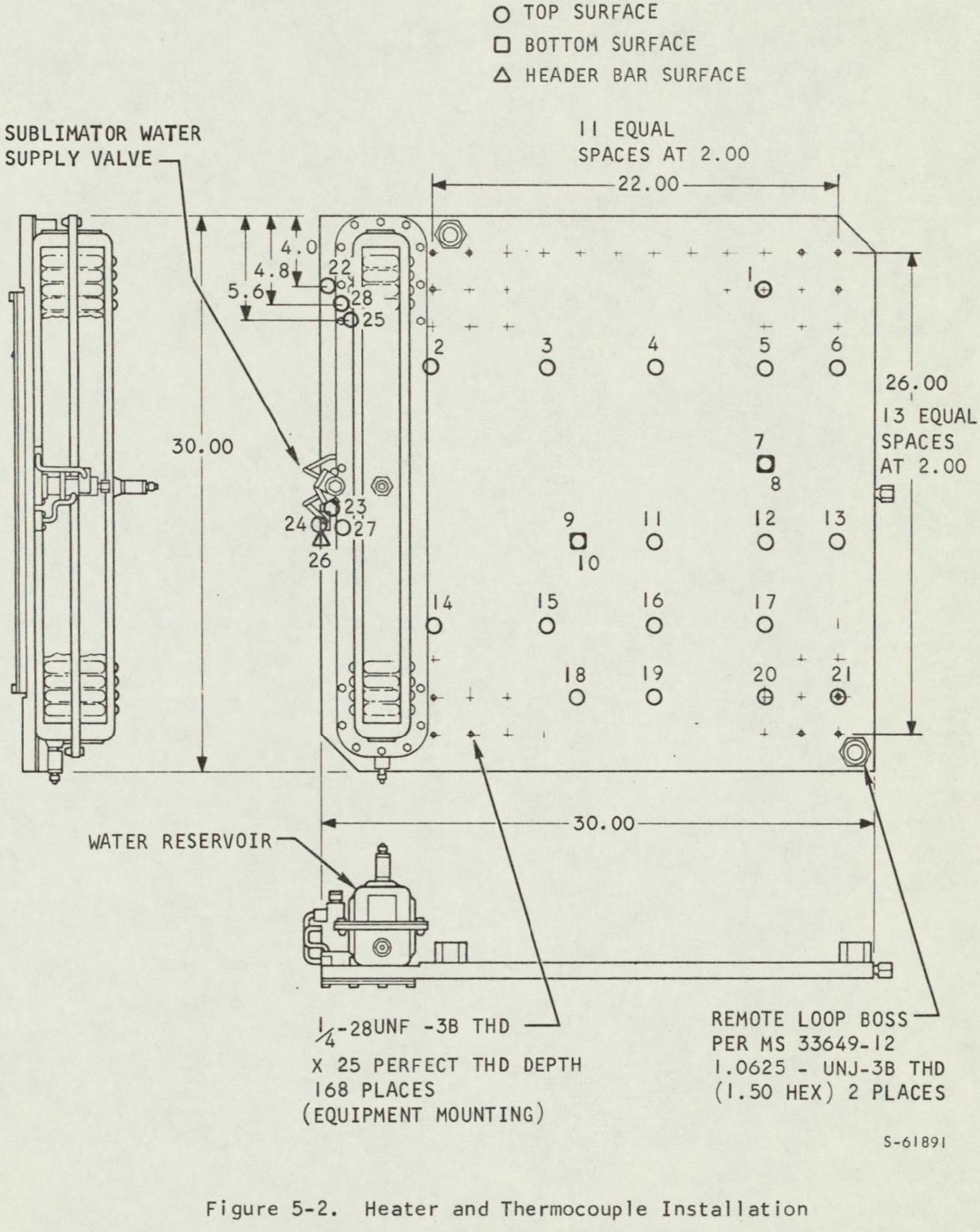


Figure 5-2. Heater and Thermocouple Installation

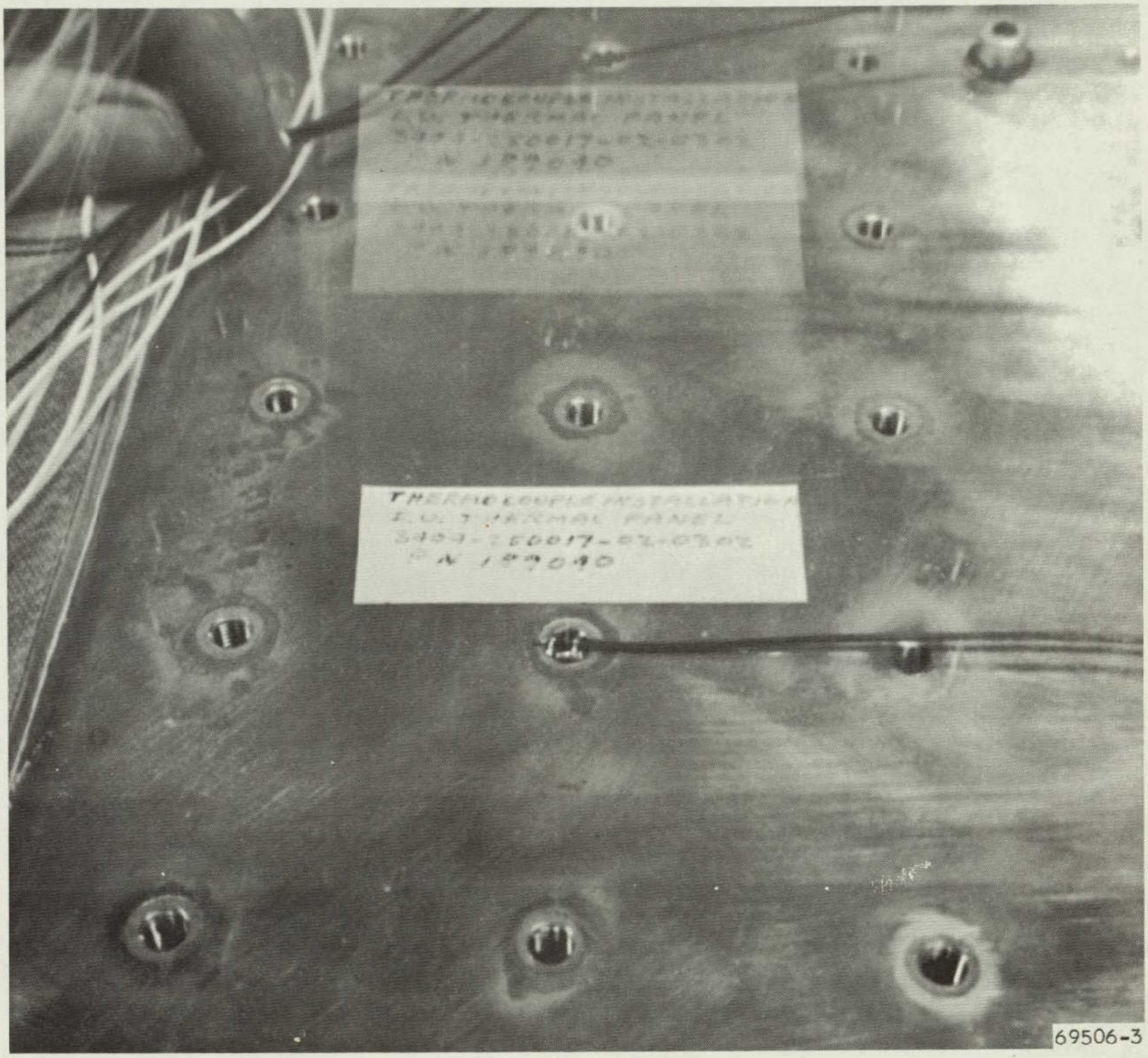




Figure 5-3. Thermocouple Installation

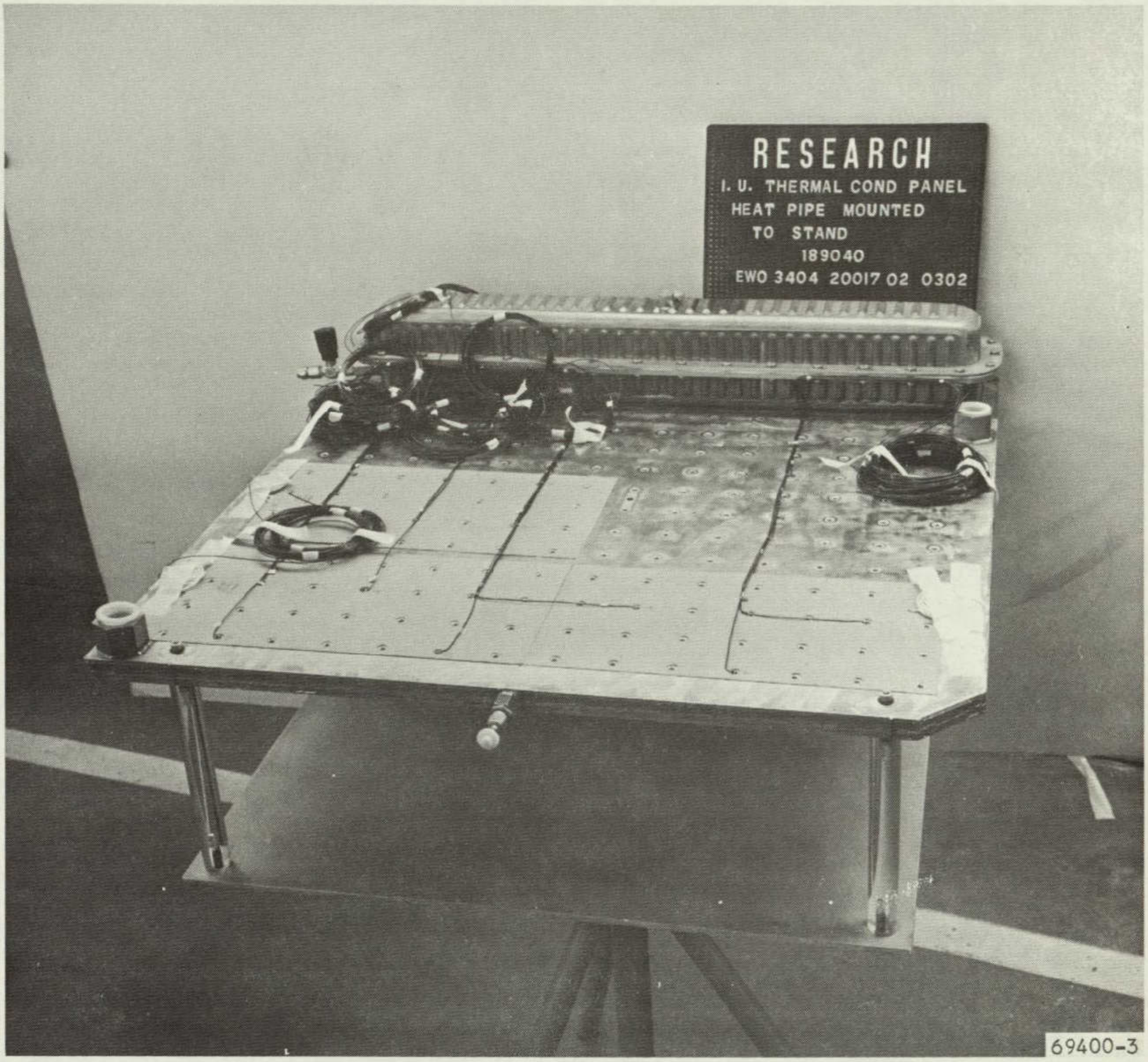


69400-3

Figure 5-4. Configuration I Heater Installation - Heater Bonded to Panel Assembly

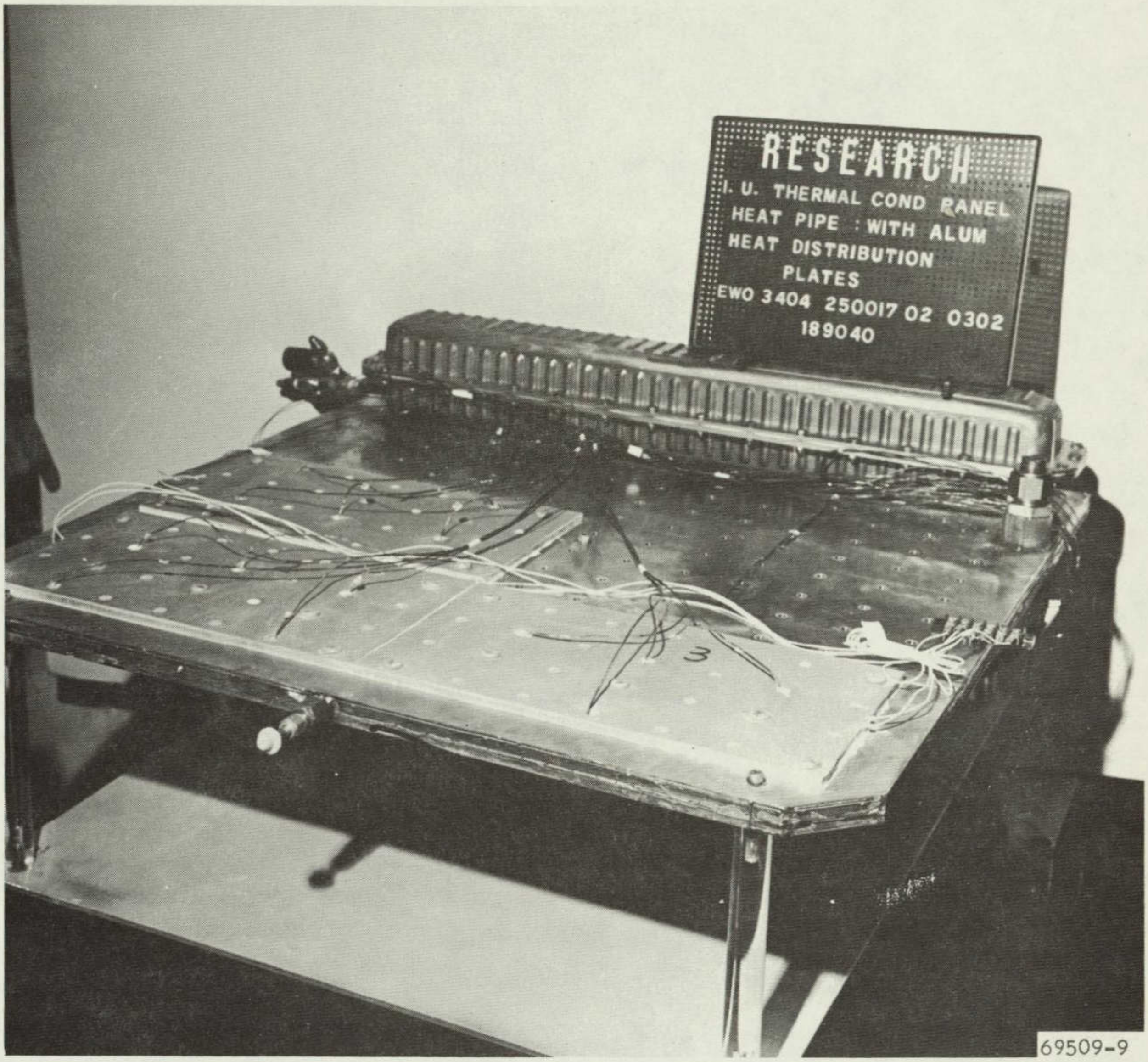


69509-9

Figure 5-5. Configuration 2 Heater Installation - Heaters Bonded to Aluminum Plates

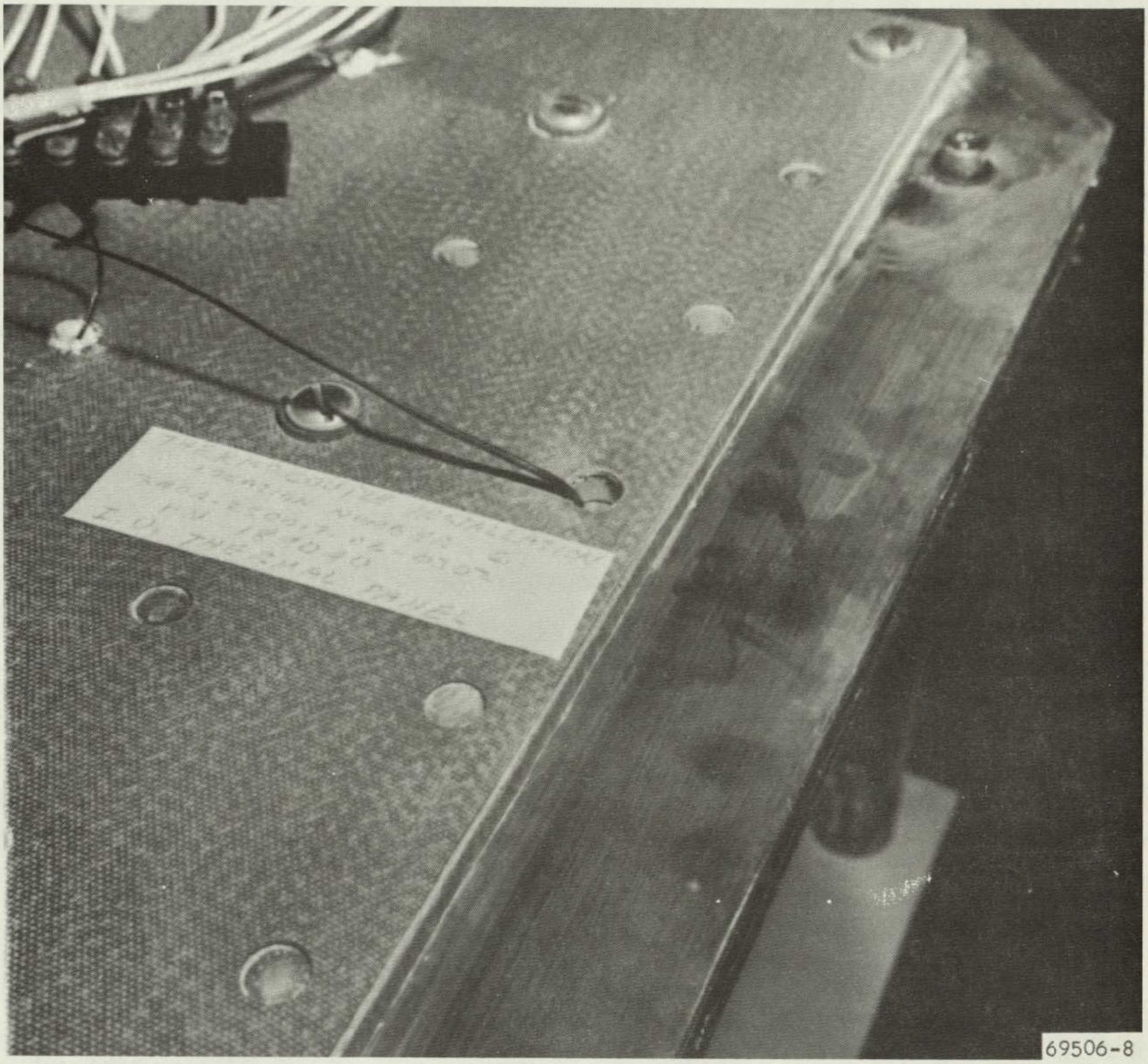

69506-8



Figure 5-6. Thermocouple Installation with Configuration 2
Heater Installation

| | Temperature, °F | | |
|---|---|---|---|
| Valve Position | Cycle 1 | Cycle 2 | Cycle 3 |
| Open | 63.0 | 63.0 | 63.0 |
| Close | 60.2 | 60.3 | 60.3 |

The opening and closing of the valve was determined by air flowing through the valve.

### Heat Pipe Filling

The charging of the heat pipe was performed in the laboratory during manufacturing. The heat pipe was filled with distilled, degassed water filtered to 10 microns using the filling setup shown in Figure 5-7.

The fill apparatus was fabricated from stainless steel and copper tubing with bellows-type vacuum valves. The assembly was vapor degreased, freon flushed, and helium leak checked prior to installation on the panel assembly. The fill apparatus was connected to the panel assembly with a combined leakage (fill apparatus and panel assembly leakage) no greater than $2.7 \times 10^{-7}$ scc/sec. The heat pipe was evacuated with a diffusion pump for 20 hr with a resulting minimum pressure of $7 \times 10^{-4}$ mm Hg abs. Heat was applied externally to the panel by heat lamps during the last 4 hr of evacuation at a panel temperature of 195°F. A volume of 959 cc of distilled, degassed water was metered into the heat pipe section of the panel. The copper fill tube (1/4 in. O.D. by 0.028-in. wall) was sealed by cold diffusion bonding using a hydraulic press.

## PERFORMANCE TESTING

Testing was performed both at a simulated altitude of 170,000 ft (0.5 mm Hg abs) using water sublimation as the means of heat rejection and at sea level using cold water as the heat sink.

### Altitude Thermal Performance Testing

The test schematic for the altitude thermal performance testing is presented in Figure 5-1 and the overall setup is shown in Figure 5-8. Water lines, thermocouple wires, sublimator pressure and fill lines, and heater wires were ducted through and sealed at the vacuum chamber bulkhead. The panel was mounted on a stand so that the sublimator porous plate was visible in a mirror adjusted for viewing from outside the chamber.

The sublimator reservoir was charged with distilled, degassed water filtered to 1 micron from a storage reservoir external to the vacuum chamber. The storage chamber, pressurized with nitrogen, was placed on a balance scale to determine the weight of water placed in the sublimator reservoir. The maximum capacity of the reservoir was measured to be 11.25 lb of water (10.5 lb fill weight). The pressurization side of the bladder was evacuated prior to filling

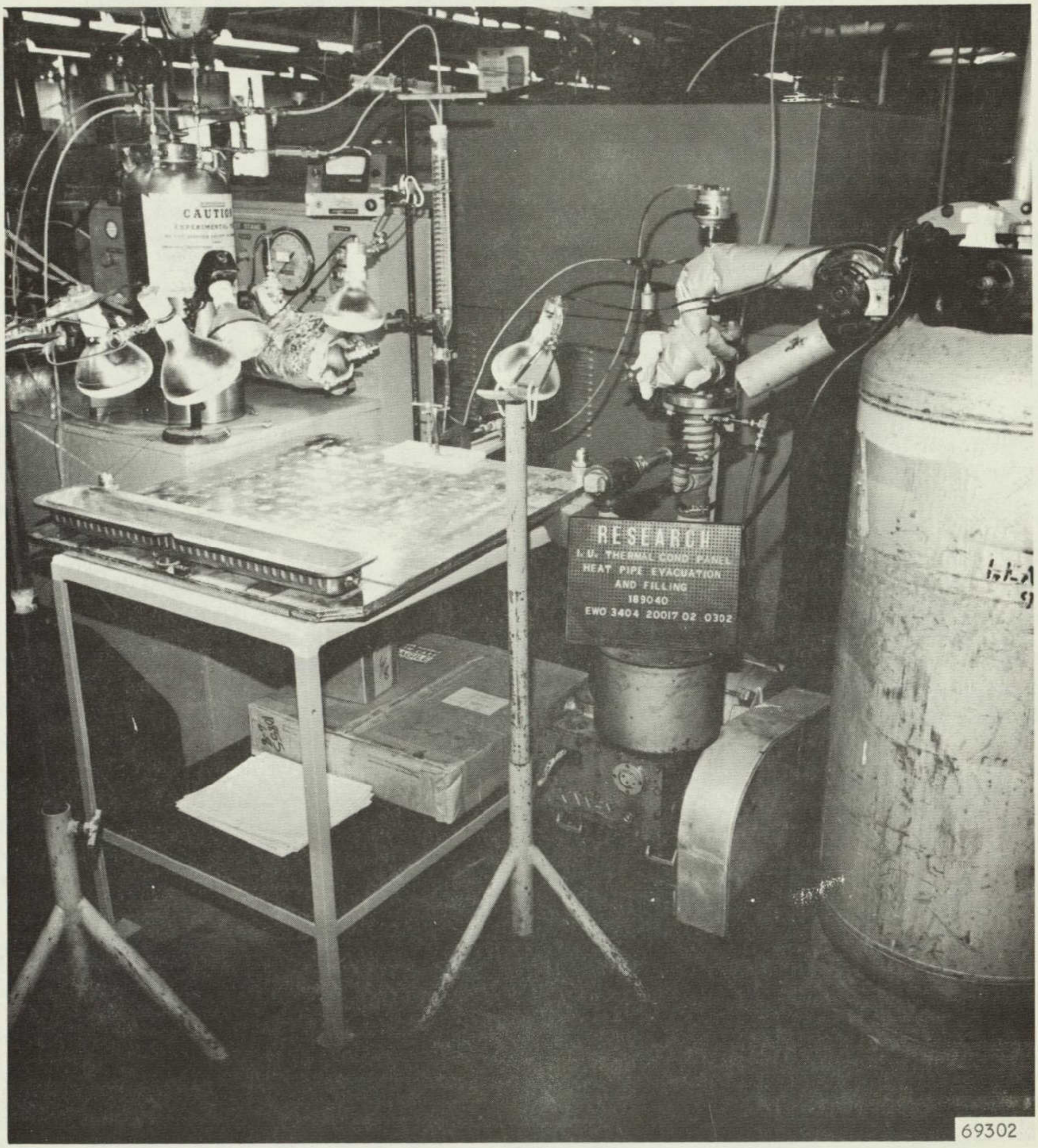


Figure 5-7. Heat Pipe Filling

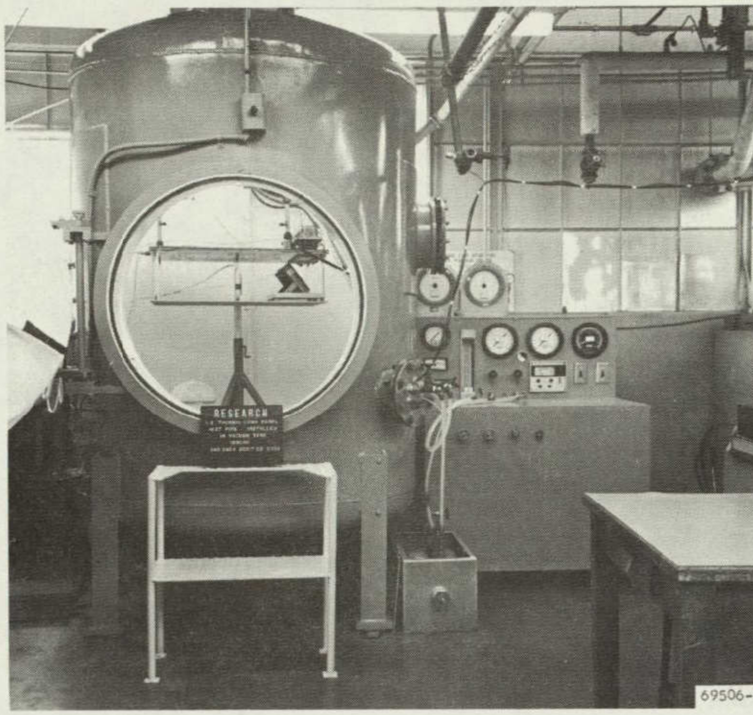


a. HEAT PIPE INSTALLED IN VACUUM CHAMBER

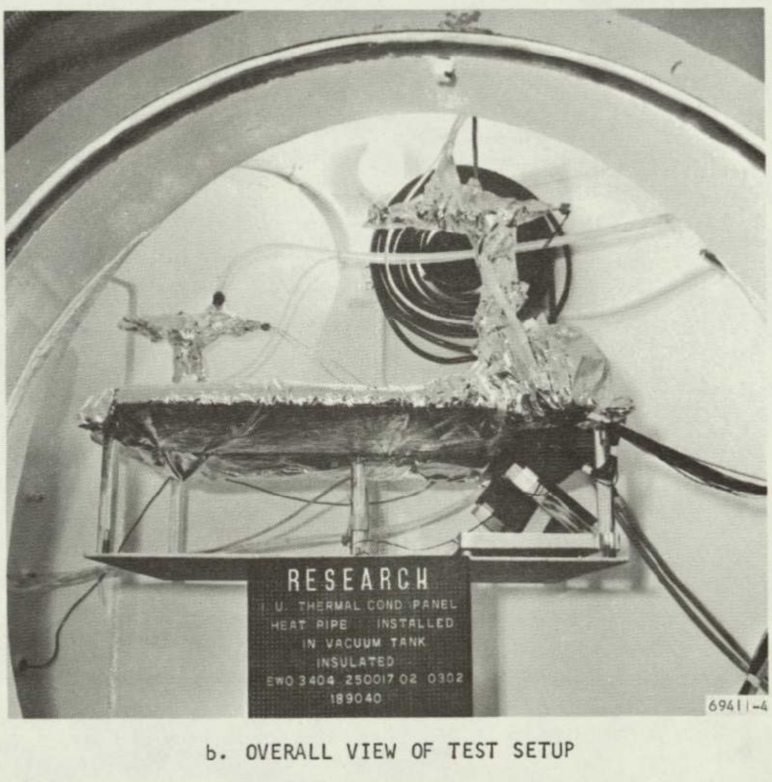


b. OVERALL VIEW OF TEST SETUP

F-12529

Figure 5-8. Thermal Conditioning Panel Test Setup the reservoir with water and then pressurized external to the vacuum chamber with dry nitrogen to a pressure of 4 psia. The panel temperature was maintained at a maximum of 60°F to ensure that the sublimator reservoir valve was closed.

Heat was applied to the panel assembly after the chamber was evacuated to a minimum chamber pressure of 0.5 mm Hg abs. Both configurations 1 and 2 heater installations were tested. Data was recorded after the panel reached steady state conditions as evidenced by monitoring the panel surface thermocouples on a 24-channel Brown recorder.

The panel was subjected to heat loads of 420, 315, 210, and 105 watts using the configuration 1 heater installation and 420, 315, and 210 watts using the configuration 2 heater installation.

Sea Level Thermal Performance Testing

The test setup for the sea level thermal performance testing is illustrated in Figures 5-9 and 5-10. The cooling water was passed through an ice bath prior to entering the pan covering the condensor (sublimator plate removed to expose the fins and the surface of the condensor). Figure 5-11 shows a view of the duct and the condensor end of the heat pipe panel in the test setup. The thermocouples were placed in contact with the sublimator fins prior to wrapping fiberglass insulation around the test assembly.

The heaters were attached thermally to the panel surface with the silastic-oxide paste using the configuration 2 heater installation technique. The heat input to the panel assembly was controlled with a variac and recorded on an ammeter and a voltmeter. The same thermocouple installation was used as the altitude performance testing with the addition of three surface thermocouples attached to the panel at the condensor end.

Four data runs were performed using the sea level performance test setup. With water as the heat pipe fluid, the panel was subjected to heat loads of 420 and 210 watts. With methanol as the heat pipe fluid, the panel was subjected to heat loads of 140 and 70 watts. Panel temperatures were recorded as in previous testing.

Remote Cooling Loop Testing

The remote cooling loop isothermal pressure drop testing was performed using water as the coolant at flow rates of 1.0, 2.0, 3.0, 4.0, 5.0, and 6.0 lb/min. Inlet and outlet pressures and temperatures as well as unit pressure drop and flow rate were recorded. The inlet fluid was maintained at a pressure of 50 psig and a temperature of 60°F.

The remote cooling thermal performance testing was performed at water flow rates of 1.0, 2.0, 3.6, 4.0, and 5.0 lb/min at heating rates of 420 and 210 watts. Inlet and outlet temperature and pressure, coolant flow rate, electrical power input, and panel surface temperature were recorded. An inlet pressure of 50 psig and an inlet temperature of 60°F was maintained for all data runs.

GARRETT
AIRESEARCH MANUFACTURING COMPANY
Los Angeles, California

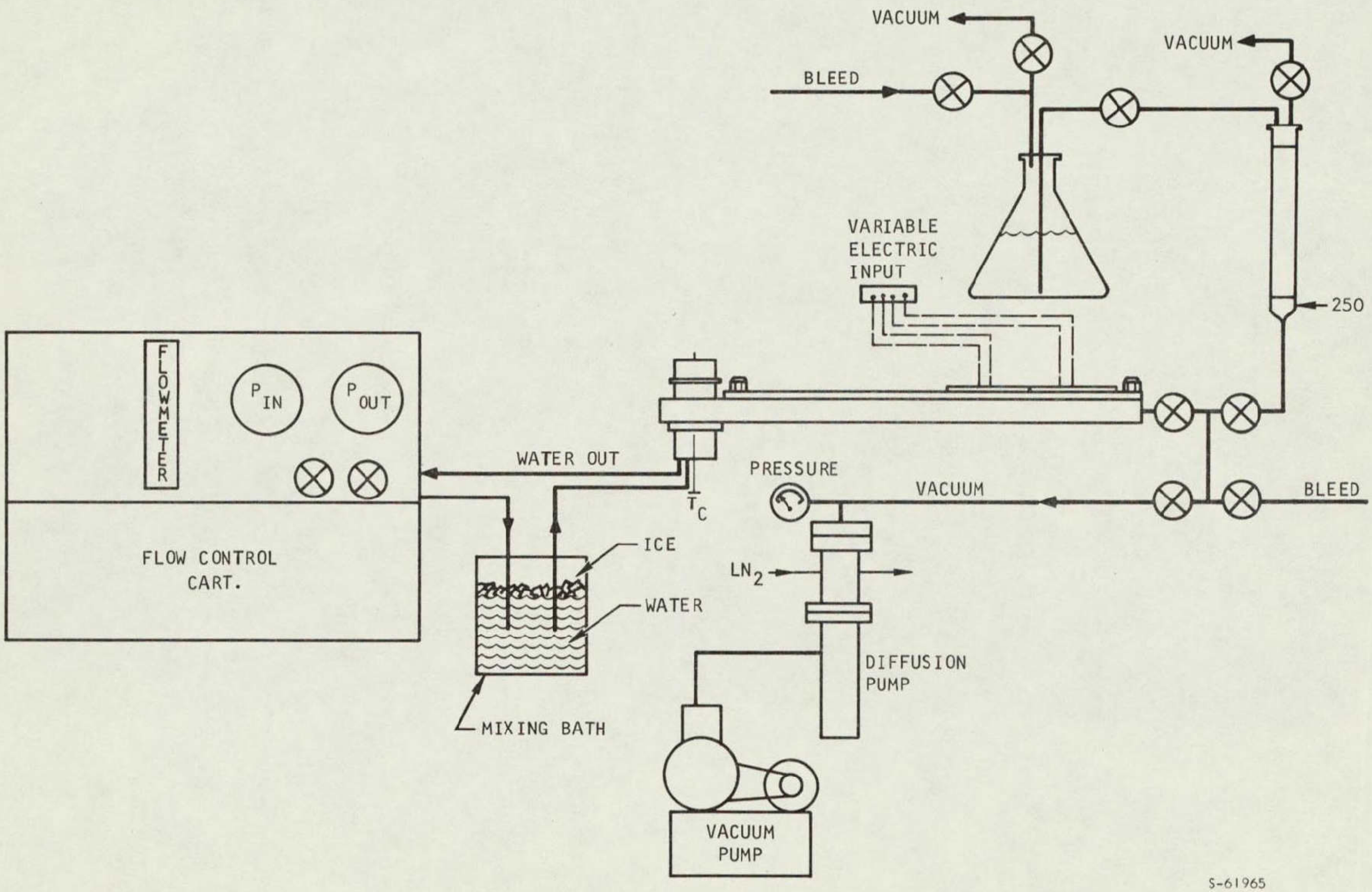


Figure 5-9. Sea Level Thermal Performance Test System with Fill Apparatus and Simulated Sublimator

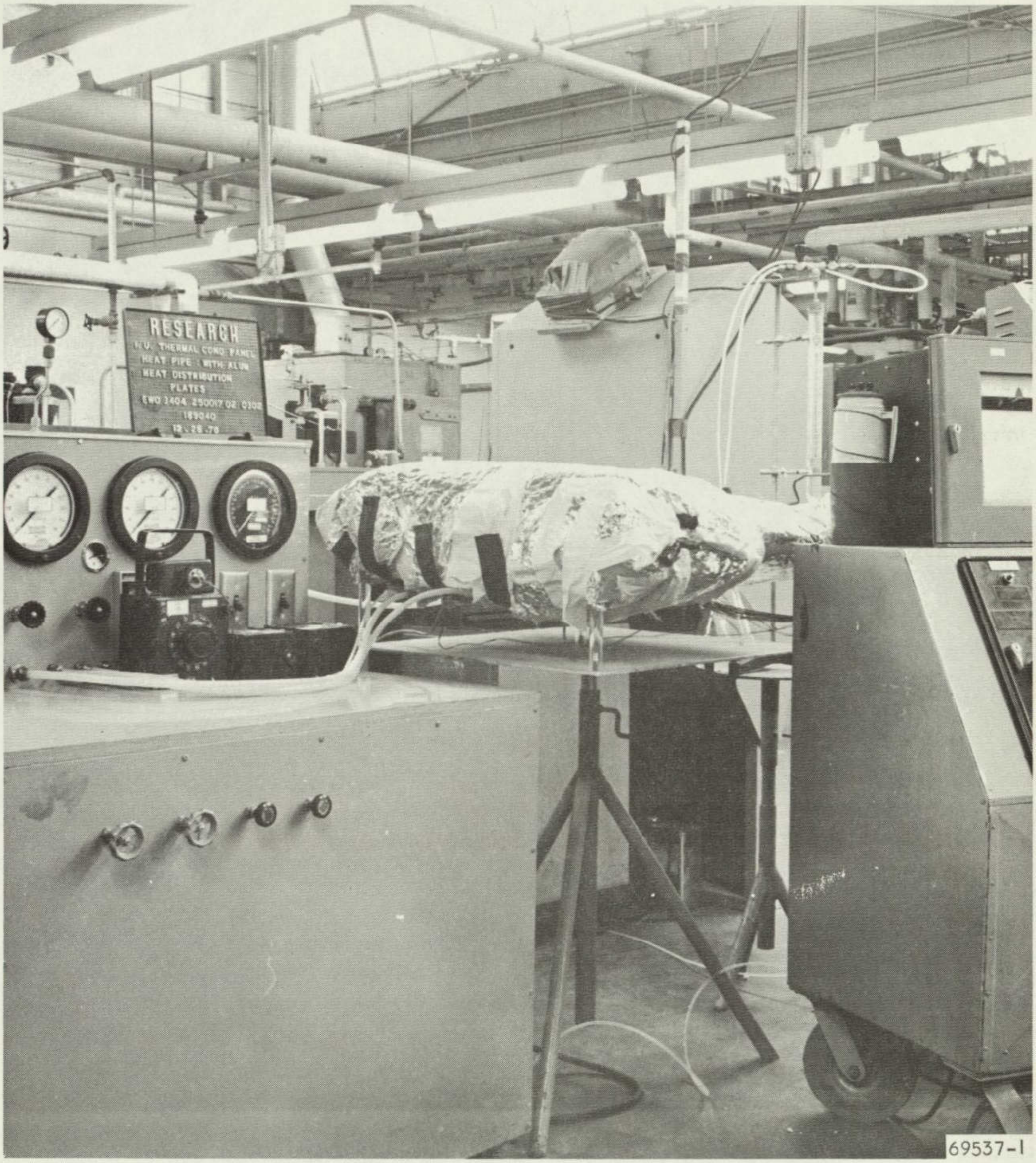




Figure 5-10. Sea Level Thermal Performance Test Setup

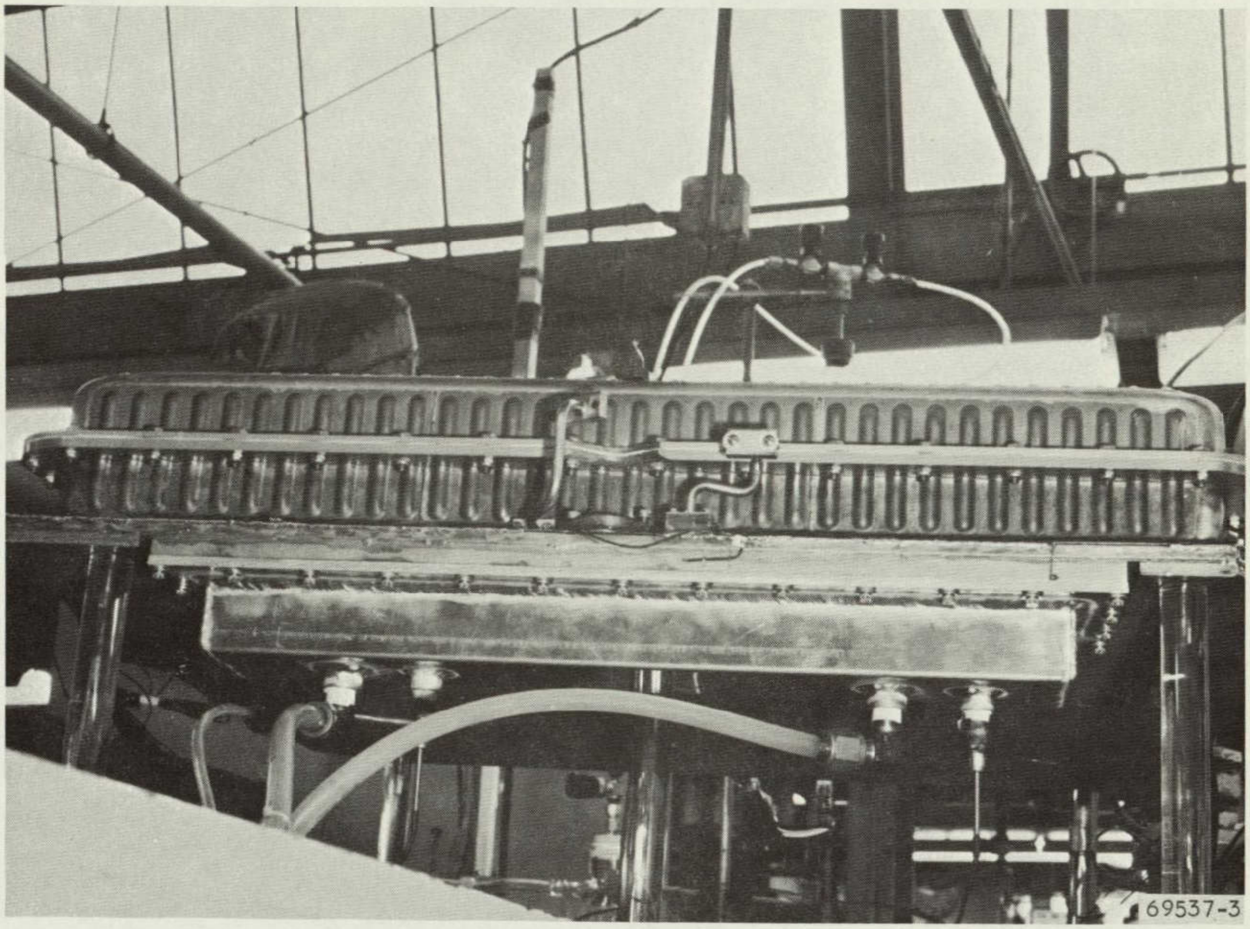

a. WATER-COOLED HEAT SINK FOR SEA-LEVEL PERFORMANCE TESTING

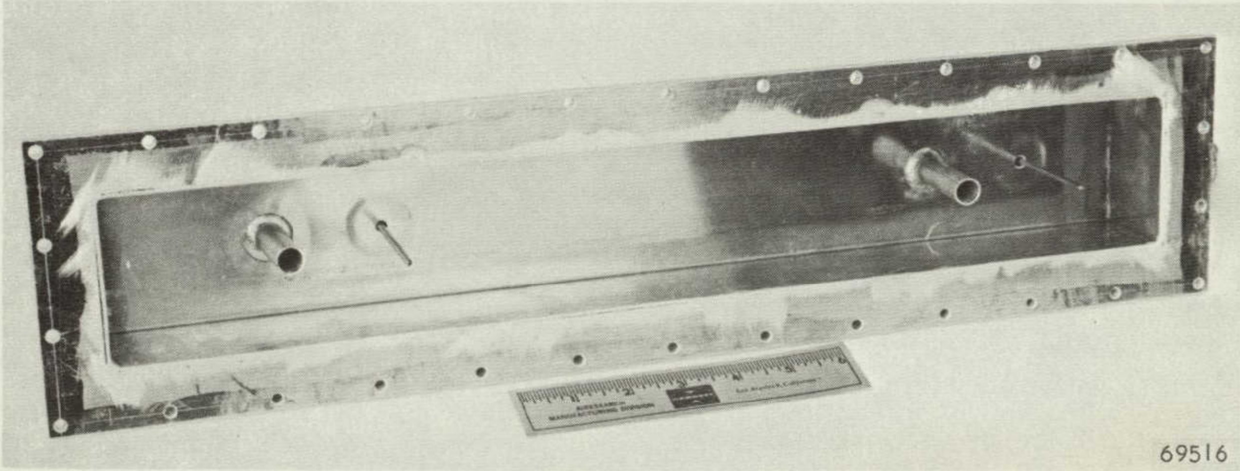

b. CLOSE-UP OF DUCT ASSEMBLY

F-12528

Figure 5-11. Ducting for Sea Level Performance Testing

## Remote Cooling Loop Performance Testing

The remote cooling loop testing included an isothermal pressure drop test and a heat transfer performance test. The pressure drop test data is shown in Figure 5-12 along with analytical predictions. Because of the bosses which extend through the remote loop, the coolant free flow area varies along the flow path. Pressure drop predictions were made based upon maximum and minimum free flow areas in order to bracket the expected performance. The predictions include contraction, expansion, and turning losses associated with the fluid entering and exiting the panel as well as turning losses within the remote loop. These losses were small compared to the friction losses, amounting to about 7 percent of the total predicted pressure drop.

The experimental overall pressure drop was about 1.5 to 2 times the predictions. Since the entrance and exit losses were such a small fraction of the analytical overall pressure drop, they alone could not account for the higher pressure loss. It is more likely that the friction losses were higher than expected, possibly due to burrs on the fins or to slight crushing of the fins during brazing.

While the pressure drop was larger than anticipated, it is noted that the remote loop was designed not to use up all of the available pressure drop in case the pressure drop was higher than expected. The data of Figure 5-12 was used to determine if the pressure drop using the design coolant, 60 percent methanol and 40 percent water, would be higher than the 6 psi maximum allowable. Using the conventional pressure drop equation, the ratio of the pressure drop of methanol-water (design coolant) to that of water (test coolant) is

$$\frac{\Delta P_m}{\Delta P_w} = \frac{\dfrac{4f_m L}{D_h}\,\dfrac{G_m^2}{2g\rho_m}}{\dfrac{4f_w L}{D_h}\,\dfrac{G_w^2}{2g\rho_w}} \qquad (5\text{-}1)$$

The friction factor f was calculated from the experimental data as a function of the Reynolds number, and was found to be

$$f = \frac{7.06}{Re^{0.655}} \qquad (5\text{-}2)$$

Using the definition of Reynolds number, $Re = GD_h/\mu$, and combining Equations (5-1) and (5-2), the pressure drop ratio becomes

$$\frac{\Delta P_m}{\Delta P_w} = \left(\frac{\mu_m}{\mu_w}\right)^{0.655} \left(\frac{\rho_w}{\rho_m}\right) \left(\frac{G_m}{G_w}\right)^{1.345} \qquad (5\text{-}3)$$

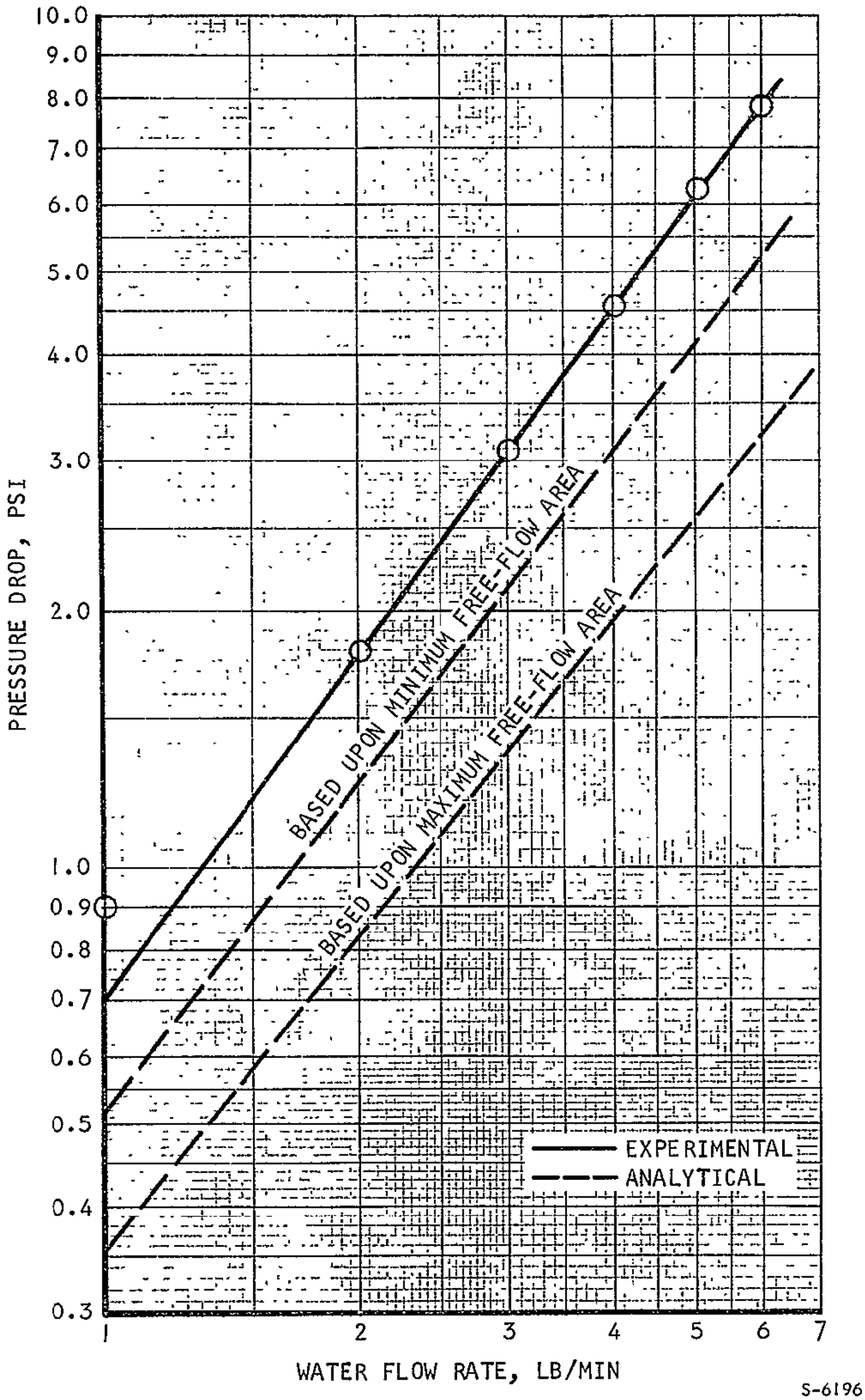


Figure 5-12. Remote Cooling Loop Pressure Drop

For the case of equal flow rates, $\Delta P_m / \Delta P_w$ = 1.41 at a temperature of 60°F. At the design flow rate of 3.6 lb/min, the data shows a pressure differential with water of 4 psi, which yields a methanol-water pressure differential of 5.6 psi. While this pressure drop is larger than the predicted 3.5 psid, it is still within the 6 psi allowable pressure drop.

Heat transfer tests were performed at half and full heat loads at coolant flow rates from 1.0 to 5.0 lb/min. The test conditions are listed in Table 5-1 with the heat balance results.

TABLE 5-1

REMOTE COOLING LOOP TEST CONDITIONS

| Run No. | Coolant Flow Rate, lb/min | Electrical Heat Input, Watts | Heat Absorbed in Coolant, Watts | Percent Heat Loss |
|---|---|---|---|---|
| 1 | 5.0 | 214 | 176 | 18 |
| 2 | 4.0 | 211 | 197 | 7 |
| 3 | 3.6 | 210 | 209 | 1 |
| 6 | 1.0 | 210 | 206 | 2 |
| 1A | 5.0 | 420 | 417 | 1 |
| 2A | 4.0 | 420 | 413 | 2 |
| 3A | 3.6 | 420 | 418 | 1 |
| 5A | 2.0 | 420 | 417 | 1 |
| 6A | 1.0 | 420 | 403 | 4 |
| 7A | 3.6 | 420 | 410 | 2 |

The heat transfer performance data from Runs 1A, 5A, 6A, and 7A is shown in Figure 5-13 where the panel surface temperature under the heaters is shown as a function of distance along the panel in the flow direction of the last pass of the remote coolant loop. The surface temperatures increase along this path because the coolant temperature increases. The panel surface temperatures were predicted analytically using the design equations (4-7) through (4-10). Since the heat input and the remote loop conductance are uniform, the coolant and panel surface temperatures increase linearly. The effect of mixing on the local coolant temperature was discussed in the remote coolant loop design section. Since this affects the local panel temperature, the predictions are shown as a range; the lower limit is for complete mixing of the coolant along its flow path and the upper limit is for no mixing. The test data showed good agreement with the analytical predictions.

## Altitude Thermal Performance Testing

Initial tests of the heat pipe-sublimator panel were performed with the configuration I heater installation in which the heater blankets were bonded directly to the panel surface. The 105-watt heat load was run first and then

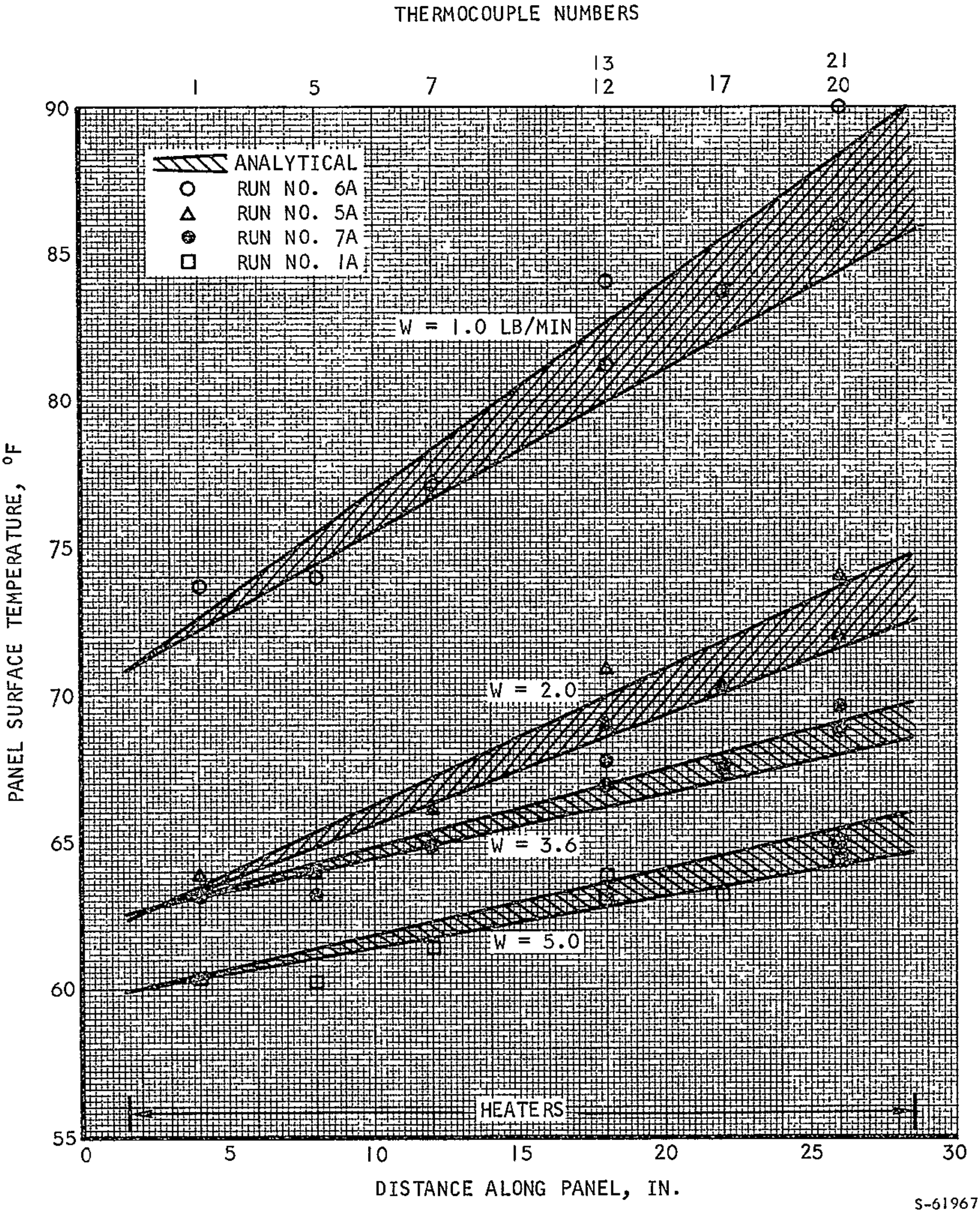


Figure 5-13. Remote Cooling Loop Thermal Performance

the heat load was increased in 105-watt increments. Thermocouple numbers 1 through 23 were recorded continuously at the rate of two readings of each thermocouple per minute. Temperatures at selected locations are shown in Figure 5-14 for the initial test run of 105 watts applied to heaters 2 and 3. Thermocouples 1 and 5 represent the maximum and minimum recorded surface temperatures underneath the area of heat input. Thermocouple 2 was typical of most of the panel surface which was not heated. Thermocouple 23 was adjacent to the copper insert in which the valve actuating temperature sensor was located. It is seen in Figure 5-14 that the panel never reached a true steady-state condition. This was of course due to the temperature level at which the sublimator water feed valve was actuated. Since this temperature was above the steady-state temperature of the cold end of the heat pipe, the panel performance was cyclical. When the sublimator is dry and heat is applied to the panel, the heat pipe will heat up until the cold end reaches the water valve actuation temperature and water is fed to the sublimator. The sublimator will provide cooling, decreasing the panel temperature below the valve actuation temperature, thereby shutting off water flow to the sublimator. The sublimator will continue to cool the panel until the water supply in the sublimator plenum runs low, at which time the panel again heats up and the cycle repeats. Figure 5-14 shows one cycle of the panel performance. When heat was applied, the panel heated up at a fairly constant rate, and when the cold end reached the water valve actuation temperature (approximately 63°F), cooling was provided by the sublimator. In this particular run the water valve was not open long enough to fill the entire plenum as evidenced by a continued increase in the panel temperature and the relatively short time (12 min) in which the temperature at thermocouple 23 began to increase. (If the plenum were full, approximately 45 min. of cooling would be provided at a heat load of 105 watts.) The valve opened again when the local temperature was high enough, and the cooling provided by the sublimator decreased the surface temperatures throughout the panel. Shortly before the end of the run, the temperature at location 23 started to increase again, indicating the beginning of another cycle.

Figure 5-14 is typical of the panel performance at the other heat loads with heater configuration 1. Near the end of the run in Figure 5-14 and at comparable times at the higher heat loads, the rate of change of the panel temperatures was very small. Panel temperatures at this quasi-steady state condition are tabulated in Table 5-2 for the four runs with heater configuration 1. At the 420-watt heat load, the panel surface reached a maximum temperature of 162°F while the cold end of the panel ran at 84°F. The temperature rise from the cold end of the heat pipe to the surface of the panel beneath the heaters ranged from 16 to 78°F as compared to a predicted rise of 14°F. The cold end of the heat pipe was running 52°F hotter than the sink temperature (32°F) instead of the predicted 31°F differential. This indicated that problems existed at both the evaporator and condensor-sublimator ends of the panel. It is noted that the smallest temperature differential under the heaters agreed with the predicted value while all others were significantly larger. The excessive temperature differentials could have been caused by (1) local dry areas in the wick where water was not available for evaporation, (2) local areas where the fins were not brazed, causing a large thermal resistance, or (3) local areas in the heaters where the heat flux was higher due to concentration of heating elements.

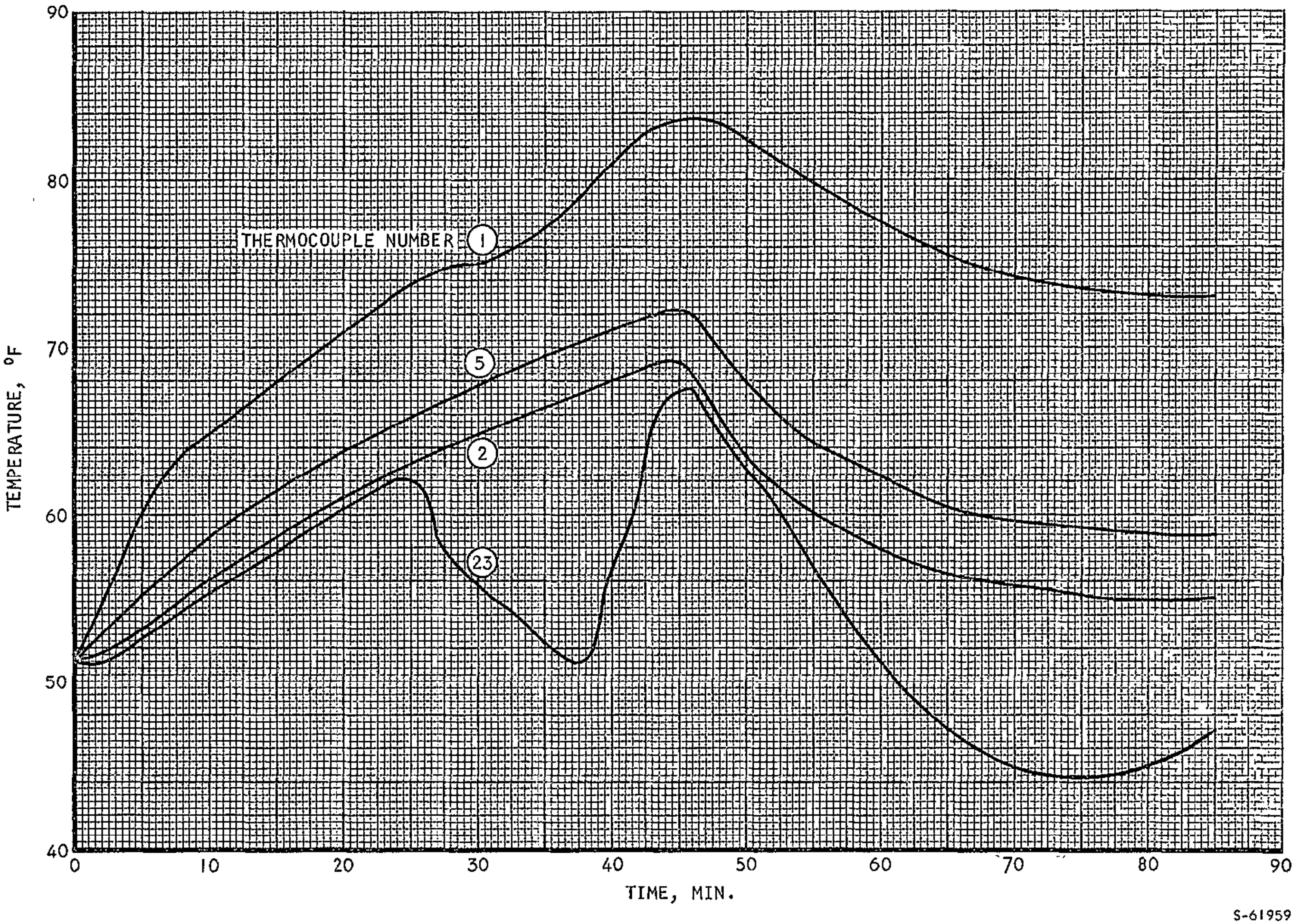


Figure 5-14. Panel Performance at a Heat Load of 105 Watts

TABLE 5-2

PANEL THERMAL PERFORMANCE DATA FOR HEATER CONFIGURATION I

| Heat Load → | 420 watts | 315 watts | 210 watts | 105 watts | 420 watts | 315 watts | 210 watts | 105 watts |
|---|---|---|---|---|---|---|---|---|
| Thermo-couple Number | Temperature, °F | | | | Temperature Difference Between Heater Panel Surface and Heat Pipe Cold End, °F | | | |
| 1 | 162 | 132 | 106 | 73 | 78 | 57 | 38 | 18 |
| 2 | 84 | 75 | 68 | 55 | | | | |
| 3 | 84 | 75 | 68 | 55 | | | | |
| 4 | 84 | 76 | 69 | 56 | | | | |
| 5 | 100 | 88 | 77 | 59 | 16 | 12 | 9 | 4 |
| 6 | NR | NR | NR | NR | | | | |
| 7 | 156 | 130 | 101 | 69 | 72 | 54 | 32 | 14 |
| 8 | 87 | 78 | 70 | 56 | | | | |
| 9 | 84 | 75 | 68 | 55 | | | | |
| 10 | 84 | 75 | 68 | 55 | | | | |
| 11 | 84 | 75 | 68 | 55 | | | | |
| 12 | 125 | 108 | 91 | 65 | 41 | 33 | 22 | 10 |
| 13 | 119 | 105 | 88 | 63 | 35 | 29 | 20 | 8 |
| 14 | 84 | 75 | 68 | 56 | | | | |
| 15 | 84 | 75 | 68 | 56 | | | | |
| 16 | 84 | 76 | 69 | 56 | | | | |
| 17 | 126 | 105 | 88 | 64 | 42 | 30 | 20 | 9 |
| 18 | 84 | 76 | 69 | 56 | | | | |
| 19 | 84 | 76 | 68 | 56 | | | | |
| 20 | 116 | 100 | 85 | 64 | 32 | 25 | 12 | 9 |
| 21 | 141 | 119 | 98 | 69 | 57 | 44 | 30 | 14 |
| 22 | 84 | 75 | 68 | 56 | | | | |
| 23 | 77 | 66 | 56 | 47 | | | | |

NR - no reading

To eliminate the potential problem of local high heat fluxes in the heaters, the heaters were mounted on the panel in configuration 2 using aluminum plates to redistribute the heat from possible areas of high heat flux. A spare heater was x-rayed to determine the locations of the heating elements. The elements appeared to be spaced uniformly enough to give a uniform heat flux into the panel. However it was decided to use configuration 2 in order to eliminate the possibility of erroneous temperature readings due to the thermocouple placement adjacent to the heating elements.

The high temperature differential at the condensor-sublimator end of the panel could have been due to (1) a contaminated sublimator porous plate, (2) an additional thermal resistance in the sublimator plenum due to the porous plate bowing away from the fins as a result of the pressure differential across it, or (3) the wick not in contact with the plate adjacent to the sublimator where no fins were present to load the wick during brazing. The second reason was thought to be likely since a significant bow was found in the plate when it was removed from the sublimator.

The first potential problem was eliminated by cleaning the porous plate with a Freon and alcohol flush prior to reassembly. The second was solved by flattening the plate and installing support channels across the outside face when it was attached to the panel so that bowing could not occur.

Three of the four original test runs were repeated and an additional single heater case was run with the changes to the heaters and the sublimator. The quasi-steady-state temperatures and temperature differential are tabulated in Table 5-3. Comparison with the temperature differential of Table 5-2 shows that the high temperature differential decreased and the low temperature differentials increased with the addition of the aluminum plates beneath the heaters. The fact that significant nonuniformity in temperature differential still existed and the evidence of the heater x-ray established that a nonuniform heat flux in the heaters was not the cause of the nonuniform surface temperature. The aluminum plates equalized the panel surface temperatures by conducting heat from the areas of poor heat transfer (the vicinity of thermocouples 1, 7, and 21) to the areas of better heat transfer (the vicinity of thermocouples 5, 13, and 20).

The unheated panel temperatures remained essentially the same as before for the 210- and 315-watt runs. At 420 watts a $7^{\circ}$F reduction was achieved, indicating that the porous plate probably had been bowed during the 420-watt run in the original set of tests.

The second set of tests had established that the nonuniform panel temperatures were not due to nonuniform heating and that the excessive condensor-sublimator $\Delta T$ was not caused by a contaminated or bowed porous plate.

The water reservoir pressure was set at 4 psia at the beginning of each set of data runs. Toward the conclusion of the 420-watt run when the panel temperature was high enough to assure that the water valve was open, the reservoir pressure was increased in 2 psi increments up to a maximum of 10 psia. With the water valve open, this same pressure existed in the sublimator reservoir, and no evidence of breakthrough was observed.

TABLE 5-3

PANEL THERMAL PERFORMANCE DATA FOR HEATER CONFIGURATION 2

| Heater ⇨ | 2 and 3 | | | 2 only | 2 and 3 | | | 2 only |
|---|---|---|---|---|---|---|---|---|
| Heat Load ⇨ | 420 watts | 315 watts | 210 watts | 252 watts | 420 watts | 315 watts | 210 watts | 252 watts |
| Thermocouple Number ⇩ | Temperature, °F ⇩ | | | | Temperature Difference Between Heated Panel Surface and Heat Pipe Cold End, °F ⇩ | | | |
| 1 | 121 | 109 | 92 | 66 | 44 | 35 | 23 | |
| 2 | 77 | 74 | 68 | 64 | | | | |
| 3 | 77 | 74 | 68 | 64 | | | | |
| 4 | 77 | 74 | 68 | 64 | | | | |
| 5 | 107 | 98 | 84 | 66 | 30 | 24 | 15 | |
| 6 | 113 | 102 | 88 | 67 | 36 | 28 | 19 | |
| 7 | 123 | 111 | 93 | 75 | 41 | 36 | 24 | |
| 8 | 79 | 76 | 70 | 65 | | | | |
| 9 | 77 | 75 | 69 | 65 | | | | |
| 10 | 77 | 75 | 69 | 65 | | | | |
| 11 | 78 | 75 | 69 | 66 | | | | |
| 12 | 119 | 106 | 90 | 106 | 42 | 32 | 21 | 42 |
| 13 | 120 | 107 | 91 | 106 | 43 | 32 | 22 | 42 |
| 14 | 77 | 74 | 68 | 65 | | | | |
| 15 | 76 | 74 | 68 | 65 | | | | |
| 16 | 78 | 75 | 70 | 67 | | | | |
| 17 | 117 | 104 | 89 | 109 | 40 | 30 | 20 | 45 |
| 18 | 77 | 75 | 69 | 66 | | | | |
| 19 | 77 | 75 | 69 | 67 | | | | |
| 20 | 110 | 99 | 85 | 102 | 33 | 25 | 16 | 38 |
| 21 | 122 | 109 | 92 | 117 | 45 | 35 | 23 | 53 |
| 22 | 77 | 74 | 68 | 64 | | | | |
| 23 | 63 | 57 | 54 | 64 | | | | |
| 24 | 64 | 58 | 60 | 65 | | | | |

## Sea Level Thermal Performance Testing

In order to determine if the high nonuniform temperature differential at the evaporator end was due to local non-wetting of the wick, it was decided to remove the water from the heat pipe and replace it with a working fluid which wet the wick, even in areas of contamination. Methanol was selected for use since, according to Reference 11, it wets all contaminated surfaces excellently. If the nonuniform panel surface temperature were still evident with the methanol heat pipe working fluid, the remaining reason for the temperature nonuniformity would be unbrazed wick areas.

As was discussed above, the sublimator porous plate was removed for these tests and replaced with a pan assembly to provide cooling by a cold circulating fluid. Two calibration tests were run with water as the heat pipe working fluid at heat loads of 420 and 210 watts. The local temperature and the temperature rise from the cold end of the heat pipe to the heated panel surface are tabulated in Table 5-4. While a comparison of the panel temperatures with those obtained in the previous set of runs is not meaningful because of different heat sink temperatures and different mechanisms of heat transfer to the heat sink, a comparison of the tabulated temperature differential is valid since the heat pipe performance is independent of the sink. Comparison with Table 5-3 showed that the temperature differentials in the sea level test averaged about 14 percent less than those run in the vacuum chamber. This was probably the result of higher heat losses since a different insulation was used in the two test setups. It is noted that the nonuniform temperatures under the heaters were still evident.

After the water calibration runs were completed, the water was removed from the heat pipe by pulling a vacuum while applying heat to evaporate the water. The heat pipe was then charged with 959 cc of reagent pure methanol. The performance test data is shown in Table 5-4. Since the surface tension of methanol is about 1/3 that of water, the liquid delivery capability is reduced by a factor of 3. Methanol runs were made therefore at 1/3 the heat load of the water runs. The nonuniformity in the temperature difference did not decrease with methanol since the same relative spread was still present for these runs. From this testing it is concluded that the nonuniform temperature differential was not the result of non-wetting of the wick, but was probably due to local unbrazed areas.

Also shown in the table are predictions of the temperature differential with methanol obtained by multiplying the water data temperature differential by the ratio of the heat loads. The methanol temperature differential was slightly lower than predicted because the portion of the temperature difference associated with the change in saturation pressure from one end of the pipe to the other is less for methanol than for water.

TABLE 5-4

SEA LEVEL THERMAL PERFORMANCE DATA USING WATER AND METHANOL AS HEAT PIPE WORKING FLUIDS

| | Calibration Test Using Water as Heat Pipe Fluid* | | | | Test Using Methanol As Heat Pipe Fluid | | | | | |
|---|---|---|---|---|---|---|---|---|---|---|
| Heat Load | 420 watts | 210 watts | 420 watts | 210 watts | 140 watts | 70 watts | 140 watts | 70 watts | 140 watts | 70 watts |
| | | | | | | | Heat Pipe Evaporator End ΔT, $^0$F | | | |
| Thermo-couple Number | Temperature, $^0$F | | Heat Pipe Evaporator End ΔT, $^0$F | | Temperature, $^0$F | | Experimental Data | | Prediction Based Upon Water Data** | |
| 1 | 125 | 88 | 38.0 | 19.3 | 81 | 67 | 10.6 | 4.7 | 12.5 | 6.3 |
| 2 | 87 | 69 | | | 72 | 62 | | | | |
| 3 | 86 | 68 | | | 71 | 61 | | | | |
| 4 | 87 | 69 | | | 72 | 62 | | | | |
| 5 | 113 | 82 | 26.1 | 13.1 | 78 | 65 | 7.0 | 3.4 | 8.7 | 4.3 |
| 6 | 116 | 85 | 29.2 | 15.6 | 81 | 67 | 9.1 | 5.1 | 9.7 | 4.9 |
| 7 | 125 | 87 | 37.6 | 18.2 | 84 | 68 | 12.1 | 6.1 | 12.5 | 6.3 |
| 8 | 88 | 71 | | | 72 | 61 | | | | |
| 9 | 87 | 69 | | | 71 | 62 | | | | |
| 10 | 86 | 68 | | | 71 | 61 | | | | |
| 11 | 88 | 69 | | | 71 | 62 | | | | |
| 12 | 124 | 88 | 36.8 | 18.9 | 83 | 67 | 10.9 | 5.2 | 12.3 | 6.1 |
| 13 | 122 | 88 | 34.7 | 18.8 | 82 | 67 | 10.6 | 5.3 | 11.6 | 5.8 |
| 14 | 87 | 69 | | | 72 | 63 | | | | |
| 15 | 87 | 69 | | | 72 | 62 | | | | |
| 16 | 88 | 70 | | | 72 | 62 | | | | |
| 17 | 122 | 86 | 34.8 | 17.5 | 82 | 67 | 10.4 | 5.0 | 11.6 | 5.8 |
| 18 | 87 | 69 | | | 72 | 62 | | | | |
| 19 | 88 | 69 | | | 72 | 62 | | | | |
| 20 | 115 | 83 | 28.0 | 14.4 | 80 | 66 | 8.4 | 4.1 | 9.3 | 4.7 |
| 21 | 127 | 89 | 39.7 | 20.4 | 82 | 68 | 10.7 | 5.7 | 13.2 | 6.6 |
| 22 | 87 | 69 | | | 72 | 62 | | | | |
| 23 | 86 | 68 | | | 46 | 43 | | | | |
| 24 | -- | -- | | | 46 | 43 | | | | |
| 25 | 85 | 67 | | | 71 | 61 | | | | |
| 26 | 65 | 55 | | | 44 | 41 | | | | |
| 27 | 87 | 69 | | | 50 | 46 | | | | |
| 28 | 87 | 69 | | | 71 | 62 | | | | |

*Water calibration run performed outside of vacuum chamber using water at approximately 40$^0$F as heat sink fluid.
**Predicted ΔT based on 420-watt water calibration run.

## Comparison with Analysis

A comparison of the analytical and experimental temperature drops in the thermal panel is presented in Table 5-5. Three temperature drops are shown: one at the heat input end, one in the vapor passage, and one at the sublimator end. The footnotes to the table explain what each $\Delta T$ includes. At the heat input end both the maximum and minimum measured $\Delta T$ are shown. This $\Delta T$ is the difference between the panel surface temperature and the vapor temperature. The vapor temperature was not measured directly; however, the temperature on the backside of the panel (Thermocouple No. 8) will be very close to the vapor temperature when the back is insulated. Because the panel was well insulated in these tests, the heat input end $\Delta T$ was taken as the panel surface temperature minus the temperature of Thermocouple No. 8. The analytical value shown at 420 w was taken from the table on Page 4-18. Values at lower heat loads were scaled from the heat flux.

In Heater Configuration 1, the lowest measured $\Delta T$ was quite close to the analytical prediction while the highest was six times that predicted. As discussed in Appendix B, it was concluded that the high $\Delta T$'s were due to local unbrazed areas between the heat pipe fin and the remote loop and between the heat pipe fin and the wick. In Configuration 2, the low $\Delta T$ increased and the high $\Delta T$ decreased. This was the result of redistributing the heat input from the areas of high thermal resistance to those with lower thermal resistance.

The vapor passage $\Delta T$ results from the difference in saturation pressure caused by the vapor flow. The vapor temperature at the hot end was again taken as the reading of Thermocouple No. 8, and the vapor temperature at the cold end was taken as the temperature of the insulated panel top surface. (Again, since no heat transfer occurs out the top of the panel when it is insulated, the panel surface will be at the vapor temperature.) These two temperatures were subtracted to yield the vapor passage $\Delta T$. Small errors in these two temperatures can yield large errors in the vapor passage $\Delta T$, so the experimental values in Table 5-5 may not be accurate. However, this is not critical since this is a small portion of the overall $\Delta T$. The analytical values shown were calculated at the experimental vapor temperatures shown. The increase in $\Delta T$ with decreasing heat load (and therefore vapor flow rate) is due to the decreasing vapor density of the progressively lower vapor temperatures.

The sublimator end $\Delta T$ is the vapor temperature minus the sublimator sink temperature which was taken as 32°F. The analytical values were taken from Figure A-2 in Appendix A and are the result of a transient analysis.

As indicated in the table, the experimental cold end $\Delta T$ ranged from 10° to 21°F higher than the analytical prediction. At a heat load of 420 w, the initial test run yielded a 52°F $\Delta T$. The porous plate was found to be bowed outward after this run, and it was suspected that the bowing increased the conduction $\Delta T$ across the sublimator plenum. Support beams were attached to hold the plate against the fins during subsequent runs, and as indicated in the table, the $\Delta T$ decreased to 47°F in the next run at this heat load. Thus, the additional $\Delta T$ unaccounted for in the analysis was 16°F at 420 w. This additional temperature drop could have been due to (1) a lower thermal

TABLE 5-5

COMPARISON OF ANALYTICAL AND EXPERIMENTAL $\Delta T$'s

| Heat Load, W | Method of Determining Temperature Drop | Temperature Drop, °F | | |
|---|---|---|---|---|
| | | Heat Input End* | Vapor Passage** | Sublimator End*** |
| 420 | Analytical ($T_{vapor}$ = 84°F) | 12.5 | 1.2 | 31 |
| | Experimental | | | |
| | Heater Configuration 1 | 13 to 75 | 3 | 52 |
| | Heater Configuration 2 | 28 to 44 | 3 | 47 |
| | Heater Configuration 2 (no sublimator) | 25 to 39 | 1 | N.A. |
| 315 | Analytical ($T_{vapor}$ = 76°F) | 9.4 | 1.5 | 29 |
| | Experimental | | | |
| | Heater Configuration 1 | 10 to 54 | 3 | 43 |
| | Heater Configuration 2 | 22 to 35 | 2 | 42 |
| 210 | Analytical ($T_{vapor}$ = 69°F) | 6.3 | 1.5 | 24 |
| | Experimental | | | |
| | Heater Configuration 1 | 7 to 36 | 2 | 36 |
| | Heater Configuration 2 | 14 to 23 | 2 | 36 |
| | Heater Configuration 2 (no sublimator) | 13 to 20 | 0 | N.A. |
| 105 | Analytical ($T_{vapor}$ = 55°F) | 3.1 | 1.9 | 13 |
| | Experimental | | | |
| | Heater Configuration 1 | 3 to 17 | 1 | 23 |

*Conduction through upper tube plate, remote coolant loop fin, tube plate and heat pipe fin, and evaporation in wick.
**Change in saturation temperature due to vapor pressure drop.
***Conduction through heat pipe wick, tube plate and sublimator plenum, and sublimation.

conductivity of the wick-water matrix, (2) a gap between the wick and the lower plate, (3) a higher thermal resistance of the sublimator water plenum, (4) a gap between the porous plate and the sublimator plenum fin, or (5) lower performance of the sublimator porous plate. Both the effective wick thermal conductivity and the porous plate performance were predicted from experimental data and therefore are not thought to be the major source of the additional $\Delta T$. Support beams were used to hold the porous plate against the plenum fins so that a gap would not exist at that location. The thermal resistance of the sublimator water plenum is a straight-forward parallel conduction calculation and therefore is thought to be quite accurate. This leaves only a gap between the wick and the lower plate to account for the higher $\Delta T$. If the wick did not braze to the plate, a water-filled gap could exist, introducing an additional thermal resistance. A water gap of 0.017 inch will sustain a $16^{\circ}F$ $\Delta T$ at the heat flux through the sublimator. A metallurgical evaluation of the thermal panel (Appendix B) indicated that the wick-plate interface was partially unbrazed. However, it was not possible to determine the average thickness of the gap. It was concluded that the additional $\Delta T$ at the cold end was most probably the result of a gap between the wick and the plate.

## Performance Map of Thermal Panel

The panel performance (surface temperatures) as a function of input heat flux and total heat load may be calculated from the performance data obtained. Over the panel surface where heat is input, the heat transfer mechanism is primarily conduction (through upper plate, remote loop fins, lower plate, heat pipe fin); therefore, the temperature difference between the panel surface and the heat pipe working fluid vapor at this location is expected to vary linearly with the input heat flux. The experimental maximum and minimum temperature drops (panel surface temperature minus vapor passage temperature) are shown in Figure 5-15 as a function of the input heat flux for the two heater configurations tested. Figure 5-15 shows that the temperatures are indeed reasonably linear with heat flux. The straight lines drawn through the date points may be used to estimate the $\Delta T$ at the heat input area of the panel.

The temperature drop between the cold end of the heat pipe and the sublimator sink temperature of $32^{\circ}F$ is shown in Figure 5-16 as a function of the heat load. This curve, based upon experimental data, may be used to estimate the cold end $\Delta T$ at a given heat load. The only temperature drop in the panel unaccounted for in the two $\Delta T$'s presented in Figures 5-15 and 5-16 is the $\Delta T$ associated with the change in saturation temperature due to the vapor passage $\Delta P$. The maximum saturation $\Delta P$ predicted for the test conditions was $2^{\circ}F$ and the maximum measured $\Delta T$ was $3^{\circ}F$. Since this small $\Delta T$ was determined experimentally by subtracting two temperatures, its accuracy is questionable, and it was thought advisable to use the analytical prediction of the vapor flow $\Delta T$ in establishing the performance map. By using Equation (4-6) for the pressure drop in the vapor passage and the laminar flow relationship of $(f)(R_e)$ = constant, the vapor passage $\Delta P$ may be expressed in terms of the heat load, the fluid properties, and the vapor flow length, as shown in the following equation:

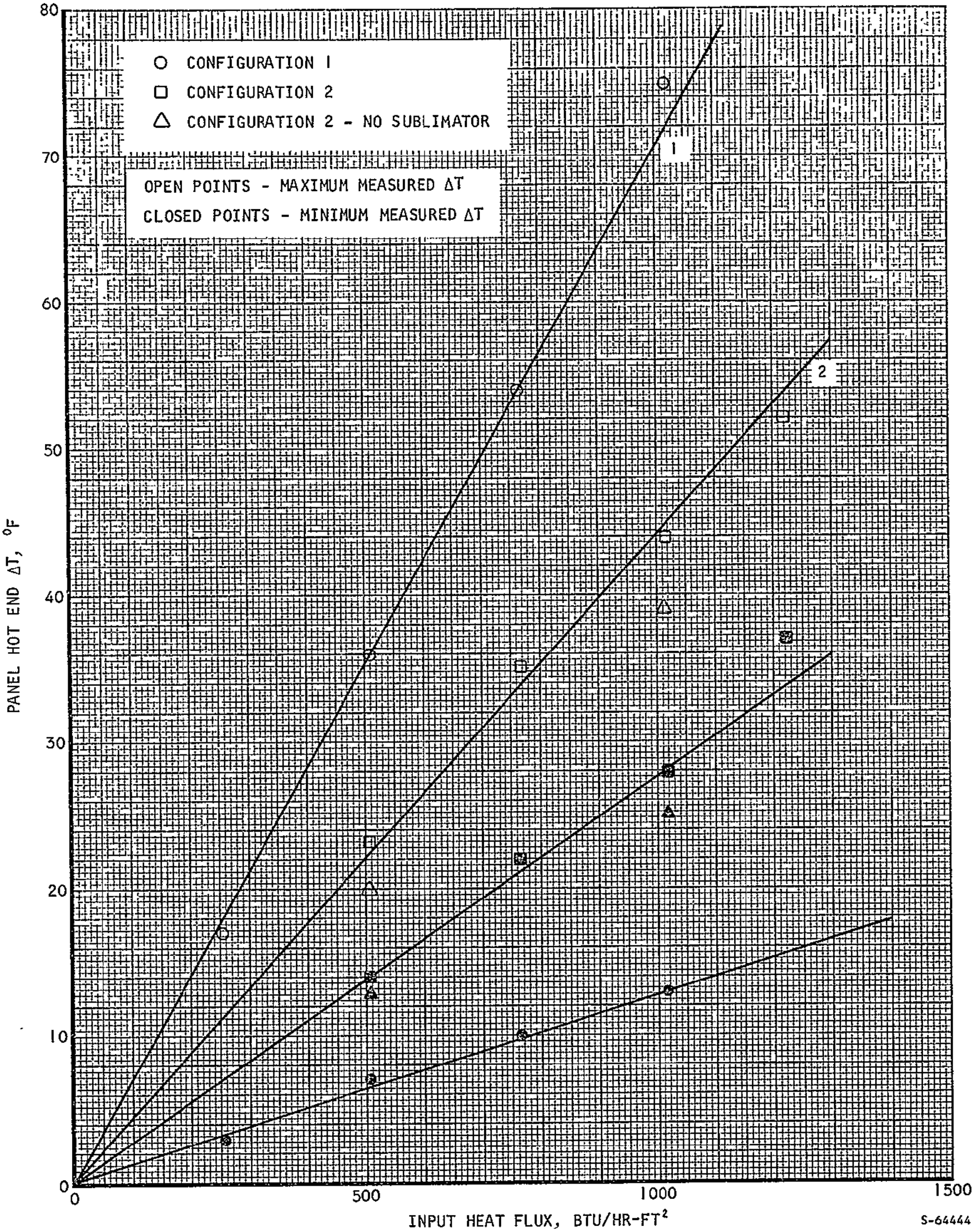


Figure 5-15. Temperature Drop at Panel Hot End

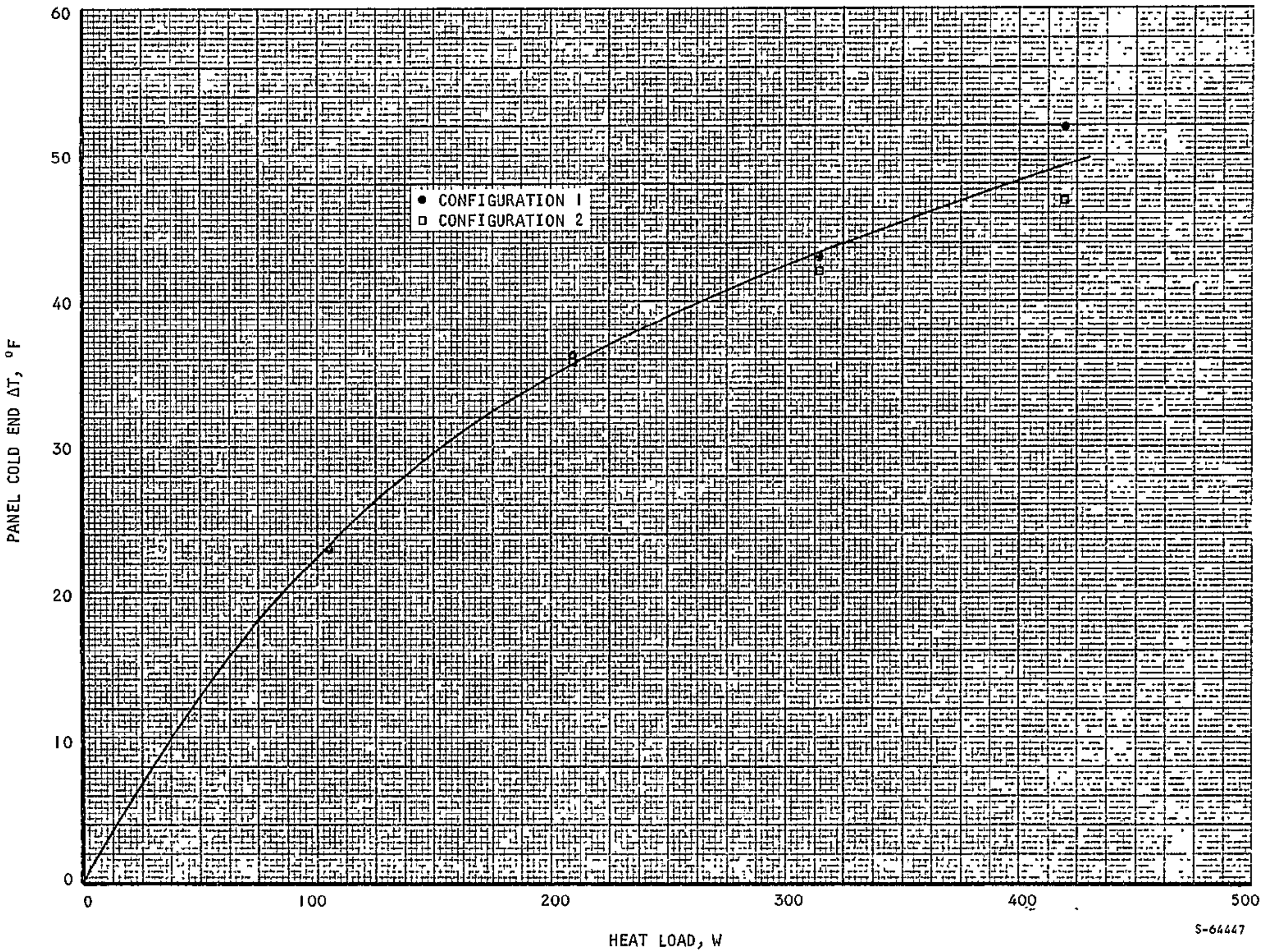


Figure 5-16. Temperature Drop at Panel Cold End

$$\Delta P = \left(\frac{2C'}{D_h^2\ g_o A_c}\right)\left(\frac{Q\mu L}{\rho h_{fg}}\right) \quad (5\text{-}4)$$

where $C'$ = constant = $fR_e$ (from Reference 19)

As shown in the sketch, the flow length L in Equation (5-4) is the distance between the midpoint of the sublimator and the midpoint of the area over which heat is input. The flow length L for the 30-in. panel is

$$L = 30 - 2.5 - 1.25 - .5\ell_2 \quad (5\text{-}5)$$

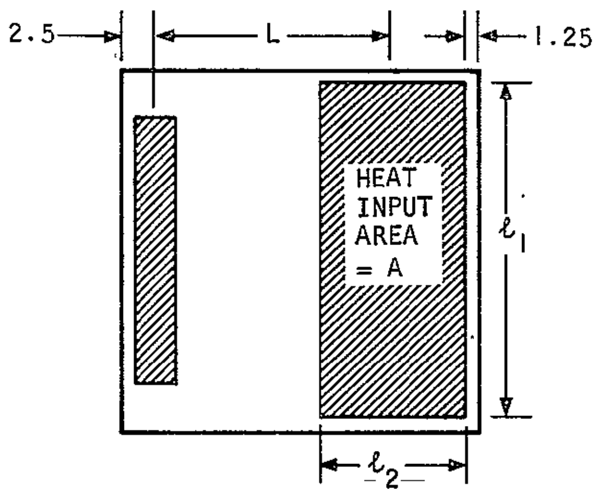


The length $\ell_2$ may be expressed in terms of the heat load Q and the input heat flux Q/A.

$$\ell_2 = \frac{A}{\ell_1} = \frac{1}{\ell_1}\ \frac{Q}{Q/A} \quad (5\text{-}6)$$

Using $\ell_1$ = 28 in. and substituting Equation (5-6) in Equation (5-5), the flow length in inches becomes

$$L = 26.25 - \frac{Q}{56\ Q/A}\left(\frac{3.414\ \text{Btu}}{\text{watt-hr}}\ \frac{144\ \text{in.}^2}{\text{ft}^2}\right) \quad (5\text{-}7)$$

where Q is in watts and Q/A in Btu-hr-ft$^2$.

By substituting Equation (5-7) in Equation (5-4), the change in saturation pressure due to the vapor flow pressure drop may be determined as a function of the heat load Q, the heat flux Q/A, and the fluid properties.

At a given heat load and heat flux, the panel maximum surface temperature is obtained as follows: The cold end $\Delta T$ is determined from Figure 5-16 at the given heat load. By adding this $\Delta T$ to the $32^0F$ sink temperature, the vapor passage temperature adjacent to the sublimator is obtained. By evaluating vapor properties at this temperature and using the given Q and Q/A, Equations (5-7) and (5-4) are solved to obtain the change in saturation pressure in the vapor passage. The saturation temperature difference is obtained by using steam tables. The hot end maximum $\Delta T$ is obtained from Figure 5-15 at the given heat flux for the heater configuration of interest, Curve 1 or 2. The cold end $\Delta T$, the rise in saturation temperature, and the hot end $\Delta T$ are added to the $32^0F$ sink temperature to obtain the maximum panel surface temperatures.

Figures 5-17 and 5-18 show the maximum panel surface temperatures as a function of the heat load and the input heat flux for Heater Configurations 1 and 2.

Comparison of Heat Pipe and Aluminum Plate

Since the function of the heat pipe section of the panel is to transfer heat with a small temperature drop, it is of interest to compare its performance with that of a solid, high-thermal-conductivity plate. The basic conduction equation is

$$dT = \frac{Q}{kA} dx \tag{5-8}$$

The heat transfer model analyzed is shown in the following sketch.

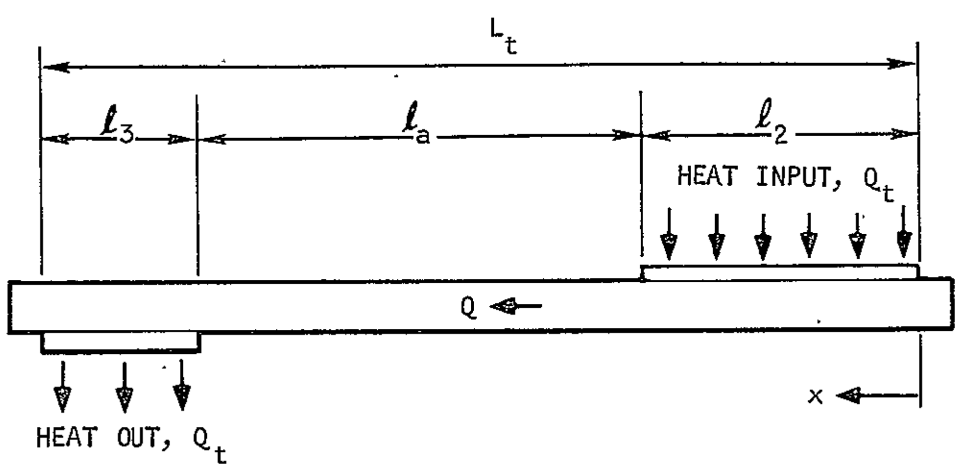


Equation (5-8) can be integrated over the length of the panel to determine the temperature drop from one end to the other. For a uniform heat load, the local heat rate in the plate in the area of heat input is as follows:

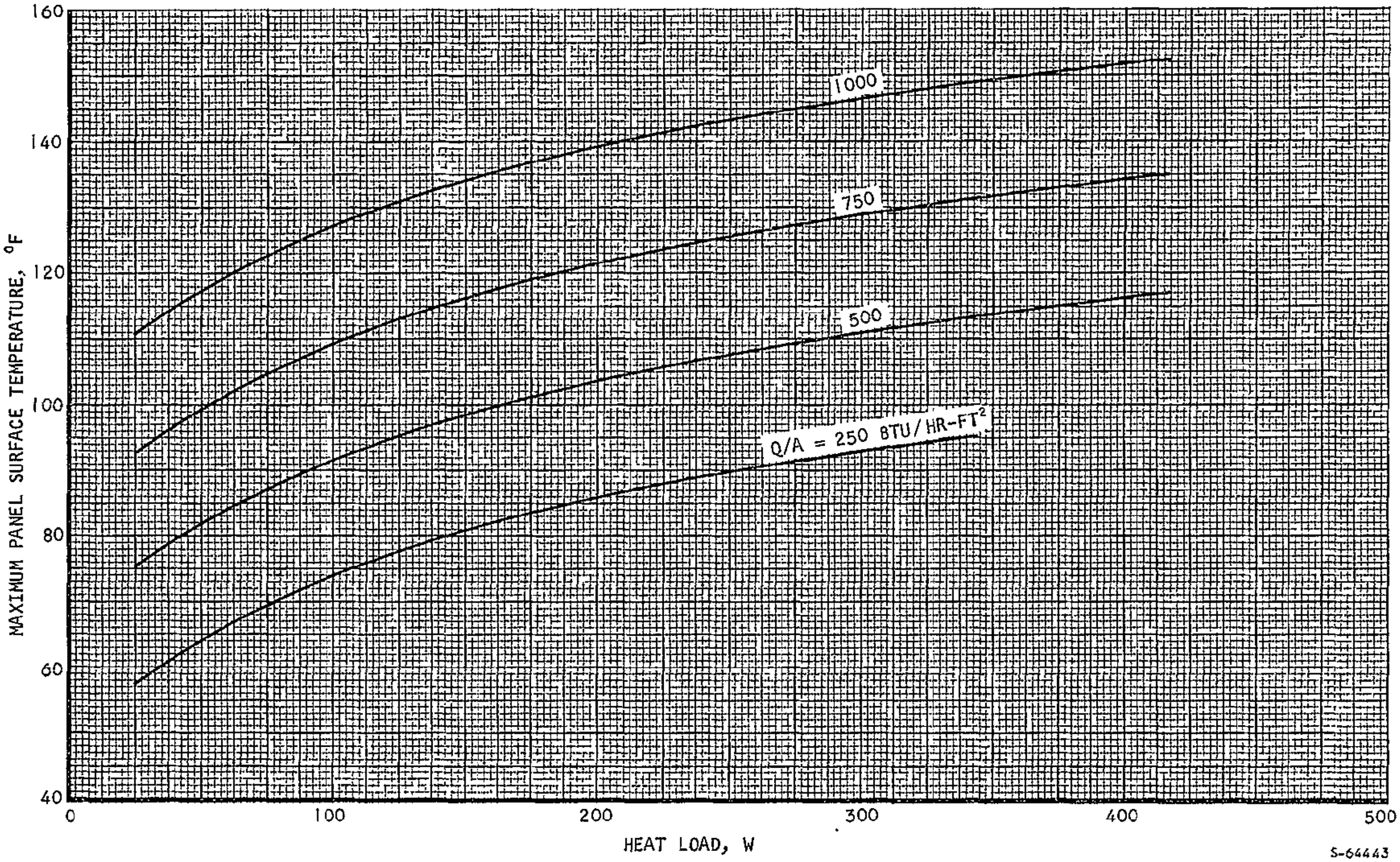


Figure 5-17. Maximum Panel Surface Temperature For Heater Configuration I

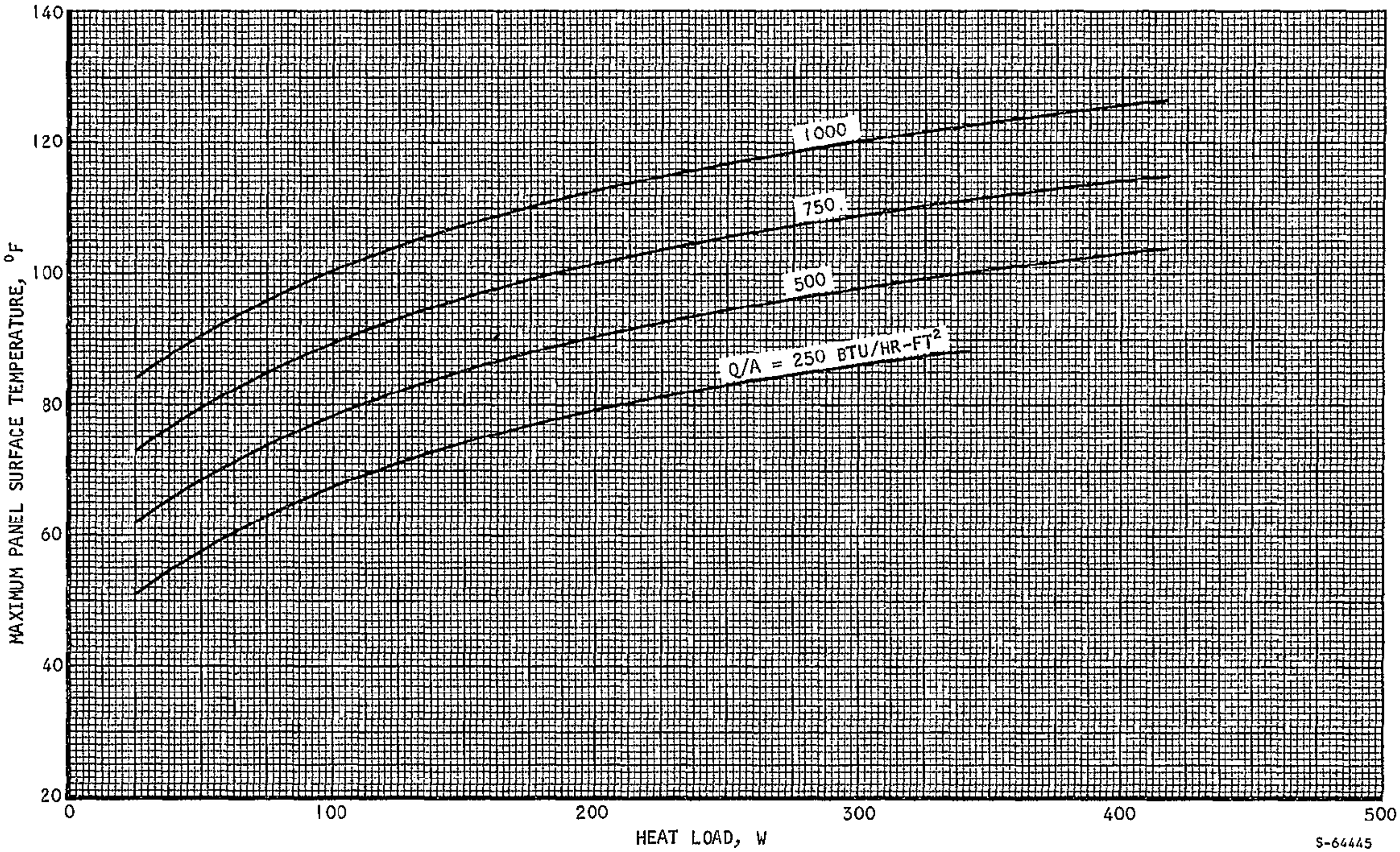


Figure 5-18. Maximum Panel Surface Temperature For Heater Configuration 2

$$Q = Q_t \frac{x}{\ell_2} \qquad (0 \le x \le \ell_2) \tag{5-9}$$

Adjacent to the sublimator, the local heat rate is

$$Q = Q_t \left(\frac{L_t - x}{\ell_3}\right) \qquad (L_t - \ell_3 \le x \le L_t) \tag{5-10}$$

In the adiabatic section, the local heat rate is $Q_t$. Equation (5-8) is integrated using the appropriate values of Q over each length interval.

$$\begin{aligned} \int_{T_{min}}^{T_{max}} dT &= \int_0^{L_t} \frac{Q}{kA}\, dx \\ &= \int_0^{\ell_2} \frac{Q_t}{kA\ell_2}\, x dx + \int_{\ell_2}^{\ell_2 + \ell_a} \frac{Q_t}{kA}\, dx \\ &\quad + \int_{L_t - \ell_3}^{L_t} \frac{Q_t}{kA} \left(\frac{L_t - x}{\ell_3}\right) dx \end{aligned} \tag{5-11}$$

The conduction area A is the product of the panel width (30 in.) and the panel thickness $\delta$. With this substitution, integration of (5-11) yields:

$$T_{max} - T_{min} = \frac{Q_t}{k\ \delta\ 30\ \text{in.}} \left[\frac{\ell_2}{2} + \ell_a + \frac{\ell_3}{2}\right] \tag{5-12}$$

The weight of the aluminum plate is determined from the density ($\rho_{al}$) and the plate volume.

$$\begin{aligned} W &= \rho_{al}\ V \\ &= \rho_{al}\ (A_p \delta - V_{holes}) \end{aligned} \tag{5-13}$$

where $A_p$ = plate projected area ≈ 900 sq in.

$V_{holes}$ = volume removed for tapped holes (less than $0.003\ A_p \delta$)

Equations (5-12) and (5-13) were solved for various plate thicknesses using the maximum heat load of 420 w and a thermal conductivity of aluminum of

100 Btu/hr-ft-°F. The bracketed length term in Equation (5-12) is equal to L in Equation (5-7) and was evaluated at an input heat flux of 1020 Btu/hr-ft$^2$. To obtain the panel overall temperature difference, a 4.7°F $\Delta T$ associated with conduction of heat through the remote cooling passage, and a 16.1°F $\Delta T$ associated with heat transfer in the sublimator were added to the aluminum plate $\Delta T$. The weights of the remote coolant loop (8.0 lb), the water tank (28.5 lb), the sublimator (4.3 lb) and a 5-percent allowance for fasteners, fluid connectors, etc. (2.0 lb) were added to the calculated aluminum plate weight to obtain a total panel weight. No structural sandwich was added since it was assumed that the plate could withstand the inertia loads without additional structure.

The overall panel temperature drop using an aluminum plate in place of the heat pipe is shown as a function of panel total weight at a heat load of 420 w and a heat flux of 1020 Btu/hr-ft$^2$ in Figure 5-19. Also shown are the experimental data points for Heater Configurations 1 and 2 as well as the analytically predicted $\Delta T$ for this condition.

It is seen that it would take an aluminum plate panel weighing over 500 lb to yield the performance that was expected and would have been achieved were it not for the unbrazed areas of the heat pipe. With the degraded heat pipe performance, the aluminum plate panel which yields the same maximum $\Delta T$ is about 50 lb heavier for Heater Configuration 1 and 100 lb heavier for Configuration 2.

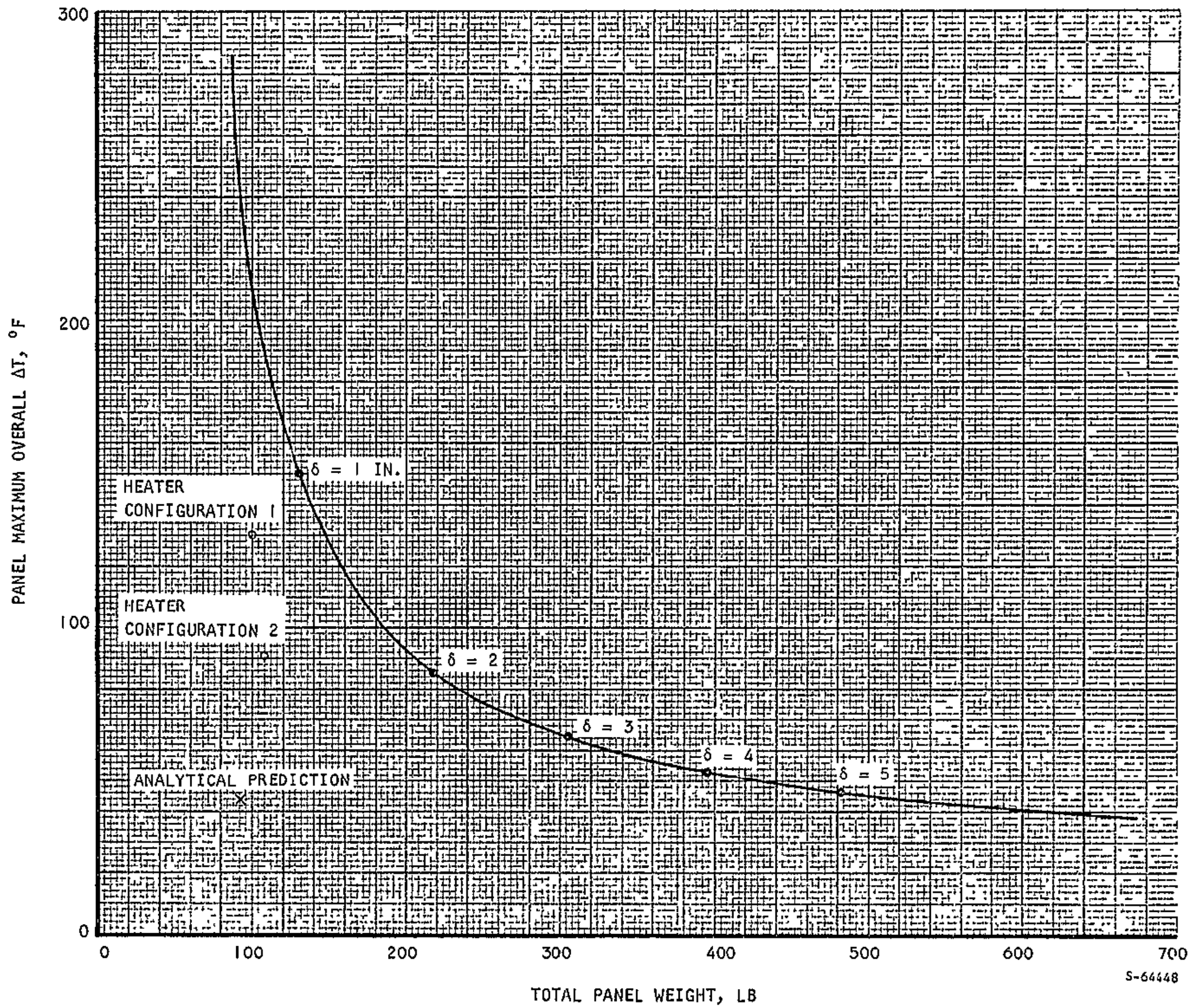


Figure 5-19. Solid Aluminum Panel ΔT as a Function of Total Weight

CONCLUSIONS AND RECOMMENDATIONS

The following conclusions were made based on the testing of the full-size thermal panel:

(a) The thermal performance of the remote cooling loop agreed well with performance predictions. On this basis a maximum panel temperature of 74°F will be achieved at maximum heat load with the design coolant (60 percent methanol 40 percent water) at the design flow rate.

(b) While the pressure drop in the remote loop was higher than predicted, the data shows that it was less than the maximum allowable at the design conditions.

(c) The heat pipe-sublimator portion of the thermal panel did not perform as expected due to unbrazed areas in the heat pipe. With the heaters installed in configuration 2, about 200 watts can be dissipated without the panel exceeding the 90°F maximum allowable temperature.

The following recommendations are made to alleviate the problems of unbrazed areas in the current panel:

(a) One of the following fabrication techniques should be used:

A machined boss and plate assembly should be used to eliminate the leakage problems associated with the panel fabrication and also any assembly tolerance stackup.

Bosses and webs should be final machined after brazing to minimize any tolerance buildup due to large braze alloy joints.

(b) A forced convection furnace braze process or a modified vacuum furnace braze technique should be used to minimize the thermal stabilization and thermal gradient problems associated with vacuum furnace brazing.

(c) The vapor passage fin should cover the condenser area to assure contact between the wick and the plate.

A recommended improved self-contained thermal panel design is shown in Figure 5-20. The new configuration is externally similar to the present configuration. Internally, an interconnecting double wick system replaces the copper fin and wick design, and the machined boss and plate assembly mentioned above is utilized. This configuration eliminates the brazing problems associated with the copper-fin-to-wick joint and eliminates many potential heat pipe leakage paths. Each wick will be brazed to the adjacent plate in separate operations so that a wick inspection is possible before the final brazing cycle.

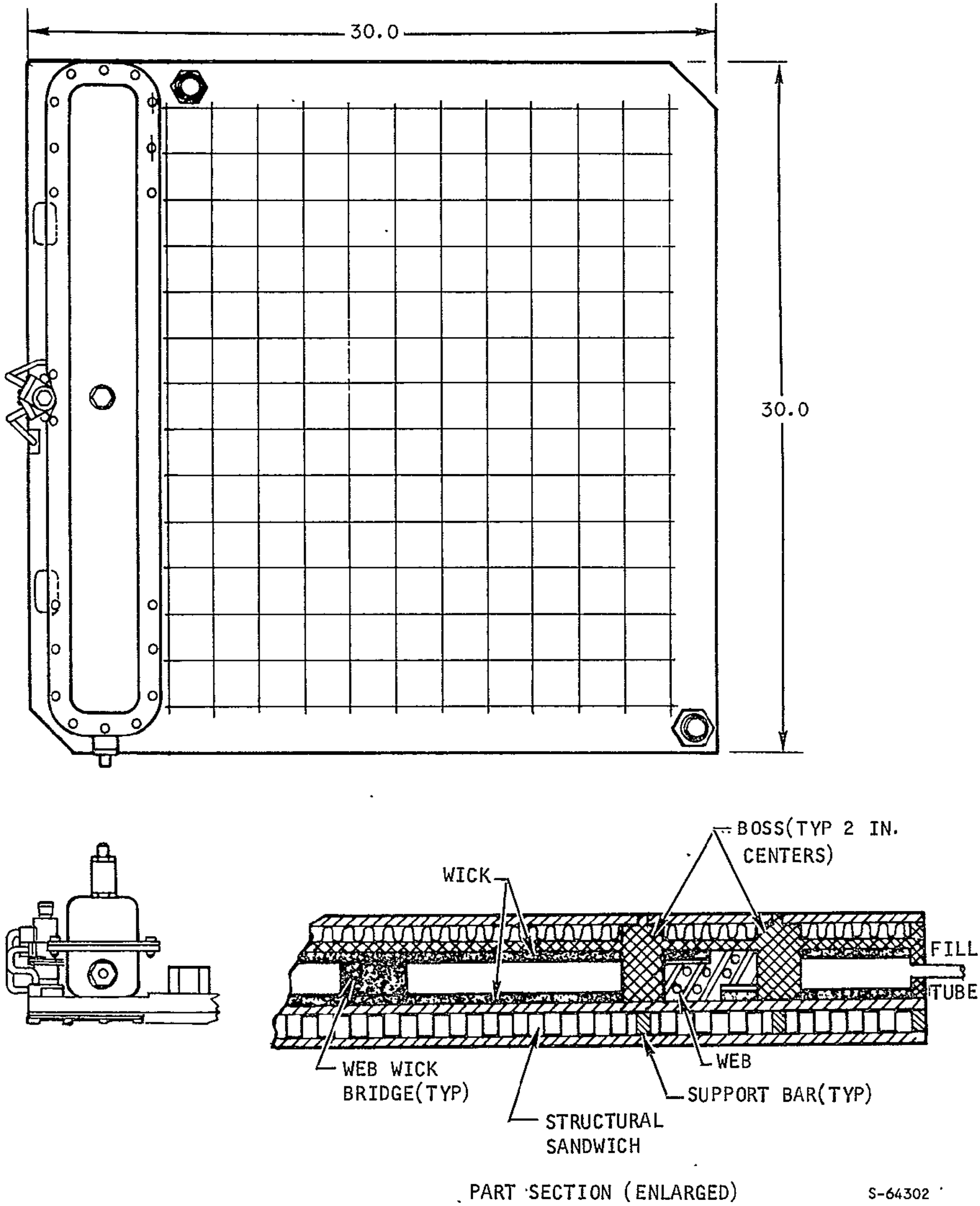


Figure 5-20. Recommended Alternate Thermal Panel Design

As shown in Figure 5-20, the wick is located directly against the heat pipe wall. In early heat pipe work there was much concern about the possibility of boiling occurring within the wick at the hot wall. It was believed that if nucleation occurred, the vapor might be trapped in the wick, resulting in liquid flow blockage and also increasing the thermal resistance of the wick by the formation of an insulating vapor blanket at the wall. While the problem of nucleation in wick structures has not been widely researched, extensive testing of the new wick configuration (Reference 2) demonstrated the effects of nucleation. At a saturation temperature of 70°F, a 15 percent dense nickel wick requires 20°F superheat for nucleation to occur with water as the working fluid. This is approximately five times the superheat that is expected in the present thermal panel application. (At 100°F, the nucleation superheat is about 12°F.) The same experimental test data also indicated that nucleation is not undesirable but, in fact, improves performance because it results in a higher heat transfer coefficient. The higher heat transfer coefficient occurs because the vapor escapes through the large pores in the wick and does not blanket the hot wall.

Liquid will return to the evaporator from the condenser through the wicks on both faces. Wick "bridges" extending across the vapor passage will deliver the liquid from the bottom wick to the wick on the heat input face.

Details of the fabrication and assembly of the improved panel configuration are discussed in Appendix B.

SECTION 6

REFERENCES


1. Graumann, D. W., and G. R. Woods, Research Study on Instrument Unit Thermal Conditioning Heat Sink Concepts, NASA-CR-97671, 1968.

2. Graumann, D. W., M. M. Soliman, and P. J. Berenson, Wicking Evaporative Heat Exchangers, AiResearch Report No. 70-6190, May 28, 1970.

3. Deverall, J. E., R. J. Kapp, and E. W. Salmi, Orbital Heat Pipe Experiment, June 5, 1967, LA-3714.

4. Neal, L. G., An Analytical and Experimental Study of Heat Pipes, January 1967, N68-12857.

5. Latimer, W. M., Oxidation Potentials, Prentice-Hall, Inc., New York, 2nd Edition, 1963, pp 198-202.

6. Kirk-Othmer, Encyclopedia of Chemical Technology, Interscience Publishers, New York, 2nd Edition, Vol. 13, pp 746.

7. Foust, R. A., Jr., Survey of Electrochemical Technology Applicable to Water Electrolysis, Energy Depot Electrolysis System Study, Allison Division General Motors Corp., Indianapolis, Indiana, EDR 3687, Vol. II, p 4-34.

8. Erb, R. A., J. Phys. Chem. 69 4, 1306 (1965).

9. Metal Surfaces: Structure, Energetics, and Kinetics, Papers presented at Seminar of American Society for Metals, October 1962.

10. Bond, G. C. Catalysis in Metals, pp 77-79, Academic Press, New York, (1962).

11. Schwartz, Anthony M., Alfred H. Ellison, The Effect of Surface Contamination on Contact Angles and Surface Potentials, NASA CR-54708, January 13, 1966.

12. Soliman, M. M., D. W. Graumann, and P. J. Berenson, Thermal Conductivity of Dry and Liquid Saturated Sintered Fiber Metal Wicks, ASME Paper No. 70-HT/SP T-40, June 1970.

13. Development of a Hydrogen Separator, Final Report, AiResearch Report 69-5358, November 1969.

14. Development of an Electrolytic Silver Ion Generator for Water Sterilization, Final Report, AiResearch Report No. 67-2158, June 1957, pp 4-20 and 4-24.

15. Latimer, W. M., Oxidation Potential, Prentice-Hall, Inc., New York, 2nd Edition, 1953, p 32.

16. Brodowsky, H., and E., Poeschel, Wasserstoff in Palladium/Silver-Liegierungen, Zeitschrift für Physikalische Chemie, Neue Folge, 44, 1965, pp 143-159.

17. Swartz, Joe, Performance Map of The Water Heat Pipe Phenomenon of Non-condensible Gas Generation, ASME Publication 69-HT-15, NASA Contract NAS7-100.

18. Kays, W. and London, A.L., Compact Heat Exchangers, McGraw-Hill Book Company, New York.

## APPENDIX A

## TRANSIENT ANALYSIS TO APPROXIMATE PANEL COLD END TEMPERATURE DIFFERENCE

A transient analysis of the panel was performed to estimate the temperature excurison between openings of the sublimator feed-water valve and to determine the minimum sublimator end $\Delta T$ as a function of the heat load. The model shown in the sketch below was used.

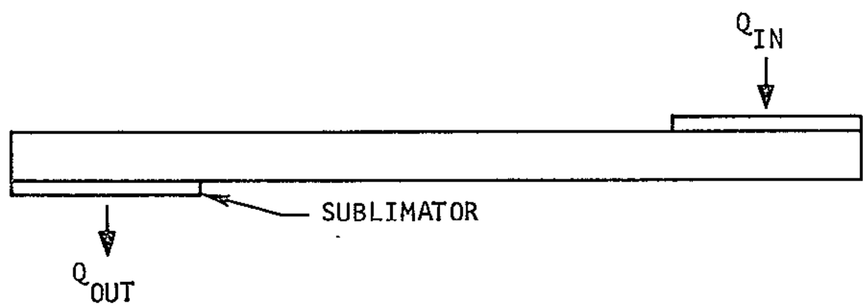


A heat balance gives

$$Q_{in} + Q_{stored} = Q_{out} \tag{1}$$

The rate at which heat is stored in the panel is approximated by

$$Q_{stored} = \Sigma WC_p \frac{d\bar{T}}{d\theta} \tag{2}$$

where: $\Sigma WC_p$ = the sum of the products of the weight and specific heat of all elements of the panel, Btu/$^0$F

$\bar{T}$ = average panel temperature, $^0$F

$\theta$ = time, hr

The rate at which heat is dissipated at the sublimator is

$$Q_{out} = \frac{T_1 - 32}{R_s} \tag{3}$$

where $T_I$ is the temperature inside the heat pipe at the cold end, $^{\circ}F$

$R_s$ = overall thermal resistance at the sublimator end of the panel, $^{\circ}F$-hr/Btu

It was assumed that as the sublimator plenum dried out (with the feed-water valve closed), the thermal resistance $R_s$ increased with time in the following manner:

$$R_s = \frac{R_i}{1 - \frac{Q_{in}\,\theta}{Q_t}} \qquad (4)$$

where $R_i$ = thermal resistance of the sublimator end of the panel with the sublimator plenum full, $^{\circ}F$-hr/Btu

$Q_{in}$ = heat input rate, Btu/hr

$Q_t$ = amount of heat required to sublime all the water in the sublimator plenum, Btu

Equation (1) becomes:

$$Q_{in} + \Sigma WC_p \frac{d\overline{T}}{d\theta} = \frac{(T_I - 32)\,(Q_t - Q_{in}\,\theta)}{R_i\,Q_t} \qquad (5)$$

Since the heat pipe theoretically maintains the panel at a fairly uniform temperature, it was assumed for this analysis that the average panel temperature $\overline{T}$ was equal to $T_I$. Making this substitution and rearranging (5), a first order linear differential equation is obtained, the solution of which is

$$T_I = \frac{e^{\left(\frac{a}{2b}\right)^2} \frac{\sqrt{\pi}}{2b} \left(\frac{Q_{in}}{\Sigma WC_p}\right) \left[\mathrm{erf}\left(b\theta - \frac{a}{2b}\right) + \mathrm{erf}\left(\frac{a}{2b}\right)\right] - 32^{\circ}F + T_o}{e^{a\theta - b^2\theta^2}} + 32^{\circ}F \qquad (6)$$

where $a = \dfrac{1}{R_i\,(\Sigma WC_p)}$

$b^2 = \dfrac{Q_{in}}{2\,R_i\,Q_t\,(\Sigma WC_p)}$

$T_o$ = temperature at which the feed-water valve opens

The solution of Equation (6) for the following typical conditions is shown in Figure A-1.

$$Q_{in} = 210 \text{ w}$$

$$Q_t = 327 \text{ Btu}$$

$$\Sigma WC_p = 9.1 \text{ Btu/}^{\circ}\text{F}$$

$$R_i = 0.0195 \text{ hr-}^{\circ}\text{F/Btu}$$

At time $\theta = 0$, the panel temperature is at 63°F and the feed-water valve opens, allowing the sublimator to operate. The panel temperature decreases and continues to decrease until $R_s$ is increased to the point where the heat cannot be dissipated at a rate to match the input heat load. The panel heats up again until it reaches 63°F at which time the valve opens again and the cycle repeats. At this heat load a minimum panel temperature of about 56°F is predicted, yielding a minimum cold end $\Delta T$ of 56 - 32 = 24°F. It is of interest to note that if the sublimator water plenum were filled all the time and the panel were allowed to come to steady state, a cold end $\Delta T$ of 14°F would be expected at 210 w.

The analysis was performed at heat loads of 105, 210, 315, and 420 w, and the minimum cold end $\Delta T$ was determined. The results are shown in Figure A-2 along with the steady state $\Delta T$ predicted for a constantly full sublimator plenum.

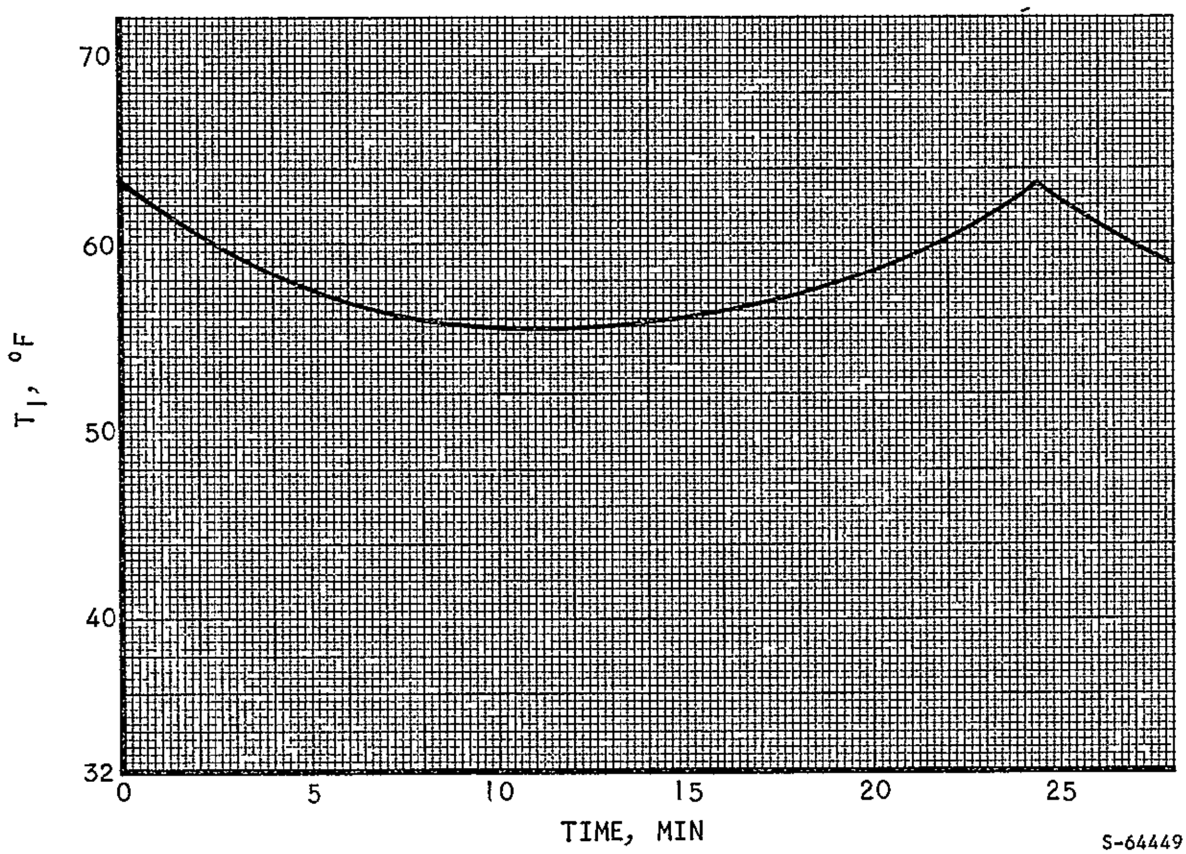


Figure A-1. Panel Cold End Temperature for 210-w Heat Load

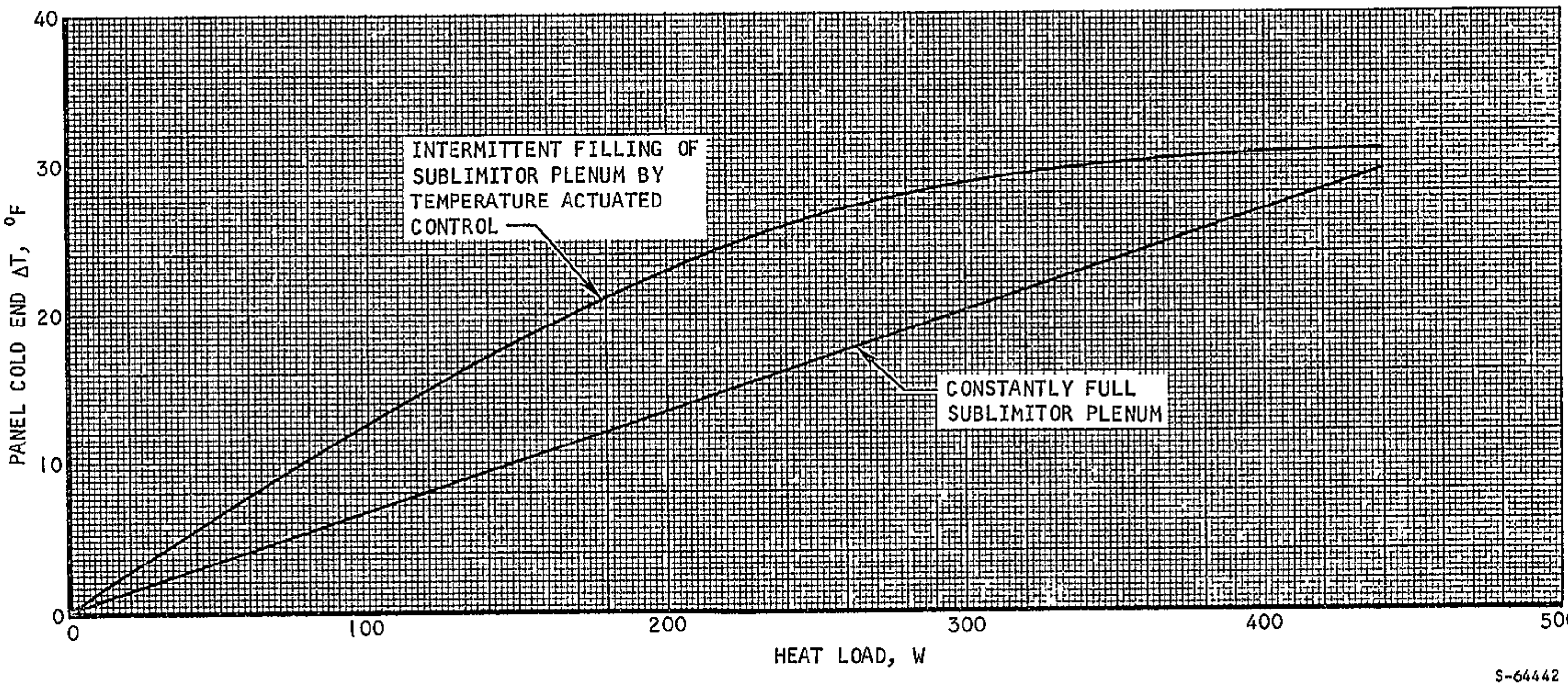


Figure A2. Minimum Panel Cold End ΔT

# METALLURGICAL EVALUATION OF BRAZED PANEL ASSEMBLY PN 189040-1

71-7343
April, 1971

Prepared by

J.C. Gibson

K.O. Parker

F.E. Carroll

Prepared for

National Aeronautics and Space Administration
George C. Marshall Space Flight Center
Huntsville, Alabama

GARRETT

AIRESEARCH MANUFACTURING COMPANY
Los Angeles, California

CONTENTS


| Section | | Page |
|---|---|---|
| 1 | INTRODUCTION | 1-1 |
| 2 | SUMMARY | 2-1 |
| 3 | THERMAL PANEL METALLOGRAPHIC EVALUATION | 3-1 |
| | Introduction | 3-1 |
| | Panel Sectioning | 3-3 |
| | Results of Metallographic Examination | 3-6 |
| | Remote Cooling Loop Evaluation | 3-13 |
| | Heat Pipe Evaluation | 3-15 |
| | Structural Sandwich Evaluation | 3-22 |
| | Conclusions | 3-25 |
| 4 | RECOMMENDED PANEL DESIGN | 4-1 |
| | Introduction | 4-1 |
| | Wicking Configuration | 4-1 |
| | Panel Fabrication | 4-3 |

## SECTION I

## INTRODUCTION

This report presents the metallographic evaluation of specimens sectioned from the Instrument Unit Thermal Conditioning Panel fabricated under Contract NAS 8-11291 to NASA Marshall Space Flight Center. The Instrument Unit Thermal Conditioning Panel was suspected of having unbrazed areas in both the evaporator and condenser end of the heat pipe. This conclusion was reached after a careful review of the performance test data. Recommendations for future work on similar types of heat pipe panels are discussed with emphasis placed on ease of manufacturing an integral, helium-leak-tight assembly.

## SECTION 2

## SUMMARY

The metallographic examination of the Instrument Unit Thermal Panel revealed many unbrazed areas and identified several distinct fabrication problems.

The stack-up of tolerances from detail part fabrication and large braze joint thickness in the boss and web joints was the single most important cause of unbrazed areas in the thermal panel assembly. The effective size (height) increase in the webs and bosses was the primary reason that the copper fins did not contact and braze to both the upper face sheet and the wick in the heat pipe section of the panel. Porosity in the copper fin due to the Kirkendall Effect was observed. Excessive braze alloy penetration into the nickel fins in the remote cooling loop and the structural sandwich was evident. Braze alloy liquation was distinctly evident in the structural sandwich and contributed to unsatisfactory brazing of the fins to one face sheet.

A thermal panel of this design and size can be successfully fabricated by some material and fabrication technique modifications. By changing the nickel fins to Type 347 stainless steel fins and by fixturing the panel assemblies so they are separated for the brazing cycle, the alloy erosion and liquation problems can be overcome. The bosses and webs must be final machined after the brazing operation to eliminate the possibility of the braze alloy joints causing fitup problems due to an excessive tolerance stack-up. The copper fin thickness must be increased to minimize the porosity due to the Kirkendall Effect.

A different design of a thermal conditioning panel using new wicking test information not available at the time the present design was conceived is presented. The new test data eliminates the necessity of the copper fin which eliminates the brazing problems associated with the Kirdendall Effect and wick-to-copper-fin brazing. The new design will meet NASA-MSFC performance and structural requirements.

SECTION 3

# THERMAL PANEL METALLOGRAPHIC EVALUATION

## INTRODUCTION

A brief description of the panel is presented below in sufficient detail to permit a discussion of features revealed by the metallographic examination.

The 30 by 30 in. thermal panel, shown in Figure 3-1, is a 3-layer, all-brazed, plate-fin sandwich assembly. The entire panel surface area is provided with internally-brazed equipment-mounting bosses on 2-in. centers, except in the condenser section which accommodates a water reservoir and sublimator on opposite sides of the panel.

Nickel fins, 0.004-in. thick, were used in both the remote-cooling loop and in the structural sandwich. Copper fins, 0.002-in. thick, and a nickel Feltmetal wick constituted the intermediate heat-pipe sandwich which was stiffened by brazed webs aligned parallel to the heat-pipe vapor flow path between the equipment mounting bosses.

In operation, heat rejected from electronic equipment would be conducted through the remote cooling loop sandwich and through the copper fins to the saturated wick where evaporation occurs. The water vapor travels to the condenser end of the panel where heat is removed by the sublimation of external, expendable water. The condensate is then returned to the evaporator section by the capillary action of the nickel wick. The interface between the remote cooling loop and the copper fins and the joints between the copper fins and the wick must be brazed to minimize the temperature differentials along the heat path. The equipment mounting bosses must be brazed to the structural-sandwich face sheet for structural integrity of the panel assembly. Bonding of the wick was required only in the condenser section of the thermal panel assembly where heat was rejected to the sublimator assembly.

The principal elements of the thermal panel were fabricated by step-brazing in the following sequence:

| Braze Cycle | Components | Brazing Alloy |
|---|---|---|
| 1 | Remote cooling loop and structural sandwiches simultaneously | AMS 4779 (2070°F) |
| 2 | Bosses and webs to remote cooling loop sandwich | Palniro RE (2025°F) |
| 3 | Heat-pipe fins, Feltmetal; bosses and webs to structural sandwich; close-outs | AMS 4778 (1970°F) |

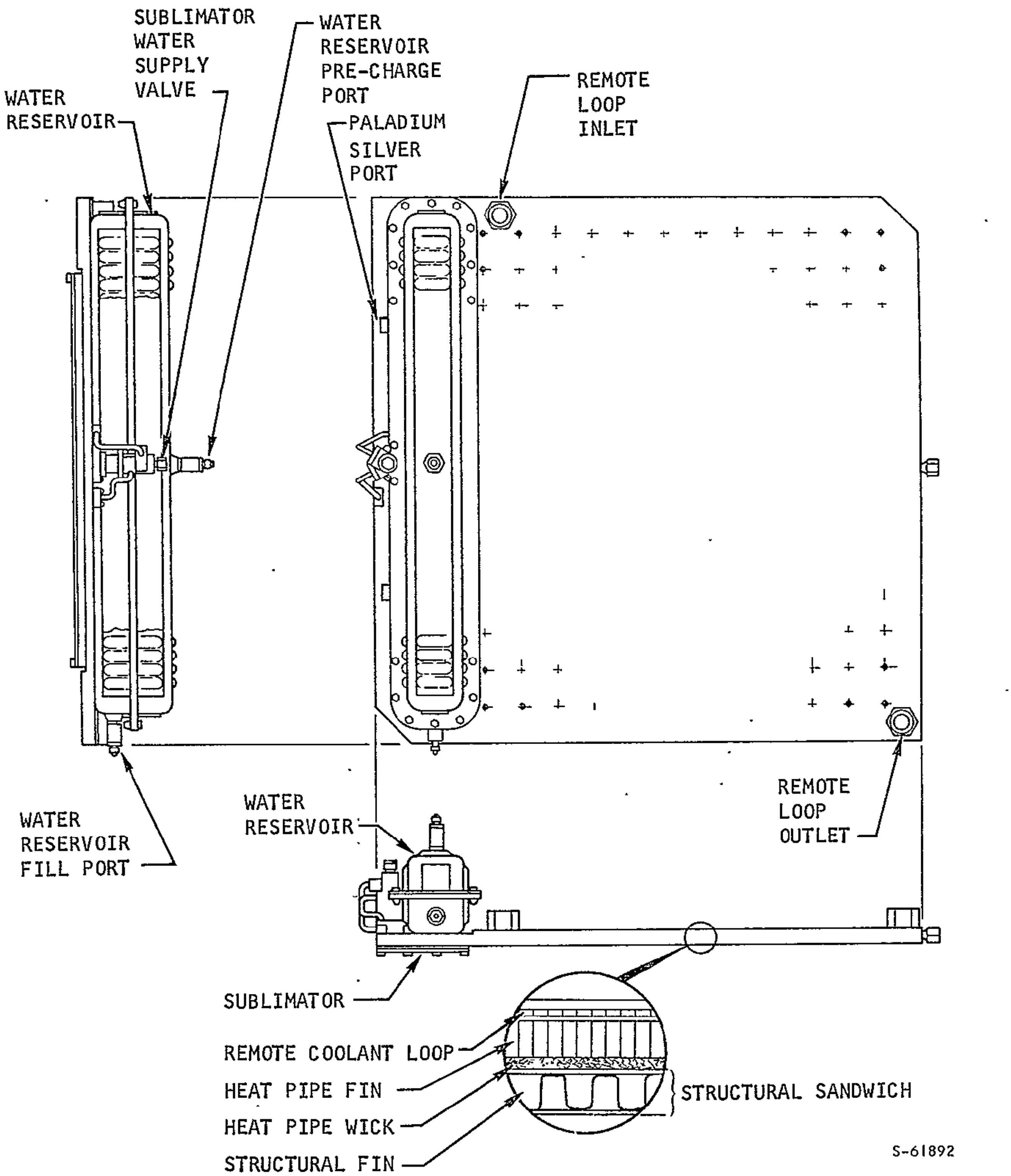


Figure 3-1. Heat Pipe Sublimator Thermal Conditioning Panel

## PANEL SECTIONING

After removal of instrumentation, mechanical attachments and external metallurgical attachments, the exposed panel was sectioned in the manner shown in Figure 3-2. Wherever possible, an abrasive cut-off machine was employed to minimize damage to the samples. Generally, four peel-test specimens and one micro-section were taken from each piece of the panel removed. Figure 3-3 shows the location, orientation, and identification of the micro-sections. Conventional matrix notation (row first, column second) was used to identify the origin of all test samples. Micro-section No. 22315 in Figure 3-3, which corresponds to point CH, was taken in an orientation normal to the heat pipe vapor flow as indicated by the heavy line through point CH. Each intersection on the grid represents an equipment-mounting boss.

Peel tests were first performed in Area 9 (Figure 3-2) to determine whether the much closer approach to predicted thermal performance at locations KC and KA than at MC could be explained in terms of brazed joint quality. The remainder of the test sample distribution was selected as a representative survey of the panel, rather than to correspond to a particular location on the thermal panel.

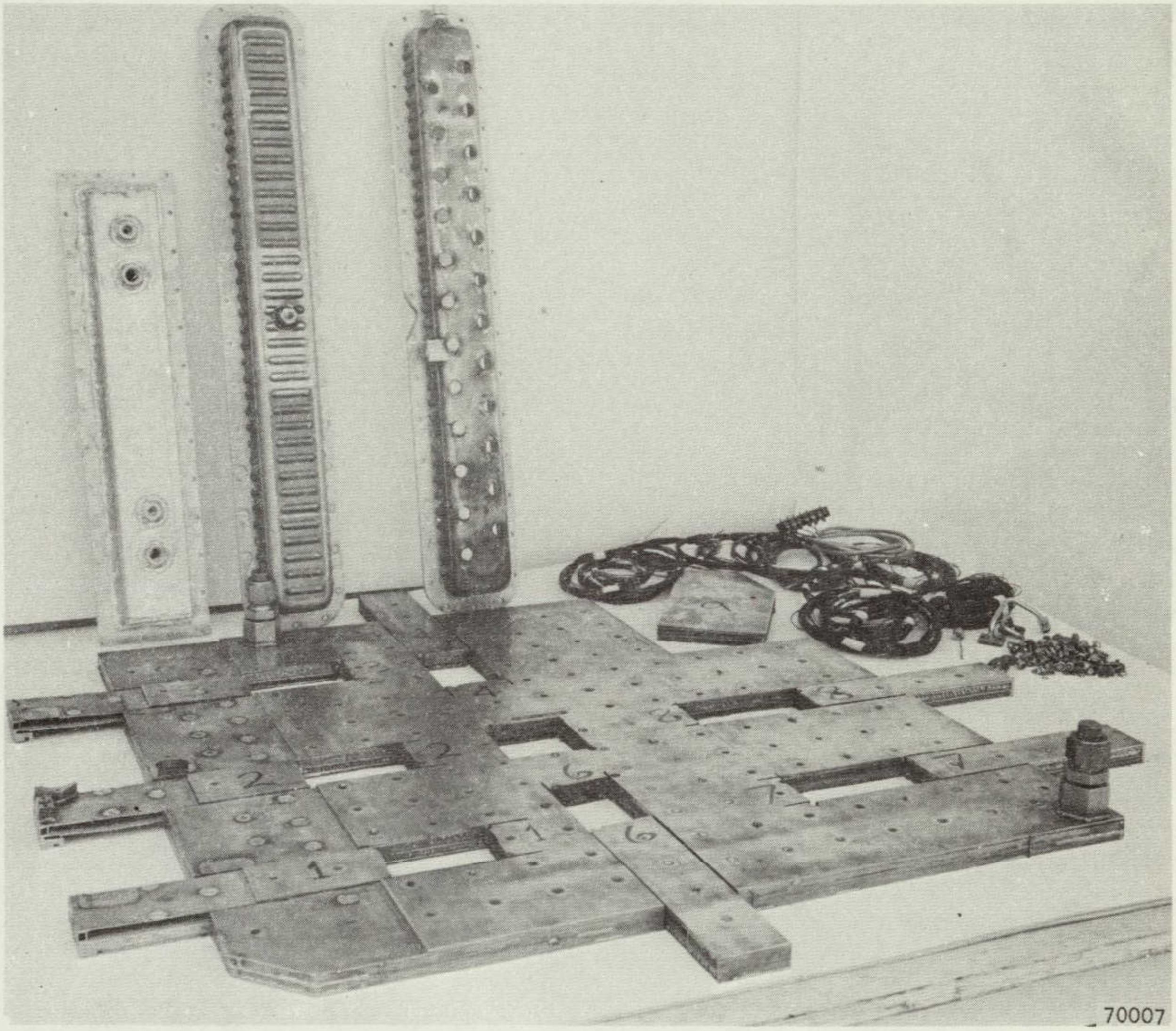


Figure 3-2. Thermal Panel After Sectioning for Metallographic Examination

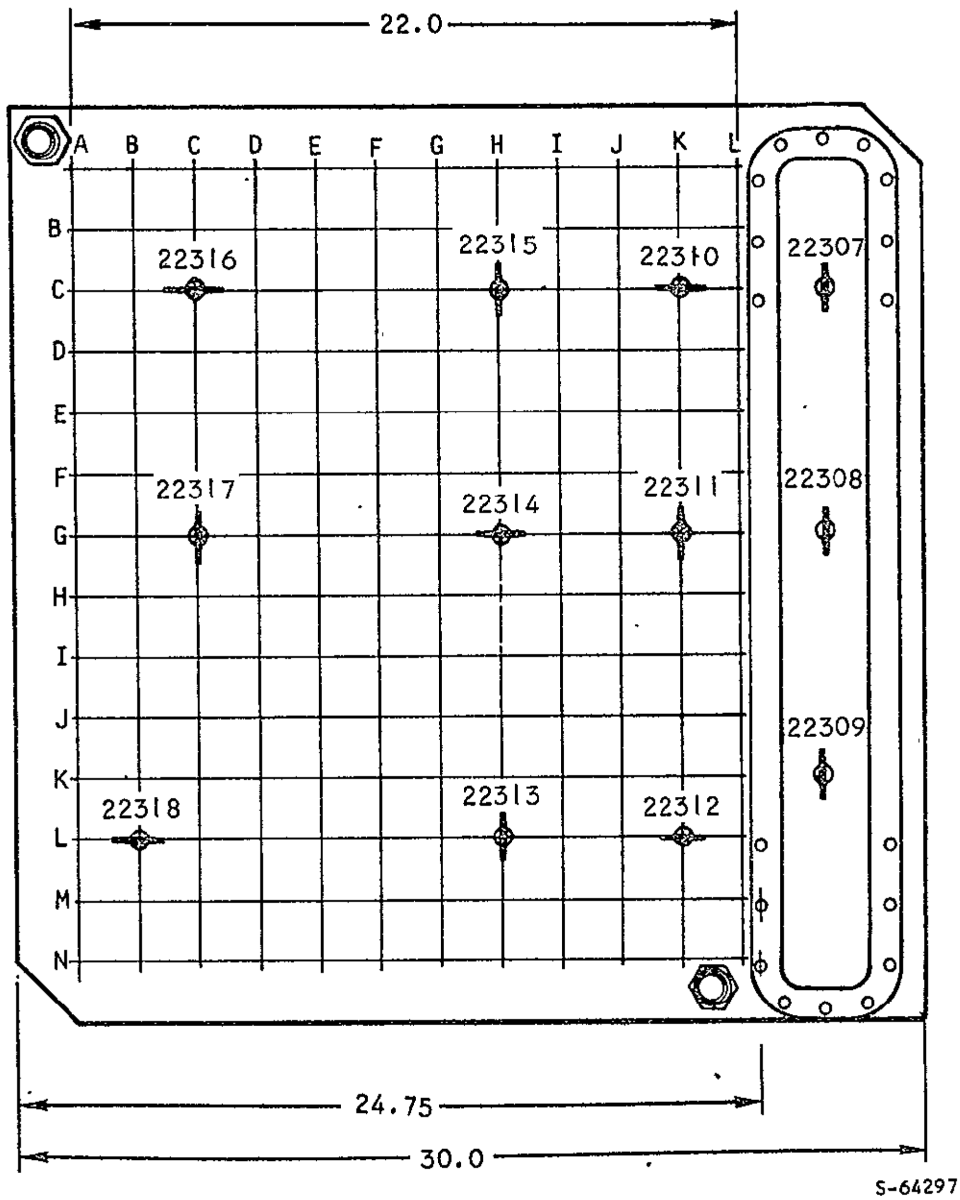


NOTE: ALL DIMENSIONS ARE IN INCHES

Figure 3-3. Location, Orientation, and Identification of Micro-Sections

RESULTS OF METALLOGRAPHIC EXAMINATION

Many unbrazed areas were revealed by the examination, and several distinct problems were identified. The results of the peel tests are summarized and shown schematically in Figures 3-4 through 3-9.

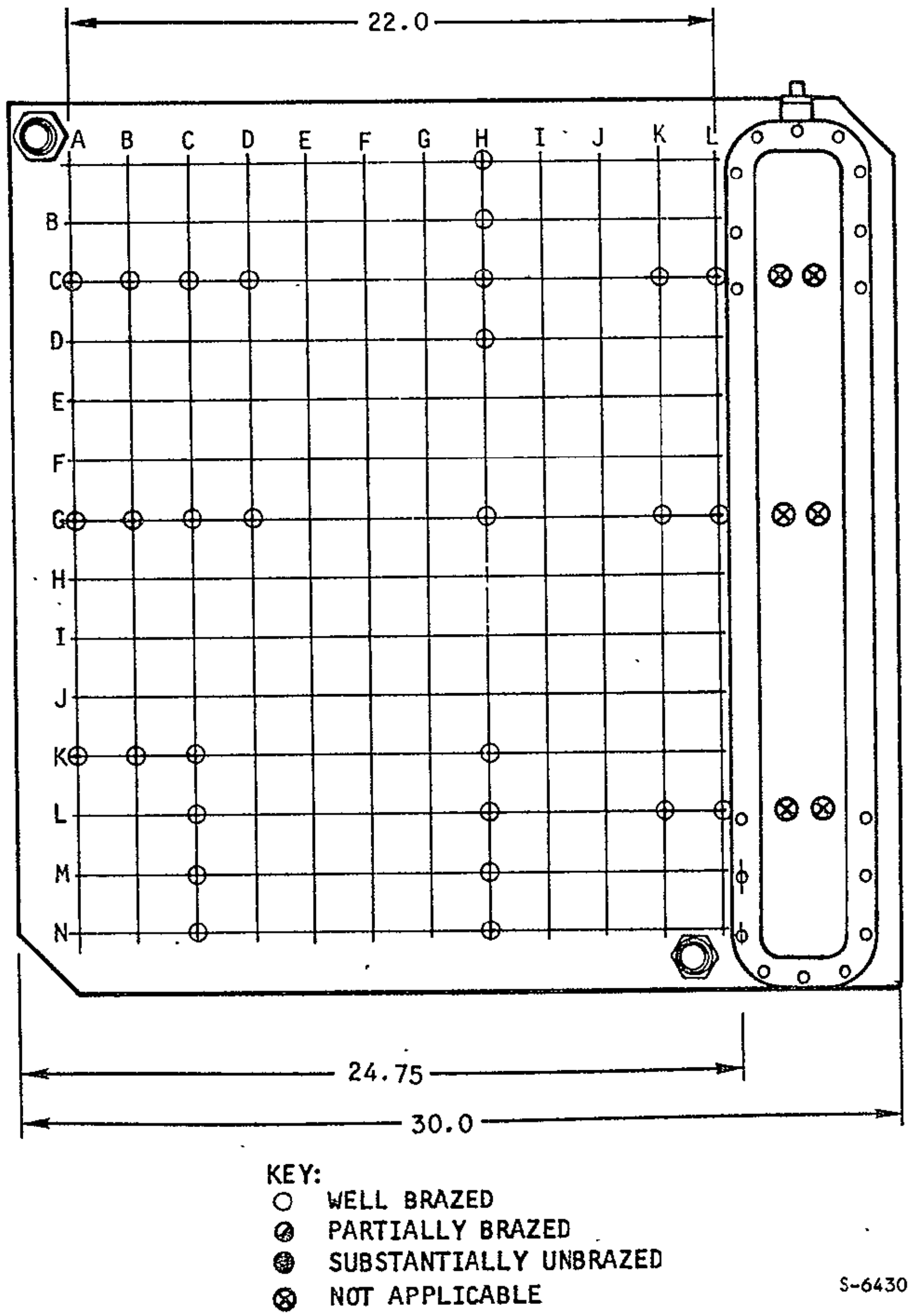


Figure 3-4. Summary of Remote-Loop Fin Joints

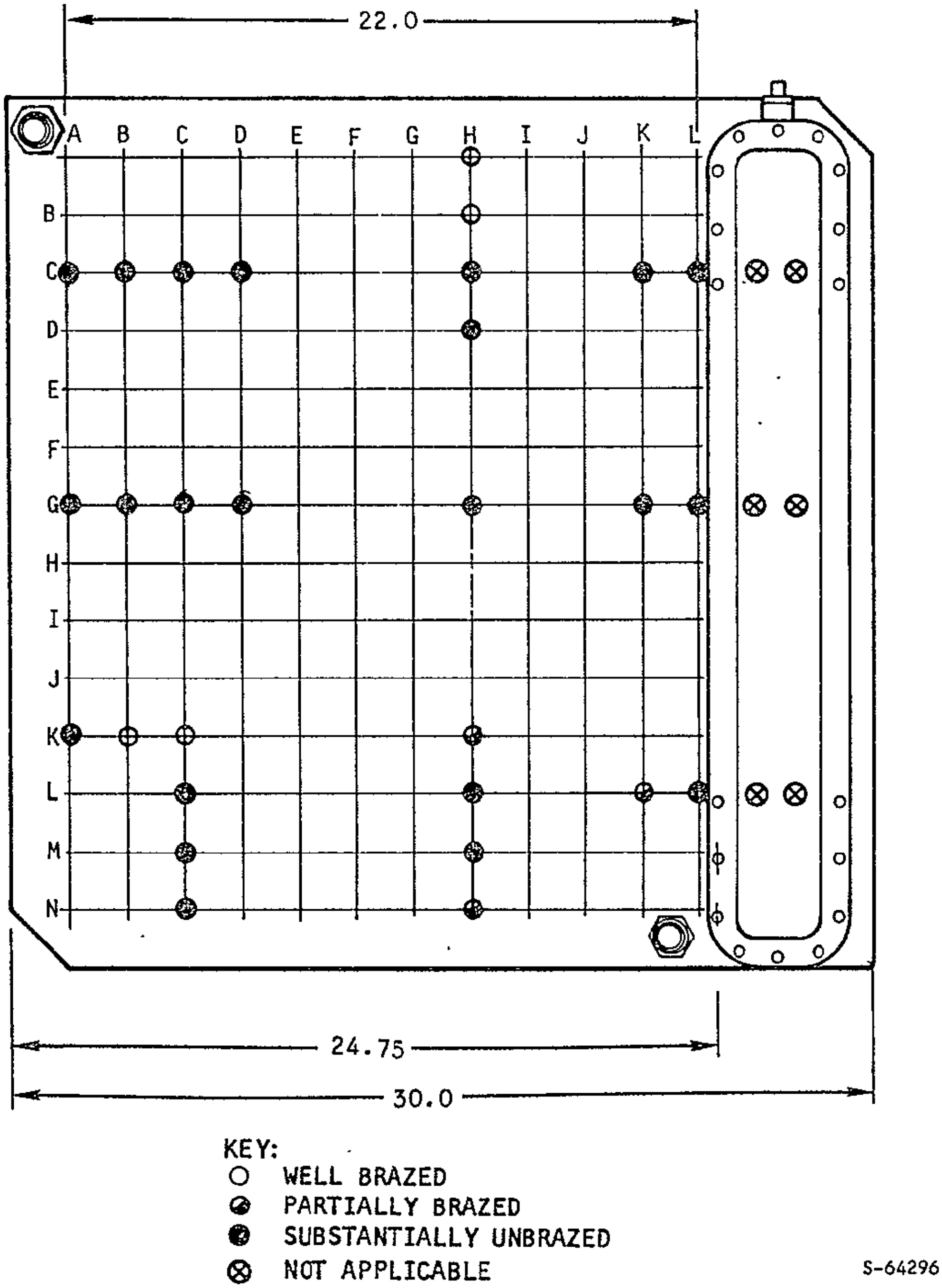


Figure 3-5. Summary of Copper-Fin-to-Remote-Loop Joints

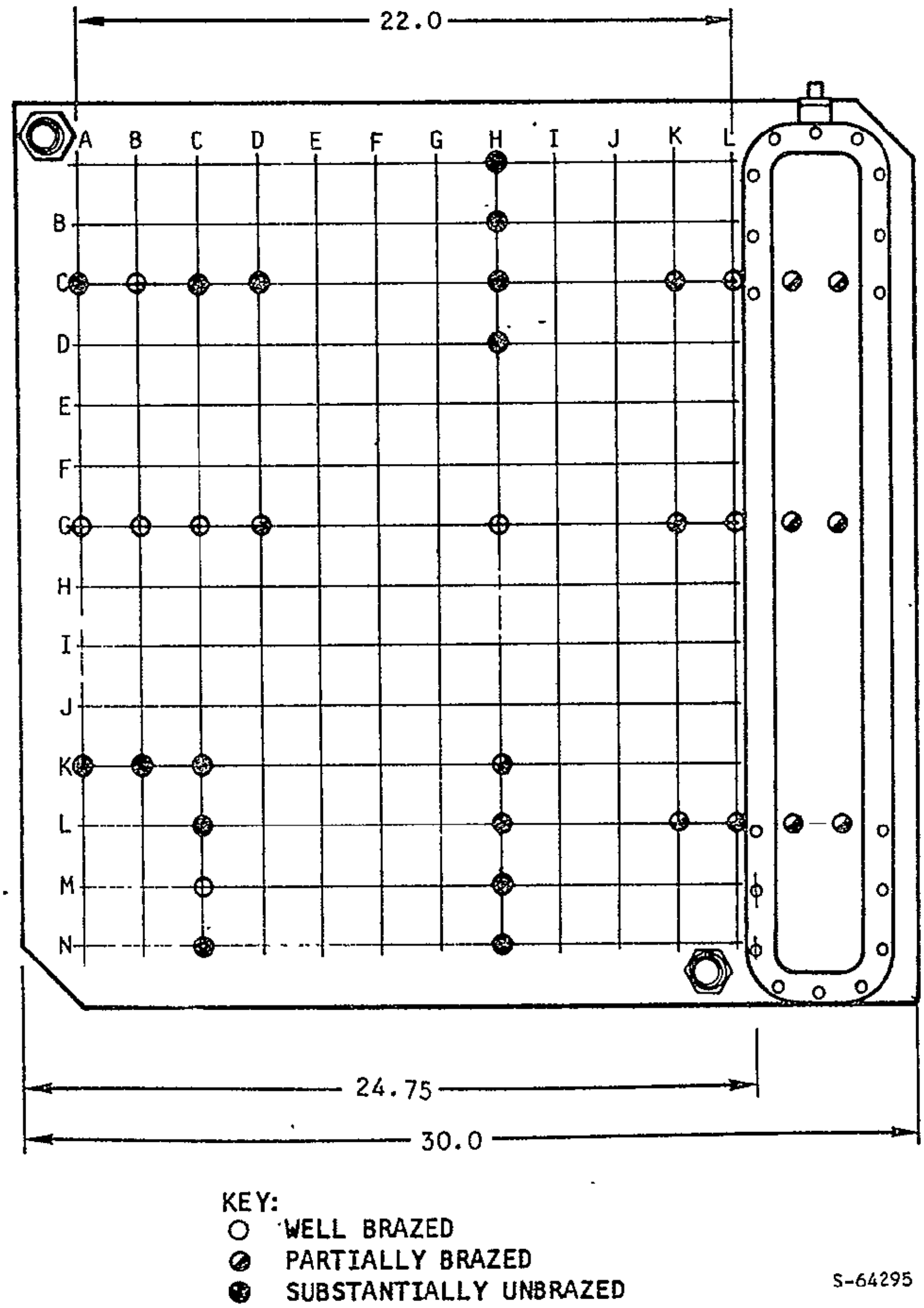


Figure 3-6. Summary of Feltmetal-Wick-to-Copper Fin Joints and Feltmetal-to-Face-Sheet Interface (Condenser Section Only)

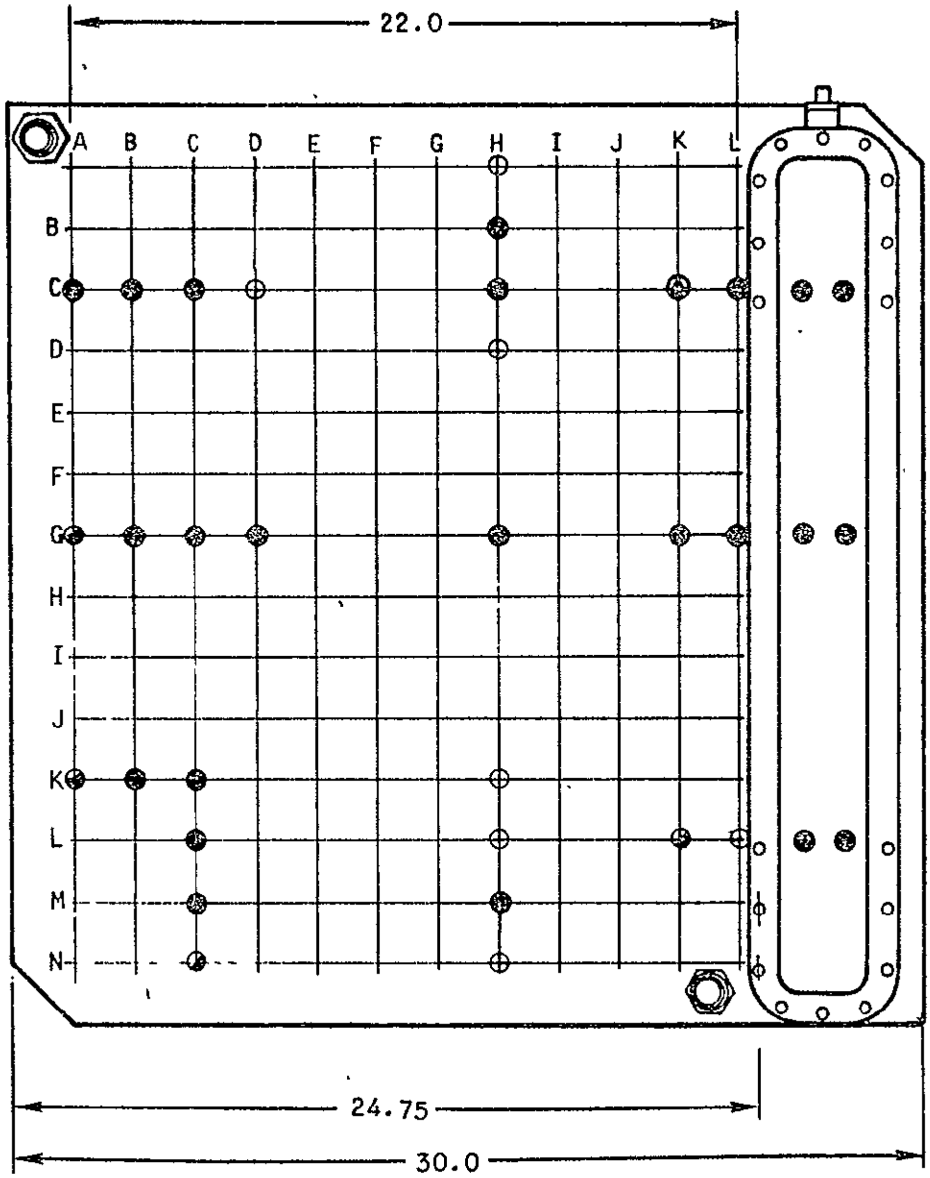


KEY:
○ WELL BRAZED
◐ PARTIALLY BRAZED
● SUBSTANTIALLY UNBRAZED
⊗ NOT EXAMINED

S-64299

Figure 3-7. Summary of Web-to-Structural-Sandwich Joints

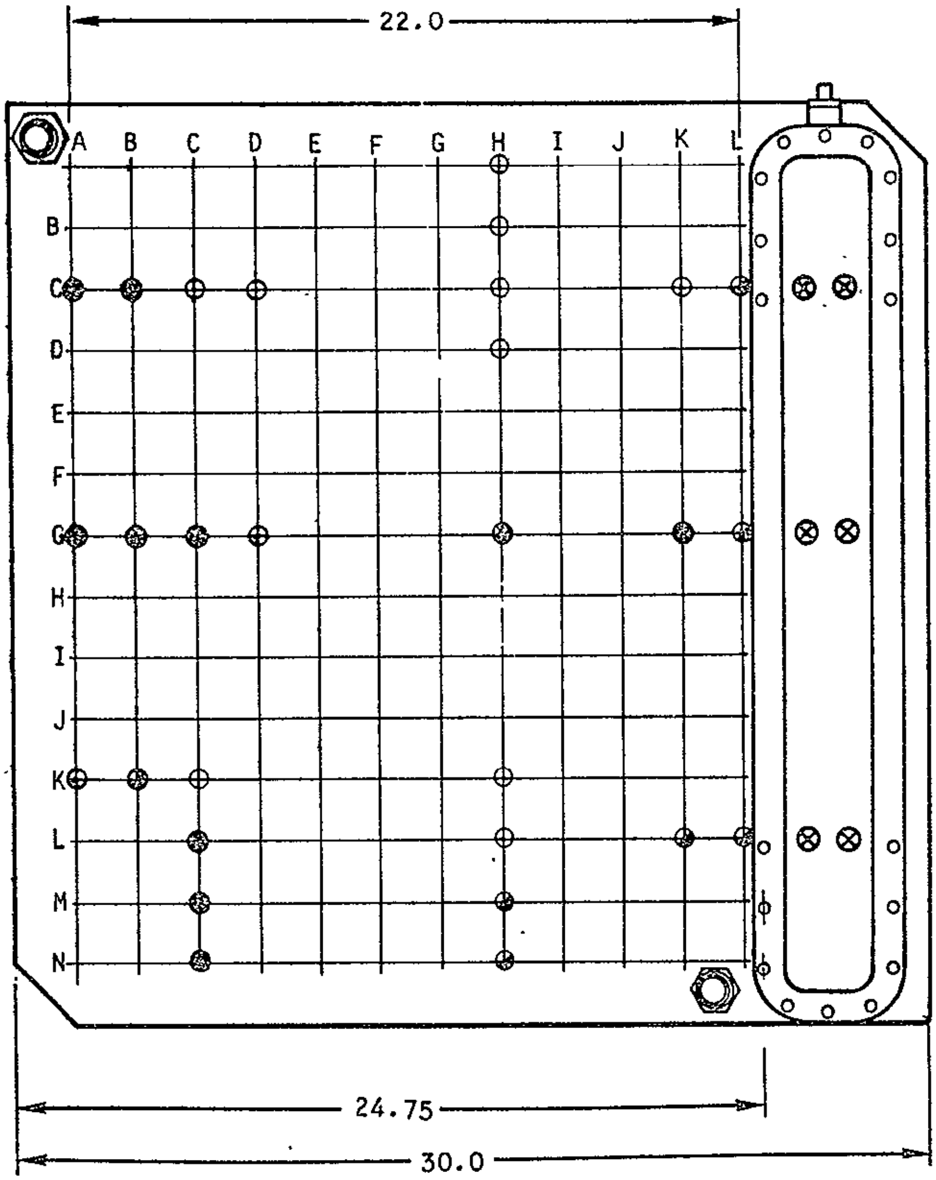


KEY:
- ○ WELL BRAZED
- ⊘ PARTIALLY BRAZED
- ⊛ SUBSTANTIALLY UNBRAZED
- ⊗ NOT APPLICABLE

S-64298

Figure 3-8. Summary of Boss-to-Structural-Sandwich Fin Joints

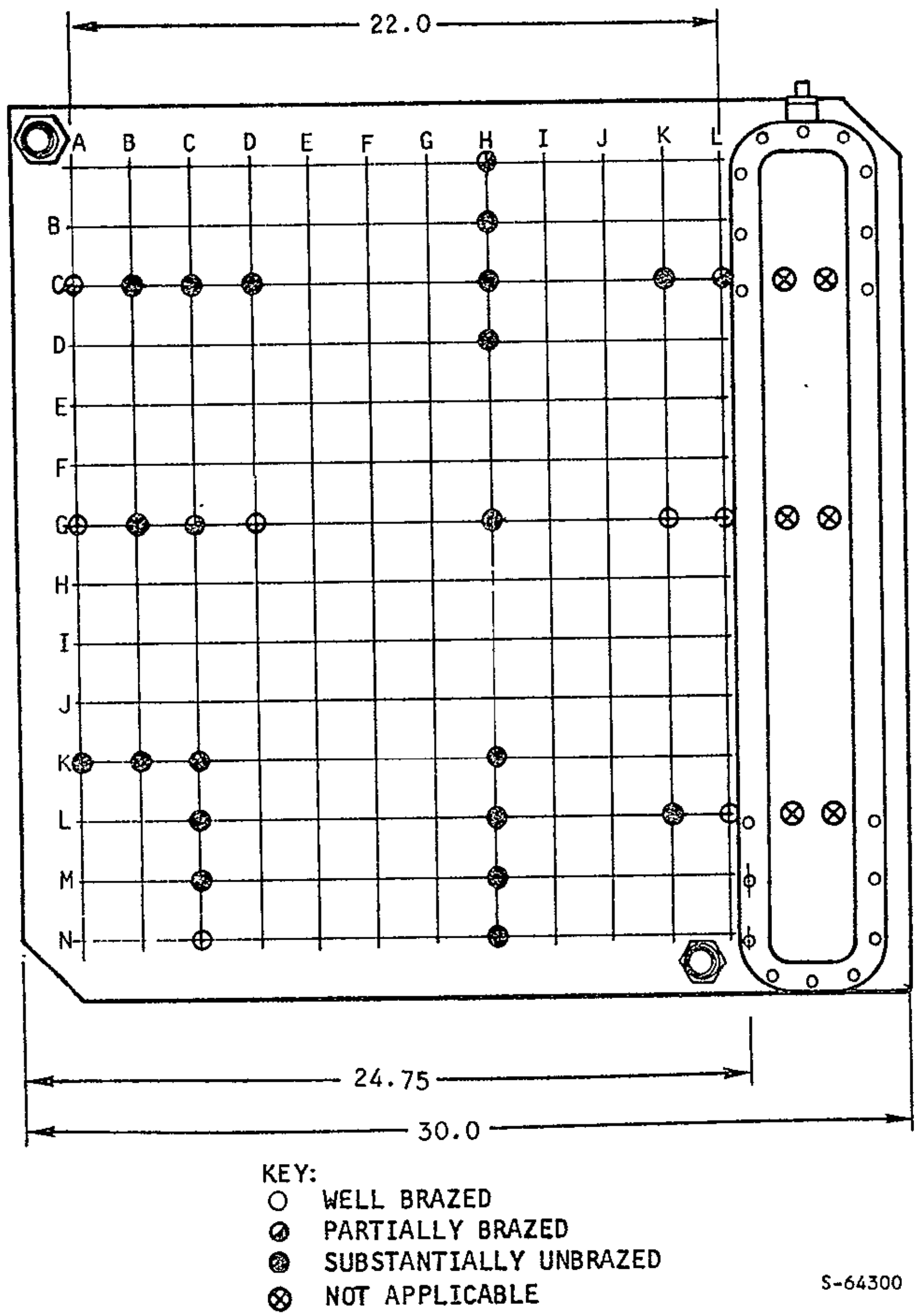


Figure 3-9. Summary of Structural-Sandwich Fin Joints

## REMOTE COOLING LOOP EVALUATION

The remote cooling loop was well brazed (see Figure 3-4) throughout the areas of the plate fin sandwich that were examined as indicated in the photomicrographs of Figures 3-10 and 3-11. Figure 3-10 indicates excellent brazing of the remote cooling loop both internally and the equipment mounting boss. Large equipment mounting boss braze joints, which are evident in both Figures 3-10 and 3-11, can cause undesirable braze tolerance buildup. Figure 3-11 shows evidence of braze alloy attack on the nickel fins due to the extended brazing cycle required for large plate fin assemblies when vacuum-furnace brazed. Forced-convection-furnace brazing or a modification of the vacuum brazing process is now recommended for panels of the design used.

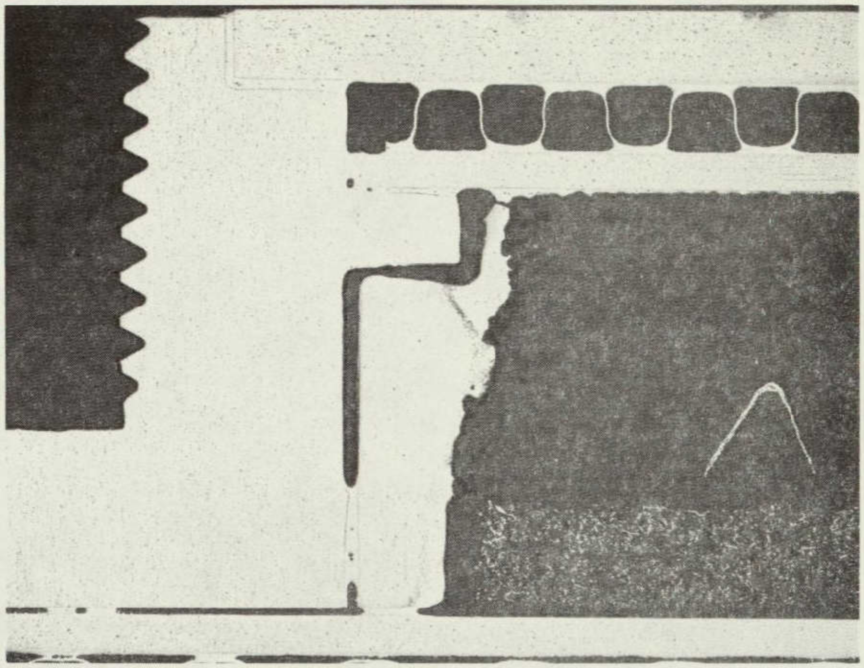

Figure 3-10. Sample LK. Note Excellent Brazing of Remote Loop Sandwich, Internally and to Boss. Etched Electrolytically in 10 percent Oxalic Acid. (Micro 22312; X6.5 Magnification)

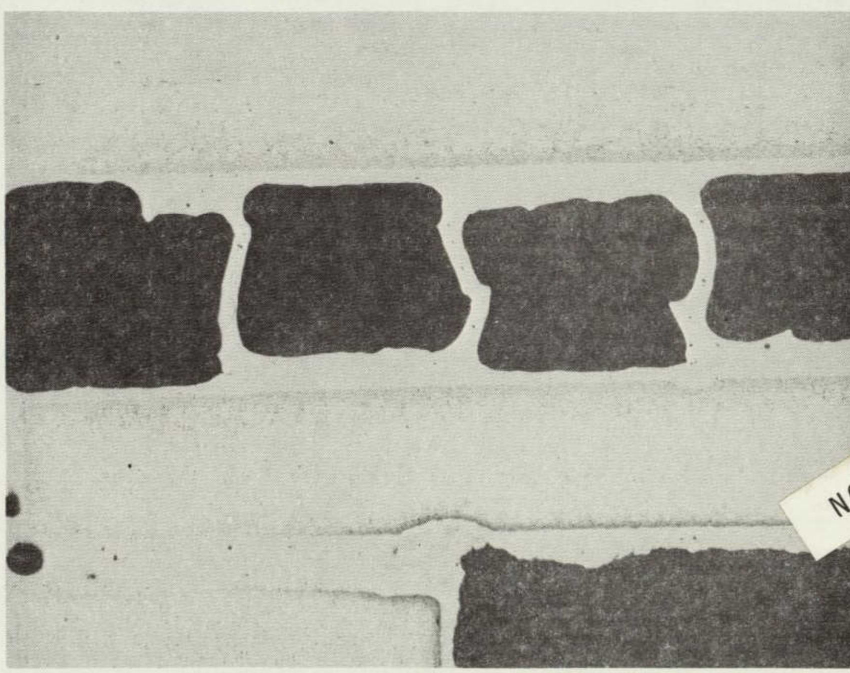


F-13142

Figure 3-11. Sample CK Showing Remote-Loop Fin Damage Caused by Protracted Brazing Cycle with Nickel-Base Brazing Alloy AMS 4779. Etched Electrolytically in 10 percent Oxalic Acid. (Micro 22310; X 25 Magnification)

## HEAT PIPE EVALUATION

The heat pipe section of the thermal panel assembly showed evidence of having inadequate brazing at all of the required brazed interfaces as summarized in Figures 3-5 and 3-8. Although 76 percent of all copper-fin-to-remote-cooling-loop interfaces were unbrazed, only 65 percent were unbrazed among the 14 samples in which the copper-fin-to-wick interface was unbrazed. This shows that on the average, brazing tended to occur only at one interface rather than at both of the required interfacial joints, thereby demonstrating a detail parts fit-up problem.

Typical conditions revealed by the peel tests of the heat pipe section are shown in Figures 3-12 through 3-17. Figures 3-12 and 3-13 show conclusively that the copper fins in sample CK were not in contact with the face sheet during panel brazing, except at an isolated point. Figures 3-16 through 3-20 illustrate conditions that were observed in several of the peel test samples. It was generally observed that the copper fins tended to braze well adjacent to the bosses and webs. These were the areas that had been coated with Palniro RE alloy in a previous brazing cycle. Brazing in these areas may be attributed to (1) slight remelting of the Palniro RE brazing alloy occurring during the final brazing cycle, (2) the fact that the locally-coated surface was more readily wetted by the AMS 4778 brazing alloy, or (3) more probably, the thickness of the Palniro RE may have been sufficient to alleviate the fit-up problem caused by the large braze joints which added an undesirable additional height to the bosses and webs. A discrepancy between the heights of the web and boss in sample CH, after brazing to the remote-loop sandwich, is suggested by Figures 3-17 and 3-18, where the web barely made contact with the structural-sandwich face sheet, and the boss was clearly well-brazed.

The photomicrographs in Figures 3-19 and 3-20 show copper fin brazing at two different locations in the heat pipe. Figure 3-19 shows the 0.002-in.-thick copper fin brazed to the remote cooling loop with a 0.002-in. AMS 4778 braze joint.

Figure 3-20 shows a copper-fin-to-wick braze joint showing fin porosity caused by a phenomenon called the Kirkendall Effect. The Kirkendall Effect is the interdiffusion between the brazing alloy and copper fin producing extensive porosity in the body of the fin. This porosity is the result of disimilar diffusion rates of two or more atomic species involved in a vacancy-exchange diffusion process in protracted high temperature brazing cycles.

The wick in the condenser section of the thermal panel was partially brazed due to lack of wick loading (fin removed in condenser section) and due to some contamination as indicated in Figure 2-21.

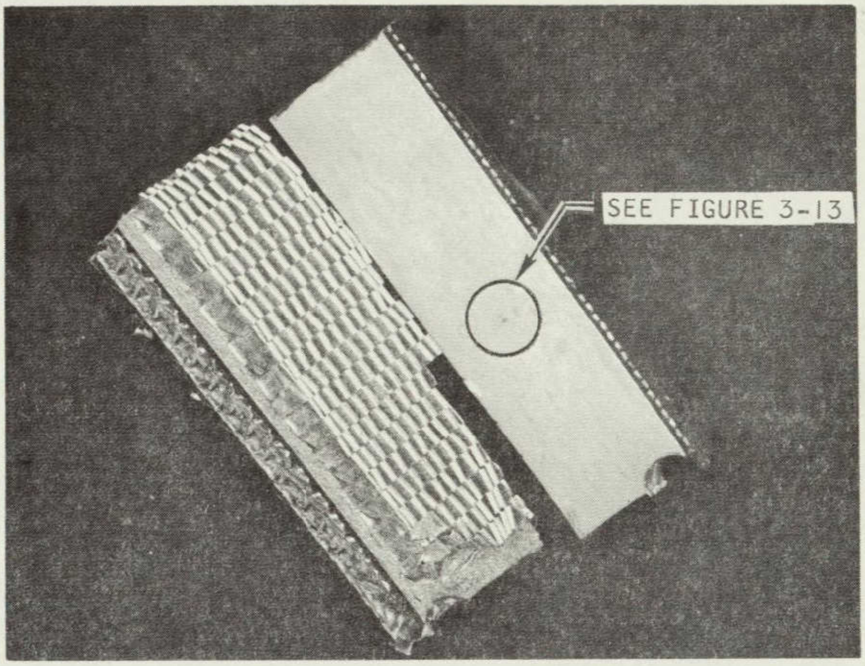


Figure 3-12. Sample CK. Note Unbrazed Interface Between Copper Fin and Remote Loop Sandwich. (X 1-1/4 Magnification)

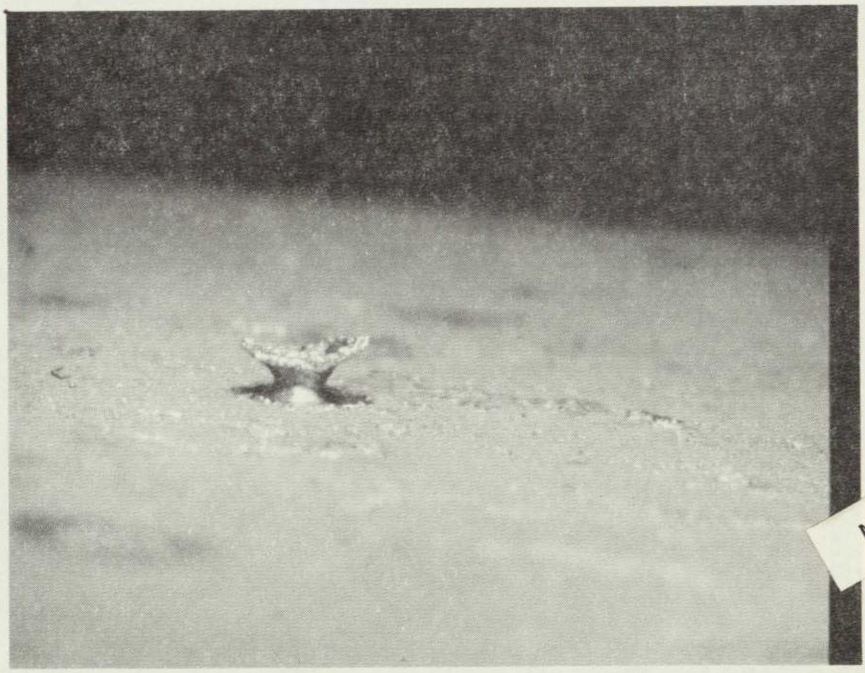



F-13137

Figure 3-13. Detail from Figure 3-12. Note Large Gap, Approximately 0.010 in., Between Crown of Solitary Brazed Copper Fin and Remote Loop Sandwich. (X 15 Magnification)

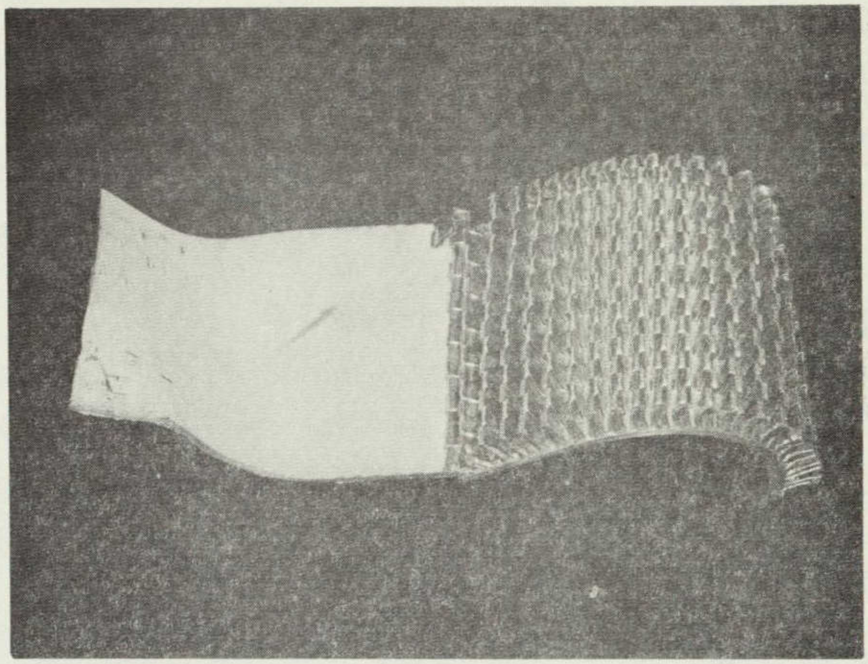

Figure 3-14. Sample MH Showing Unbrazed Face Sheet on Thermal Panel Side of Structural Sandwich. (X 2/3 Magnification)

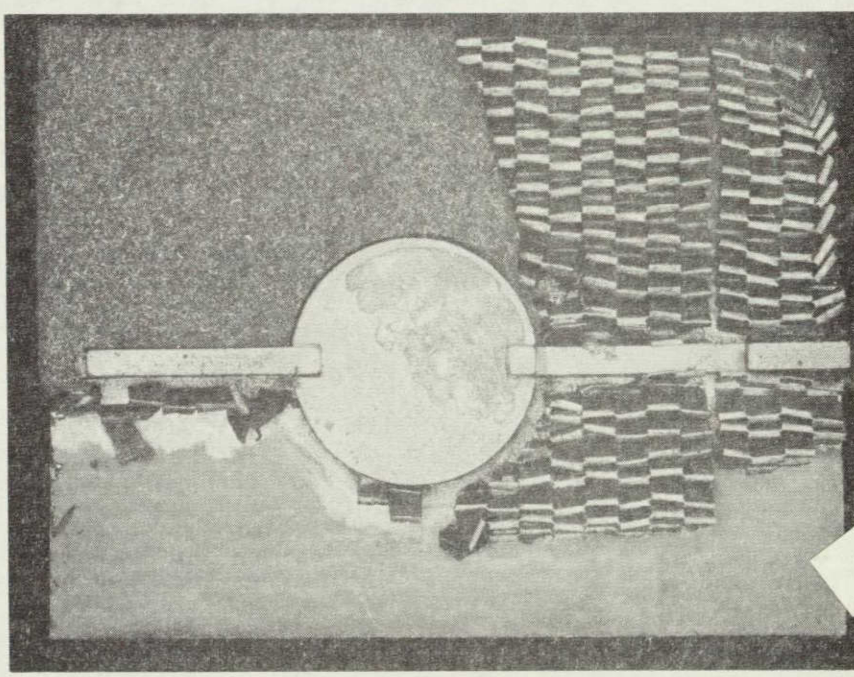



F-13138

Figure 3-15. Sample MH Showing Partially Brazed Boss, Unbrazed Web, and Unbrazed Areas at the Felt Metal-Copper Fin and Copper Fin-Remote Loop Interfaces. (X 1-1/2 Magnification)

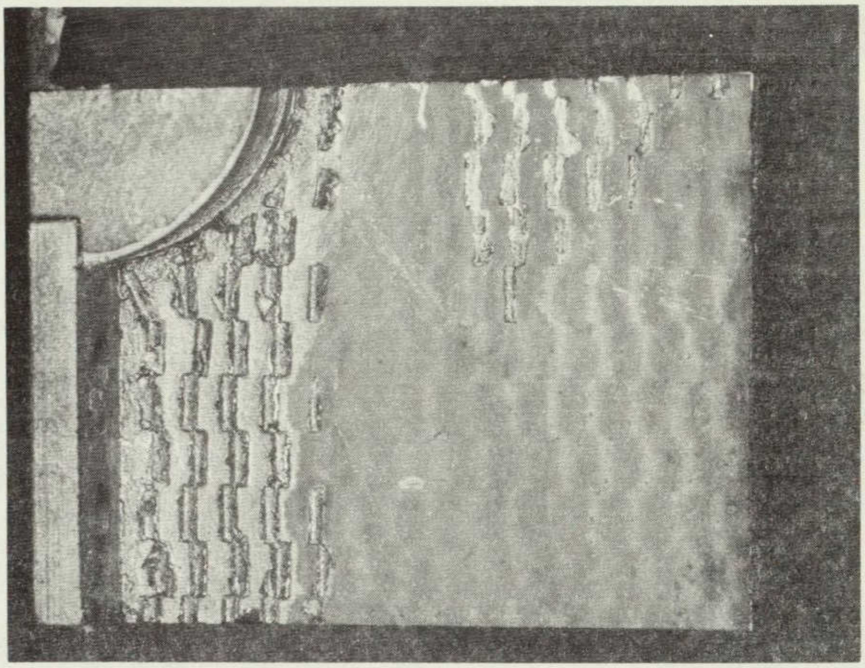

Figure 3-16. Sample CH. Note that the Copper Fins are Well-Brazed Adjacent to the Web and Boss but not Elsewhere. The Web and Boss Area was coated with Palniro RE in a Previous Brazing Cycle. (X 3 Magnification)

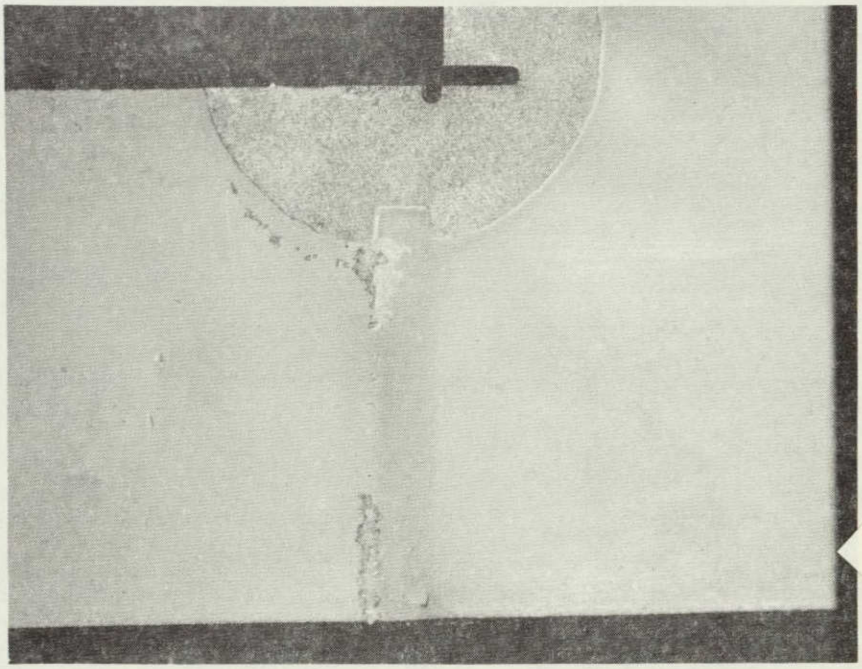



F-13139

Figure 3-17. Sample CH Showing Panel-Side Face Sheet of Structural Sandwich After Peel Test. The Boss was Well-Brazed, but the Web was Substantially Unbrazed. (X 3 Magnification)

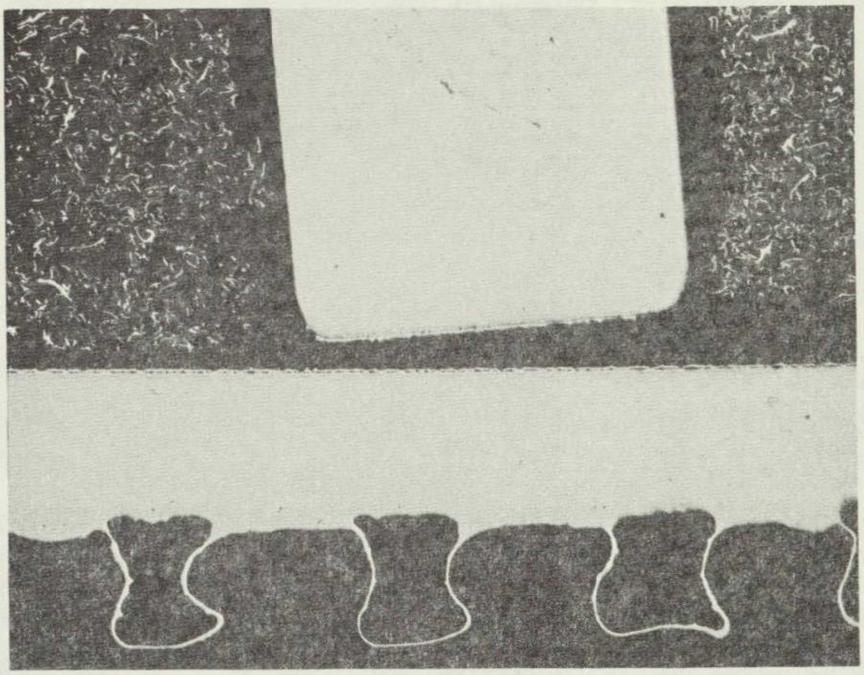

Figure 3-18. Micro 22309 Showing Lack of Contact Between Web and Face Sheet in Panel Condensor Section. (Unetched; X 20 Magnification)

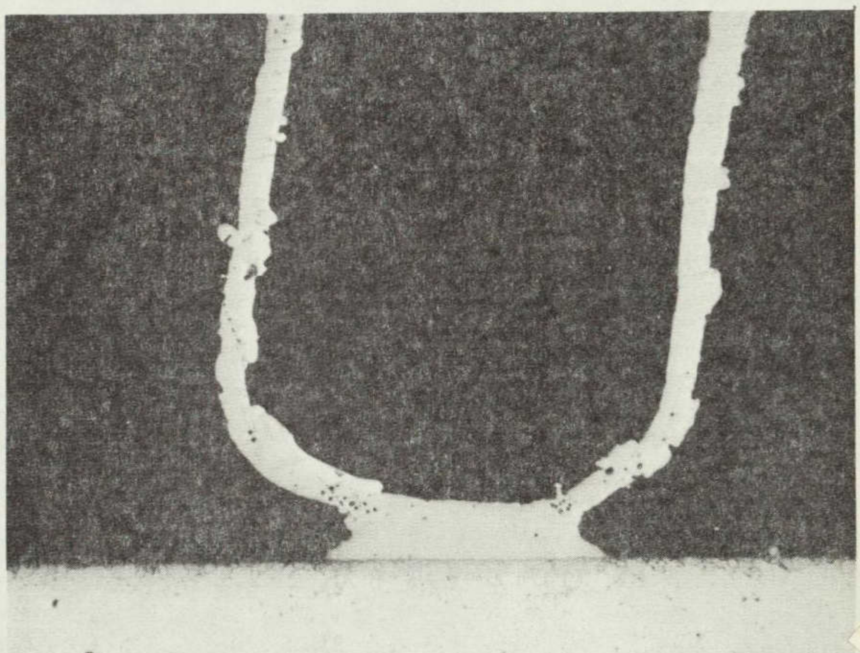



F-13941

Figure 3-19. Sample CH Showing Copper Fin Brazed to Remote-Loop Face Sheet. (Micro 22315; Unetched; (X 80 Magnification)

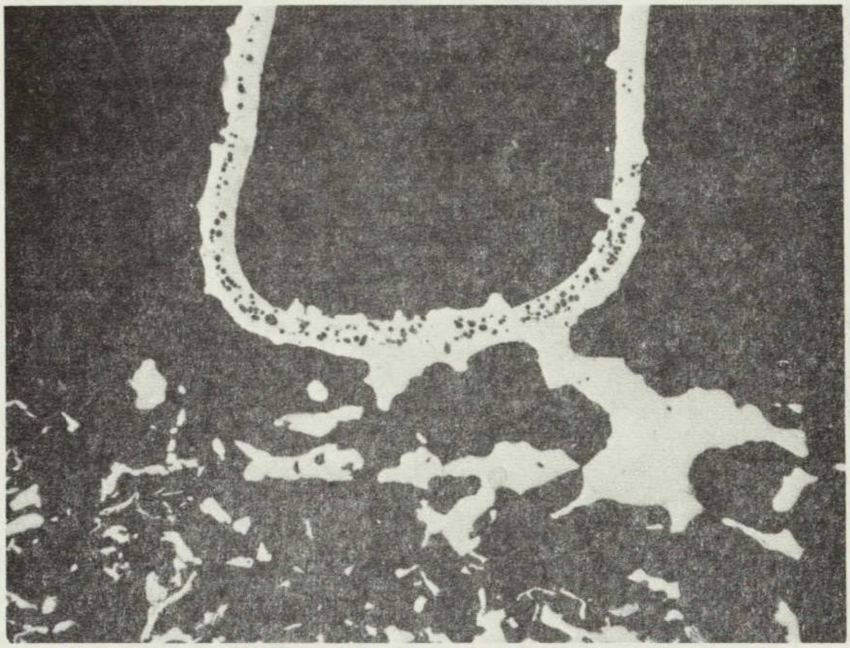

Figure 3-20. Sample LH Showing Copper Fin Brazed to Nickel Felt Metal. The Fin Porosity is Caused by Interdiffusion Between the Copper and the Brazing Alloy. (Micro 22313; Unetched; X 80 Magnification)

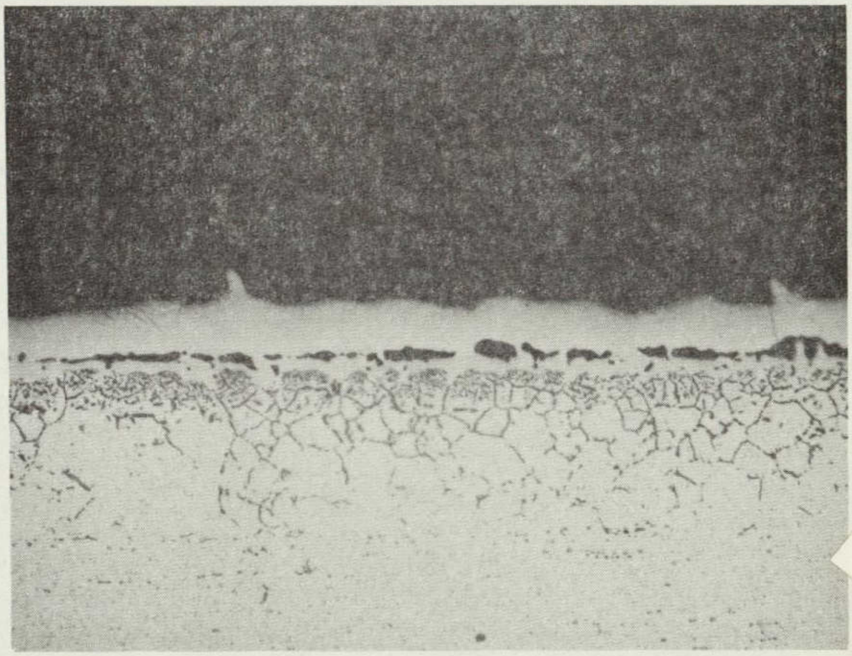



F-13145

Figure 3-21. Micro 22309 Showing Failure of Brazing Alloy to Wet Condenser-Section Face Sheet. Etched Electrolytically in 10 percent Oxalic Acid. (X 300 Magnification)

## STRUCTURAL SANDWICH EVALUATION

The structural sandwich metallurgical evaluation is summarized in Figure 3-9. The photomicrograph evaluation is presented in Figures 3-22 through 3-25. The structural sandwich showed evidence of excellent fin-to-sheet brazing on the external sheet but evidence of braze alloy liquation on the internal (heat pipe side) face sheet. Extensive brazing alloy liquation, which results from an excessive dwell in the braze alloy freezing range, was observed wherever the structural sandwich fins failed to braze to the heat-pipe face sheet.

Brazed and unbrazed fins are shown in Figures 3-24 and 3-25. Figure 3-24 illustrates well brazed fins and a smooth flow of adjacent brazing alloy. Figure 3-25 shows evidence of unbrazed fins caused by braze alloy liquation alone. Evidence of structural fin damage is illustrated in Figure 3-22 where the fins have failed along grain boundaries penetrated by the AMS 4779 brazing alloy. The unbrazed heat-pipe face sheet, also shown in Figure 3-22, was unbrazed due to the liquation of the braze alloy as discussed above.

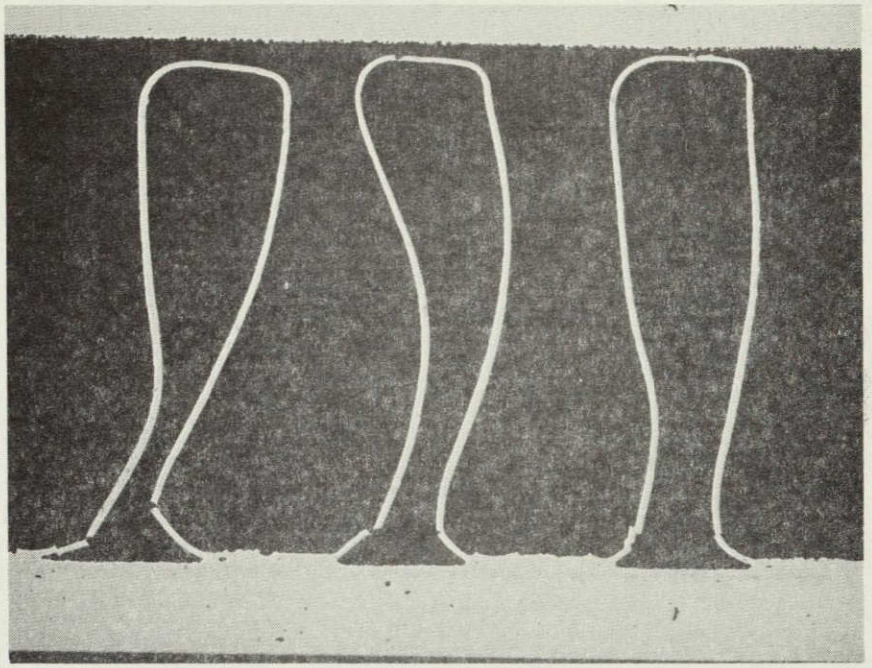

Figure 3-22. Sample LB Showing Evidence of Fin Crushing but no Brazing at Panel-Side Face Sheet. Etched Electrolytically in 10 percent Oxalic Acid. (Micro 22318; X 12 Magnification)

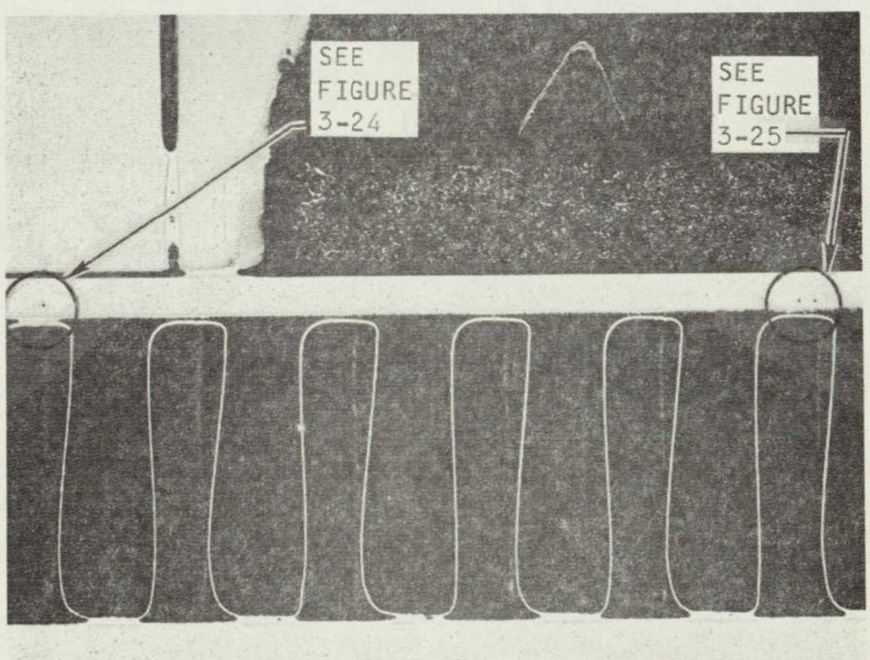




F-13143

Figure 3-23. Sample LK Showing Brazed and Unbrazed Structural-Sandwich Fins Identified by Micro-Hardness Impressions Etched Electrolytically in 10 percent Oxalic Acid. (Micro 22312; X 6.5 Magnification)

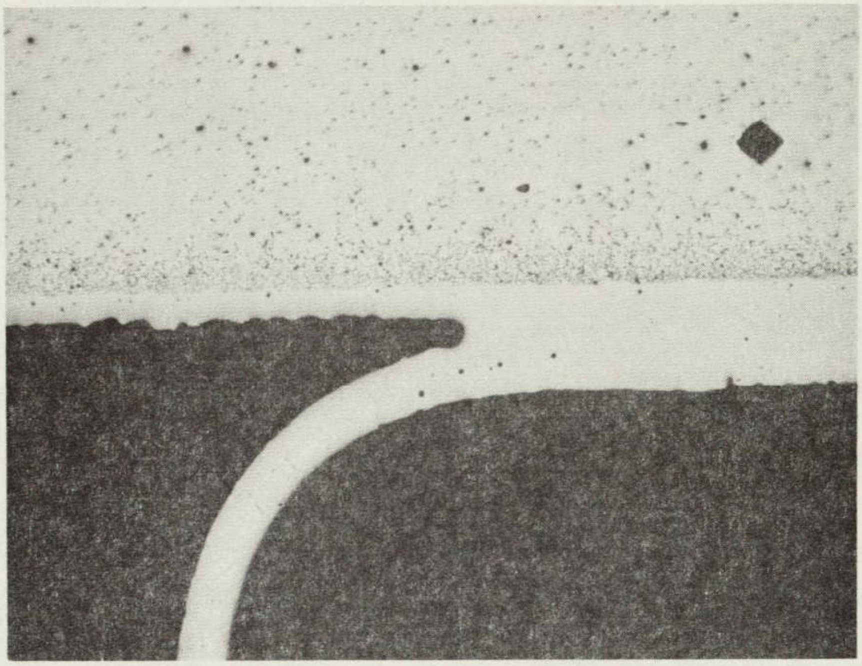

Figure 3-24. Detail From Figure 3-23. Note Well-Brazed Fin and Smooth Flow of Adjacent Brazing Alloy. Etched Electrolytically in 10 percent Oxalic Acid. (Micro 22312; X 100 Magnification)

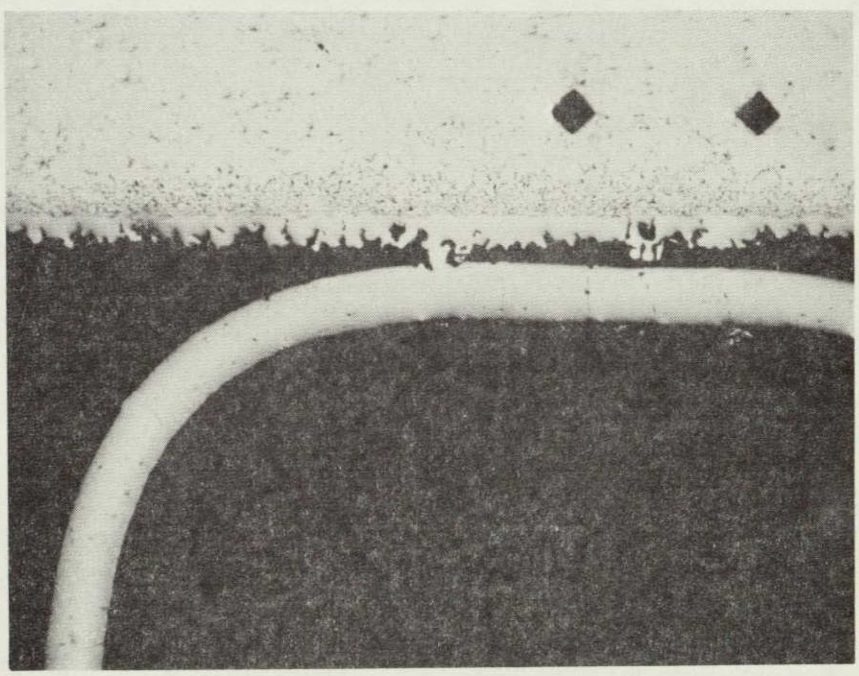



F-13144

Figure 3-25. Detail from Figure 3-23. Note Unbrazed Fin and Brazing Alloy Liquation. Etched Electrolytically in 10 percent Oxalic Acid. (Micro 22312; X 100 Magnification)

## CONCLUSIONS

The observation from the metallurgical analysis discussed above show that with some slight design modifications a thermal panel of this large size could be successfully fabricated. In the remote cooling loop and the structural sandwich, the problem of fin degradation due to braze alloy penetration could be eliminated by using a Type 347 stainless steel fin rather than the nickel fin which is less resistant to braze alloy erosion. The difficulties associated with the liquation of the braze alloy can be eliminated by brazing the remote cooling loop and the structural sandwich in separate brazing cycles or in the same brazing cycle but loaded separately instead of adjacent to one another. The heat pipe sandwich brazing would have the same configuration but would use thicker copper fins to minimize the problems associated with the Kirkendall Effect. The bosses and webs should be final machined after brazing to minimize any tolerance build up due to large braze alloy joints. The alternate fabrication technique would be the use of a machined boss and plate assembly as described in Section 4. In conclusion, a forced convection furnace braze process or a modification of the vacuum furnace braze technique should be used on complex large flat panels of the design used in the MSFC panel program to minimize the thermal stabilization and thermal gradient problems associated with vacuum furnace brazing.

## SECTION 4

## RECOMMENDED PANEL DESIGN

### INTRODUCTION

A recommended improved thermal conditioning panel design is shown in Figure 4-1. Externally, the new configuration is similar to the present configuration. The major difference is internal in the heat pipe section of the panel where the copper fin and wick system is replaced by an interconnecting double wick system and the upper sheet of the heat pipe is machined from a thick plate, eliminating many potential helium leak paths. The recommended configuration will eliminate the brazing problems encountered in the present panel by the removal of the copper fin and by the addition of the support bar in the structural sandwich.

### WICKING CONFIGURATION

The new thermal panel heat pipe concept incorporates wicking structures on both the planar surfaces. The heat transfer mechanism on the heat input face of the panel is primarily conduction. Heat is conducted through the remote coolant loop and through the liquid saturated wick to the surface of the wick where evaporation of the working fluid occurs. At the condenser end of the heat pipe, the vapor condenses and the heat given up in phase change is conducted through the wick-water matrix to the sublimator where heat is removed from the panel during sublimation of water in the heat sink.

In early heat pipe work there was much concern about the possibility of boiling occurring within the wick at the hot wall. It was believed that if nucleation occurred, the vapor might be trapped in the wick, resulting in liquid flow blockage and also increasing the thermal resistance of the wick by the formation of an insulating vapor blanket at the wall. While the problem of nucleation in wick structures has not been widely researched, extensive testing of the new wick configuration demonstrated the effects of nucleation.* At a saturation temperature of $70^{\circ}F$, a 15 percent dense nickel wick requires $20^{\circ}F$ superheat for nucleation to occur with water as the working fluid. This is approximately five times the superheat that is expected in the present thermal panel application. (At $100^{\circ}F$, the nucleation superheat is about $12^{\circ}F$.) The same experimental test data also indicated that nucleation is not undesirable but, in fact, improves performance because it results in a higher heat transfer coefficient. The higher heat transfer coefficient occurs because the vapor escapes through the large pores in the wick and does not blanket the hot wall.

Liquid will return to the evaporator from the condensor through the wicks on both faces. Wick "bridges" extending across the vapor passage will deliver

---

*Wicking Evaporative Heat Exchanger, AiResearch Report No. 70-6190, NASA Manned Spacecraft Center, Contract NAS 9-8253, Graumann, D., et al.

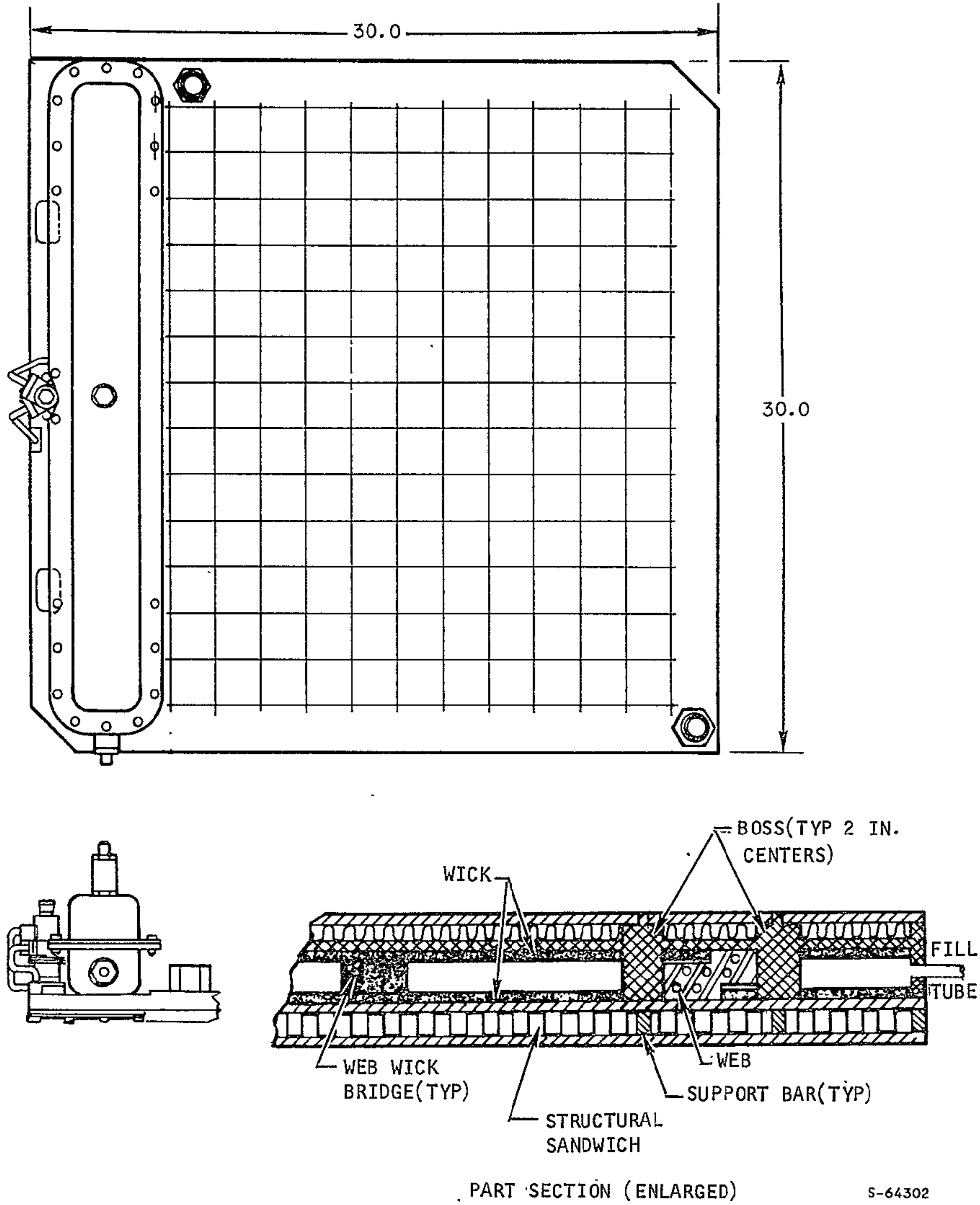


Figure 4-1. Recommended Thermal Panel Design

the liquid from the bottom wick to the wick on the heat input face. Optimization would result in a minimum thickness evaporator wick with the primary liquid delivery to the evaporator being through the wick bridges from the second wick.

PANEL FABRICATION

The panel fabrication discussed below describes the fabrication of the plate-fin assemblies, wick brazing, and the sequence used for brazing and assembling the thermal panel assembly. A forced-convection furnace braze process or a modification of the vacuum furnace braze technique would be used to minimize the thermal stabilization and thermal gradient problems associated with vacuum furnace brazing.

Plate-Fin Assembly

The remote cooling loop will be fabricated using plate-fin construction with a 3-pass coolant flow path. The fins, flow dividers, the 0.040-in.-thick Type 347 stainless steel top sheet, and the 0.040-in. thick machined bottom plate assembly will be brazed into an integral assembly with AMS 4779 (2070°F). After brazing the panel assembly will be subjected to a Stresscoat pressure test to ensure the integrity of the braze joints. Following a successful pressure test, a helium leak test will be performed to verify the integrity of the assembly between the heat pipe side of the machined plate and the remote cooling loop plate-fin sandwich.

The structural plate fin sandwich will be fabricated and tested using the same techniques used in the fabrication of the remote cooling loop assembly with the sublimator fin brazing being done in the same braze cycle. The structural sandwich will have support bars running normal to the webs in the heat pipe section of the panel for support of the bosses during the final brazing cycle. Like the remote cooling loop, the structural plate fin sandwich will be subjected to a Stresscoat pressure test followed by a helium leak test to ensure braze joint integrity.

Wick Brazing

The wicks which have machined cutouts for boss and web clearances will be brazed to the structural assembly and the remote cooling loop assembly using the gold-based braze alloy Palniro RE (2025°F). The alloy foil will be preplaced on the plate-fin assembly around the web and boss locations. The brazing fixture for the structure sandwich will be a machined stainless steel plate with machined spacers to control the wick crush as shown in Figure 4-2. The plate will be machined flat with the spacer height set to obtain a fixed amount of wick crushing to ensure sufficient contact for brazing over the 900 sq in. The brazing of the wick to the remote cooling loop assembly will use a machined plate that uses the equipment mounting bosses for a location reference. The bosses will function as machined spacers to ensure an integral braze joint between the wick and the plate over the entire panel surface areas. This fixturing technique is also shown in Figure 4-2.

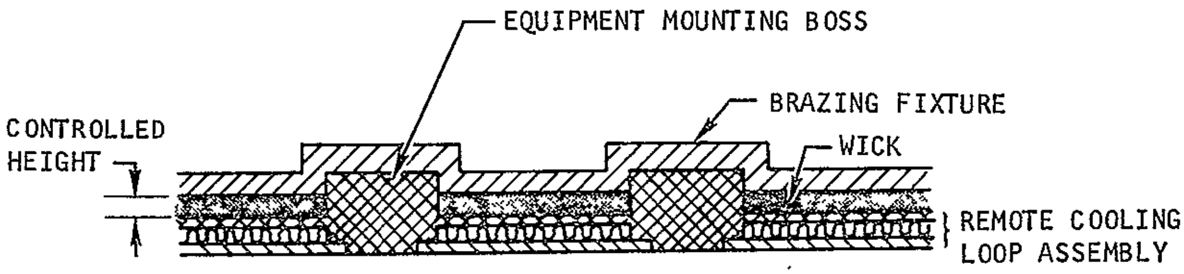


a. Wick Brazing to Remote Cooling Loop

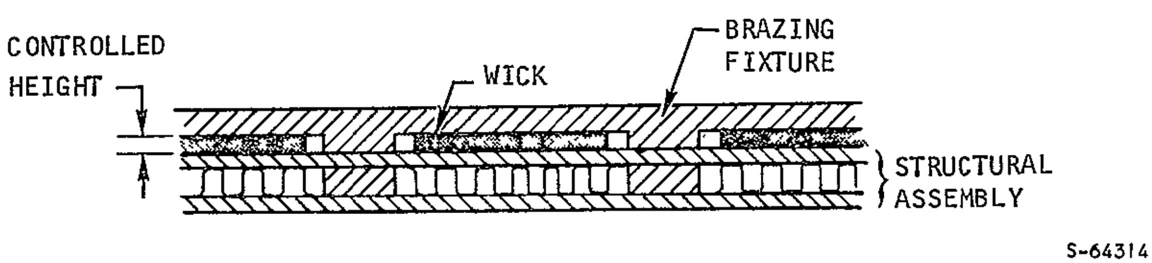


b. Wick Brazing to Structural Assembly

Figure 4-2. Fixturing Techniques for Wick Brazing

## Thermal Panel Assembly

The two plate-fin subassemblies will be joined to form an integral assembly brazing by (1) the webs to both the remote cooling loop and structural panel assemblies, (2) the bosses to the structural panel assembly, and (3) the header bar periphery of the heat pipe section to the structural sandwich assembly. As one of the assembly procedures for the final brazing cycle, the web wick bridges will be installed using mechanical attaching clips on the remote cooling loop assembly. A mechanical contact joint will be the interfacial joint between the web bridge and the wicks. This joint will be made positive by allowing the web bridge to slightly crush the wick at the local contact point. The AMS 4786 (1970°F) braze alloy selected for the brazing of the final assembly will be used in both the foil and powder forms. The foil will be preplaced for brazing of all joints except the web-to-boss joints which must use braze powder due to geometry considerations. The heat pipe will be radiographically inspected, pressure tested, and helium leak tested to ensure that both of the brazed subassemblies have been brazed into an integral helium leak tight assembly.

## Attaching Parts

The final assembly operations for completing the thermal panel assembly will be to attach the paladium-silver diffusion ports, thermistor and thermistor mounting cup, sublimator water reservoir, remote cooling loop and ports, and the sublimator plate assembly to the brazed assembly.